COPPE
UFRJ

SIMULATION AND CONTROL OF A TEMPERATURE SWING ADSORPTION NATURAL GAS DEHYDRATION UNIT

Camila Simões da Costa Cunha Vasconcellos

Dissertação de Mestrado apresentada ao Programa de Pós-graduação em Engenharia Química, COPPE, da Universidade Federal do Rio de Janeiro, como parte dos requisitos necessários à obtenção do título de Mestre em Engenharia Química.

Orientadores: Argimiro Resende Secchi
José Manuel Gonzalez Tubio Perez

Rio de Janeiro
Fevereiro de 2020

SIMULATION AND CONTROL OF A TEMPERATURE SWING ADSORPTION NATURAL GAS DEHYDRATION UNIT

Camila Simões da Costa Cunha Vasconcellos

DISSERTAÇÃO SUBMETIDA AO CORPO DOCENTE DO INSTITUTO ALBERTO LUIZ COIMBRA DE PÓS-GRADUAÇÃO E PESQUISA DE ENGENHARIA (COPPE) DA UNIVERSIDADE FEDERAL DO RIO DE JANEIRO COMO PARTE DOS REQUISITOS NECESSÁRIOS PARA A OBTENÇÃO DO GRAU DE MESTRE EM CIÊNCIAS EM ENGENHARIA QUÍMICA.

Examinada por:

Prof. Argimiro Resende Secchi, D.Sc.

Prof. Maurício Bezerra de Souza Jr., D.Sc.

Prof. André Luiz Hemerly Costa, D.Sc.

Eng. José Manuel Gonzalez Tubio Perez, D.Sc.

RIO DE JANEIRO, RJ – BRASIL
FEVEREIRO DE 2020

Vasconcellos, Camila Simões da Costa Cunha

Simulation and Control of a Temperature Swing Adsorption Natural Gas Dehydration Unit/Camila Simões da Costa Cunha Vasconcellos. – Rio de Janeiro: UFRJ/COPPE, 2020.

XXXII, 176 p.: il.; 29,7cm.

Orientadores: Argimiro Resende Secchi

José Manuel Gonzalez Tubio Perez

Dissertação (mestrado) – UFRJ/COPPE/Programa de Engenharia Química, 2020.

Referências Bibliográficas: p. 168 – 176.

1. Desidratação. 2. Gás natural. 3. Peneira molecular. 4. TSA. 5. Controle. 6. Modelagem. 7. Condensação retrógrada. I. Secchi, Argimiro Resende *et al.* II. Universidade Federal do Rio de Janeiro, COPPE, Programa de Engenharia Química. III. Título.

I dedicate these pages to all people who suffer from depression and who have had their cognitive capacities doubted because of it. Your abilities are only limited by your own free will. Let no one set boundaries to your dreams.

Acknowledgments

I am thankful to my family, friends and colleagues for all the support. I am most of all thankful to God, for providing me with the strength to continue this work when I could not see beyond my limitations.

Thank you Carlos Henrique Ferreira Brasil for standing by me throughout the whole process, for the tutoring, for encouraging me when I wanted to give up, for the forwarded e-mails, for making me believe that it was possible, for providing me with space to work and for the countless rides. I could not have done it without your help. You rock!

Thank you Antônio Rennó for helping me keep my sanity during tough times, for teaching me to breathe and for keeping my heart warm and cozy.

Thank you Ursula Simões da Costa Cunha Vasconcellos for being such a great sister and an inspiration, for sharing your experience and for trying to help even though you have already had your share of academic challenges.

The following people have aided me directly with the daunty tasks of finishing my classes, with the elaboration and with the revision of this dissertation and I feel their names must be mentioned: André Neves de Moraes, Thiago Ribeiro Sant'Anna Chaves, Felipe Eduardo Braun, Larissa Barreto Paiva, Luiz Carlos de Azevedo Fonseca, Ataíde Souza Andrade Neto and Bianca de Pley Almeida Teixeira.

I would also like to thank my advisors for their patience. Thank you Professor Argimiro for being kind and supportive and for finding the time to fit regular meetings into your busy schedule.

Thank you Pedro da Fonseca Vieira, Gilberto Teixeira Jr. and Márcio Mattoso de Pádua for allowing me to pursue the dream of achieving my Masters Degree while remaining employed.

"Everyone's under pressure and you just have to learn how to deal with it."

(Richard Simmons)

Resumo da Dissertação apresentada à COPPE/UFRJ como parte dos requisitos necessários para a obtenção do grau de Mestre em Ciências (M.Sc.)

SIMULAÇÃO E CONTROLE DE UMA UNIDADE DE DESIDRATAÇÃO DE GÁS NATURAL POR ADSORÇÃO COM VARIAÇÃO DE TEMPERATURA

Camila Simões da Costa Cunha Vasconcellos

Fevereiro/2020

Orientadores: Argimiro Resende Secchi
José Manuel Gonzalez Tubio Perez

Programa: Engenharia Química

A desidratação de gás natural por adsorção em leito fixo é uma tecnologia amplamente adotada na indústria do petróleo, mostrando-se especialmente útil nos casos em que é necessário reduzir o teor de água a níveis mais baixos do que o tratamento convencional por trietileno glicol é capaz. As unidades de desidratação de gás (GDU) por adsorção operam em processos cíclicos (adsorção-regeneração). Em plantas offshore, este comportamento é viabilizado por meio do aquecimento dos vasos de adsorção utilizando gás apropriado – processo conhecido como *Temperature Swing Adsorption* (TSA). Para reservatórios de petróleo do pré-sal pode ocorrer um fenômeno conhecido como condensação retrógrada caso a GDU esteja operando próximo à curva de ponto de orvalho. Este cenário é observado em algumas unidades de produção *offshore*. Devido à queda de pressão e a variações de temperatura, ocorre a formação de condensado, que reduz a vida útil das peneiras moleculares. A estratégia de controle proposta nesta dissertação consiste em um controle de temperatura do gás de alimentação, em malha retroalimentada, com controlador Proporcional-Integral, que busca manter a diferença entre a menor temperatura medida nos leitos e a temperatura de orvalho determinada em função da condição da alimentação igual a um valor constante (*set-point*). Observou-se que a estratégia é capaz de reduzir o tempo em que o processo permanece dentro do envelope de fase, ainda que ocorra um aumento de 10% nas frações molares de CO_2, H_2O e C_5H_{12} do gás de alimentação. A GDU considerada para a simulação dinâmica e controle possui três vasos operando em TSA de forma a processar fluido com composição característica das correntes provenientes dos reservatórios do pré-sal.

Abstract of Dissertation presented to COPPE/UFRJ as a partial fulfillment of the requirements for the degree of Master of Science (M.Sc.)

SIMULATION AND CONTROL OF A TEMPERATURE SWING ADSORPTION NATURAL GAS DEHYDRATION UNIT

Camila Simões da Costa Cunha Vasconcellos

February/2020

Advisors: Argimiro Resende Secchi
José Manuel Gonzalez Tubio Perez

Department: Chemical Engineering

Dehydration of natural gas by fixed bed adsorption is a technology widely adopted in the oil industry, proving to be especially useful in cases where it is necessary to reduce the water content to lower levels than conventional triethylene glycol treatment is capable of. Adsorption gas dehydration units (GDU) operate in cyclic processes (adsorption-regeneration). In offshore industrial plants, this behavior is made possible by heating the adsorption vessels using appropriate gas - a process known as Temperature Swing Adsorption (TSA). For pre-salt oil reservoirs, a phenomenon known as retrograde condensation may occur if the GDU is operating close to the dew-point curve. This scenario is observed in some offshore production units. Due to pressure drop and temperature variations, condensate formation occurs, which reduces the lifespan of molecular sieves. The control strategy proposed in this dissertation consists of a feed gas temperature feed-back control loop which adopts a Proportional-Integral controller with the objective of maintaining the difference between the lowest measured temperature of the beds and the dew-point temperature determined as a function of feed stream conditions at a fixed value (set-point). It was observed that the strategy is capable of reducing the time that the operating point remains inside the phase envelope, even if there is a 10% increase of the CO_2, H_2O and C_5H_{12} molar fractions in the feed gas. The GDU considered for the dynamic simulation and control consists of three vessels operating in TSA to process fluid with a characteristic composition of pre-salt feed streams.

Contents

List of Figures

List of Tables

List of Symbols

Latin symbols

Symbol	Units	Description
a	m^2/m^3	Specific particle surface
a_P	m^2/m^3	Specific particle surface per unit volume bed
A	m^2	Area
c_k	$kmol/m^3$	Molar concentration of component k
c_{pg}	$MJ/kmol/K$	Specific gas phase heat capacity at constant pressure
c_{ps}	$MJ/kg/K$	Specific heat capacity of adsorbent
D_b	m	Bed diameter
D_{ek}	m^2/s	Effective adsorbed phase diffusivity of component k
D_{ki}	m^2/s	Knudsen diffusion coefficient of component i
D_{mk}	m^2/s	Mean molecular diffusion coefficient of component k
E_{zk}	m^2/s	Axial dispersion coefficient of component k
f	$-$	Function
f_{eq}	$-$	Equilibrium (isotherm) relationship
H_b	m	Height of adsorbent layer
H_i	$MJ/m^3/s$	Rate of change of heat of adsorbed phase

Symbol	Units	Description
H_R	$MJ/m^3/s$	Combined heats of homogeneous and heterogeneous reactions
H_{Ti}	$MJ/m^3/s$	Heat of adsorption contribution to solid phase energy balance
ΔH_i	$MJ/kmol$	Heat of adsorption of component i
HTC	$MJ/m^2/s$	Gas-solid heat transfer coefficient
IP	$*$	Isotherm parameter, *units depend on isotherm
j	N/A	Colburn j-factor for heat or mass transfer
J_k	$kmol/m^3/s$	Mass transfer rate of component k to/from adsorbent per unit volume
k_{0k}	m/s	Pre-exponential factor for Arrhenius relationship
k_{0Pk}	m/s	Pre-exponential factor for pressure dependent Arrhenius relationship
k_{fk}	m/s	Film mass transfer coefficient of component k
k_g	$MW/m/K$	Gas phase thermal conductivity
k_{gr}	$MW/m/K$	Effective radial gas phase thermal conductivity
k_{gr}^{dyn}	$MW/m/K$	Dynamic contribution to k_{gr}
k_{gr}^{stat}	$MW/m/K$	Static contribution to k_{sr}
k_i	$1/s$	Effective, lumped mass transfer coefficient of component i
k_s	$MW/m/K$	Solid thermal conductivity
k_{gz}	$MW/m/K$	Effective axial gas phase thermal conductivity
k_{sr}	$MW/m/K$	Effective radial solid phase thermal conductivity
k_{sr}^{stat}	$MW/m/K$	Static contribution to k_{gr}
k_{sz}	$MW/m/K$	Effective axial solid phase thermal conductivity

Symbol	Units	Description
k_W	$MW/m/K$	Thermal conductivity of column wall
K_{K_i}	m^3/kg	Isotherm slope of component i (Henry's coefficient)
$\bar{K}_{K_i}$	$-$	Dimensionless isotherm slope of component i (Henry's coefficient)
K_{mac}	$1/s$	Macropore mass transfer coefficient
K_{mic}	$1/s$	Micropore mass transfer coefficient
K_p	$bar \cdot s/m^2$	Darcy's constant
K_{Pi}	m^2/s	Macropore diffusion coefficient
L	m	Length of horizontal bed
M	$kg/kmol$	Molecular weight
MTC_g	$1/s$	Gas film mass transfer coefficient
MTC_s	$1/s$	Solid film mass transfer coefficient
N_{u_W}	$-$	Nusselt number for gas wall heat transfer
P	bar	Pressure
P_c	bar	Critical pressure
P_i^0	bar	IAS vapor pressure
P_k	bar	Partial pressure of component k
P_M	bar	Pressure associated with the point of highest temperature on the phase envelope
P_{sat}	bar	Saturation pressure
P_T	bar	Point of highest pressure on the phase envelope
P_{e_K}	$-$	Component Peclet number for mass transfer
P_r	$-$	Prandtl number
r	m	Radial co-ordinate (in packed bed or particle)

Symbol	Units	Description
Δ_r	m	Radial discretization distance
r_p	m	Particle radius
R	$bar \cdot m^3/kmol/K$	Universal gas constant
R_e	$-$	Particle Reynolds number
S_{c_k}	$-$	Component Schmidt number
Sh_k	$-$	Component Sherwood number
t	s	Time
t_{cycle}	s	Adsorption cycle time
T	K	Temperature
T_0	K	Equal to T_{amb} or T_W depending on context used
T_{amb}	K	Ambient temperature
T_c	K	Critical temperature
T_M	K	Maximum temperature on phase envelope
T_s	K	Solid phase temperature
T_T	K	Temperature associated with the point of highest pressure on phase envelope
T_g	K	Gas phase temperature
v_g	m/s	Gas phase superficial velocity
w_k	$kmol/kg$	Loading
w_k^*	$kmol/kg$	Loading at equilibrium
Y_k	$-$	Mole fraction of component k in the gas phase
z	m	Axial coordinate
Z	$-$	Gas compressibility factor

Greek symbols

Symbol	Units	Description
α	$-$	Alpha function used in the Peng-Robinson equation
ϵ_B	m^3/m^3	Total bed voidage
ϵ_i	m^3/m^3	Inter-particle voidage
ϵ_P	m^3/m^3	Intra-particle voidage
ϕ	$-$	Relative pressure: $P_k/P_{sat,k}$
γ	$-$	Factor used in k_{sr}^{stat} calculation
γ_i	$-$	Activity coefficient of component i
Γ_i	$*$	Property being evaluated at coordinate i of discretized z axis. *Units depend on which property is being evaluated.
μ	$N \cdot s/m^2$	Dynamic viscosity
ρ_g	$kmol/m^3$	Gas phase molar density
ρ_s	kg/m^3	Adsorbent bulk density
ψ	$-$	Particle shape factor (sphericity)
$\tau_{10\%}$	s	Controller's response time, i.e. time that the process variable takes to reach its steady state value within a 10% margin.

List of Abbreviations, Acronyms and Initialisms

ADSIM	ASPEN Adsorption Simulator
ANP	Brazilian National Agency of Petroleum, Natural Gas and Biofuels (Portuguese: *Agência Nacional do Petróleo, Gás Natural e Biocombustíveis*)
bpd	Barrels per Day
BTX	Mixture of benzene, toluene, ortho-xylene, meta-xylene and para-xylene
DAE	Differential Algebraic Equations
DCS	Distributed Control System
DEPS	Differential Evolution and Particle Swarm Optimization
EZ	Equilibrium Zone
FDM	Finite Difference Method
FVM	Finite Volume Method
GDU	Gas dehydration unit
JT	Joule-Thomson
LDF	Linear Driving Force
LUB	Length of Unused Bed
MEG	Monoethylenglycol
MTZ	Mass Transfer Zone

NG	Natural Gas
NGL	Natural Gas Liquids
NLP	Nonlinear Problem
OPEC	Organization of Petroleum Exporting Countries
OPEX	Operational Expenditure
ORB	OPEC Reference Basket
PLC	Programmable Logic Controller
PPP	Petroleum Primary Processing
PSA	Pressure Swing Adsorption
ppmV	Parts per Million by Volume
PTSA	Pressure Temperature Swing Adsorption
SSE	Sum of Squared Errors
TEG	Triethylene Glycol
TSA	Temperature Swing Adsorption
UDS	Upwind differentiating Scheme
VPSA	Vacuum Pressure Swing Adsorption
WTI	West Texas Intermediate

Chapter 1

Introduction

Natural gas dehydration by fixed bed adsorption, more specifically by molecular sieve adsorption, is a widely adopted practice in the petroleum industry. This technology is especially useful in cases where it is necessary to reduce the water content of gaseous hydrocarbon streams to levels lower than the conventional triethylene glycol (TEG) treatment is capable of achieving. According to MOKHATAB (2019), molecular sieve adsorption allows natural gas water content to be reduced to less than 1 ppmV.

In an offshore vessel, when a hydrocarbon stream leaves its reservoir through production wells and reaches the topsides industrial facility, it undergoes a primary processing treatment, which aims to guarantee adequate product specification to prevent damage to downstream equipment, proper flow of fluid streams and meet contractual custody transfer requirements. Figure 1.1 summarizes the main units of a primary processing plant.

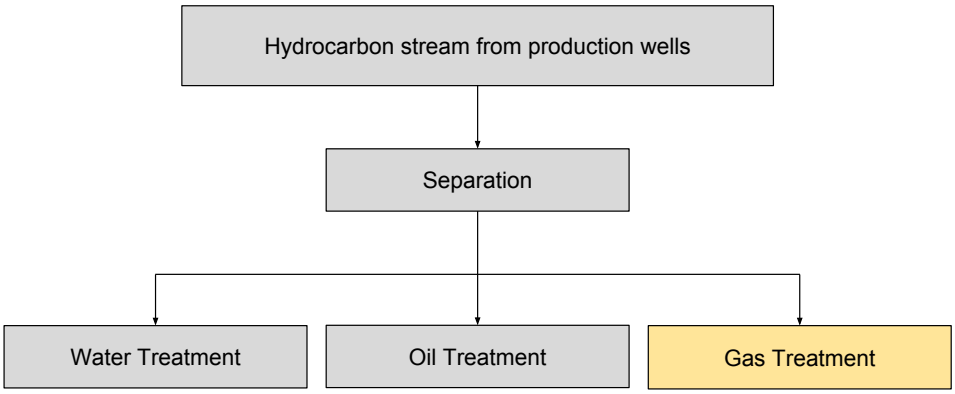

Figure 1.1: Primary Processing Plant on offshore production units.

Since the hydrocarbon streams arrives with many contaminants, including water, natural gas dehydration units (GDU) are important parts of a primary processing plant Gas Treatment system (see Figure 1.2). A packed bed adsorp-

tion GDU operates in cyclic batches (adsorption-regeneration). It is common to find multiple adsorption vessels in the same unit in order to allow the regeneration to occur parallel to the gas processing, and it is not necessary to stop the unit to replace the sieves of the saturated bed. In offshore plants, the cyclic behavior is feasible by heating the adsorption vessels using appropriate gas - a process known as Temperature Swing Adsorption (TSA). The TSA is more suitable when compared to the Pressure Swing Adsorption (PSA) process due to the lower energy consumption.

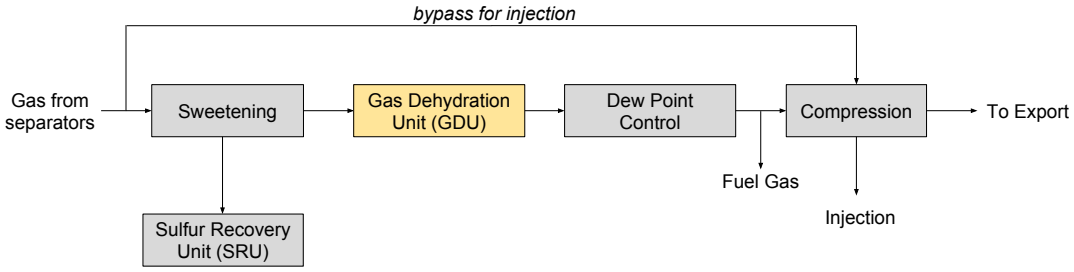

Figure 1.2: Offshore natural gas treatment plant.

In this dissertation, a temperature control strategy was proposed as an attempt to minimize condensation of the feed stream, which damages molecular sieves and causes significant impacts to the GDU.

1.1 Current Scenario of Oil and Gas Exploration and Production

Although discouraged by drastic barrel price drop from 2014 to 2016, crude oil production is still increasing. As stated by OPEC (2019),

> "The year 2018 saw substantial global supply growth. Total oil liquids production increased significantly by 2.60 million barrels/day, outpacing oil demand growth by more than 1 million bpd in 2018. The increase was once more driven by outstanding production gains in North America, particularly in the United States."

The major benchmark crude prices are slowly recovering, although still far from the elevated price plateau reached between the years 2011 and 2014 (see Figure 1.3).

According to ANP (2019), Brazil's pre-salt petroleum production has increased from 469.9 million barrels in 2017 to 521.5 million barrels in 2018. Pre-salt reservoirs are responsible for 55.2% of total national petroleum production.

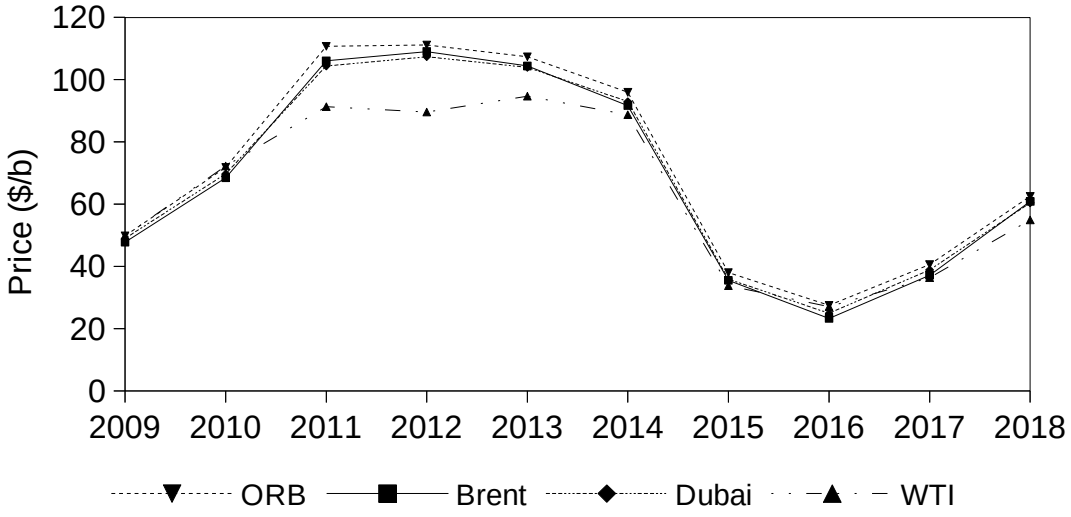

Figure 1.3: Price development of ORB and major benchmark crudes (OPEC, 2019). Authorized by the copyright owner.

Although pre-salt production imposes a series of technological challenges regarding exploration, production and logistics in general, the gains for exploring these reservoirs are significant. For this reason, there is a national tendency to stimulate offshore production in spite of its challenges.

1.2 Offshore Petroleum Primary Processing Units

When a fluid stream comes from an oil production well, it reaches an offshore production unit and undergoes a primary processing phase before being stored in the cargo tanks. It is first separated into three phases: free water, oil and wet gas. The wet gas must be treated in order to be injected for secondary recovery methods, used as gas-lift, as fuel gas on the platform's turbo-generators or to be exported.

Figure 1.2 shows a typical gas treatment plant found on many offshore production platforms. There may be one or more process units that are not represented or that are indeed represented, but may not be needed, according to the characteristics of the reservoir and composition of the produced gas. However, for units designed to operate on offshore pre-salt production fields, the Gas Dehydration Unit (GDU) is an essential component of the gas treatment if the gas is to be exported, or used as fuel gas.

Some of the reasons that explain the importance of the GDU for removing the water from natural gas are the following:

- Natural gas in the right conditions can combine with liquid or free water to form solid hydrates that can plug valve fittings or even pipelines.

- Water can condense in the pipeline, causing slug flow and possible erosion and corrosion.
- Hydrate formation and plugging of pipeline can imposes a risk to process safety due to hydraulic shocks, which may cause noise, vibration and pipe collapse.
- Water vapor increases the volume and decreases the heating value of the gas.
- Sales gas contracts and/or pipeline specifications often have to meet the maximum water content of 5 ppmV. This ensures that water-based problems will not hamper downstream operations.

1.3 The Need for Natural Gas Dehydration

Water is one of the many impurities present in natural gas. Great part of the produced natural gas is close to mixture dew-point at production temperature and pressure conditions. Water present in natural gas may cause all of the problems mentioned in the previous section. In order to minimize these risks, dehydration becomes an essential part of an offshore unit's primary processing plant.

Besides the dangers to the processing facility, there is also a problem regarding logistics. Pre-salt reservoirs contain a substantial amount of natural gas which is produced along with oil. This gas must either be burned, re-injected or exported to onshore natural gas processing facilities in order to be treated and delivered to consumers. For environmental reasons, the amount of flared gas shall be as little as possible and there is a limit to the amount of gas that can be re-injected due to the reservoir's production cycle. Gas transportation to onshore facilities becomes the main form of dealing with the great volume of produced natural gas.

The offshore production sites are far away from the coast and pipelines are at great ocean depths (larger than 2,000 m). The exportation pipelines are therefore subject to high pressures (200 bar or greater) and low temperatures (2 to 5 $^{\circ}C$). This favours hydrate formation due to condensation of water and lighter components.

Since exported natural gas will be received onshore by a Natural Gas Processing facility, there are contractual specification requirements, among which a low water content must be guaranteed. For the aforementioned reasons, produced natural gas dehydration technologies shall be adopted in order to guarantee

low water contents that will prevent hydrate formation and attend contract requirements. The required water content by contract is usually 5 ppmV. For this reason, the natural gas exported by primary processing plants usually has a 1 ppmV specification.

1.4 Using Molecular Sieves to Achieve Low Water Contents

Molecular sieves are desiccant materials with a crystal structure of uniform pore sizes which are commonly used in adsorption processes. The pore diameters or molecular sieves are comparable to the diameters of the molecules to be adsorbed. The desiccant is tailored or chosen for specific applications so that molecules with diameters greater than that of the pore diameters cannot enter the structure or be adsorbed. The application of molecular sieves ranges widely including separation processes, purifying processes and chromatography. When used in packed beds for dehydration, it is capable of achieving the lowest water contents when compared to other conventional technologies. For this reason, molecular sieve adsorption dehydration units units are widely employed at offshore production facilities.

1.4.1 Temperature Swing Adsorption (TSA)

According to BERG *et al.* (2019), the temperature swing adsorption (TSA) technology for natural gas processing is well established and has been patented and used since the 1950s, being most frequently adopted in dehydration applications. It consists in a method for continuously regenerating desiccants in packed beds by varying temperature, without the need to stop production. By employing adequate design techniques, i.e. sizing of the adsorption vessels and selecting cycle times, it is possible to process high flow rates while keeping the product within specified range.

During a TSA cycle, the temperature of the packed bed varies significantly. In the adsorption phase, it operates at feed stream temperature. During the regeneration phase, it is heated since the solid phase typically has lower adsorption capacity at high temperatures (WOOD *et al.*, 2018). The reduced capacity causes the adsorbate to be released and the desiccant to be recovered.

1.5 Condensation in Packed Beds and Its Inconvenience

1.5.1 Phase Behaviour of Petroleum Hydrocarbons

Petroleum is a very complex mixture of hydrocarbons. According to API (2011), besides hydrocarbons in the carbon number range from C1 to C60+, crude oil also contains organometallic complexes, such as sulfur and vanadium, dissolved gases such as hydrogen sulfide and other contaminants. Petroleum is usually found associated with contaminants such as water, carbon dioxide and hydrogen sulfide. Table 1.1 shows the typical elemental composition of an "average crude oil".

Table 1.1: Typical elemental composition of an average crude oil, according to API (2011)

Element	Composition (wt%)
Carbon	84
Nitrogen	14
Sulfur	1-3
Nitrogen	1
Oxygen	1
Minerals and salts	0.1

Although natural gas has lighter components, it is still a complex mixture. To understand the behavior of such a mixture, a *phase diagram* is useful. It is used to show the phase behavior of a mixture according to pressure, temperature, volume and other conditions. The pressure versus temperature plot is quite commonly used. For fluid mixtures, this phase diagram usually takes on the shape of an envelope (see Figure 1.4). It is thus referred to as a *phase envelope*. The vapor-liquid equilibrium (VLE) data is usually represented in the phase diagram, since it defines the envelope. For a liquid at a certain temperature, the pressure at which the first vapor bubble is formed is called the *bubble-point pressure*. For multiple temperatures, the bubble pressure points form the *bubble-point curve*. It is the curve that defines the upper portion of the phase envelope (for low temperatures). For a gas at a certain temperature, the pressure at which the first droplet of liquid is formed is called the *dew-point pressure*. For multiple

temperatures, the respective dew-point pressures form the *dew-point curve*. It defines the inferior outline of the envelope.

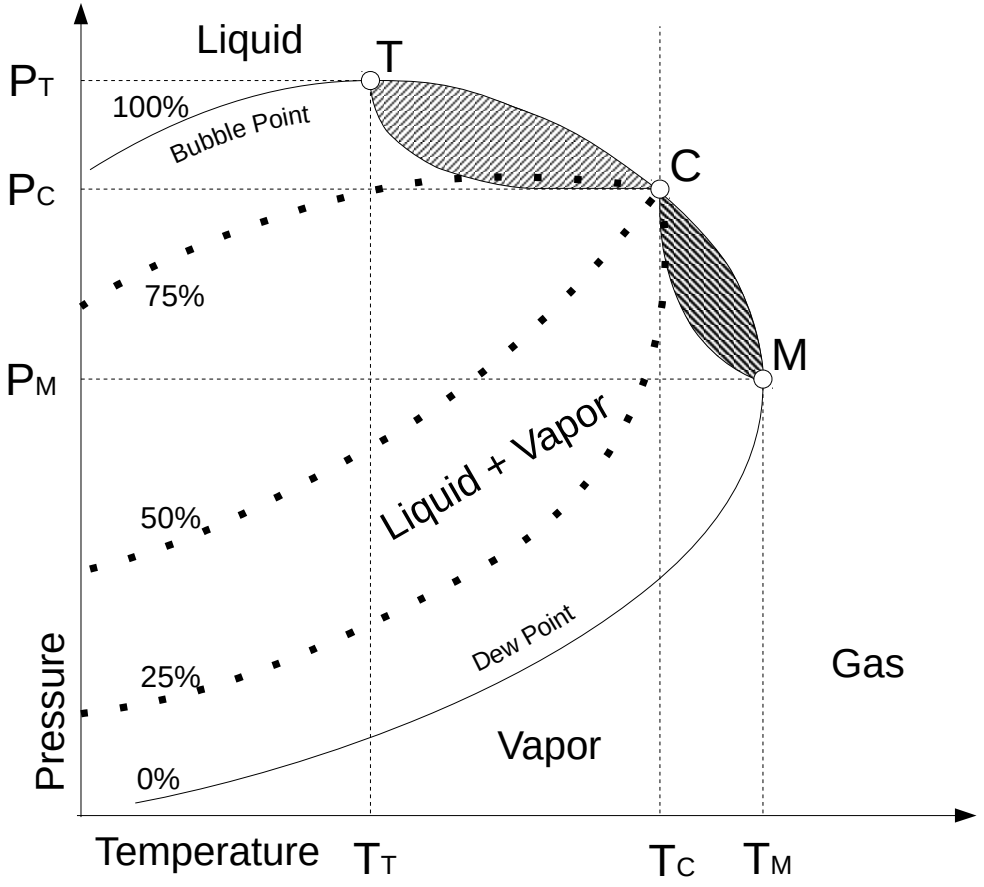

Figure 1.4: Phase envelope of a complex mixture.

The point at which the dew-point and the bubble-point curves meet is known as the *critical point* (see BERCHE *et al.* (2009)). It is defined by the *critical temperature*, T_c and *critical pressure*, P_c. At this point, the gaseous and liquid phases become indistinguishable. When fluid temperature and pressure are above critical temperature and critical pressure, the fluid is known as a *super-critical fluid*. The critical point is usually found at high temperatures and pressures. However, for many offshore primary processing units, the operating point is located close to the critical point, which is why it is so important to understand fluid behavior in this region. The maximum temperature observed on the phase envelope, T_M, defines the *cricondentherm*. The maximum observed pressure on the phase envelope, P_M, defines the *cricondenbar*. These curves are important since their position related to the critical point defines if there is the possibility of *retrograde condensation* or *retrograde vaporization*.

Figure 1.4 presents the phase envelope of a complex mixture. Curve TC is the bubble-point curve. For operating points on top of this curve, the phase is completely liquid. Curve CM is the dew-point curve and operating points on top of this curve are completely gaseous (saturated vapor). Inside the phase envelope, two phases are observed. The dotted curves represent different liquid and vapor percentages. The cross-hatched areas between curves TC and CM represent retrograde behavior.

1.5.2 Retrograde Condensation and Vaporization

As can be observed on Figure 1.4, a peculiar phenomenon occurs between T_c and T_M: isothermal compression or expansion may move from a 0% liquid to another 0% liquid condition, both on the dew-point curve CM, crossing the two-phase region. For a gas with pressure greater than P_M and $T_c < T < T_M$, isothermal expansion will lead the system into the cross-hatched region, in which liquid percentage increases. This behavior is different from what would be originally expected for pure substances. For this reason, it is called *retrograde condensation*. Further expansion will cause the system to leave the cross-hatched area, and liquid percentage will be reduced, as would be normally expected for pure substances. For this reason, outside the cross-hatched area, condensation is no longer retrograde.

Similar behavior is expected within the region $P_c < P < P_T$, where the phenomenon is called *retrograde vaporization*. For a liquid with pressure greater than P_c and smaller than P_T, isobaric cooling or heating will lead the system from a 100% liquid to another 100% liquid condition, both on the bubble-point curve, crossing the two-phase region. If temperature is greater than T_T, initial cooling will cause vapor formation to increase until a certain temperature is reached. This behavior is also different from what would be expected for pure substances. Therefore, it is called *retrograde vaporization*. Further cooling will cause vapor percentage to decrease, as would be normally expected for pure substances. In this case, vapor is no longer considered retrograde.

Retrograde phenomena were first observed by KUENEN (1892). As examined by KATZ and KURATA (1940), there was a disagreement among papers on study of phase behaviour of complex mixtures regarding the definition of the term "retrograde condensation". In recent years, the term has been used as a general term applying to all isothermal phase changes above the critical temperature and all isobaric changes above the critical pressure which were opposite to normal behavior.

1.5.3 Effects of Condensate on Packed Beds

When operating with saturated vapors, one can expect liquids to form due to pressure drop across packed beds and cyclic temperature variations, for retrograde condensation or just regular (normal) condensation. Even though it can be computer-simulated, due to model uncertainties and stream composition variations, it is difficult to accurately estimate the amount of liquids that will form and stay in the molecular sieve pores (see MOKHATAB (2019)). Condensation may shorten the lifespan of desiccants, increasing operational costs. According to TERRIGEOL (2012), liquid deposits (water or hydrocarbon) blocks access to molecular sieve micro-pores, which results in an overall decrease of the adsorption capacity. In addition, heavier hydrocarbon cracking and polymerization may occur during regeneration. Increased undesired pressure drop and channelling may occur across the bed. Both TERRIGEOL (2012) and MOKHATAB (2019) pointed out that the most efficient solution is to avoid the retrograde region as much as possible by increasing the feed temperature. Preheating the inlet stream by 3°C up to 5°C is usually recommended.

1.5.4 Controlling the Feed Stream Temperature

Feed stream composition varies during a production unit's life time and pressures vary along the packed beds. For this reason, adopting a fixed temperature set-point for the feed stream is not an ideal solution. Instead, assuming that the stream composition varies little in the packed bed, it would be a better approach to maintain the difference between the lowest measured temperature of the beds and the dew-point temperature determined as a function of feed stream conditions at a fixed value. The recommended 3°C up to 5°C would be applied above feed stream dew-point temperature. This is the main idea behind the control strategy proposed in this work.

1.6 Objectives

This dissertation aims to simulate the Temperature Swing Adsorption (TSA) gas dehydration process of a unit containing three packed beds, verify stream behavior along the packed bed, identifying the occurrence of condensation and propose a control scheme to reduce adsorbent exposure to the phenomenon.

1.7 Dissertation Structure

This work is composed of five chapters, structured as follows:

- Chapter 1 is the Introduction. It contextualizes and sets the backdrop for the motivation of this dissertation. Key terms and concepts which are essential for understanding the problem are introduced. A description of the problem is stated and dissertation objectives are defined.
- Chapter 2 is the Literary Review. It explains in more detail the context in which this work is inserted and some significant references on the topics related to modeling and control of Temperature Swing Adsorption (TSA) process units are discussed. TSA cyclic operational principles are explained.
- Chapter 3 concerns the Methodology. The process description of the unit used for simulation is presented. The simulation models are derived according to simplifying hypotheses. The numerical method used to solve the system of Differential Algebraic Equations (DAE) is explained and simulation parameters are depicted. Simulations for assessing the control strategy are proposed.
- Chapter 4 presents a discussion of the simulation results and a qualitative comparison to the temperature time plot for the GDU of a real production unit. The effectiveness of the proposed control strategy is evaluated by comparison of simulation results (with and without the proposed control strategy).
- Chapter 5 presents the conclusions of this dissertation and future work proposals.

Chapter 2

Literature Review

This literature review comprehends published material covering mainly the modeling of adsorption vessels and control applied to industrial Temperature Swing Adsorption plants. Although plenty of material was found on adsorption process modeling, not much was available on the second topic. This chapter summarizes information about natural gas dehydration technologies, including adsorption; desiccant materials, with emphasis to zeolite molecular sieves; commonly used packed bed model equations; typical problems concerning packed beds, including the presence of contaminants in the feed stream; operational and control aspects of Temperature Swing Adsorption natural gas dehydration units; and an outline of publications that are closely related to this work.

Figure 2.1 presents the three main natural gas dehydration principles (CAMPBELL, 2014) and the most commonly adopted cyclic adsorption processes (SHAFEEYAN, 2014): Temperature Swing Adsorption, Pressure Swing Adsorption, Vacuum Pressure Swing Adsorption, and Pressure Temperature Swing Adsorption, which will also be described in this chapter.

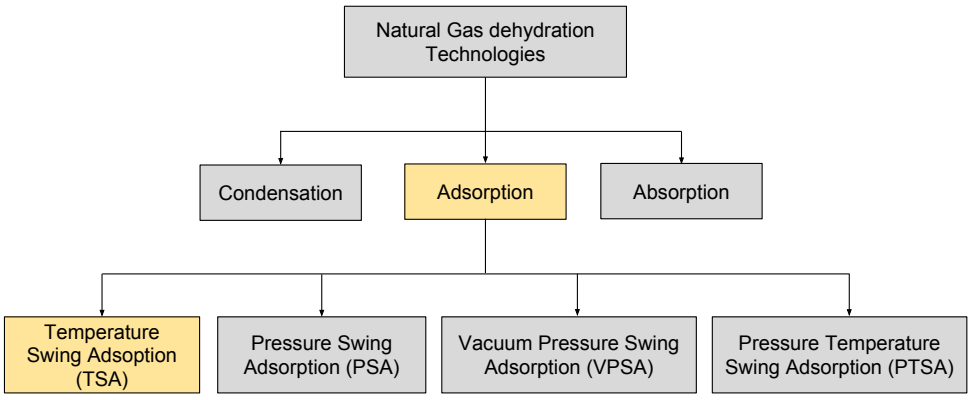

Figure 2.1: Natural gas dehydration principles and adsorption technologies.

2.1 Natural Gas Dehydration Technologies

According to MOKHATAB (2019), the most commonly employed natural gas dehydration principles are condensation, absorption, and adsorption, being the last two widely employed when low mixture dew-points are required. NETUSIL and DITL (2011) presented a comparison of these three technologies according to energy demand and suitability for use (see Table 2.1). This section briefly describes sample process plants that adopt the aforementioned principles and highlights their advantages and disadvantages. Emphasis is given to the adsorption process since it is adopted in the gas dehydration unit concerned in this work.

Table 2.1: Comparison of natural gas dehydration technologies according to energy demand and achievable dew-point depression as presented by NETUSIL and DITL (2011) and CAMPBELL (2014). The symbols -, + and ++ refer to *least energy demand*, *greater energy demand* and *highest energy demand*, respectively.

Technology	**Energy Demand According to Gas Pressure**			ΔT_{DEW} **[°C]**
	< 130 bar	**130 - 160 bar**	**> 160 bar**	
Absorption	-	-	+	-40 to -50
Adsorption	+	++	++	-80
Condensation	++	+	-	-60 to -70

2.1.1 Condensation

Dehydration by direct cooling, also called *chilling*, employs the condensation method to reduce the dew-point of natural gas. As can be observed in Figure 2.2, a feed stream consisting of wet natural gas is cooled and then routed to a flash drum. Upon expansion, due to the Joule-Thomson effect, water vapor condenses and is removed from the stream through the inferior portion of the vessel. Further cooling and entering a second flash drum also causes the condensation of higher hydrocarbons. Therefore, it is possible to achieve simultaneous dehydration and natural gas liquid recovery with the same plant.

A downside of the condensation method is that since it involves cooling, the formation of *methane hydrate* is likely to occur. Cooling causes great amounts of methane to be trapped within the crystal structure of water, forming an ice-resembling solid. As mentioned in Chapter 1, hydrate formation is a cause of

major problems such as the plugging of pipelines and valve fittings and shall, by all means, be avoided. In Figure 2.2, this is achieved by injecting hydrate inhibiting chemical products before each cooling step. Methanol or monoethylenglycol (MEG) are usually applied. In this case, hydrate inhibitor regeneration is also required.

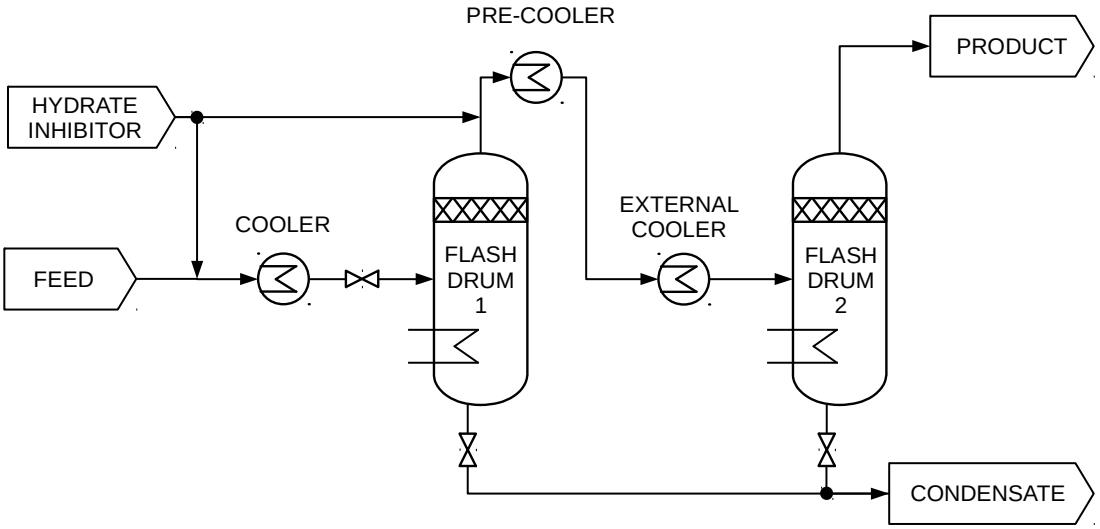

Figure 2.2: Typical natural gas dehydration plant which adopts the condensation principle.

Table 2.1 presents a comparison between natural gas dehydration technologies. According to CAMPBELL (2014), chilling with MEG injection allows dew-point temperature depressions between 60 and 70°C, which is a better result than what is obtained with absorption. However, the demanded energy for natural gas pressures below 130 bar is the highest among compared technologies.

2.1.2 Absorption

Water absorption is generally performed by contacting a wet natural gas feed stream with a hygroscopic, non-corrosive solvent, usually triethylene glycol (TEG). For this reason, the process is called *glycol dehydration* and it takes place in a tray column or packed bed called a *contactor*. According to CAMPBELL (2014), this is the most common dehydration process used to meet pipeline custody transfer specifications and field requirements being sometimes used in conjunction with adsorption processes.

Figure 2.3 presents an example of a natural gas dehydration plant which adopts the TEG absorption technology. First, the feed stream enters a scrubber to remove free water. The wet natural gas then ingresses the contactor through

the bottom of the vessel and flows upwards in counter-current with the "lean" solvent entering from the top. The dry gas leaves through the top of the contactor and enters a gas-glycol heat exchanger, where it cools down the lean TEG stream. After contact with the wet gas, the TEG is enriched with water molecules and leaves the contactor through the bottom.

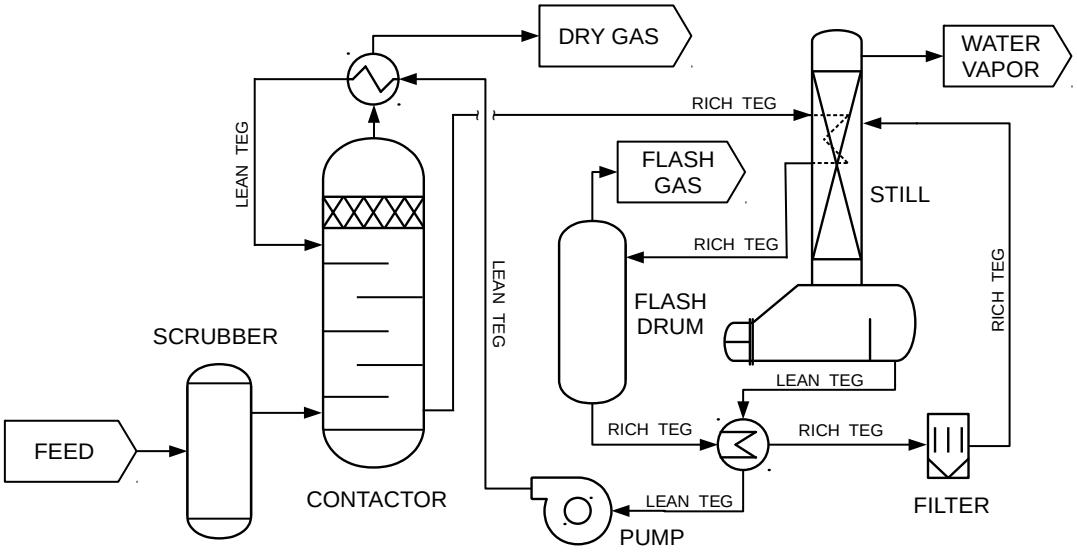

Figure 2.3: Example of absorption plant which adopts triethylene glycol (TEG) dehydration technology.

The rich TEG enters a reflux condenser at the top of a still column where it serves as a cooling medium. Then, it enters a flash tank where most of the volatile components are vaporized (CAMPBELL, 2014), goes through a rich/lean heat exchanger where it serves as a cooling medium for the lean TEG, passes through a filter, and finally, enters the still where the absorbed water is removed by distillation. At the bottom of the still column there is a re-boiler where the glycol concentration is increased to the required value. The flash gas may be routed to the gas treatment plant of the unit, be used as fuel gas, or be directed to flare. The equipment part of the portion of the plant where rich glycol enters and lean glycol leaves is called the *regeneration unit* and it operates mostly at atmospheric pressure (CAMPBELL, 2014).

2.1.3 Adsorption

The term *adsorption* refers to a multi-step surface phenomenon in which an *adsorbate* from a bulk phase becomes attached to the surface of a solid particle, the *adsorbent*. The adsorbate can be any species such as atoms, ions or molecules from a fluid or dissolved solid which is, in many applications, an impurity to be

removed by adsorption from the fluid stream. The adsorption process is usually modeled as happening in three steps: first, there is the diffusion of a component from the bulk phase to the laminar boundary layer surrounding the solid particle; second, the component moves from the boundary layer into the pores of the solid particle; finally, there is the binding of that component to the solid surface inside a pore of the adsorbent. This transport phenomenon is driven by concentration gradients (WOOD *et al.*, 2018). Adsorption is classified depending on the nature of the bonding between adsorbent and adsorbed components. When the species are attached to the adsorbent by weak van der Waals forces, the process is characterized as *physisorption*. When the attachment is due to covalent bonding or electrostatic attraction, it is classified as *chemisorption*. The nature of the bonding depends on the details of the species involved (CAMPBELL, 2014).

As can be observed on Table 2.1, adsorption presents the largest dew-point depressions with an intermediate energy demand for pressures lower than 130 bar, when compared to other dehydration technologies.

Figure 2.4 presents an example of an adsorption plant in which one bed is in adsorption mode while the other one is regenerating. The feed gas stream with wet gas enters one of the adsorption vessels through the top. As it flows downwards, adsorption occurs as the adsorbates interact with the packed bed. The dry stream leaves through the bottom of the vessel. At the same time, dry regeneration gas is routed through the bottom of a second bed. The gas is heated to the adequate regeneration temperature according to the bed's desiccant material and enters the vessel. As the hot gas flows upwards, it caries the desorbed components and leaves through the top of the bed. The regeneration stream goes through a cooler and then enters a vessel where water and hydrocarbon are separated.

There is a great number of adsorbents available, to be chosen depending on the application. For the drying of natural gas, physical adsorption is used. As stated by CAMPBELL (2014), physical adsorbents usually have at least the following characteristics: large surface area and pore volume (500 to 800 m^2/g); high mass transfer rate; can be viably regenerated; adsorption capacity is maintained in reasonable levels with time; provide low pressure drop throughout the lifespan of the unit; have high mechanical strength to resist crushing, dust formation and thermal damage; are inexpensive, non-corrosive, chemically inert and non-toxic; have high bulk density and high capacity; present little change in volume during adsorption-desorption cycles; retain strength when wet; and are commercially available and field-proven. Some of the materials that present these characteristics are alumina, silica gel, activated carbon and molecular sieves. Due to the very low outlet dew-points and higher useful capacity, molec-

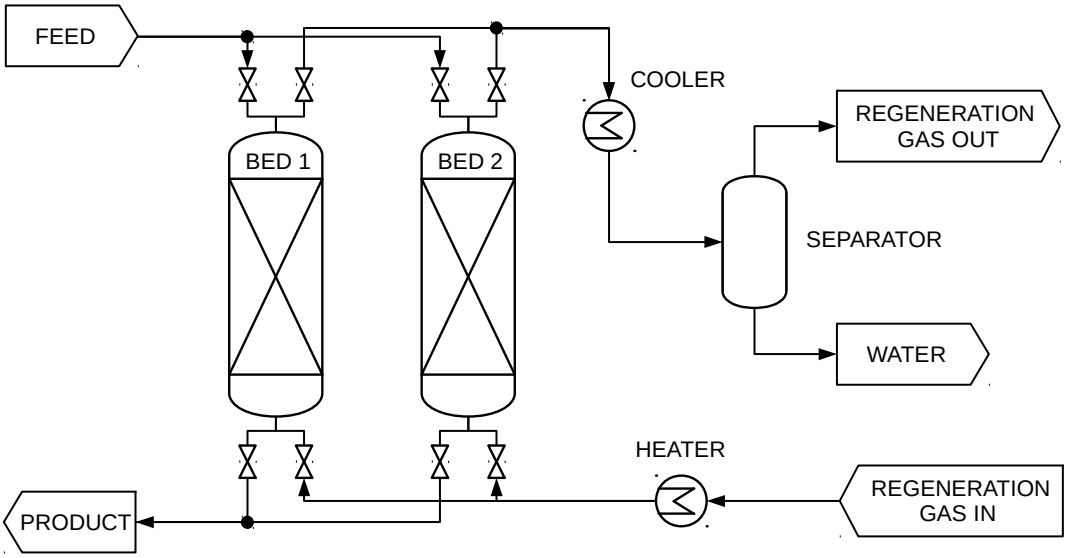

Figure 2.4: Example of an adsorption plant.

ular sieves are usually the first choice when it comes to natural gas dehydration on offshore applications (CAMPBELL, 2014).

Zeolite Molecular Sieves

Unlike silica gels and activated alumina, which are amorphous and present a wide range of pore openings, molecular sieves have uniform sized pore diameters (CAMPBELL, 2014). According to ROUQUEROL *et al.* (1994), the International Union of Pure and Applied Chemistry (IUPAC) adopts the following nomenclature regarding the size of pores: *micropores* have widths smaller than 2 nm; *mesopores* have widths between 2 and 50 nm and *macropores* have widths larger than 50 nm. Molecular sieves are microporous materials with two fundamental features: the ability to selectively adsorb molecules and to exchange their non-framework cations (SZOSTAK, 1992). This allows these adsorbents to be tailored for specific applications.

Zeolites are special types of molecular sieves consisting of porous crystalline aluminosilicate minerals (RUTHVEN, 1984) commonly used as commercial adsorbents. Zeolites can occur naturally, but can also be synthetically produced. According to RUTHVEN (1984), the zeolite framework consists of an assembly of SiO_4 and AlO_4 tetrahedra organized in regular arrangements through shared oxygen atoms. This forms an open "crystal lattice containing pores of molecular dimensions into which molecules can penetrate" (RUTHVEN, 1984). Figure 2.5 shows the structures of zeolites type A and X.

Zeolites have the potential of providing precise and specific separation of

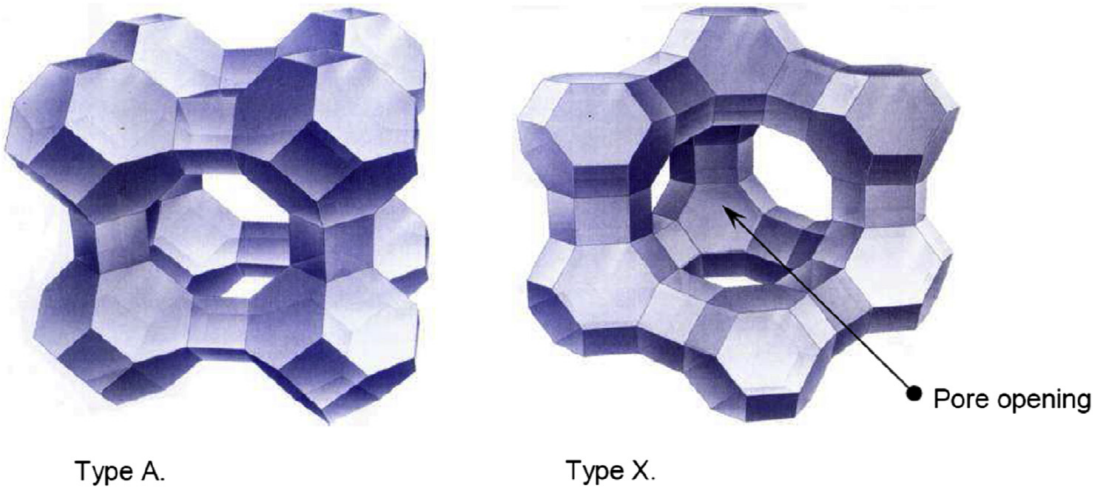

Figure 2.5: Type A and type X molecular sieve structures. Reprinted from Handbook of Natural Gas Transmission and Processing, MOKHATAB (2019), Natural Gas Dehydration and Mercaptans Removal, pages 307-348, Copyright (2019), with permission from Elsevier.

gases, including the removal of H_2O, CO_2 and SO_2 from low-grade natural gas streams (ZOU, 2019). Figure 2.6 shows a guide for the selection of molecular sieves. The pore sizes are usually measured in Å, which is equivalent to 0.1 nm. It may be observed that for dehydration, 3Å molecular sieves are ideal. However, if the gas stream is not rich in MeOH or H_2S, the 4Å molecular sieves may also be used.

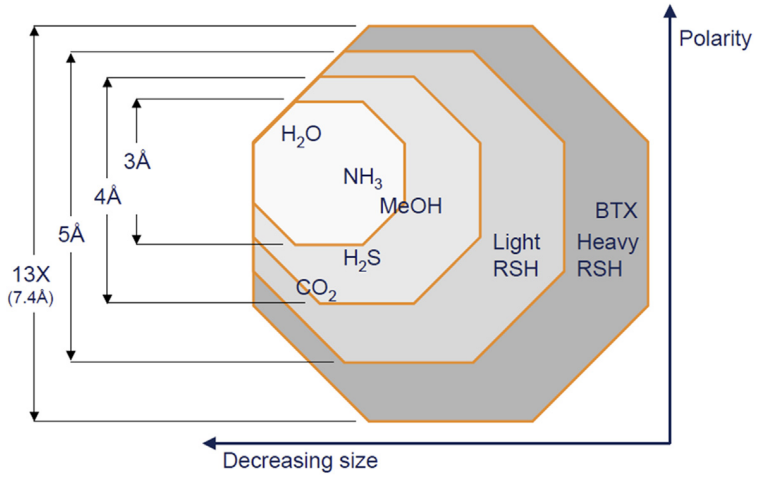

Figure 2.6: Molecular sieve selection guide according to size of the adsorbent molecules. Reprinted from Handbook of Natural Gas Transmission and Processing, MOKHATAB (2019), Natural Gas Dehydration and Mercaptans Removal, pages 307-348, Copyright (2019), with permission from Elsevier.

Regeneration

The use of molecular sieves on drying processes consist of a series of adsorption-regeneration cycles. During the regeneration phase, the adsorbate is removed from the desiccant. There are two main methods for regeneration of molecular sieves: Pressure Swing Adsorption (PSA), which consists in promoting a pressure reduction, which reduces the molecular sieve capacity; and Temperature Swing Adsorption (TSA), which consists in heating the packed bed, while purging with a carrier gas. Variants of these methods include, Vacuum Pressure Swing Adsorption (VPSA), Pressure Temperature Swing Adsorption (PTSA), Rapid Thermal Swing Adsorption (RTSA), among others (SHAFEEYAN (2014), BONNISSEL *et al.* (2001)). In TSA, regeneration temperatures range from 149°C to 316°C depending on molecular sieve type (see Appendix C).

The heating step for the regeneration is usually done slowly, linearly and in stages. According to TERRIGEOL (2012), when the heating step is done too fast, *hydro-thermal damaging* occurs. Water is more quickly desorbed from the lower layers of the packed bed since the regeneration gas enters the molecular sieve adsorption vessels from the bottom. This generates a significant pressure gradient: while the lower layers are hot (at regeneration temperature), the upper sections of the bed are still at adsorption temperature. Once the regeneration gas reaches these cooler upper layers, it gets over-saturated and "retro-condensation" of water occurs. This phenomenon is also known as *water reflux* and is observed especially near the walls of the vessel. On the outlet temperature curve of the regeneration gas, water reflux translates as a plateau typical of physical state change. The temperature of the bed increases resulting in boiling of the water. This effect is accentuated by low regeneration gas flow rates and high pressures (TERRIGEOL, 2012).

Water condensation presents significant damage to molecular sieves, including weakening of the binder and of the zeolite structure. The binding clay is leached from the molecular sieve structure and turns into dust and powder. Under the action of water soluble salts that can exchange ions with the zeolite, it forms agglomerates throughout the vessel wall and cement the structure. This may be the cause of preferential paths, high pressure drop along the bed and can even make it difficult to remove the desiccant material from the vessel. The attrition resulting from these gas-liquid interactions at high temperature can cause bed movements responsible for uneven flow distribution and pressure drop increase. The crystal structure of the zeolite suffers a loss of capacity and in some cases, it can be completely destroyed (as is the case with zeolite X crystals). The effects on zeolite A crystals is less dramatic: due to a “pore closure” effect that

concerns mainly the external surface of the crystal (especially for zeolite 3A), a decrease in the kinetics of adsorption occurs (TERRIGEOL, 2012).

The solution to hydro-thermal damaging consists of the application of a suitable heating procedure. This is typically done by increasing the regeneration temperature a few degrees per minute with a preliminary heating step of around 80 to 130°C. In cases where it is possible to reduce regeneration pressure and/or increase regeneration gas flow rate, these procedures are also recommended to reduce hydro-thermal damage. Increasing regeneration flow rate allows more water to be removed and the upper sections of the bed to be heated faster (TERRIGEOL, 2012).

Adsorption Kinetics

As explained by MOKHATAB (2019), physical adsorption is an equilibrium process, in which for a given vapor phase concentration and temperature, an equilibrium concentration exists on the adsorbent surface that has a maximum value for the adsorbate. The amount of gas adsorbed for different values of partial pressures at a constant temperature results in a set of data known as *adsorption isotherm*. The shape of the isotherm varies according to type of adsorbent, adsorbate, and inter-molecular interactions between the gas and the surface. In addition, polarity and size dictate adsorbate concentration on the absorbent surface. The theory of solid bed adsorption has been thoroughly reviewed in a number of publications (MOKHATAB, 2019).

As previously mentioned, in industry, adsorption is usually carried out in a vertical vessels with a fixed packed bed of adsorbents. When the feed gas enters the bed from the top, the top portion of the bed becomes saturated first. In the saturation zone, an equilibrium between the water partial pressure in the gas and the water adsorbed on the desiccant is established and no additional adsorption occurs. This is called the equilibrium zone (EZ). While the bed remains in the adsorption phase, the EZ grows as more adsorbent id adsorbed. The depth of bed from saturation to initial adsorption is known as the mass transfer zone (MTZ). In this region, mass is transferred from the gas stream to the surface of the desiccant. During the adsorption phase, the MTZ continuously moves downward through the bed, and water displaces the previously adsorbed gases until the entire bed becomes saturated with water vapor (in the case of dehydration). When the leading edge of the MTZ reaches the end of bottom of the vessel, the product gets contaminated. This means that *breakthrough* occurs. It is ideal to make the duration of the adsorption phase to be as long as it takes for breakthrough to occur. This maximizes cycle time, which extends bed

life because temperature cycling causes degradation to the bed, and minimizes regeneration costs. However, since it is more important to guarantee product specification, most plants operate using fixed cycle times to ensure no adsorbate breakthrough (MOKHATAB, 2019).

It is a common practice to model the transferring of mass from the gas phase to the solid phase by considering a film model with linear driving force (LDF) in which the transfer effects are lumped into a constant coefficient. Although there are many other approaches to model adoption kinetics, the LDF model is usually in accordance with experimental results (SHAFEEYAN, 2014).

Adsorption Equilibrium

A number of isotherm models in conjunction with error analysis techniques such as Sum Squared Errors (SSE), chi-square test (χ^2), and Standard deviation of relative errors (S_{RE}) are usually used for fitting experimental loading data. FOO and HAMEED (2010) presented a state of the art review of the modeling of adsorption isotherm systems, nonlinear fitting methods and applications of linear and nonlinear forms of isotherm models.

A substance on the fluid phase is adsorbed differently when there are other components in the mixture. This happens because adsorbed components of different species interact on the adsorbent material's surface. For this reason, mixture isotherms are needed. However, obtaining data for such an isotherm may be tedious and time-consuming to perform (ADSIM, 2017). Thus, it is useful to predict the mixture isotherms from pure component isotherms. There are a number of methods which may be used for this prediction such as the Vacancy Solution Theory (SUWANAYUEN and DANNER, 1980), Extended Langmuir Approach (KAPOOR *et al.*, 1990), Ideal Adsorbed Solution Theory (IAST) (MYERS and PRAUSNITZ, 1965), Real Adsorbed Solution Theory (RAST) (MYERS and PRAUSNITZ, 1965), Dual-Site Langmuir (TANG *et al.*, 2016) and Heterogeneous Ideal Adsorbed Solution Theory (HIAST) (VALENZUELA *et al.*, 1988).

Molecular Sieve Contaminants

Besides the hydrocarbons that constitute natural gas, other undesired components known as *contaminants* are also present in smaller concentrations. They are responsible for a series of undesired effects that may be either harmful or inconvenient to process, logistics and personnel. As noted by OBERLAENDER (2015), water, acid gases (CO_2, H_2S, COS, CS_2 and mercaptans), inert gases (N_2 and He) and elemental mercury (Hg) may be found among natural gas contaminants. Regarding molecular sieve adsorption on packed beds, the undesired ef-

fects usually include premature breakthrough and unacceptable pressure drops. TERRIGEOL (2012) described the most common contaminants that affect molecular sieve packed beds along with their effects, consequences and mitigation.

Although pre-treatments such as acid gas, sulfur removal and dehydration are usually done prior to molecular sieve adsorption, contaminants may still be found on the feed stream of a packed bed. TERRIGEOL (2012) stated that the adsorption process can be significantly disturbed by the presence of such contaminants in many ways: adsorption competition, degradation of the structure, partial blocking of the bed and side reactions. Independently of the contaminant, the consequences are usually poor performance leading to premature breakthrough, unacceptable pressure drop and / or adsorbent unloading difficulties.

The typical contaminants described by TERRIGEOL (2012) are oxygen, liquid water, salts, liquid hydrocarbons, liquid amines and caustic carryover.

2.2 Packed Bed Models and Related Publications

The modeling of packed beds is well consolidated in related literature. SHAFEEYAN (2014) has published an extensive review of mathematical models of fixed-bed columns for carbon dioxide adsorption applications. Although the objective of this work is to model and simulate a natural gas dehydration process, and besides the fact that most of the models presented by SHAFEEYAN (2014) are for PSA applications, the packed bed modeling for TSA remains essentially the same. Table 2.2 presented in this section contains the adsorbents; isotherms; the mass, momentum and energy balance equation considerations found on literature to model packed bed behaviour specifically for TSA applications; and a summary of the main results of each work.

According to Table 2.2, it can be observed that most of the natural gas dehydration applications use Zeolite 3A/4A. It can also be observed that most of the TSA applications consider the Ergun equation for representing pressure drop across a packed bed. The Langmuir isotherm is the most common choice for TSA natural gas dehydration since it can be well adjusted to experimental data for this type of application. For the same reason and due to its simplicity, the LDF for mass transfer resistance is considered by most of the authors. This information will be used for defining the simplifying assumptions of the model used in the simulations of this work.

There are a few publications closely related to this thesis in the sense that similar process units are considered. However, none of these publications mention the control aspect of the process. The works by AMBRÓSIO (2014), SANTOS

(2016) and BRAUN (2018) consider a gas dehydration unit that uses fixed bed molecular sieve adsorption operating in a TSA cycle for the dehydration of natural gas. Since these publications were used as reference for this dissertation, their aspects that are most useful to this work will be briefly described in this section.

2.2.1 Gas-Solid Equilibrium Isotherms and the Operational Impact of Elevated CO_2 Concentrations

SANTOS (2016) developed the dynamic simulation of a complete operation cycle of a dehydration unit of CO_2 rich natural gas encompassing multicomponent adsorption and desorption with molecular sieve zeolite 4A via the commercial simulator Aspen Adsorption. Taking as base scenario the Libra Field gas case, it was set up typical operating conditions by varying the CO_2 content in the water saturated gas stream as well as the pressure of the adsorption bed in order to analyze the impact of these variables on the dehydration performance. After the simulations, it was found that the dry gas meets specification of water content less than 1 ppm. In connection with an analysis of phase behavior, it was found that low CO_2 contents (less than 50%) do not present operational risks in terms of retrograde condensation during gas dehydration. For the high CO_2 content cases (50% up to 90%) it was found that CO_2 condensation will not occur during adsorption if pressure is kept equal or less than $50 bar$.

Retrograde condensation of natural gas was not an issue considering the composition and operation point of the analyzed process.

The thesis by SANTOS (2016) focuses on the calibration of adsorption isotherm models with gas-solid equilibrium data from literature. Multicomponent adsorption concerning H_2O, CO_2 and CH_4 was considered contacting the commercially available 4A zeolite. Langmuir isotherm parameters were obtained for each of these components. Regarding the elevated CO_2 concentrations, SANTOS (2016) observed that there is a competition for sites of adsorption between the CH_4, CO_2 and H_2O molecules. This effect is more significant between the last two components. SANTOS (2016) also observed that most of the water is desorbed during the TSA regeneration phase, significant methane and carbon dioxide residues are left at the end of the cycle. It was also reported that the residue increases with increasing CO_2 concentrations of the feed stream.

2.2.2 Analysis of Dehydration Performance for Different Temperature, Pressure and Feed Stream Compositions

AMBRÓSIO (2014) studied a process plant similar to that of SANTOS (2016). The dehydration performance was analysed for different temperature, pressure and feed stream compositions adding up to a total of 147 scenarios. It was observed that an increase in temperature is accompanied by an increase in the concentration of methane in the product stream, i.e., the greater the co-adsorption effect decreased with increasing temperature, both for medium and high pressures. The results obtained for the medium and high pressure scenarios showed that there is a tendency to increase the amount of methane in the pores of the molecular sieve.

2.2.3 Optimization Applied to the Design of a TSA Molecular Sieve Gas Dehydration Unit

BRAUN (2018) compared the traditional packed bed GDU design by predefined design guidelines to that of a new method consisting of the application of optimization using phenomenological model and operational and performance constrains. It was pointed out that significant savings can be achieved by applying optimization of the main variables involved in the project, when compared to simply applying heuristic rules and principles from previous projects. It was observed that phenomenological models provide more accurate results when compared to empirical models for the properties of desiccants. For this reason, using the first type is more appropriate for basic design engineering. It was highlighted that phenomenological models can also be used for operational monitoring.

It was observed that the phenomenological approach suggested the adoption of more "severe" conditions, such as maximizing the regeneration temperature, ΔP by length and the adoption of rapid cycles. However, the applicability of these conditions depends on whether or not the zeolite is capable of supporting them. This implies that the cost is strongly influenced by the quality of the adsorbent considered in the design phase. The challenge is to develop a solid which at the same time has high resistance to high flow rate of gases and high temperatures, without reducing its lifespan, without fragmenting or deteriorating, with high mechanical resistance and mainly with high capacity (high porosity, diffusivity and adsorption), when some of these characteristics compete with each other (e.g. high porosity and high mechanical resistance).

BRAUN (2018) also stated that the imposed restrictions have a great influ-

ence on the cost. The importance of carefully analyzing restrictions when they represent limiting factors was emphasized. Especially because some of these restrictions are recommendations of a practical and historical nature, which may not be relevant as technology evolves.

Specifically for the studied case, the configurations with 2 adsorbing beds and 1 regenerating bed were the ones that best suited the restrictions, presenting lower cost. However, it is not possible to establish a general rule for defining the best configuration. Each available option shall be optimized and analyzed individually.

2.2.4 An Example of Control Applied to a TSA Dehydration Unit

Not much literature was found on the controllability of TSA dehydration processes. ATUONWU *et al.* (2012) studied the controllability of heat-integrated zeolite adsorption dryers. The work analyses the ease with which decentralised control can be satisfactorily applied to an adsorption drying system for set-point tracking, disturbance rejection and optimal energy and quality performance using well-established controllability indicators.

Figure 2.7 shows the studied process plant. Mean product moisture content, temperature and vitamin C concentration (representative of product quality) were considered as controlled variables. Set-point tracking and disturbance rejection controllability metrics were considered in addition to energy performance sensitivity.

In adsorption dryers, the adsorption system introduces extra degrees of freedom of which some input–output pairs are promising. For corresponding inputs, adsorption dryers are shown to have higher steady-state gains than equivalent conventional dryers due to correlation between dehumidification, adsorption heat and the controlled variables. They also show improved resilience to ambient air disturbances due to adsorbent subsystem-induced self-regulation properties.

The encouraging mechanisms of the self-regulation are adsorption heat, kinetic and equilibrium properties of the adsorbent. Due to the high correlation between product moisture content and temperature, improved controllability was observed when vitamin C concentration was used as an output variable instead of product temperature. It is thus proposed that on the availability of reliable soft sensors or state estimators, instead of product temperature, vitamin C or some other temperature-dependent quality measure should be controlled in addition to product moisture in decentralised drying system control.

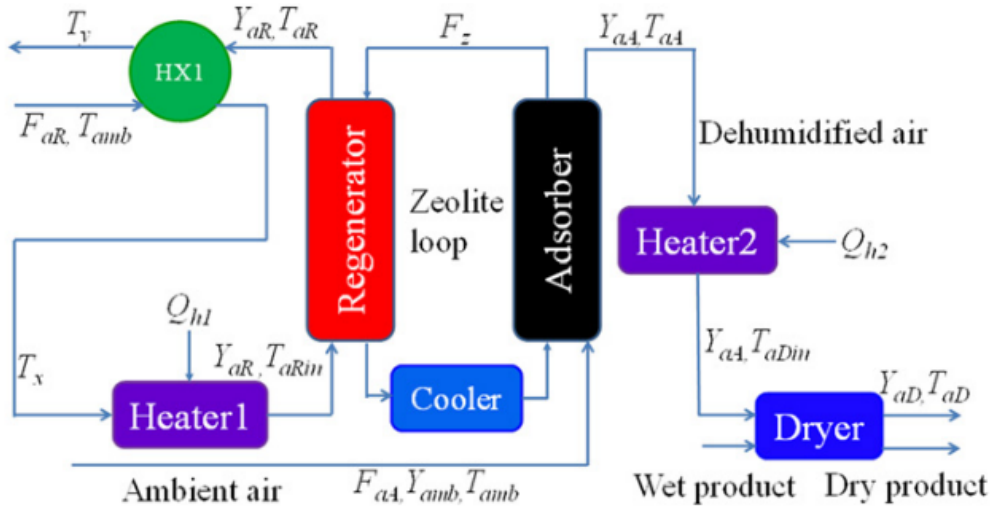

Figure 2.7: Heat integrated adsorption dryer. Reprinted from Chemical Engineering Science, Vol 80, ATUONWU *et al.* (2012), On the controllability and energy sensitivity of heat-integrated desiccant adsorption dryers, Page 135, Copyright (2012), with permission from Elsevier."

Under perfect rejection of unfavourable disturbances like ambient temperature drop and humidity rise, the energy performance of adsorption dryers is not significantly degraded, whereas, it is for conventional systems.

Table 2.2: Summary of dynamic models for fixed bed Temperature Swing Adsorption (...continued on next page)

Reference	Isotherm	Momentum	Flow Pattern	Mass Transfer	Heat Effects	Adsorbent	Application	Solution	Results and Comments
BRAUN (2018)	Langmuir	Ergun	Axially-dispersed plug flow	LDF	Non-isothermal; adiabatic	Zeolite 4A	Natural gas dehydration	Finite differences. Matlab ODE23T	Ideal gas. GDU ideal config. is 2/3.
JOSS *et al.* (2017)	Binary Sips	Ergun	Plug flow with axial dispersion	LDF	Non-isothermal; non-adiabatic; Local Thermal Equilibrium (LTE); axial conductivity neglected	Zeolite 13X	N_2 and CO_2. Post-combustion CO_2 capture	Cyclic steady state determined using the successive substitution method	Binary mixture CO_2/N_2
MARX *et al.* (2016)	Sips + IAST	Ergun	Plug flow with axial dispersion	LDF	LTE. Non-adiabatic	Zeolite 13X	Post-combustion CO_2 capture	Experiments. Matlab *fmincom* for parameter estimation. FVM. Van Leer Method. Gear's method. IMSL DIVPAG solver.	CO_2 adsorption kinetics is strongly impacted by heat transfer.
SANTOS (2016)	Langmuir	Ergun	Plug flow. No axial dispersion.	LDF	Adiabatic; Non isothermal; no conduction; constant HTC and heat of adsorption.	Zeolite 4A	Natural gas dehydration	Aspen Adsorption. First order upwind differentiating scheme. 20 axial nodes.	Langmuir 3 presented a better fit to experimental data than Langmuir 1. Not all CH_4 is desorbed during regeneration.

Table 2.2: (...continued) Summary of dynamic models for fixed bed Temperature Swing Adsorption

Reference	Isotherm	Momentum	Flow Pattern	Mass Transfer	Heat Effects	Adsorbent	Application	Solution	Results and Comments
NTIAMOAH *et al.* (2016)	Dual-site Langmuir	Ergun	Plug Flow	LDF	Non-isothermal; no solid conduction; non-adiabatic	Zeolite NaUSY	CO_2 capture	Aspen Adsorption. UDS-1. Implicit Euler integrator. 150 nodes. $1 \times 10{-}5$ CSS tolerance.	Ideal Gas. Product purities > 91% can be achieved using purge with hot gas stream with composition equivalent to the product.
GABRUŚ *et al.* (2015)	Langmuir-Freundlich / dual-site Langmuir-Langmuir	N/A	N/A	N/A	N/A	Zeolite 3A/4A	Aliphatic alcohols de-watering	Experimental. Intelligent Gravimetric Analyzer.	Water loss from molecular sieves temperature range: 40-400°C for 3A and 40-500°C for 4A. Water desperation temperature shall be greater than 130°C.
SALVADOR *et al.* (2015)	N/A	N/A	N/A	N/A	N/A	Activated Carbon	Regeneration of carbonaceous adsorbents	Literature Review	According to the regeneration agents, there are 8 methods of TSA.

Table 2.2: (...continued) Summary of dynamic models for fixed bed Temperature Swing Adsorption

Reference	Isotherm	Momentum	Flow Pattern	Mass Transfer	Heat Effects	Adsorbent	Application	Solution	Results and Comments
AMBRÓSIO (2014)	Langmuir	Burke-Plummer	Plug flow with no axial dispersion.	LDF	Adiabatic; non-isothermal; no conduction	Zeolite 4A	Natural gas dehydration	Aspen Adsorption. UDS-1. 20 nodes.	An increase in T is accompanied by an increase in the concentration of CH_4 in product stream.
PIRNGRUBER *et al.* (2013)	Langmuir	Constant drop	N/A	N/A	N/A	polyethyleneir (PEI) deposited on a silica support (Cariact G10)	Post-combustion CO_2 capture	Theoretical analysis	Fixed bed process is the most energy efficient when compared to isothermal fluidized bed and adiabatic fluidized bed.
ATUONWU *et al.* (2012)	—	—	—-	—-	Adiabatic	Zeolite	Air drying for vitamin C purification (food processing)	—-	It is preferable to control product moisture and vitamin C concentration in a 2x2 decentralized control system.

Table 2.2: (...continued) Summary of dynamic models for fixed bed Temperature Swing Adsorption

Reference	Isotherm	Momentum	Flow Pattern	Mass Transfer	Heat Effects	Adsorbent	Application	Solution	Results and Comments
ATUONWU *et al.* (2011b)	—	—	—-	—-	Adiabatic	Zeolite	Air drying for food processing	—-	Heat integration is considered as part of the adsorber design. 15% improvement in energy efficiency was observed.
ATUONWU *et al.* (2011a)	—	—	—-	—-	Adiabatic	Zeolite	Air drying for food processing	—-	Energy efficiency is improved by 45% in low-temperature dryer by optimizing regeneration temperature, flow rates and heat recovery from exhausts.
MOATE and LEVAN (2010)	Multi-temperature Toth	Constant pressure; Darcy's law	Plug flow with axial dispersion	LDF. Inert N_2 and O_2	Adiabatic; non-isothermal.	Zeolite 5A	Post-combustion CO_2 capture	Comsol Multi-Physics finite element software	By bed geometry, regeneration efficiency increased by 55%.

Table 2.2: (...continued) Summary of dynamic models for fixed bed Temperature Swing Adsorption

Reference	Isotherm	Momentum	Flow Pattern	Mass Transfer	Heat Effects	Adsorbent	Application	Solution	Results and Comments
NASTAJ and AMBROŻEK (2009)	Two-site Dubinin-Radushkevich	Constant pressure	Plug Flow with axial dispersion	LDF	Non-equilibrium; Non-isothermal; non-adiabatic	Silica gel	Air drying	NMOL; Finite Differences; 50 nodes; DIVPAG from IMSL; Adams Moulton or Gear BDF method.	Inlet air temperature and humidity significantly effect adsorption and desorption in TSA.
TLILI *et al.* (2009)	Langmuir	N/A	N/A	N/A	N/A	Zeolite 5A	CO_2 recovery	Experimental	Recovery of CO_2 under vacuum leads to 99% purity, but limited recovery (85%).
AMBROŻEK (2009)	Langmuir	Constant pressure	Plug flow with axial diffusion	LDF	Axial conduction; non-isothermal; non-equilibrium; non-adiabatic	Activated Carbon	Removal of VOCs	NMOL; DIVPAG from IMSL; second-order central differentiating scheme; 30 nodes	Breakthrough curves not significantly affected by axial thermal conductivity and axial diffusion.
GIRAUDET *et al.* (2009)	Langmuir; O'Brian and Myers	Constant pressure	Plug flow with axial dispersion	LDF	Non-isothermal; non-adiabatic	Activated carbon	Removal of VOCs	NMOLS with adaptive space remeshing	Differences between adsorbents were explained with different coefficients of axial dispersion of heat.

Table 2.2: (...continued) Summary of dynamic models for fixed bed Temperature Swing Adsorption

Reference	Isotherm	Momentum	Flow Pattern	Mass Transfer	Heat Effects	Adsorbent	Application	Solution	Results and Comments
RIBEIRO *et al.* (2008)	Multi-site Langmuir	Constant drop	Axially dispersed plug flow	LDF	—-	Activated carbon	Post-combustion CO_2 capture	MATLAB *fmins*; gPROMS, orthogonal collocation of finite elements	Multi-site Langmuir provided better fit for high pressures. However, experimental isosteric heats were higher than the obtained with this isotherm.
AMBROZEK (2008)	Dubinin-Astkhov	Ergun	Axially-dispersed plug flow	LDF	—-	Activated carbon	Removal of VOC from waste air	NMOL; DIVPAG/IMSL; second-order central differentiating scheme	In closed-loop system, VOC can be easily recovered at condenser T equal to surroundings. For open-flow, low condensation T is required.

Table 2.2: (...continued) Summary of dynamic models for fixed bed Temperature Swing Adsorption

Reference	Isotherm	Momentum	Flow Pattern	Mass Transfer	Heat Effects	Adsorbent	Application	Solution	Results and Comments
LI (2007)	Langmuir; Freundlich; Sips; Flory-Huggins; Toth; Multi-site Langmuir; Dual-site Langmuir; IAST; Statistical model; Extended Sips	N/A	N/A	N/A	N/A	MFI, β-zeolite, Zeolite NaY and Zeolite 13X	Flue gas, landfill gas, natural gas and enhanced oil recovery	Non-linear regression; non-linear solver; Newton's method; MS Excel solver.	CO_2 is more adsorbed than CH_4 because of its higher quadrupole moment. 2 parameter: Langmuir is better than Freundlich.
MOREIRA *et al.* (2006)	Langmuir	N/A	Axially-dispersed plug flow	LDF	Isothermal	Hydrotalcite	Post-combustion CO_2 capture	Minimization of average residual error. PDECOL; orthogonal collocation; 100 elements; two interior collocation points.	MG50 presents good capacity for CO_2 adsorption at any T. CO_2 retained by carbonation + adsorption. CO_2 released by thermal treatment > 350°C.

Table 2.2: (...continued) Summary of dynamic models for fixed bed Temperature Swing Adsorption

Reference	Isotherm	Momentum	Flow Pattern	Mass Transfer	Heat Effects	Adsorbent	Application	Solution	Results and Comments
CLAUSSE *et al.* (2004)	O'Brien-Myers + IAST for co-adsorption	Ergun	Axially Dispersed Plug flow	LDF	LTE; adiabatic; non-isothermal; no conduction / isothermal; near-adiabatic w/ no conduction; no conduction w/ heat-exchanger	Activated Carbon	Co-adsorption of ethane anc CO_2 from N_2 (VOC removal)	NMOL + FVM. 80 grid points. DASPK 2.0	MTC < 0.01-> numerical breakthrough curves too dispersive compared to the experimental. MTC > 0.01-> numerical curves agreed with the experimental.
KIM *et al.* (2004)	Langmuir-Freundlich	Constant pressure	Axially Dispersed Plug flow	LDF	LTE; Non-isothermal; no solid conduction; near-adiabatic	Zeolite 13X	Air drying	gPROMS; MOLS; CFDM of second order; 15-30 nodes; DASOLVE	When heat of adsorption is high, concentration breakthrough of 2D resembles 1D with column-wall energy balance.

Table 2.2: (...continued) Summary of dynamic models for fixed bed Temperature Swing Adsorption

Reference	Isotherm	Momentum	Flow Pattern	Mass Transfer	Heat Effects	Adsorbent	Application	Solution	Results and Comments
CLAUSSE *et al.* (2003)	Experimental isotherms + IAST for co-adsorption	N/A	N/A	N/A	Internal heat exchanger	Carbonaceous adsorbent	VOC removal	Experimental.	CO_2 reduces column capacity to capture ethane and increases necessary regeneration time.
BONJOUR *et al.* (2002)	Toth	Darcy's Law	Axially dispersed plug flow	LDF	Isothermal wall; non-adiabatic; non-isothermal (bed)	Activated Carbon	VOC removal	SIMPLE algorithm	The new TSA process with indirect cooling and heating provided small axial T gradients and purity higher than 99.995%.
KO *et al.* (2001)	Extended Langmuir	Constant Pressure	Axially dispersed plug flow	LDF	Non-isothermal; non-equilibrium; non-adiabatic	Activated Carbon	Purifying BTX	MOLS; CFDM (2nd order, 20 elements); gPROMS; DASOLVE	Experimental breakthrough agreed with model. Jacketed TSA is more energy saving.

Table 2.2: (...continued) Summary of dynamic models for fixed bed Temperature Swing Adsorption

Reference	Isotherm	Momentum	Flow Pattern	Mass Transfer	Heat Effects	Adsorbent	Application	Solution	Results and Comments
HUANG and FAIR (1989)	Langmuir + Flory Huggins (Vacancy Solution Model)	Constant Pressure	Axially-dispersed plug flow	LDF	Non-isothermal; non-adiabatic	Activated carbon	Parametric analysis for multi-component adsorption (ethane - propane) separation	Experimental and NMOL with second-order central differencing. DGEAR with Gear's method. 2nd order bachwards differencing at L (for Neumann boundary condition). 24 nodes.	Breakthrough curve of key component is little effected by the non-key component when both concentrations are low. N_2 competes with ethane for adsorption on activated carbon.
HUANG and FAIR (1988)	Langmuir + Flory Huggins (Vacancy Solution Model)	Constant Pressure	Axially-dispersed plug flow	LDF	Non-isothermal; non-adiabatic	Activated carbon	Separation of ethane / propane mixture from nitrogen or helium	NMOL with second-order central differencing. DGEAR with Gear's method. 2nd order bachwards differencing at L (for Neumann boundary condition). 24 nodes.	Surface diffusion dominates intra-particle mechanism. N_2 is competitive with ethane on AC when its partial pressure is much higher than that of ethane.

Table 2.2: (...continued) Summary of dynamic models for fixed bed Temperature Swing Adsorption

Reference	Isotherm	Momentum	Flow Pattern	Mass Transfer	Heat Effects	Adsorbent	Application	Solution	Results and Comments
SCHORK and FAIR (1988)	Redlich-Peterson	Constant Pressure	Axially-dispersed plug flow	LDF	Non-isothermal; non-adiabatic	Activated Carbon	Nitrogen - propane separation	NMOLS; 2nd order central differencing scheme. 24 - 28 nodes. DGEAR - IMSL; Gear's method with variable order and step size. 2nd order bachwards differencing at L (for Neumann boundary condition)	Ideal gas. Single adsorbate. 1D. Regeneration energy efficiency is improved by increasing contact time in adiabatic bed. In non-adiabatic, there is an optimum contact time.
TSAI *et al.* (1985)	Langmuir	Constant Pressure	Plug flow. No axial dispersion.	Pore diffusion. Parabolic intra-particle concentration profile.	Isothermal	Activated Carbon	Separation of H_2 from CH_4	Integration by 4th order predictor - corrector method. Crank-Nicolson method.	Ideal Gas. 1D. Only CH_4 adsorbed. Pore diffusion is important in this application. Parabolic concentration inside particle.

Table 2.2: (...continued) Summary of dynamic models for fixed bed Temperature Swing Adsorption

Reference	Isotherm	Momentum	Flow Pattern	Mass Transfer	Heat Effects	Adsorbent	Application	Solution	Results and Comments
TSAI *et al.* (1983)	Langmuir	Constant Pressure	Plug flow. No axial dispersion.	Pore diffusion	Temperature of solid and gas are equal	Activated Carbon	Separation of H_2 from CH_4 at elevated pressures	Crank-Nicolson method. SIMPLE algorithm.	Ideal Gas. 1D. Only CH_4 adsorbed.
BASMADJIAN (1975)	N/A	N/A	N/A	N/A	Non-isothermal; LTE	Silica gel; activated carbon; 3A, 4A and 5A Zeolites	Drying; desulfurization; CO_2 removal, solvent recovery	—	Possibility of omitting cooling step in TSA cycles when (q_P/Y_F) / (C_{ps}/Cpb) > 1.5.

Chapter 3

Methodology

This chapter presents the methodology used for modeling and simulation of a Gas Dehydration Unit (GDU). First, the process of an existing unit is explained along with a description of the feed stream and the expected output stream. An adequate equation of state (EOS) is chosen in order to accurately predict fluid properties and behaviour. Simplifications are applied to the feed stream in order to reduce computational time and complexity without compromising phase behaviour representation. Afterwards, a simplified mathematical model of the packed bed is obtained. These models are used to formulate the system of Differential-Algebraic Equations (DAEs) that will be solved periodically, composing the Temperature Swing Adsorption (TSA) cycles. For each model equation, the necessary parameters and their calculation methods are presented. The numerical method used as discretization procedure for the model equations is also presented. Finally, the TSA simulation algorithm and Aspen Adsorption simulation software are described.

3.1 Process Description of a Real Unit

As explained on Chapter 1, the GDU is the part of the Gas Treatment System required to meet the specifications in the produced natural gas from the production wells prior to be used as fuel gas, gas-lift, exportation gas and injection gas. For the particular production unit with which this work is concerned, the GDU comes after the Main Compression Unit and before the Hydrocarbon Dew Point Control Unit. It consists mainly of the following equipment: feed gas heater (P-01), gas coalescer filter (FT-01), condensate coalescer filter heater (P-04), molecular sieve adsorber vessels (BED 1, BED 2 and BED 3), particulate filter (FT-02), regeneration gas compressor (UC-01), regeneration gas pre-heater (P-02), regeneration gas heater (P-03), regeneration gas cooler (P-05) and regeneration gas

separator (FT-03). Since the GDU is placed after the Main Compression Unit, the equipment and materials have to be suitable for high pressures which may vary from 65 bar up to 82 bar, being 74 bar the nominal pressure of the Main Compressor Unit. Figure 3.1 presents the Process Flow Diagram (PFD) of the real GDU.

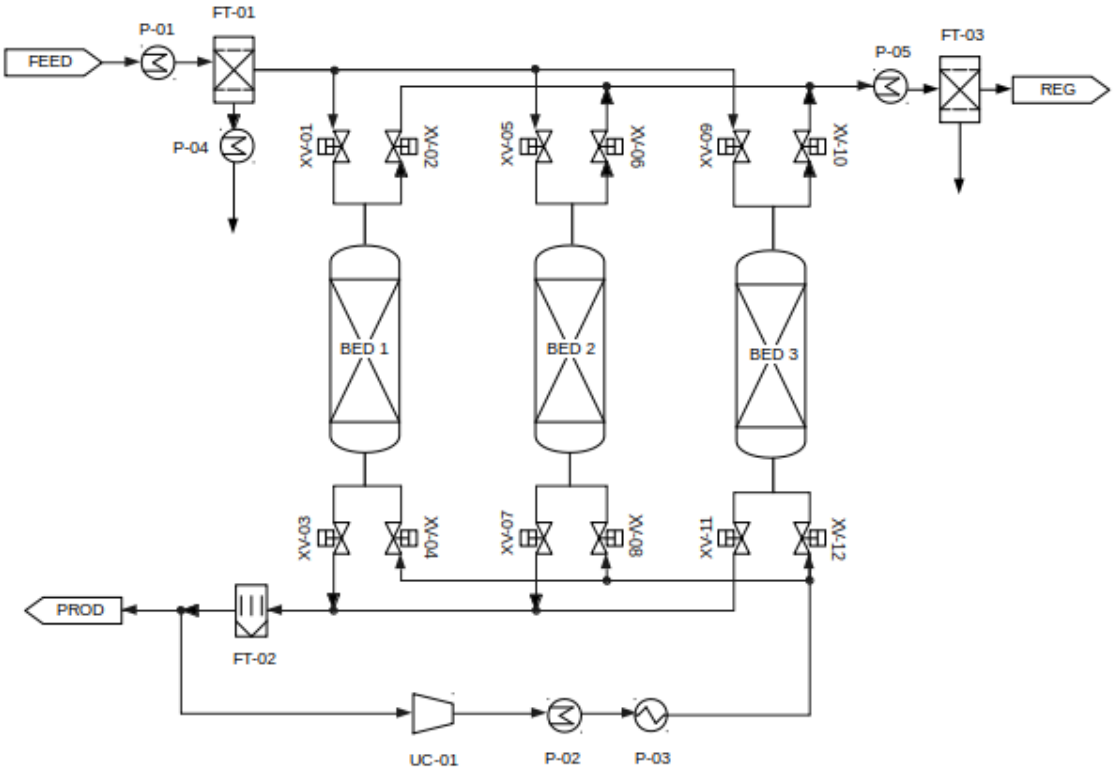

Figure 3.1: Process Flow Diagram of an existing Gas Dehydration Unit.

Regarding construction, each of the three vertically oriented vessels containing the desiccant bed for water adsorption (molecular sieves) has an internal diameter of 2.75 m. Considering the refractory material which lines the bed's interior, this diameter reduces to 2.60 m, which is the diameter of the volume that will be actually filled with desiccants. There is an empty hemisphere at the top of the bed with a radius of 1.40 m and an empty cylindrical space of 0.87 m of height and the same diameter as the bed. After this space there is a 0.15 m layer of 1" ceramic balls followed by a mesh screen and a 0.32 m layer of silica gel to guard the molecular sieves. This is followed by a 5.37 m layer of 4A molecular sieves of mixed types (pellets, beads etc.), a 0.08 m layer of 1/4" ceramic balls, a 0.08 m layer of 1/2" ceramic balls, mesh screens and a grid supporting ring. After the mesh screens there is a cylindrical empty space of 0.97 m height and diameter of the bed and a hemisphere equal to the one found at the top of the bed.

During normal operation, two vessels work on adsorption mode, with the gas

flowing downwards, and one vessel works on regeneration mode (desorption by heat), with the gas flowing upwards. The state of the on-off valves (XV-01 through XV-12) are defined depending on whether the bed is in adsorption or regeneration mode.

3.1.1 Adsorption Mode (Dehydration)

The gas stream from the regeneration gas coalescer filter at approximately 40°C is routed back to be mixed with the Main Compression Unit gas at 25°C to 28°C (see Figure 3.2).

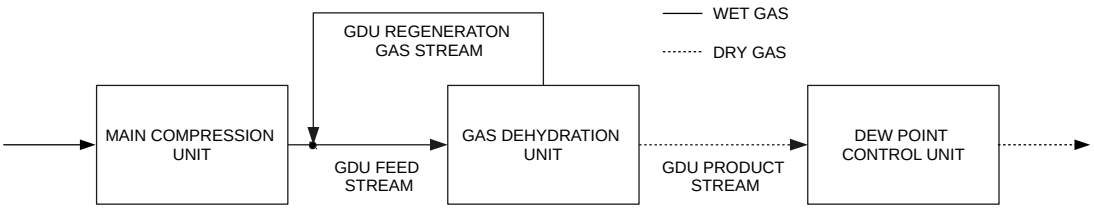

Figure 3.2: Process Flow Diagram of an existing Gas Dehydration Unit

This mixture composes the feed stream of the GDU at approximately 33°C. The sum of these two gas streams is heated up in the feed gas heater, which consists of a gas-gas heat exchanger, aiming to achieve the dew-point temperature of about 34 to 36°C. This mixed stream enters the gas coalescer filter where free liquids (water and hydrocarbons) are removed. If the temperature of the condensed liquids is below 30°C, it is heated in the condensate coalescer filter heater to prevent hydrate formation. The saturated gas is then routed to the top of the molecular sieve beds, entering the two beds in adsorption mode from the top. A gas flow rate of about 13,289.3 kmol/h (3.69 kmol/s) is expected to feed the GDU, which means that each bed in adsorption mode is expected to receive an inlet gas flow rate of 1.85 kmol/s. The dehydrated gas stream that leaves the GDU must comply with water content less than 1 ppmv. This stream is filtered in a particulate filter before proceeding to the Hydrocarbon Dew-Point Control Unit in order to avoid carrying dust material to downstream systems. A total pressure drop of about 1 bar is expected as the feed stream passes through the complete GDU.

3.1.2 Regeneration Mode (Desorption)

Part of the filtered dehydrated gas (about 10% to 11%) that leaves the two molecular sieve adsorber vessels in adsorption mode is used as regeneration gas. This

means that the bed in regeneration mode will receive a feed flow rate of about 0.41 kmol/s. This gas fraction is boosted through the regeneration gas compressor to provide an increase in pressure, since there is a slight pressure drop as the gas runs through the packed beds. Then, it is heated in the regeneration gas heaters. There is a pre-heater (P-02) and an electric heater (P-03). The pre-heater is a gas-gas heat exchanger, used to increase gas temperature as much as possible by exchanging heat with hotter gas streams from other parts of the primary processing plant. The exchanged heat obtained from the pre-heater by itself is usually not enough to raise the regeneration gas stream temperature up to the molecular sieve regeneration temperature of 230°C. For this reason, an electric heater is used together with it. The electric heater starts by linearly (ramp set-point) raising the temperature to about 120°C. During this time, the set-point of the pre-heater is 0°C and it is bypassed. Once 120°C are reached, the set-point of the pre-heater is changed to 120°C, it is no longer bypassed and the set-point of the electric heater is linearly increased to 230°C. This gas stream at 74 bar and 230°C is fed to the molecular sieve adsorber vessel in regeneration mode from its bottom. This will heat the desiccant bed in order to recover water retained in the molecular sieves. The regeneration gas leaving (upwards) the vessel is then cooled down in the regeneration gas cooler to 40°C in order to condense the desorbed water and directed to the regeneration gas coalescer filter where the water and condensate are separated from the original stream. The condensate collected in the inlet gas coalescer filter is heated in the condensate coalescer filter heater and routed to a safety knock-out drum. It is then routed back to the primary processing plant's separation stage.

3.1.3 Expected and Observed Cyclic Behaviors

The GDU considered in this text was designed to operate in TSA cycles of 18 hours duration (see Figure 3.3).

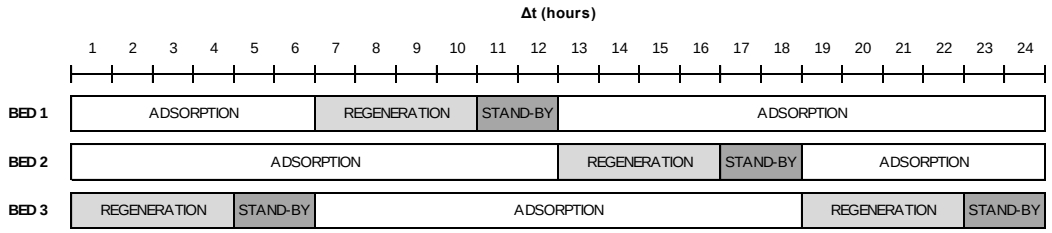

Figure 3.3: Different phases of TSA cycle for BED 1, BED 2 and BED 3.

During these 18 hours, a bed will be in adsorption mode for 12 hours, regeneration mode for 4 hours and stand-by mode for 2 hours. As stated before, the

switching of the on-off valves XV-01 through XV-12 is responsible for directing the gas feed and regeneration streams to the desiccant beds in adsorption mode and regeneration mode, respectively. Although applying a control strategy to modulate the duration of each TSA cycle stage would be beneficial, in the sense that it would allow to extend molecular sieve life, it is beyond the scope of this work. Valve switching for the studied GDU is established by using an on-off controller set by a global timer, i.e., valve state is driven by fixed time intervals determined during the unit design phase.

In order to guarantee a continuous batch process where no two beds are regenerating at the same time, the cycles of the three vessels have to be shifted by 6 hours. Suppose for example that at time $t = 0h$ BED 1 had already been in adsorption mode for 6 hours, BED 2 had just entered adsorption mode and BED 3 had just entered regeneration mode. This is the case presented in Figure 3.3. Six hours later, BED 1 would have been adsorbing for 12 hours and would enter regeneration mode. The on-off valves XV-01 and XV-03, responsible for routing the feed stream to BED 1 would be shut-off and valves XV-02 and XV-04, responsible for routing the regeneration gas to BED 1 would be turned on. At the same time, BED 3 would have been regenerating for 6 hours and would enter adsorption mode. Valves XV-10 and XV-12, responsible for routing the regeneration gas to BED 3 would be shut-off and XV-09 and XV-11, responsible for routing the feed gas to BED 3 would be turned on. No change would be observed for the states of BED 2 valves until six hours later, when BED 2 would enter regeneration mode, BED 1 would enter adsorption mode and BED 3 would remain in adsorption mode. Table 3.1 presents the state of each valve during different times of a TSA cycle previously described.

Figure 3.4 shows the temperature profile observed at the top of three packed beds of a real Gas Dehydration Unit for a full TSA cycle.

At time $t = 0h$, BED 2 is still regenerating while BED 1 and BED 3 are adsorbing. At about $t = 3.267hrs$, BED 3 starts regenerating, while BED 1 and BED 2 are adsorbing. The particular shape observed for the temperature profile is due to the heating sequence of the regeneration gas. At the time a bed enters regeneration mode, both the regeneration gas pre-heater and heater are bypassed. First, the by-pass valve for the pre-heater is closed and the equipment set-point is linearly increased from 55°C to about 120°C at a rate of approximately 1.5°C per minute. Once the 120°C set-point is reached by the pre-heater, the regeneration gas heater bypass valve is closed. The heater set-point is immediately changed to 120°C. Both set-points remain unchanged for about an hour in order to account for bed dynamics. This is enough time for the bed to asymptotically reach the set-point. The regeneration gas heater set-point is then, once again increased

Table 3.1: Valve state during Temperature Swing Adsorption cycle. Gray cells indicate that the bed is in regeneration/stand-by mode.

Bed	Valve	Time (hours) 0	6	12	18	24
BED 1	XV-01	ON	OFF	ON	ON	OFF
	XV-02	OFF	ON	OFF	OFF	ON
	XV-03	ON	OFF	ON	ON	OFF
	XV-04	OFF	ON	OFF	OFF	ON
BED 2	XV-05	ON	ON	OFF	ON	ON
	XV-06	OFF	OFF	ON	OFF	OFF
	XV-07	ON	ON	OFF	ON	ON
	XV-08	OFF	OFF	ON	OFF	OFF
BED 3	XV-09	OFF	ON	ON	OFF	ON
	XV-10	ON	OFF	OFF	ON	OFF
	XV-11	OFF	ON	ON	OFF	ON
	XV-12	ON	OFF	OFF	ON	OFF

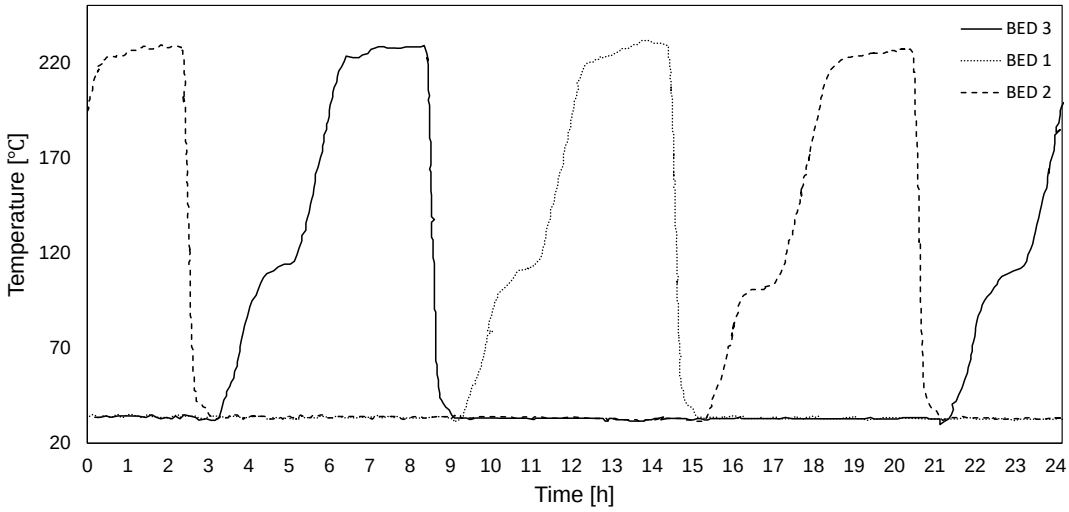

Figure 3.4: Temperature at the top of three packed beds of a real unit.

linearly at a rate of approximately 1.5°C per minute from 120°C to about 230°C, the molecular sieve regeneration temperature. The set-points remain unchanged for about two hours, so that the bed may have enough time to regenerate. After that, the set-points for both heaters are immediately reduced to zero and both heaters are bypassed. The temperature at the top of the bed is then reduced back to the starting temperature of of about 34°C. Due to bed dynamics, it takes about half an hour for the bed top temperature to reach the initial temperature. During this time and for another one and a half hours, the bed is in stand-by mode. The bed is then ready to be switched back to adsorption mode and a new TSA cycle begins.

Figure 3.5 shows the regeneration gas pre-heater and heater set-point temperatures during the regeneration phase of a TSA cycle. The observed temperature variation at the top of a molecular sieve adsorption vessel is also presented.

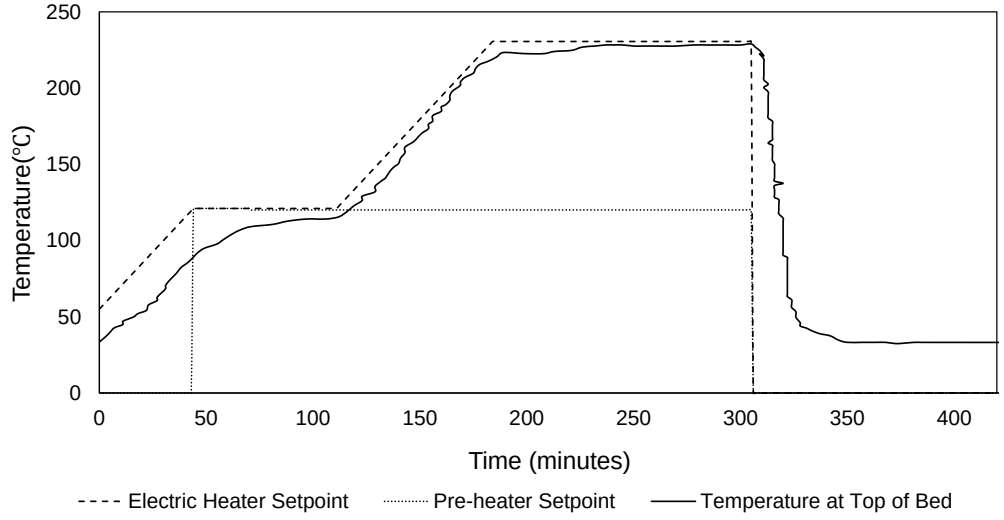

Figure 3.5: Regeneration gas pre-heater and heater set-points and actual temperature variation at top of bed.

3.1.4 Inlet Stream Composition, Characteristics and Expected Behaviour

As previously mentioned, the GDU receives a feed stream of about 3,289.3 kmol/h at 33°C and 74 bar resulting from the mixture of regeneration gas and main compressor outlet gas. Table 3.2 presents the expected composition of this mixture as determined from a laboratory test on a sample extracted from a pre-salt production unit. It can be observed that the gas feed stream is composed mainly of methane with significant amount of carbon dioxide, although CO_2 content is not as high as observed for other pre-salt reservoirs such as described

Table 3.2: Composition of the gas stream

Component	Molecular Formula	Molar Mass $[g/mol]$	Molar % Before Dehydration
Water	H_2O	18.02	0.0884
Nitrogen	N_2	28.01	0.5772
Carbon Dioxide	CO_2	44.01	24.9844
Methane	CH_4	16.04	55.1655
Ethane	C_2H_6	30.07	8.9069
Propane	C_3H_8	44.10	5.8208
i-butane	C_4H_{10}	58.12	0.9227
n-butane	C_4H_{10}	58.12	1.9503
i-pentane	C_5H_{12}	72.15	0.3877
n-pentane	C_5H_{12}	72.15	0.7996
Hexane	C_6H_{14}	86.17	0.2399
Heptane	C_7H_{16}	100.20	0.1164
Octane	C_8H_{18}	114.23	0.0306
Nonane	C_9H_{20}	128.25	0.0082
Decane	$C_{10}H_{22}$	142.28	0.0012
Undecane	$C_{11}H_{24}$	156.31	0.0002

by SANTOS (2016). Nitrogen, ethane, propane and other heavier unsaturated hydrocarbon compounds are also present, but in smaller amounts. The molar percentage of water is 0.0884, which means that the dehydration stage is necessary in order to reach the required 1 ppmv specification (0.0001 molar percentage). For this reason, it is said that the stream is composed of "wet" gas.

Figure 3.6 presents the phase envelope for the GDU feed stream composition of Table 3.2, calculated considering the Peng-Robinson equation of state (EOS). It can be observed that the operating point lies on the dew-point curve, i.e. the feed stream is composed of saturated vapor. This means that any minor expansion of its volume will lead to condensation. The slight pressure drop generated by the packed bed will cause the operating point to enter the phase envelope, so a condensed phase is expected. This is due to the high working pressures. From the phase envelope diagram, it can be observed that if the working pressure were lower, say for example below 46 bar, a pressure drop would not cause any condensation. Instead, the operating point would move further away from the phase envelope.

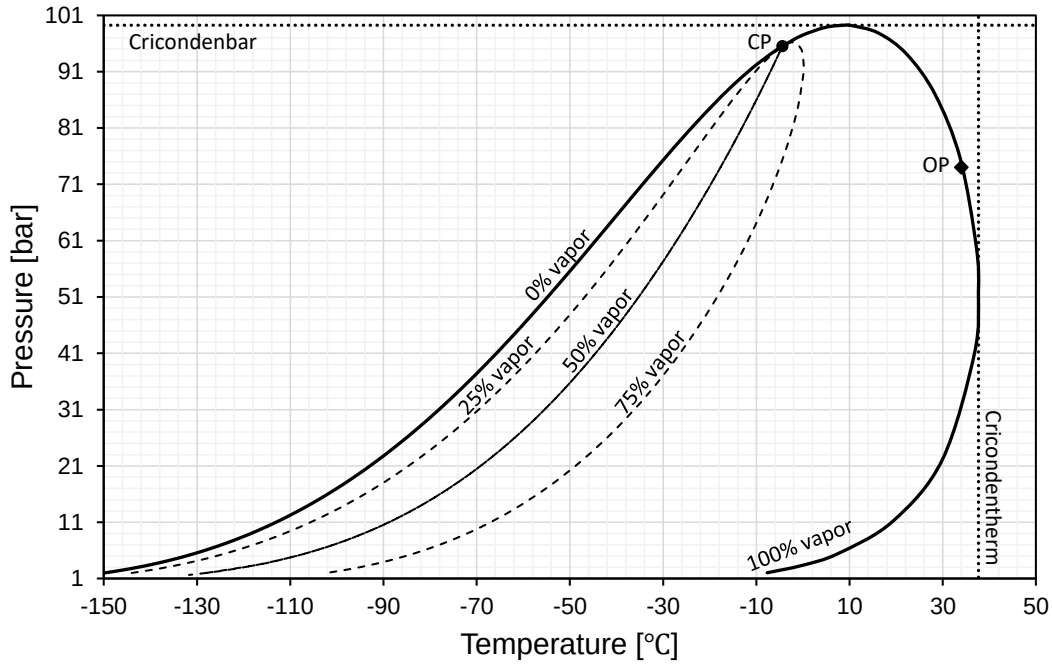

Figure 3.6: Phase envelope for stream composition, before dehydration, presented in Table 3.2. CP is the critical point at $T_c = -4.4$ °C and $P_c = 95.5$ bar. OP is the operating point at $T_{OP} = 34$ °C and $P_{OP} = 74$ bar. The cricondenbar is designated by maximum pressure $P_M = 99.2$ bar and the cricondentherm by maximum temperature $T_M = 37.7$ °C. Values obtained considering the Peng-Robinson equation of state.

3.2 Simulation Premises, Model Assumptions and Parameters

This section presents a packed bed abstraction, which will be used to represent the molecular sieve adsorber vessels most important physical characteristics. It also describes the methodology used for modeling the GDU including the method used for calculating thermodynamic states and properties of the gas stream, feed gas stream simplification method, packed bed abstraction, model assumptions and parameter calculation. The model equations serve as input to the commercial simulation software Aspen Adsorption (version 10) from Aspentech, which was used to solve the system of equations. The Aspen Properties software was also used along with the property method which will be described in this section.

3.2.1 Property Method

In order to model and analyze the fluid stream behavior, calculation procedures are needed to determine the thermodynamic properties (e.g. fugacity coefficient, enthalpy and volume) and transport properties (e.g. viscosity, thermal conductivity and diffusion coefficient). For the sake of consistency with the Aspen Properties simulation tool, this set of calculation procedures will be called a *property method*. The property method used to represent the behavior of the feed stream described in Table 3.2 is presented in this section.

Due to the high pressures involved, the gas streams involved in this simulation are not well represented by the ideal gas law. The phase envelope presented in Figure 3.6 was calculated considering the PENG-ROB property method, according to the Aspen Properties nomenclature. As can be observed, the phase behavior was analyzed for the petroleum mixture for a wide range of pressures, varying from very low (1 bar) to very high (100 bar). The PENG-ROB property method uses the Peng-Robinson EOS for all thermodynamic properties except liquid molar volume, which is calculated using the API method for liquid molar volume of pseudocomponents and the Rackett model for real components. This property method presents reasonable results at all temperatures and pressures and is consistent in the critical region. However, the results are least accurate in the region near the mixture critical point.

Peng-Robinson EOS

The Peng-Robinson EOS was developed in 1976 by Ding-Yu Peng and Donald Robinson at the University of Alberta and its standard equation was published in

PENG and ROBINSON (1976). The Peng-Robinson EOS presents the following characteristics: the parameters are expressed in terms of the critical properties and the acentric factor; the model provides reasonable accuracy near the critical point, particularly for calculations of the compressibility factor and liquid density; and the equation is applicable to the calculations of all fluid properties in natural gas processes.

The standard form of the Peng-Robinson EOS is given by Equation 3.1 where R is the universal gas constant, T is the temperature, V_m is the molar volume, T_c is the critical temperature of the mixture, P_c is the critical pressure of the mixture and α if the alpha function, which depends on the acentric factor ω. The binary parameters k_{ij} are usually determined from regression of phase equilibrium data such as VLE data, but the Aspen Properties software has a database with built-in values for a large number of component pairs, including for the components used in this work.

$$P = \frac{RT}{V_m - b} - \frac{a}{V_m^2 + 2 \cdot b \cdot V_m - b^2} \tag{3.1}$$

$$a = \sum_i \sum_j x_i \cdot x_j (a_i \cdot a_j)^{0.5} (1 - k_{ij}); \quad a_i \approx \alpha_i \cdot 0.45724 \frac{R^2 T_{c_i}^2}{P_{c_i}}$$

$$k_{ij} = k_{ij}^{(1)} + k_{ij}^{(2)} T + k_{ij}^{(3)} T^{-1}, \quad k_{ij} \neq k_{ji}$$

$$\alpha_i = \left[1 + \left(0.37464 + 1.54226\omega_i - 0.26992\omega_i^2 \right) \left(1 - \sqrt{\frac{T}{T_{ci}}} \right) \right]^2$$

$$b = \sum_i x_i b_i; \quad b_i \approx 0.07780 \frac{RT_{c_i}}{P_{c_i}}$$

Liquid Molar Volume Calculation

The model for calculating the liquid molar volume of a mixture uses the API procedure and the Rackett model. Ideal mixing is assumed:

$$V_m^l = x_p \cdot V_p^l + x_r \cdot V_r^l \tag{3.2}$$

where x_p is the mole fraction of pseudo-components and x_r is the mole fraction of real components.

For pseudo-components, the API procedure is used:

$$V_p^l = fcn(T, T_b, API) \tag{3.3}$$

where fcn is a correlation based on API procedure 6A3.5 (DANNER *et al.*, 1983).

At high density, the Ritter equation is used (adapted from RITTER *et al.* (1958)):

$$V_p^l = \frac{1}{62.3636}\left[SG^2 - \frac{\left(1.2655 \cdot SG - 0.5098 + 8.011 \times 10^{-5} T_b\right)(T - 519.67)}{T_b}\right]^{-1/2} \tag{3.4}$$

where SG is the specific gravity, T_b is the mean average boiling point in Rankine, T is the temperature of the system in Rankine, and the mass specific volume is produced in units of cubic feet per pound-mass.

The effect of pressure is automatically accounted for using procedure 6A3.10.

For real components, the Rackett mixture model is used.

$$V_r^l = \frac{R \cdot T_c \cdot Z^{R \cdot A\left[1+\left(1-\frac{T}{T_c}\right)^{2/7}\right]}}{P_c} \tag{3.5}$$

3.2.2 Feed Composition Simplifications

The feed composition presented in Table 3.2 has sixteen components. In order to reduce model complexity and increase simulation speed, a simplified composition was obtained. The simplified composition has a phase envelope similar to the original composition in both shape and cricondentherm value and is composed of only four species: H_2O, CO_2, CH_4 and C_5H_{12}. The mole fraction of each component in the simplified stream is presented on Table 3.3. The molar percentages of the original stream is also presented for comparison purpose.

First, the mole fractions of heavier components were summed and concentrated in the n-pentane fraction. Ethane, propane and nitrogen fractions were concentrated in the carbon dioxide fraction. Finally, the values obtained for the mole fractions of water, carbon dioxide, methane and n-pentane were visually adjusted in order to obtain a composition with phase envelope similar to the phase envelope of the original stream composition.

Figure 3.7 shows the phase envelopes for the original composition and for the

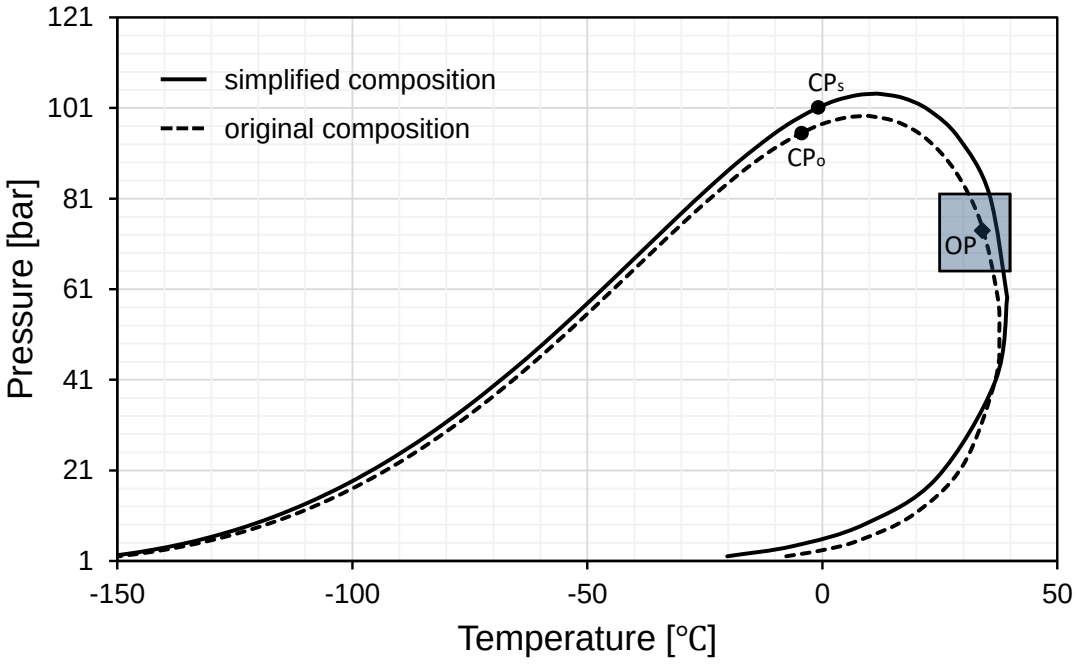

Figure 3.7: Phase envelopes for the original and simplified feed stream compositions (see Table 3.3). The critical point for the simplified composition CP_s is located at critical pressure P_c = 101.2 bar and at critical temperature T_c = -0.9°C. The cricondenbar is at maximum pressure P_M = 104.2 bar and the cricondentherm is at maximum temperature T_M = 39.3°C. The critical point for the original stream CP_o was already defined in Figure 3.6. OP is the operating point at T = 34 °C and P = 74 bar. The box overlapping both curves represents the area where the operating point may fall due to process disturbances, which may cause pressure and temperature variations during adsorption mode.

Table 3.3: Simplified composition of the gas feed stream

Component	Molecular Formula	Molar Mass $[g/mol]$	Molar % of Original Stream	Molar % of Simplified Stream
Water	H_2O	18.02	0.0884	0.08
Nitrogen	N_2	28.01	0.5772	
Carbon Dioxide	CO_2	44.01	24.9844	47.00
Methane	CH_4	16.04	55.1655	48.30
Ethane	C_2H_6	30.07	8.9069	
Propane	C_3H_8	44.10	5.8208	
i-butane	C_4H_{10}	58.12	0.9227	
n-butane	C_4H_{10}	58.12	1.9503	
i-pentane	C_5H_{12}	72.15	0.3877	
n-pentane	C_5H_{12}	72.15	0.7996	4.62
Hexane	C_6H_{14}	86.17	0.2399	
Heptane	C_7H_{16}	100.20	0.1164	
Octane	C_8H_{18}	114.23	0.0306	
Nonane	C_9H_{20}	128.25	0.0082	
Decane	$C_{10}H_{22}$	142.28	0.0012	
Undecane	$C_{11}H_{24}$	156.31	0.0002	

simplified composition. The figure also shows a rectangle delimiting the pressure (65 bar to 82 bar) and temperature (25°C to 40 °C) ranges which may occur due to process disturbances during adsorption mode. The operating point variation region during regeneration mode was not represented in the plot because regeneration temperature is high (230 °C). In this TSA cycle phase, the operating point lies far away from the phase envelope and there is no risk of condensation due to pressure drop in the packed bed.

3.2.3 Packed Bed Model Assumptions and Parameters

This section presents a packed bed abstraction, describes the model assumptions and simplifications for the packed bed and presents the calculations executed in order to obtain the necessary parameters. Each model assumption serves as input to the Aspen Adsorption software.

Adsorption Vessel Abstraction and Bed Parameters

Three molecular sieve adsorber vessels exist in the GDU described in Section 3.1. In order to simulate the unit, it is necessary to provide a mathematical model capable of representing the most important characteristics of the vessels. The abstraction presented in this section will be the basis for formulating the packed

bed model.

As was previously discussed, the real adsorber vessels are composed of multiple layers of ceramic balls and adsorber material. There is a thin layer of silica gel on top of the 4A molecular sieves. The layer of silica gel is very thin compared to the layer of 4A molecular sieves. For that reason, only the 4A molecular sieve adsorbent layer will be considered. The molecular sieves are also of mixed type, which means that there are beads and pellets mixed together. However, for the sake of simplicity and to reduce simulation complexity, it will be considered that only 4A molecular sieve beads are present. It will also be considered that the beads are evenly distributed along the bed, so that the bed if composed of a single, homogeneous adsorbent layer. Figure 3.8 presents the bed abstraction. For solving the packed bed models, it will be assumed that the layer of adsorbent material has a total height of 5.682 m and a bed diameter of 2.6 m.

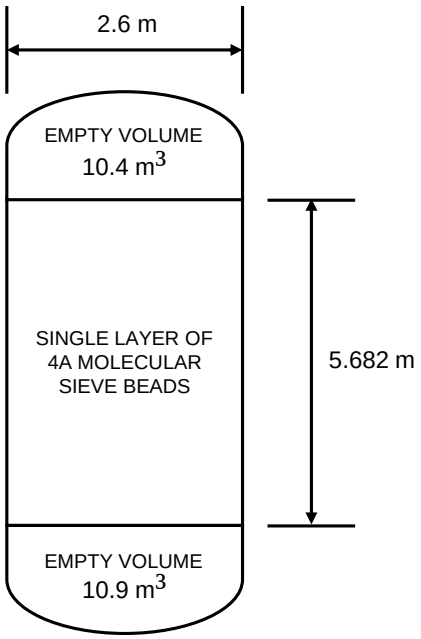

Figure 3.8: Molecular sieve adsorption vessel abstraction.

The molecular sieve material characteristics such as particle radius r_p, surface area a_p, shape factor (sphericity) ψ, intra-particle voidage ϵ_p, bulk solid density ρ_s and specific heat capacity C_{p_s} can be obtained from commercial 4A molecular sieves. For these parameters, the values presented in AHN *et al.* (2004) will be considered. The inter-particle voidage ϵ_i is an important parameter which influences pressure drop in packed beds. For an industrial sized adsorption vessel filled with spherical adsorbent particles, ϵ_i can be considered equal to 0.39 (BENYAHIA and O'NEILL, 2005). Table 3.4 summarizes the packed bed and adsorbent particle parameters.

Table 3.4: Packed bed and adsorbent material parameters

Parameter	Value	Units	Description	Reference
H_b	5.682	m	Height of adsorbent layer	N/A
D_b	2.6	m	Internal diameter of adsorbent layer	N/A
ϵ_i	0.39	m^3/m^3	Inter-particle voidage	BENYAHIA and O'NEILL (2005)
ϵ_p	0.34	m^3/m^3	Intra-particle voidage	AHN *et al.* (2004)
ρ_s	720	kg/m^3	Bulk solid density of adsorbent	AHN *et al.* (2004)
r_p	0.00166	m	Adsorbent particle radius	AHN *et al.* (2004)
ψ	1.00	N/A	Adsorbent shape factor (sphericity)	N/A
a_p	1807.23	$1/m$	Specific surface area of adsorbent ($3/r_p$)	N/A
C_{p_s}	0.00084	$MJ/kg/K$	Adsorbent specific heat capacity	AHN *et al.* (2004)

TSA Cycle Considerations and Parameters

The TSA cycle of the GDU was previously described in Section 3.1. This section will summarize the cycle parameters. For the simulations in this work, the stand-by mode will be incorporated into the regeneration phase. Instead of linearly increasing the set-point of the regeneration gas heater and pre-heater, a step wave form will be used. It will be considered that the bed is in adsorption mode for 12 hours and in regeneration mode for 6 hours. During adsorption, it will be assumed that the feed gas temperature is at 34°C and during regeneration, 230°C. The feed gas pressure will be considered constant and equal to 74 bar throughout the whole cycle. Table 3.5 summarizes the TSA cycle parameters.

Table 3.5: TSA cycle parameters

Phase	Duration	Value [hrs]	Temperature	Value [°C]
Adsorption	Δt_{ads}	12	T_{ads}	34
Regeneration	Δt_{reg}	6	T_{reg}	230

Packed Bed Model Considerations (Simplifying Hypothesis)

In this section, a simplified set of equations for the packed bed model is derived. The considerations for simplification for the mass, energy and momentum balance will be presented. The kinetic model and chosen equilibrium isotherm will be described. For each equation, the necessary parameters will also be presented.

In order to determine the concentration of each component along the packed bed, a mathematical model is needed. Considering a phenomenological approach, a *mass balance*, also called a *material balance* equation may be derived. It is obtained by applying the law of conservation of mass to the analysis of the physical system. Such an approach is straightforward and the complexity of the resulting equation may vary according to the effects that one desires to consider.

$$Input + Generation = Output + Accumulation + Consumption \tag{3.6}$$

Equation 3.6 shows the general equation for the material balance of any control volume.

The following assumptions were applied to the **mass balance**:

- It is assumed that there is no solid formation.
- It is assumed that no chemical reactions occur inside the adsorption vessels.
- It is assumed that there is no radial dependence of concentration and solid loading, in which case the concentration and loading values adopted represent cross-sectional average values (SHAFEEYAN, 2014).
- Aspen Adsorption **Mass Balance Assumption**: "Convection Only with Estimated Dispersion".
- The linear driving force (LDF) with constant mass transfer coefficient is assumed as the kinetic model.

The overall mass balance for a multi-component gas phase accounts for the convection of material and mass exchanged between the gas and the solid phases. Equation 3.7 shows the overall mass balance for the gas phase. In this equation, v_g is the gas phase superficial velocity in m/s, ρ_g is the as phase molar density in kmol/m^3, z is the bed coordinate where the properties are being considered, ρ_s is the adsorbent bulk density in kg/m^3 and ω_k is the bed loading with component k. This equation shows that the overall gas molar concentration will increase or decrease according to the rate with which the amount of each component k is desorbed or adsorbed in the considered packed bed volume of adsorbents, respectively. The first term of Equation 3.7 accounts for the convection of material and the second term for the mass exchange between gas and solid phase.

$$\frac{\partial \left(v_g \cdot \rho_g\right)}{\partial z} + \rho_s \cdot \sum_k \frac{\partial w_k}{\partial t} = 0 \tag{3.7}$$

A mass balance equation may also be derived for each component in the gas phase. It consists in an equation similar to Equation 3.7, but with extra terms for accumulation and axial dispersion.

In a real packed bed, the ideal plug flow condition may not be adequate, since axial mixing happens as a fluid flows through the vessel. This undesired effect reduces the efficiency of separation and efforts are made to minimize it during bed design. There are three main sources of axial dispersion in gases: from wall effects due to non-uniformity of packing, either at the wall (wall effects) or in the core section of the packing (channeling). This may be avoided by having a sufficiently large ratio of bed-to-particle diameters; from molecular diffusion effects and from turbulent mixing effects arising from the splitting and recombining of flows around the adsorbent particles. In general, the molecular diffusion and turbulent mixing effect are additive and proportional to the second order spatial concentration derivative, so they can be lumped together into a single effective dispersion coefficient, E_{zk}.

Equation 3.8 presents the mass balance equation for component k and its boundary conditions. The first term on the left accounts for the axial dispersion. No radial dispersion is considered (third simplifying hypothesis). The second term is the convective term. The third term accounts for accumulation inside the bed. The effects due to reactions and adsorption are grouped in J_k. Since no reaction are considered (second simplifying hypothesis), J_k is the mass transfer rate of component k to/from adsorbent per unit volume, given in kmol/m^3/s.

$$-\epsilon_i \cdot E_{zk} \cdot \frac{\partial^2 c_k}{\partial z^2} + \frac{\partial \left(v_g \cdot c_k\right)}{\partial z} + \epsilon_B \cdot \frac{\partial c_k}{\partial t} + J_k = 0 \tag{3.8}$$

$$[z = 0]: \quad -\epsilon_i \cdot E_{zk} \cdot \frac{\partial c_k}{\partial z} + (vg \cdot c_k)\,|_{z=0} = vg \cdot c_k$$

$$[z = L]: \quad \frac{\partial c_k}{\partial z} = 0$$

In this equation, ϵ_i is the inter-particle voidage, ϵ_B is the total bed voidage (sum of the inter and intra-particle voids, i.e., $\epsilon_i + \epsilon_P$) and c_k is the molar concentration of component k, given in kmol/m^3.

Since the LDF model was considered as the kinetic model, J_k is given by equation 3.9, where w_k is the instant solid loading for component k and w_k^* is the solid loading at equilibrium, which is given by the adsorption isotherm for component k in the adsorbent, and MTC is the mass transfer coefficient.

$$J_k = \frac{\partial w_k}{\partial t} = MTC_k \left(w_k^* - w_k\right) \tag{3.9}$$

The isotherm used in this thesis was a sub-type of the Langmuir isotherm in which the original Langmuir parameters are functions of temperature (see Equation 3.10). ADSIM refers to this as the Langmuir 3 isotherm.

Table 3.6 shows the Langmuir 3 isotherm parameter values which were adopted for the simulations. Since the C_5H_{12} molecules are too large to be adsorbed by the 4A zeolite molecular sieves, only the H_2O, CO_2 and CH_4 isotherms were needed. Parameters for H_2O and CO_2 were estimated by SANTOS (2016). Parameters for the CH_4 adsorption isotherm are presented in Annex C.

$$w_k^* = \frac{(IP_1 - IP_2 \cdot T) \cdot IP_3 \cdot e^{IP_4/T} \cdot P_k}{1 + IP_3 \cdot e^{IP_4/T} \cdot P_k} \tag{3.10}$$

The adsorbed solution theory adopted for predicting the mixture isotherm from the individual isotherms is the Ideal Adsorbed Solution (MYERS and PRAUSNITZ, 1965). According to the ADSIM User Manual (ADSIM, 2017), many systems have shown strong correlation between experimental data and predictions by IAS theory, including ternary mixtures on zeolites.

The axial dispersion coefficient E_{zk} of component k at coordinate z is esti-

Table 3.6: Langmuir 3 isotherm parameters for H_2O and CO_2 estimated by SANTOS (2016). Parameters for CH_4 estimated in Annex C.

Component	IP_1 (kmol/kg)	IP_2 (kmol/kg/K)	IP_3 (bar^{-1})	IP_4 (K)
H_2O	0.015358000	2.29060E-05	5.38030E-08	6314.671300
CO_2	0.004949088	6.29477E-06	0.001906942	3020.342254
CH_4	0.003152522	0	6.82223E-05	2381.605255

mated using the following correlation (KAST, 1988):

$$E_{zk} = 0.73 \cdot D_{mk} + \frac{v_g \cdot r_p}{\epsilon_i \left(1 + 9.49 \cdot \frac{\epsilon_i \cdot D_{mk}}{2 \cdot v_g \cdot r_p}\right)} \tag{3.11}$$

where D_{mk} is the molecular diffusivity of component k in the mixture, v_g is the gas velocity, ϵ_i is the interparticle voidage and r_p is the particle radius.

The molecular diffusivity D_{mk} of component k in a mixture of n components is estimated according to equation Equation 3.12 (BRAUN, 2018), in which Y_k is the mole fraction of component k in the mixture, Y_j is the mole fraction of component j in the mixture and D_{kj} is the binary molecular diffusivity of component k in component j.

$$\frac{D_{mk}}{1 - Y_k} = \left(\sum_{\substack{j=1 \\ j \neq k}}^{n} \frac{Y_j}{D_{kj}} \right)^{-1} \tag{3.12}$$

The molecular diffusivities D_{kj}, in c^2m/s, for binary gas systems composed of species k and j at pressure P and temperature T are obtained using Equation 3.13.

$$D_{kj} = \frac{10^{-3} \cdot T[K]^{1.75} \cdot \left(\frac{1}{M_k} + \frac{1}{M_j}\right)^{0.5}}{P[atm] \left[\left(\sum V_k\right)^{1/3} + \left(\sum V_j\right)^{1/3} \right]^2} \tag{3.13}$$

in which M_k is the molar mass of component k, M_j is the molar mass of component j and $\sum V_k$ and $\sum V_j$ are the total diffusive volumes of components k and j, respectively, according to FULLER *et al.* (1966). The Special Atomic Diffusion Volumes were corrected in FULLER *et al.* (1969) and the final diffusive volumes

for the feed gas components are presented in Table 3.7.

Table 3.7: Diffusion Volumes obtained from FULLER *et al.* (1969).

Species	Diffusion Volume
CH_4	25.14
CO_2	26.7
H_2O	13.1
C_5H_{12}	107.22

Using Equation 3.13 and the diffusion volume values presented at Table 3.7, the binary molecular diffusivity coefficient was calculated for each pair of feed stream gas components. Since the TSA cycle takes place at two different temperatures: 34°C during the adsorption phase and 230°C during the regeneration phase, each D_{kj} was calculated for these two values. The pressure was considered constant and equal to 74 bar. Table 3.8 presents the results.

Table 3.8: Binary Molecular Diffusivity Coefficient in $10^{-4} \cdot cm^2/s$, at $P = 74bar$.

Species	D_{kj}	Adsorption $34°C$	Regeneration $230°C$
CH_4	D_{12}	25.69397	60.94504
	D_{13}	37.89919	89.89532
	D_{14}	14.44094	34.25331
CO_2	D_{21}	25.69397	60.94504
	D_{23}	30.19582	71.62326
	D_{24}	9.85259	23.36995
H_2O	D_{31}	37.89919	89.89532
	D_{32}	30.19582	71.62326
	D_{34}	16.08524	38.15351
C_5H_{12}	D_{41}	14.44094	34.25331
	D_{42}	9.85259	23.36995
	D_{43}	16.08523	38.15351

Equation 3.12 and the values obtained at Table 3.8 were used to calculate the molecular diffusivity coefficient of each species in mixture. The values were once again calculated for the two operation temperatures of the TSA cycle. The results are presented on Table 3.9.

In order to avoid having to create a task for the D_{mk} value to change during the TSA cycles, a weighted average was used to estimate a single value, $\widehat{D}_{mk}$, to be used for the whole simulation. Equation 3.14 shows that the TSA cycle

Table 3.9: Molecular Diffusivity Coefficient of species k in mixture. Units are given in $10^{-7} \cdot m^2/s$, at $P = 74bar$.

Species	D_{mk}	Adsorption $T_{ads} = 34°C$	Regeneration $T_{reg} = 230°C$	$\widehat{D}_{mk}$
CH_4	D_{m1}	2.40139	5.69599	3.49959
CO_2	D_{m2}	2.25250	5.34285	3.28262
H_2O	D_{m3}	3.20337	7.59826	4.66833
C_5H_{12}	D_{m4}	1.17424	2.78524	1.71124

times Δt_{ads} and Δt_{reg} were used as weights for multiplying the molecular diffusivity coefficient at each cycle temperature. These results are also presented on Table 3.9.

$$\widehat{D}_{mk} = \frac{\Delta t_{ads} \cdot D_{mk}(T_{ads}) + \Delta t_{reg} \cdot D_{mk}(T_{reg})}{\Delta t_{ads} + \Delta t_{reg}} \tag{3.14}$$

The mass transfer coefficient for species k, MTC_k is given by Equation 3.15, which provides a correlation with the Sherwood number, Sh (WAKAO and FUNAZKRI, 1978).

$$Sh = \frac{2 \cdot MTC_k \cdot r_p}{D_{mk}} = 2 + 1.1 \cdot Sc^{1/3} \cdot Re^{0.6} \tag{3.15}$$

In Equation 3.15, Sc is the Schmidt number, given by Equation 3.16 and Re is the Reynolds number, given by Equation 3.17.

$$Sc = \frac{\mu}{\rho_g \cdot D_{mk}} \tag{3.16}$$

$$Re = \frac{\rho_g \cdot v_g \cdot r_p}{\mu} \tag{3.17}$$

Table 3.10 presents the Mass transfer coefficients (MTC) between fluid components and 4A zeolite, calculated using Equation 3.15. The mass transfer coefficient for each component also varies with temperature, so the same procedure adopted for calculating $\widehat{D_{mk}}$ was used for calculating $\widehat{MTC}_k$ (see Equation 3.18).

The results are also presented on Table 3.10.

$$\widehat{MTC}_k = \frac{\Delta t_{ads} \cdot MTC_k(T_{ads}) + \Delta t_{reg} \cdot MTC_k(T_{reg})}{\Delta t_{ads} + \Delta t_{reg}} \tag{3.18}$$

Table 3.10: Mass transfer coefficients (MTC) between fluid components and 4A zeolite. Units are given in $10^{-3} \cdot s^{-1}$, at $P = 74bar$.

Species	MTC_k	Adsorption $T_{ads} = 34°C$	Regeneration $T_{reg} = 230°C$	$\widehat{MTC}_k$
CH_4	MTC_1	4.43528	17.60296	8.82451
CO_2	MTC_2	4.24709	16.86072	8.45163
H_2O	MTC_3	5.39234	21.37315	10.71927
C_5H_{12}	MTC_4	2.73381	0.25632	1.90798

As fluid moves along a packed bed, there is a slight pressure drop due to viscosity and to reduction of kinetic pressure. The form with which the pressure varies along the bed may be obtained by means of a *momentum balance*. The momentum balance specifies how the adsorption bed layer model will treat gas velocity and pressure. Since packed beds are usually designed as to minimize pressure drop, assuming constant pressure or a fixed, small pressure drop along the bed would be a reasonable approximation. Nonetheless, this section presents a correlation typically used to model pressure variation and gas velocity on packed beds.
The following assumptions were applied to the **momentum balance**:

- Pressure drop and gas velocity changes across the packed bed are considered.
- Both the viscous and kinetic pressure drop effects are considered.
- The Ergun Equation is used to model axial pressure drop and velocity changes.
- Aspen Adsorption **Momentum Balance Assumption**: "Ergun Equation".

Equation 3.19 combines both the Carman–Kozeny and the Burke–Plummer (BURKE and PLUMMER, 1928) equations. It is therefore valid for laminar and turbulent flows. For this reason, it is most frequently used. This equation is called Ergun Equation or Ergun Correlation (ERGUN, 1952). The second term

on the right hand side corresponds to the pressure drop due to viscosity and the first term, to the loss of kinetic pressure.

$$-\frac{\partial P}{\partial z} = \frac{1.5 \cdot 10^{-3} \cdot \mu \cdot (1-\epsilon_i)^2}{\left(2 \cdot r_p \cdot \psi\right)^2 \cdot \epsilon_i^3} \cdot v_g + \frac{1.75 \cdot 10^{-5} \cdot M \cdot \rho_g \cdot (1-\epsilon_i)}{2 \cdot r_p \cdot \psi \cdot \epsilon_i^3} \cdot v_g^2 \quad (3.19)$$

$$[Z = L]: \quad P|_{z=L} = P|_{z=L^+}$$

In order to calculate the temperature of the gas along the packed bed, an *energy balance* is needed.
The following assumptions were applied to the **energy balance**:

- The system is non-isothermal, i.e., the temperature varies along the bed during each phase of the TSA cycle.
- Only gas conduction was considered.
- The heat of adsorption, ΔH_k, the gas thermal conductivity, K_g, and the solid phase heat capacity, C_{P_s} were assumed to be constant.
- Due to thermal insulation, the heat loss through the wall and heat accumulation in the wall are considered negligible in comparison to the amount of heat caused by the heat of adsorption. This results in operation close to adiabatic behavior.
- Heat transfer is assumed to occur between the two phases according to a film resistance model. The heat transfer coefficient, HTC, is estimated using Equation 3.20, presented on the ADSIM User Manual (ADSIM, 2017).

In order to estimate the heat transfer coefficient, HTC, for the film resistance model, which will be used to calculate the rate of heat transferred per m^3 of the packed bed, Equation 3.20 was used. In this equation, j is the j-factor, equal to $1.66 \cdot Re^{-0.51}$ if $Re < 190$, or equal to $0.983 \cdot Re^{-0.41}$ otherwise (ADSIM, 2017). P_r is the Prandtl Number, which can be calculated by Equation 3.21 (SHEIKHOLESLAMI and GANJI, 2017).

$$HTC = j \cdot C_{P_g} \cdot v_g \cdot \rho_g \cdot Pr^{-2/3} \quad (3.20)$$

$$Pr = \frac{\mu \cdot C_{P_g}}{K_g \cdot M} \quad (3.21)$$

The gas phase energy balance and its boundary conditions are presented on Equation 3.22. The first term on the left is the thermal conduction term. It is responsible for modeling the axial thermal dispersion. ϵ_i is the inter-particle voidage and K_g is the gas phase thermal conductivity, which was estimated using Aspen Properties (version 10) for the feed stream composition and pressure equal to 74 bar. The following values were calculated for K_g at each of the TSA cycle phase temperatures: $K_g(34°C)$ = 2.46575×10^{-8} MJ/m/K and $K_g(230°C)$ = 4.75694×10^{-8} MJ/m/K. Since this value was considered constant in the simulation, a weighted average was done using Equation 3.23 and $\widehat{K}_g$ = 3.22948×10^{-8} MJ/m/K was obtained.

$$-K_g \cdot \epsilon_i \cdot \frac{\partial^2 T_g}{\partial z^2} + C_{vg} \cdot v_g \cdot \rho_g \cdot \frac{\partial T_g}{\partial z} + \epsilon_B \cdot C_{vg} \cdot \rho_g \cdot \frac{\partial T_g}{\partial t} + P \cdot \frac{\partial v_g}{\partial z} + \\ + HTC \cdot a_p \cdot \left(T_g - T_s\right) = 0 \tag{3.22}$$

$$[z = 0]: \quad K_g \cdot \epsilon_i \cdot \frac{\partial T_g}{\partial z}|_{z=0} = \left(\rho_g \cdot_{vg} \cdot v_g \cdot T_g\right)|_{z=0^+} - \left(\rho_g \cdot_{vg} \cdot v_g \cdot T_g\right)|_{z=0^-}$$

$$[z = L]: \quad \frac{\partial T_g}{\partial z}|_{z=L} = 0$$

$$\widehat{K}_g = \frac{\Delta t_{ads} \cdot K_g(T_{ads}) + \Delta t_{reg} \cdot K_g(T_{reg})}{\Delta t_{ads} + \Delta t_{reg}} \tag{3.23}$$

The second term of Equation 3.22 is the convective term, in which C_{vg} is the specific gas phase heat capacity at constant volume. The third term models thermal accumulation and the fourth term includes the effect of compression. The last term is the heat transfer from gas to solid, given by the film resistance model (fifth simplifying hypothesis), in which a_p is the specific particle surface per unit volume of packed bed.

The solid phase energy balance is given by Equation 3.24. The first term on the left is the accumulation of heat on the solid phase, in which ρ_s is the adsorbent bulk density and C_{P_s} is the specific heat capacity of the adsorbent. The second term is the rate of heat generation by adsorption of each component k per unit mass of solid. It depends on the local rate of mass transfer, i.e., the change in the amount of material adsorbed. The constant for heat of adsorption, ΔH_k, is given in Table 3.11. Since pentane is not an adsorbed species, its heat of adsorption is not considered.

$$\rho_s \cdot C_{ps} \cdot \frac{\partial T_s}{\partial t} + \rho_s \cdot \sum_{i=1}^{n} \left(\Delta H_k \cdot \frac{\partial w_k}{\partial t} \right) - HTC \cdot a_p \cdot \left(T_g - T_s \right) = 0 \tag{3.24}$$

Table 3.11: Constant for heat of adsorption ΔH_k in $MJ/kmol$ as presented by WYNNYK (2019)

Parameter	Value
ΔH_{CH_4}	-18.3
ΔH_{CO_2}	-36.2
ΔH_{H_2O}	-50.2
$\Delta H_{C_5H_{12}}$	N/A

The last term in Equation 3.24 corresponds to the gas-solid heat transfer from the fluid phase to the solid phase. It is expressed in terms of the film resistance, where the heat transfer area is proportional to the area of the adsorbent particles.

3.3 Numerical Method

The model equations presented on the previous section make up a system of Partial Differential Equations with time and spacial derivatives (along the z axis). This system can be solved by the Method of Lines (MOL), which consists in first, discretizing the equations with respect to the spatial coordinates, resulting in a system of nonlinear differential-algebraic equations of index 1. The equations can then be solved as an Initial Value Problem.

Figure 3.9 shows, on the left, a simplified diagram of vertically oriented adsorption vessel. Considering that the vessel is composed of a one-layered homogeneus packed bed, the properties on the interior of the vessel are considered to be the same and radially uniform. Thus, the average values of the properties are considered and analyzed for each coordinate along the z axis.

On the right side of Figure 3.9, the discretization scheme for the vessel in uniform volumes is presented. The problem is presented in cylindrical coordinates considering only variations along the z axis.

Among the many methods for the spacial discretization, the first order accurate Upwind differentiating Scheme (UDS) was chosen for its unconditional stability and least simulation time (PAUL, 2003). Equations 3.25 and 3.26 show the first and second order derivative approximations, respectively. The number

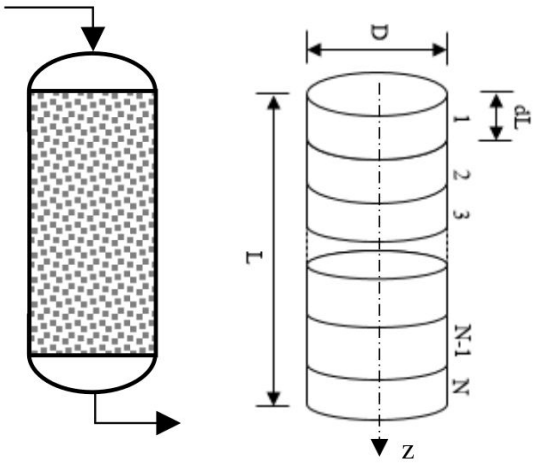

Figure 3.9: On the left, a simplified representation of the packed bed. On the right, the adopted discretization scheme.

of discretization nodes to be used will be analyzed during simulation 1.

$$\frac{\partial \Gamma_i}{\partial z} \approx \frac{\Gamma_i - \Gamma_{i-1}}{\Delta z} \tag{3.25}$$

$$\frac{\partial^2 \Gamma_i}{\partial z^2} \approx \frac{\Gamma_{i+1} - 2\Gamma_i + \Gamma_{i-1}}{\Delta z^2} \tag{3.26}$$

In order to obtain the equations on the first an last volumes, the boundary conditions are needed. For the material balance on the fluid phase, the boundary conditions adopted were the Danckwerts conditions.

3.3.1 Solver Options

A ASDIM's non-linear solver was used in standard mode with a Mixed Newton method and residual convergence criterion. The maximum number of divergent steps was 20. The maximum step reductions was 20. The maximum number of iterations was 500. The "Return to Best Point on Failure" option was selected. Absolute and relative variable tolerances were each set to 1×10^{-5}. The absolute equation tolerance was also set to 1×10^{-5}. So were the numerical derivative absolute and relative perturbation tolerances.

3.4 Proposed Simulations

In order to test the control strategy proposed in this chapter, the derived process models will be used in a dynamic simulation of the Gas Dehydration Unit. The commercial process simulation suit Aspen Plus (version 10.0) by Aspentech shall be used. This software suit includes Aspen Adsorption^{TM}, Aspen Dynamics and Aspen Properties.

The simulations shall be executed progressively, starting with a simple one vessel simulation and building up in complexity to the full unit. A brief description of each simulation is presented below along with the initial conditions of each.

- SIMULATION 1: First, a single vessel in the adsorption phase of the TSA cycle will be simulated. This is necessary first, to obtain the temperature profile along the bed during adsorption, since this variable is critical for the control strategy. It is also needed in order to observe the variation of loading of the adsorbent with time. This will be crucial for verifying if the duration of the cycle is adequate. This first simulation is also useful to check if the behavior provided by the model is according to the expected and to evaluate the number of nodes to be used for the discretization method. Since the composition of the dehydrated gas is not initially known, it is assumed that the vessel is filled completely with methane. The adsorbent particles are considered to be initially unloaded. The temperature of the bed is considered to be equal to the feed stream temperature.

- SIMULATION 2: The second simulation consists of a vessel in the desorption phase. The purpose of this is mainly for verification of the desorption dynamics. This will also be used in order to determine the cycle duration. The initial conditions of the packed bed for simulation 2 are the variables of simulation 1 at t = 12 hours (the end of a full adsorption cycle). Simulation 1 is executed in Aspen Adsorption until t = 12 hours. Then, the flow sheet is modified so that the regeneration gas flows from the bottom of the vessel to the top. The composition of the regeneration gas is set as equal to the product of simulation 1.

- SIMULATION 3: The third simulation consists of a two-vessel simulation. It is an intermediate step between building the single-vessel flow sheet and the three-vessel flow sheet in the Aspen Adsorption software. In order to guarantee suitable initial conditions to the simulation, every ADSIM flow sheet has to start simple. The initial values have to be adjusted so that the

simulation converges for each step. If this is true, other components can be gradually added to the flow sheet increasing its complexity gradually.

- SIMULATION 4: The fourth simulation consists in the complete Gas Dehydration Unit with the typical control loops and TSA cycle. This will be used to verify how the gas operating point moves on the phase envelope plot, compare with the results obtained from a real unit and verify the performance of the typical control loops. This simulation consists of simulation 3 with an additional packed bed from simulation 2. The initial condition for the packed bed in regeneration is the condition at the end of 6 hours of simulation 2.

- SIMULATION 5: Finally, the fifth simulation consists in the complete GDU with all control loops, including the feed temperature control loop to reduce retrograde condensation. Instead of building on to simulation 4, simulation 5 was based on a previous simulation 3 and simulation 2 runs. The initial conditions are the conditions at the end of a 12 hours simulation for the two beds in adsorption (simulation 3) and a six hour simulation for the bed in regeneration (simulation 2).

3.5 Control Design

3.5.1 Typical Control Loops

In order to guarantee adequate regeneration gas flow rate and temperature in case of feed stream disturbances, two control loops are employed: FFIC-1 and TIC-1. The first control loop consists of two orifice plates, one compressor or blower (UC-01) and a programmable logic controller (PLC) or distributed control system (DCS). The *manipulated variable* is the compressor inlet volumetric flow rate, in m^3/s. The *process variable* is the total flow rate (in kmol/s) from the two beds in adsorption phase. In a real industrial unit, gas flow rate is usually measured using an *orifice plate*. A transmitter sends this value to the PI controller. Since the desired regeneration flow rate is 11% of the total flow rate, an orifice plate is placed at the regeneration stream pipeline. The instantaneous regeneration flow rate (in kmol/s) is then divided by 0.11 and this is the control loop *flow set-point*. According to DE CAMPOS and TEIXEIRA (2010), this particular control strategy is known as *ratio control*. The user input to FFIC-1 is the *ratio set-point*, which, in this case, is 0.11.

The second control loop (TIC-1) consists of the electric heat exchanger (P-03), a temperature sensor and transmitter (TIT-7), and a PLC or DCS controller. The

temperature transmitter, placed after the electric heater, sends the temperature of the regeneration stream to the controller. This is the control loop process variable. The set-point is the desired regeneration temperature (230°C). The manipulated variable, which is the output of the controller is the heat exchanger duty Q, in MW.

3.5.2 Control for Reducing Condensation

The control strategy designed to reduce the occurrence of condensation in the Gas Dehydration Unit and the control loop elements are described in this section. It consists of a simple solution to which Classical Control methods apply. Figure 3.10 shows the Piping and Instrumentation Diagram (P&ID) of the Gas Dehydration Unit.

Loop Elements

As can be observed in Figure 3.10, asides from the typical control loops, the control strategy for reducing condensation is represented. For the physical implementation of the control loop, the following instruments and equipment are necessary:

- P-01: one heat exchanger;
- TIC-2: one PLC or DCS controller;
- TIT-1, TIT-2, TIT-3, TIT-4, TIT-5 and TIT-6: six temperature sensors (two for each adsorption vessel) with their respective temperature transmitters;
- AIT-1: one dew-point analyzer.

The pressure transmitter (PIT-1) represented in Figure 3.10 may be considered as part of the dew-point analyzer, since the pressure is necessary in order to estimate the theoretical value of the dew-point temperature, T_{DEW}.

The temperature sensors usually consist of a thermowell (TW) with a thermocouple or a thermoresistor (TE) which are generally not represented in P&IDs for simplicity of the drawing. Two temperature sensors will be installed at each molecular sieve adsorption vessel: one at the top of the packed bed and one at the bottom. TIT-1 and TIT-2 are installed in BED 1. TIT-3 and TIT-4 are installed in BED 2. TIT-5 and TIT-6 are installed in BED 3.

A Gas Dehydration Unit is usually supplied as a package unit which includes the vessels (BED 1, BED 2 and BED 3), the on-off valves (XV-01 to XV-12), filters

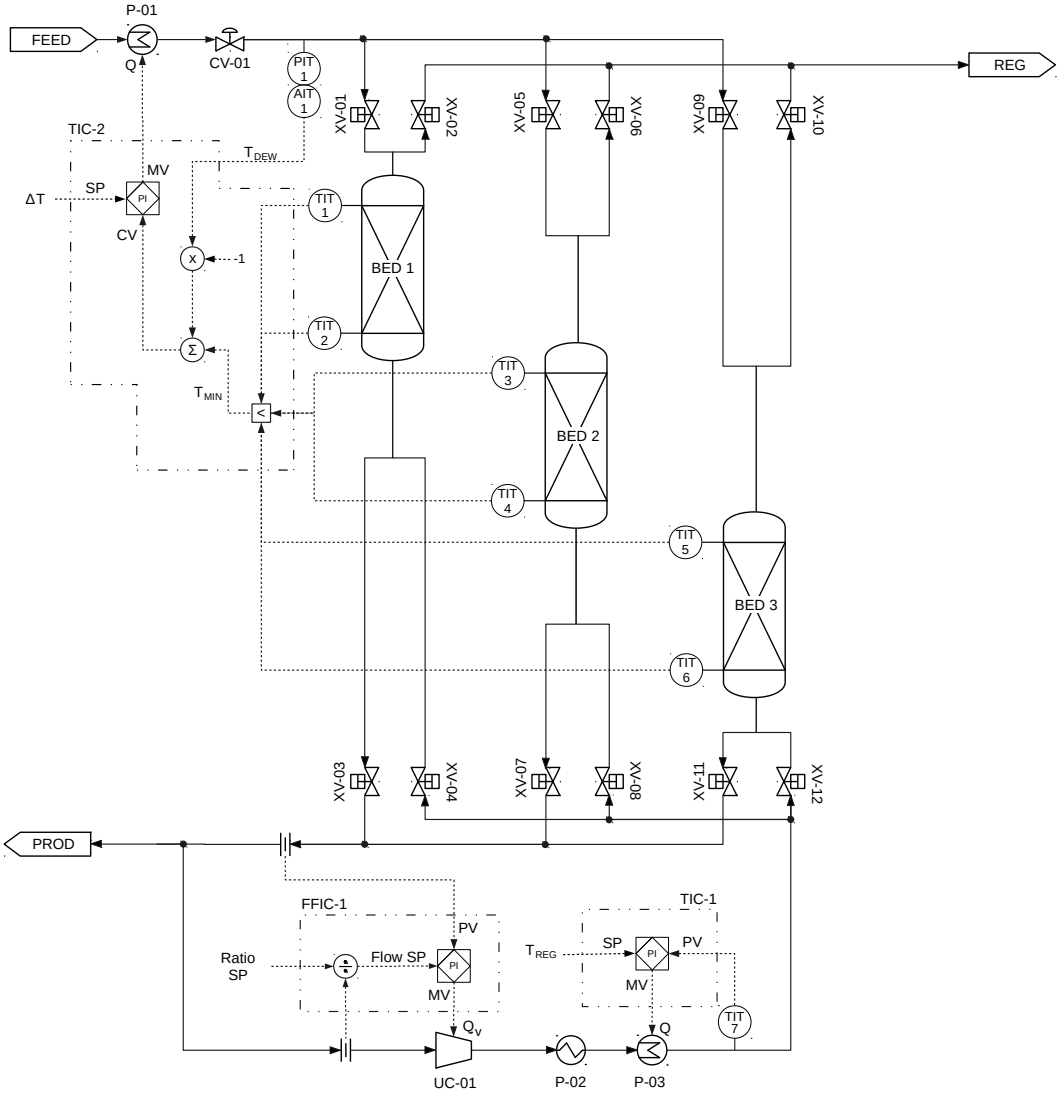

Figure 3.10: Gas Dehydration Unit with Control Loops.

(not represented), temperature transmitters (at the top, center and bottom of the beds) and moisture analyzers (not represented).

It is not common for GDU packages to be supplied with dew-point analyzers. This instrument would have to be acquired separately. The dew-point analyzer provides as its output a $4 - 20mA$ signal representative of the dew-point temperature T_{DEW} of the sample. This output will serve as input to the TIC-2 and shall be employed in the control strategy.

Control Strategy

The control strategy consists of a temperature control loop which will actuate on the heat capacity Q, in MW, of heat exchanger P-01. This heat capacity is the *manipulated variable* (MV).

The controller is represented by TIC-2 and consists of a classical PI controller with additional arithmetic function blocks to manipulate the input signals in order to obtain the *controlled variable* (CV). Function blocks for the execution of subtraction and a comparative block are needed. Equation 3.27 shows the mathematical expression of CV.

$$CV = min(T_1, T_2, T_3, T_4, T_5, T_6) - T_{DEW} \tag{3.27}$$

The main idea of this control strategy is to keep the lowest temperature of the unit at a fixed distance ΔT from the dew-point temperature. This way, a drop of pressure would also cause an increase in temperature and the operation point would not enter the phase envelope, thus preventing condensation from occurring. Figure 3.11 illustrates the idea of the proposed strategy.

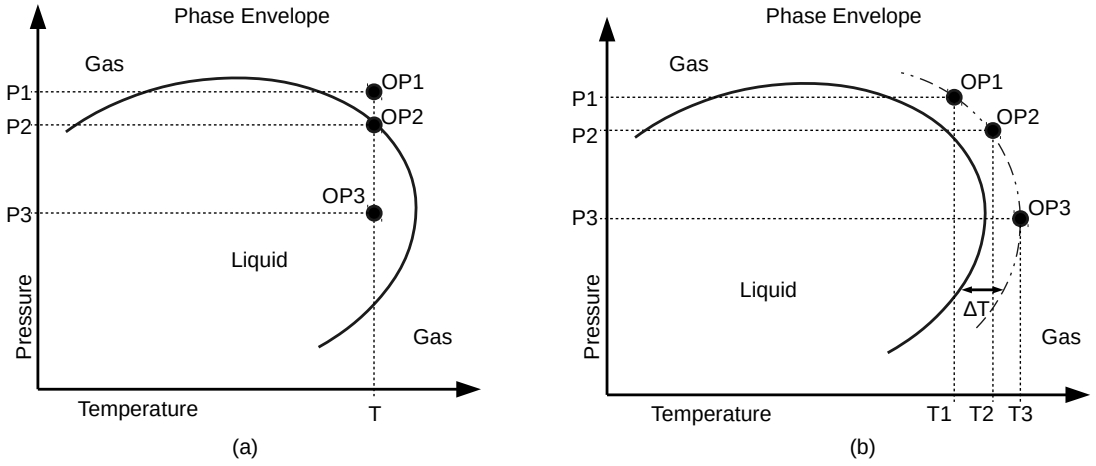

Figure 3.11: Phase diagrams with operating points: (a) without the proposed control strategy, (b) with the proposed control strategy.

Suppose that the the GDU is operating, without the control strategy presented in this section, at an operating point of OP1 with pressure P1 and temperature T. This is the case presented in Figure 3.11.(a). As the gas enters the bed, there is a slight pressure drop. This pressure drop moves the operating point to OP2, with pressure P2 and temperature approximately T (there would also be a slight temperature decrease). Depending on the pressure drop along the bed, the operating point may enter the phase envelope, such as is the case with OP3. In this case, condensation would occur.

Figure 3.11.(b) illustrates the case of the same GDU with the control strategy implemented. Starting at OP1, once the gas entered the bed and the pressure drop occurred, T_{DEW} would increase, causing the difference between the actual lowest temperature and the dew-point temperature to become smaller than the set-point ΔT of the controller. This would cause an increase in Q, the manipulated variable (MV), which would heat up the feed gas and the temperature at the new operating point would increase to $T_2 = T_{DEW} + \Delta T$. This would also happen if the pressure dropped further, moving the operating point to OP3.

This fixed distance in temperature ΔT between the lowest temperature T_L and the dew-point temperature of the gas is the *set-point* of the PID controller. It is a constant, user-defined value and shall not be smaller than the accuracy of the dew temperature analyzer (typically $0.5°C$).

It is important to observe that Figure 3.11 is an exaggerated representation of the process and was only elaborated as such with the intention of better explaining the idea of the control strategy.

The Point of Lowest Temperature

In order for the proposed control strategy to effectively reduce condensation damage to the molecular sieves, it is essential to place the temperature instruments at the point of lowest temperature along the bed. As will be shown in the following sections, this point oscillates between the top and the bottom of the bed.

Even though temperature may initially increase in the bed due to the adsorption process being exothermic, this will generate a peak of temperature in the beginning, which will be dispersed at the end of the bed (the next chapter properly clarifies this effect).

It is important to observe that, as can be seen in Equation 3.27, no distinction is made among the beds as to which are in the adsorption phase and which is in the regeneration phase. This is because in the regeneration phase, the temperature along the bed rises since the regeneration temperature is 230°C.

Since the controller considers the minimum among the temperatures, during the comparison the temperatures measured on the bed that is in the regeneration phase are the highest, and are, therefore, discarded by the controller.

3.5.3 Additional Considerations

For the proposed control strategy, it is assumed that there is little variation in the mole concentration of the stream components, so that the phase envelope of the gas would remain approximately constant throughout the unit. However, this is not what happens in reality. A more realistic approach would be to include a dew-point analyzer at the top and bottom of each bed and choose the smallest $T - T_{DEW}$ as the controlled variable. However, dew-point analyzers are expensive and including two analyzers for each bed would increase both capital expenditure (CAPEX) and operational expenditure (OPEX). An even more ideal approach would be to use the analyzers and a bed model to estimate the phase envelope and temperature curve for each axial direction along the bed. The estimated minimum difference ($\widehat{T}_{MIN} - \widehat{T}_{DEW}$) would serve as the CV. For this last approach, more computer processing power would be needed and the algorithm would take longer to process.

In cases where it is not possible to include an analyzer, an adapted, but less efficient version of this control strategy consists in programming a simplified phase envelope (see Appendix B) into the TIC-2 controller and using it to obtain the dew-point temperature. This is useful when the phase envelope varies more for the range of temperature and pressure. In this case, it is necessary to run a laboratory analysis to find at least some points of the feed stream phase envelope. The controller would also have to be reprogrammed in case the feed stream composition changed.

Chapter 4

Results and Discussion

This chapter details how simulations 1, 2, 3, 4 and 5, mentioned in Chapter 3 were executed. The plots for temperature, pressure, velocity, mole fractions and concentration profiles along BED 1, BED 2 and BED 3 are explained. For simulations 4 and 5, a discussion of the control loop responses, phase behavior, and product specification are also presented and analyzed. For each simulation, the packed bed and balance equation parameters presented and calculated in Chapter 3 were used.

4.1 Simulation 1: Single Vessel Adsorption

The first simulation consists of a single vessel in the adsorption phase. Figure 4.1 shows the schematic used for the simulation. As recommended by Aspen Adsorption User Manual (ADSIM, 2017) fixed values of pressure were defined for the feed and product, and a control valve was used to ensure the adequate flow rate. The operating conditions for this simulation are presented in Table 4.1. It was considered that the packed bed was initially filled only with CH_4 and initial temperature was considered to be 34.0°C.

4.1.1 Temperature and Number of Nodes

Since adsorption is an exothermic process, energy is transferred to the gas inside the adsorption vessels as dehydration occurs. For this reason, a considerable temperature increase is expected as gas travels through the bed and this can be observed in simulation 1. Figures 4.2 and 4.3 show the temperature variation at different axial bed coordinates with time. L is the dimensionless length. The

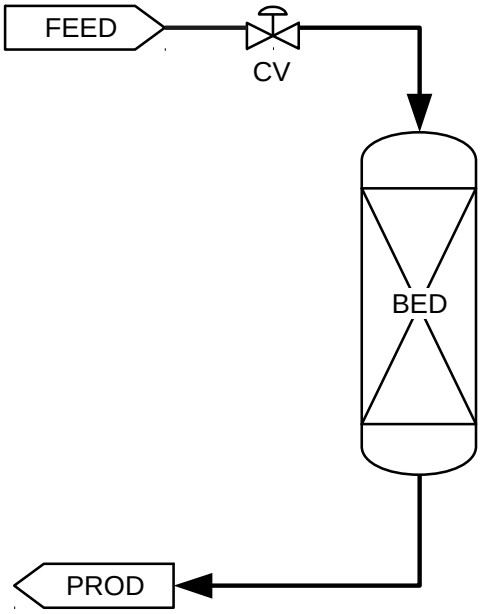

Figure 4.1: Molecular sieve bed adsorption schematic for simulation 1.

Table 4.1: Operating conditions for simulation 1

Parameter	Value	Unit	Description
P_f	74.09	bar	Feed stream pressure
P_p	73.07	bar	Product stream pressure
T_f	34.0	°C	Feed temperature
F_f	1.85	$\mathrm{kmol\,s^{-1}}$	Feed stream flow rate
C_{v_i}	18.32	$\mathrm{kmol\,s^{-1}\,bar^{-1}}$	Valve's initial flow coefficient
Y_{CH_4}	0.4830	mol / mol	Molar fraction of CH_4 at feed stream
Y_{CO_2}	0.4700	mol / mol	Molar fraction of CO_2 at feed stream
Y_{H_2O}	0.0008	mol / mol	Molar fraction of H_2O at feed stream
$Y_{C_5H_{12}}$	0.0462	mol / mol	Molar fraction of pentane at feed stream

temperature plot was broken up into two figures in order to better explain the different behaviors observed at particular time intervals.

Figure 4.2 shows the temperature variation from the beginning of the adsorption phase (t = 0 hours) up to t = 0.18 hours. The temperature along the bed is initially at 34.0°C. Since initially the molecular sieves are completely unloaded and concentration of adsorbable components suddenly increases, the adsorption rate is the highest. For this reason, a temperature peak appears and the temperature at the end of the bed (L = 1.0) reaches 105.7°C. Due to the convective term of the energy balance, the peak travels along the bed and since the dispersion term was also considered, the peak widens as it moves forward axially. During this first time interval, after the first minute of adsorption, the bottom of the bed

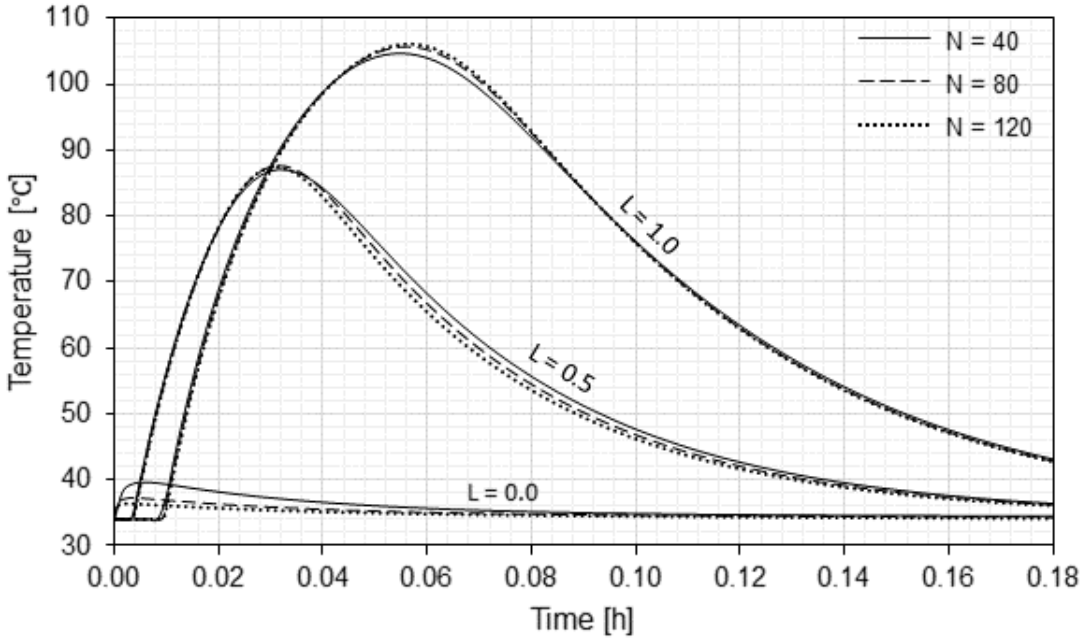

Figure 4.2: Temperature on different axial distances across packed bed for t < 0.18 hours. L is the dimensionless length, being L = 0 the top of the bed and L = 1, the bottom. The temperature was evaluated for simulations with different numbers of nodes.

is the hottest spot and the top of the bed is the coolest spot. The lowest temperature happens at the top of the bed and is equal to 34.0°C, which is equal to the temperature of the feed stream.

In Figure 4.2, it can also be observed that for each axial coordinate (L = 0.0, L = 0.5 and L = 1.0), there are three curves. These curves were obtained by running simulation 1 with different numbers of discretization nodes: N = 40, N = 80 and N = 120. For N smaller than 40 nodes, convergence issues were observed and simulation was interrupted due to "Integration failure.". For N greater than 120 nodes, the simulation became very time consuming (see Table 4.2).

Table 4.2: Simulation times for different number of discretization nodes, N. Δt_{ref} is the time it took to execute simulation 1 until time t = 3,000 seconds. $\Delta \hat{t}_6$ is the estimated time it will take to run 6 cycles, which is equivalent to t = 108 hours.

N	Δt_{ref} [minutes]	$\Delta \widehat{t_6}$ [hours]
40	2.57	5.6
80	3.92	8.5
120	7.73	17.0

For comparison purposes, the simulation was executed once for each node number from t = 0 seconds to t = 3,000 seconds. For each run, the times at start

and finish were recorded for evaluation. For N = 40, the execution time Δt_{ref} was relatively quick (2.57 s). When the number of nodes was doubled (N = 80 nodes), the execution time increased by more than 50% (Δt_{ref} = 3.92 s). When the number of nodes was once again increased by 40, Δt_{ref} almost doubled. Although a better estimate would be obtained if the simulation were executed for different time intervals and for more node numbers, a rough estimate can be made by observing the results of this short experiment: the simulation time seems to increase exponentially with the number of nodes.

Assuming that execution time varies linearly with simulation interval length, an estimate was obtained for how long it would take to execute six TSA cycles, $\Delta \widehat{t_6}$ (this is the duration for simulations 4 and 5). As mentioned on Chapter 3, each cycle lasts 18 hours, so 6 cycles corresponds to an interval of 108 hours. Table 4.2 shows that it would take about 5.6 hours to run 6 TSA cycles using 40 discretization nodes, 8.5 hours using 80 nodes and 17 hours using 120 nodes. With 40 nodes the simulation is already too time consuming. This is a critical factor because the Aspen software licenses were remotely accessed, thus being subjected to connection losses due to network fluctuations. In fact, the connection was frequently lost after random time intervals that varied from 7 to 12 hours. As a consequence of these connection losses, the simulation would be interrupted and once restarted, the TSA cycle would not resume from the point where it stopped. Instead, a new cycle would start before finishing the previous one.

Although it would be ideal to increase N until the curves on Figure 4.2 no longer varied and then choose that node number for the simulation, it can be observed that the shapes of the curves remain essentially the same, with the temperature peak initially more pronounced for a greater N. However, this significant difference due to N only happens for a short amount of time and for t greater than 0.04 hours, this effect becomes less pronounced. For a qualitative analysis, it is enough to observe the shape of the curves and since the objective of this work is to compare a GDU with and without the feed stream's temperature control strategy, using a smaller number of nodes does not impose an issue. For this reason, 40 nodes will be used for the rest of simulation 1 and for simulations 2, 3, 4 and 5.

Returning to the temperature analysis of simulation 1 (adopting the selected number of nodes), after 2.4 hours adsorbing, the concentration gradients are smaller and temperature along the bed converges to a value between 33.5 and 34.3°C, which is close to the feed stream temperature. A moving front may be observed in Figure 4.3. For this phenomenon to be observed, the curves on more axial coordinates has to be plotted. The temperature difference between

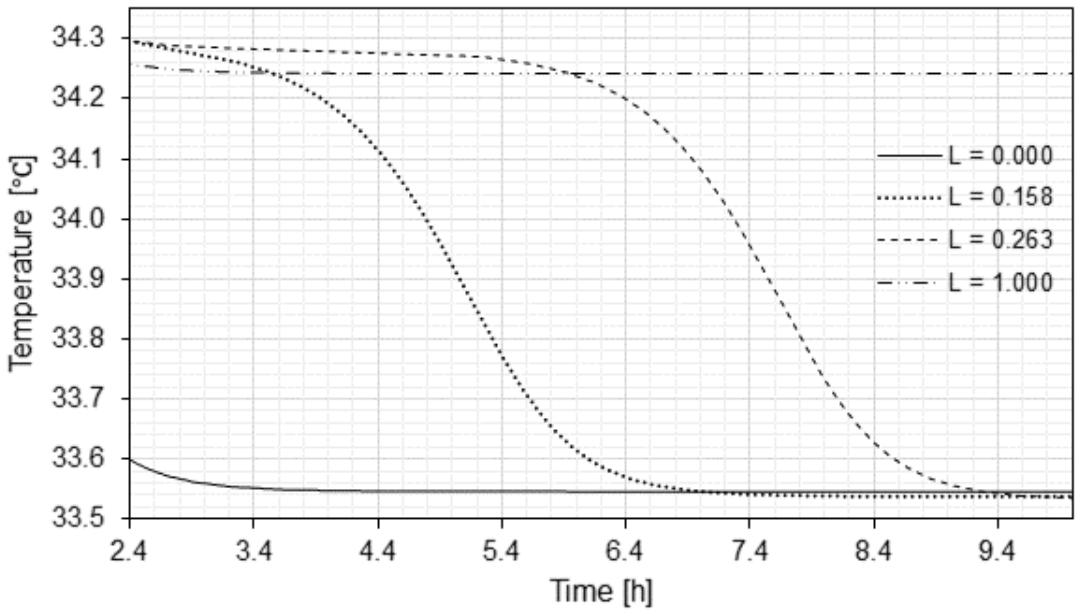

Figure 4.3: Temperature on different axial distances across packed bed for t > 2.4 hours. L is the dimensionless length, being L = 0 the top of the bed and L = 1, the bottom.

bed coordinates is smaller than 1°C. The temperature does, however, drop to a minimum value of 33.5°C, which is lower than the feed temperature. This is due to the expansion when the feed stream reaches the adsorption vessel. It can be observed on the plot that the point of lowest temperature moves from the top downwards in the axial direction as the mass transfer zone moves along the bed and if adsorption time is increased, it will eventually reach the bottom of the bed.

As will be shown in the Vapor-Liquid Equilibrium section, for the operation pressure range, the dew-point temperature is practically constant and equal to 35.5°C. According to the temperature profile table, at t = 0.102 hours the bed temperature of the top of the bed has already dropped below T_{DEW}, i.e. condensation occurred. During the adsorption phase, the temperature of at least some portion of the bed remained below T_{DEW} for at least 11.9 hours.

4.1.2 Pressure

As the fluid stream flows through the packed bed, a slight pressure drop is expected. However, beds are usually designed for this pressure drop to be small (usually less than 1 bar). Figure 4.4 shows the pressure profile along the packed bed for different simulation times. It can be observed that the profile is quite linear and that pressure drop across the bed becomes small (less than 0.28 bar)

after the first minutes of adsorption. This indicates that considering the pressure profile to be constant along the packed bed or even the pressure itself to be constant during the whole process would be good approximations.

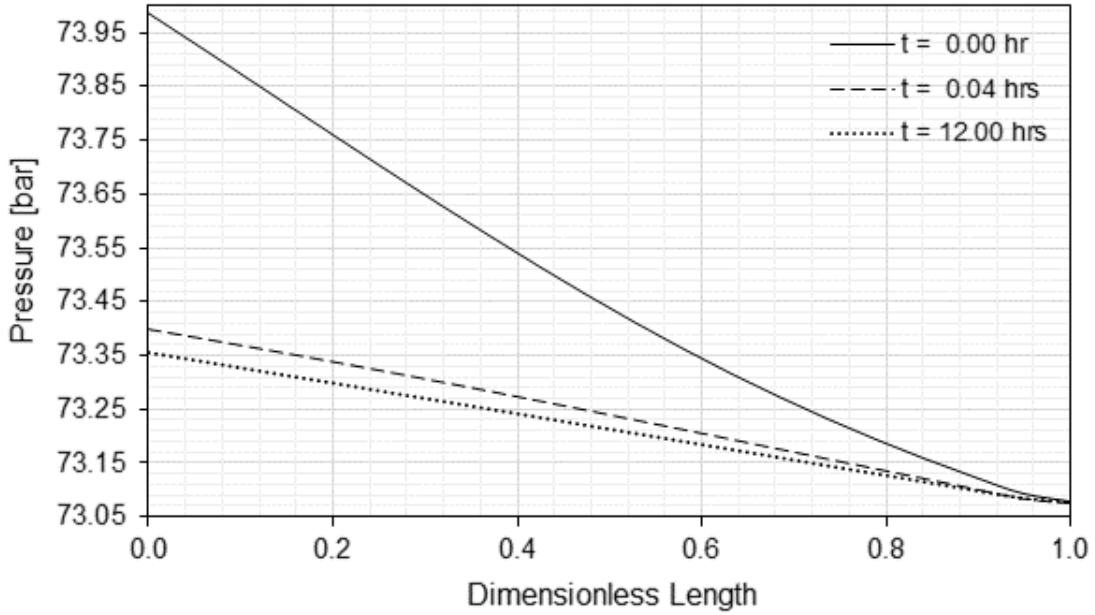

Figure 4.4: Pressure profile across packed bed for different time intervals. L = 0 is the top of the bed and L = 1, the bottom.

4.1.3 Velocity

The velocity of the fluid stream is expected to vary along the packed bed. As was done with the temperature plots, the gas velocity was also plotted in two different figures to describe the particular behaviors observed at different time intervals. Figures 4.5 and 4.6 show the gas velocity curves for three discrete axial bed coordinates: L = 0.0 being the top of the bed, L = 0.5, the middle and L = 1.0, the bottom. The different behavior patterns occurred at time intervals similar to the intervals in which change of behavior was observed for the temperature. This suggests that the gas velocity is greatly influenced by the temperature changes.

During the first time interval ($t \in [0, 0.3]$ hours), the gas velocity presented the greatest variations, both in time and along the bed. Since the pressure is linear and presents little variation, it can be assumed that this is due to the temperature changes, which are also the most drastic at the beginning of the adsorption phase. For $t < 0.05$ hours, there is a drop in velocity caused by the change of gas composition due to feed stream, which contains heavier components, and to the adsorption of lighter components. About 6.5 kmol are removed from the gas inventory by adsorption. After this, the temperature increases while the ad-

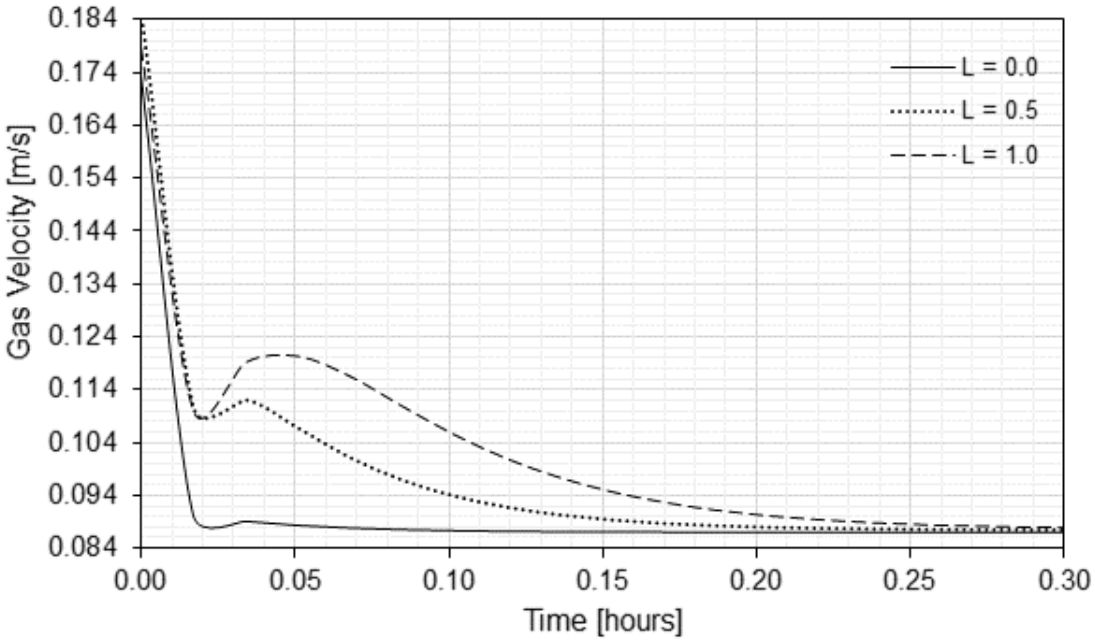

Figure 4.5: Gas velocity profile across packed bed for t < 0.3 hours, at different bed lengths. L = 0 is the top of the bed and L = 1, the bottom.

sorption of components other than water is reduced, which causes the velocity to increase. This behavior can be observed in Figure 4.5. After the initial velocity drop, the velocity peak increases and disperses along the bed, as happens with the temperature.

Figure 4.6 shows the gas velocity for t > 0.3 hours. It can be observed that the velocity profile becomes constant after 2.3 hours. From this time in the cycle, it was observed that the pressure profile changes very little, and although the temperature profile presents a front that propagates along the bed, the temperature variation is very small (less than 1°C) when compared to the initial time interval. This reflects directly in the gas velocity profile.

4.1.4 Mole Fractions

The mole fractions of the feed stream components are expected to change as the fluid stream travels through the molecular sieve vessels due to the adsorption process. Since the process was designed for natural gas dehydration and the 4A molecular sieve was chosen specifically for this application, it is expected that most of the water is removed from the wet gas. The product is expected to have a mole fraction of water smaller than 0.0001 at all times. This should be observed in the simulation, since the modeled unit was designed accordingly. Although the intention is to remove only water, it was observed in previous chapters that the 4A molecular sieves also adsorb CH_4 and CO_2, which are present in sig-

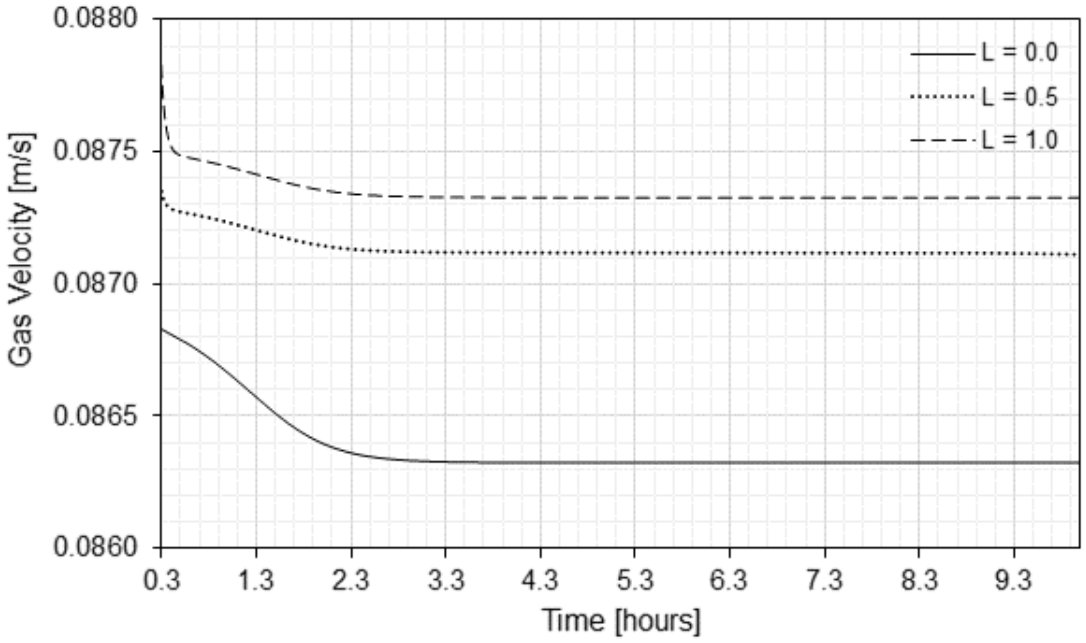

Figure 4.6: Gas velocity profile across packed bed for t > 0.3 hours, at different bed lengths. L = 0 is the top of the bed and L = 1, the bottom.

nificant amount in the feed stream. For this reason, a reduction is expected in the mole fractions of water, methane and carbon dioxide. Despite not being adsorbed, the pentane mole fraction is expected to increase, due to the reduction of the mole fractions of the other components.

Figure 4.7 shows the H_2O mole fraction profile (breakthrough curve) for different moments of the adsorption phase of the TSA cycle. As previously stated, the adsorption cycle was designed to have a duration of 12 hours. After 6 hours of adsorption, 20% of the bed is saturated and at the end of the adsorption phase (t = 12 hours), only 40% of the bed is saturated. The bed is designed like this since with time, the mass transfer zone tends to widen and eventually, regeneration will not be capable of recovering the top portion of the bed. Molecular sieve adsorbers for GDUs are usually designed to last for about 25 years, which is the lifetime of an FPSO, so it is important to leave enough space between the mass transfer zone and the end of the bed during design. This is because the capacity of the molecular sieve decreases with time due to irreversible degradation after each cycle. The molecular sieve degradation factor was not considered in the model.

Figure 4.8 shows how the mole fraction of methane for the gas varies with time for three different bed coordinates. Inside the bed, the mole fraction of CH_4 is initially 1. It drops to 0.4830, the mole fraction of methane on the feed stream, in less than 12 minutes and remains constant for the rest of the adsorption phase (t = 12 hours). The reduction in Y_{CH_4} happens because the bed was initially

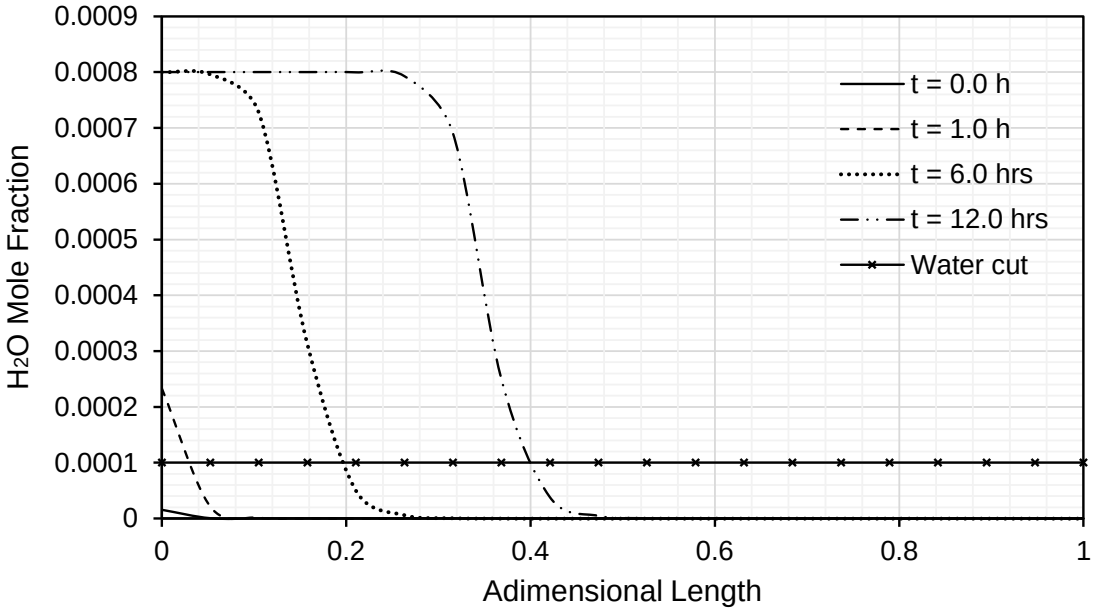

Figure 4.7: Water mole fraction of gas across packed bed. L = 0 is the top of the bed and L = 1, the bottom.

filled with methane, so the initial composition was greater than the feed stream composition.

Regarding the mole fraction of carbon dioxide, it was initially equal to 0 along the bed and equal to 0.4700 at the feed stream. It remains constant at Y_{CO_2} = 0.4700 for L = 0.0 throughout the whole adsorption phase, but as gas travels through the bed, carbon dioxide is also adsorbed, so there is a gradual increase along the axial direction, happening faster at the top of the bed. As time goes by, the packed bed also becomes saturated in CO_2 and the mole fraction of this component on the gas stream starts to increase until it eventually reaches the feed stream composition. This behavior can be observed in Figure 4.9.

As expected, the pentane mole fraction initially increases to 0.0465 at the beginning of the bed, and as the gas travels to the bottom of the vessel, it eventually reaches a peak at 0.0530 (see Figure 4.10). As the bed becomes saturated with the other components, the feed stream slowly converges back to its initial mole fractions and $Y_{C_5H_{12}}$ returns to its initial composition of 0.0462.

At the end of the adsorption phase, the mole fractions of the product stream are basically the mole fractions of the feed stream without the water. Since the packed bed does not saturate its capacity of holding H_2O, but does so for the other components, the mole fraction of water is reduced while the mole fraction of the other components increase slightly to compensate for the reduction of Y_{H_2O}. The resulting mole fractions are presented in Table 4.3.

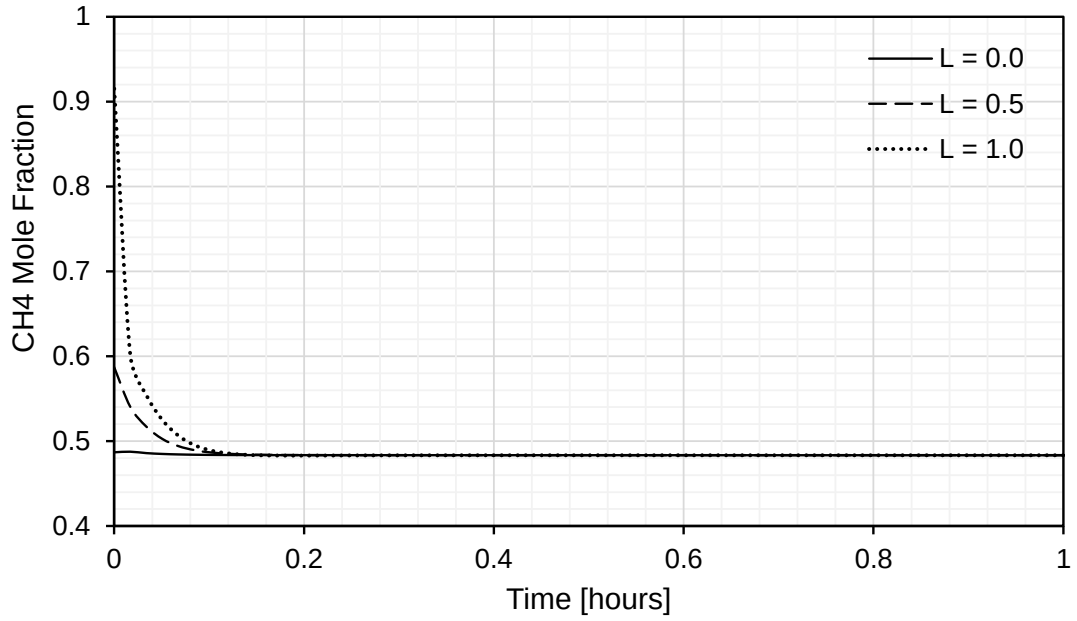

Figure 4.8: Methane mole fraction on solid phase for different bed lengths during full adsorption cycle. L = 0 is the top of the bed and L = 1, the bottom.

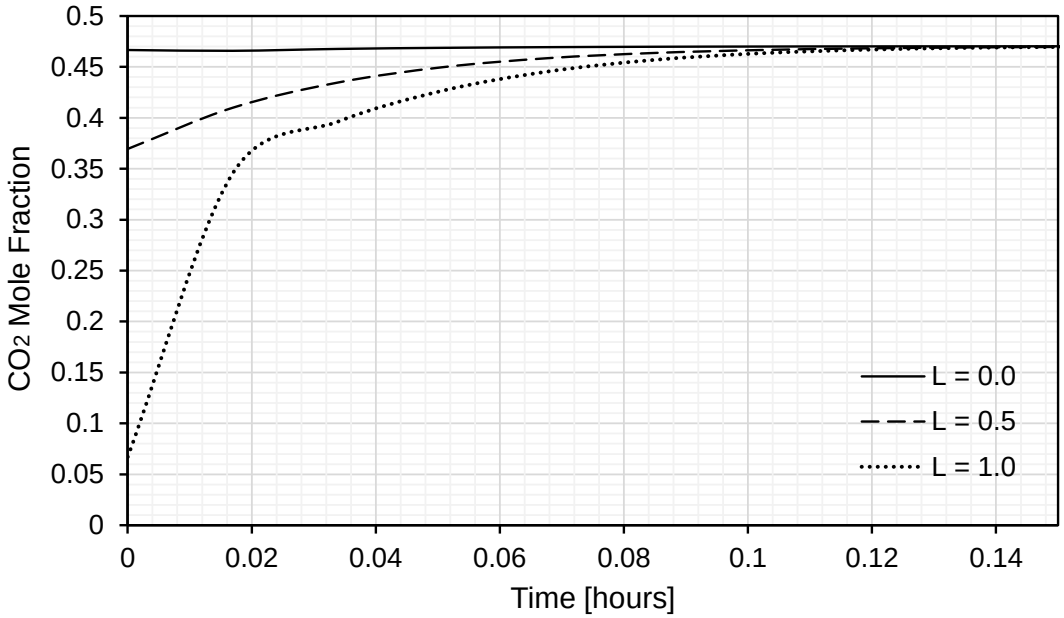

Figure 4.9: Carbon dioxide mole fraction on solid phase for different bed lengths during full adsorption cycle. L = 0 is the top of the bed and L = 1, the bottom.

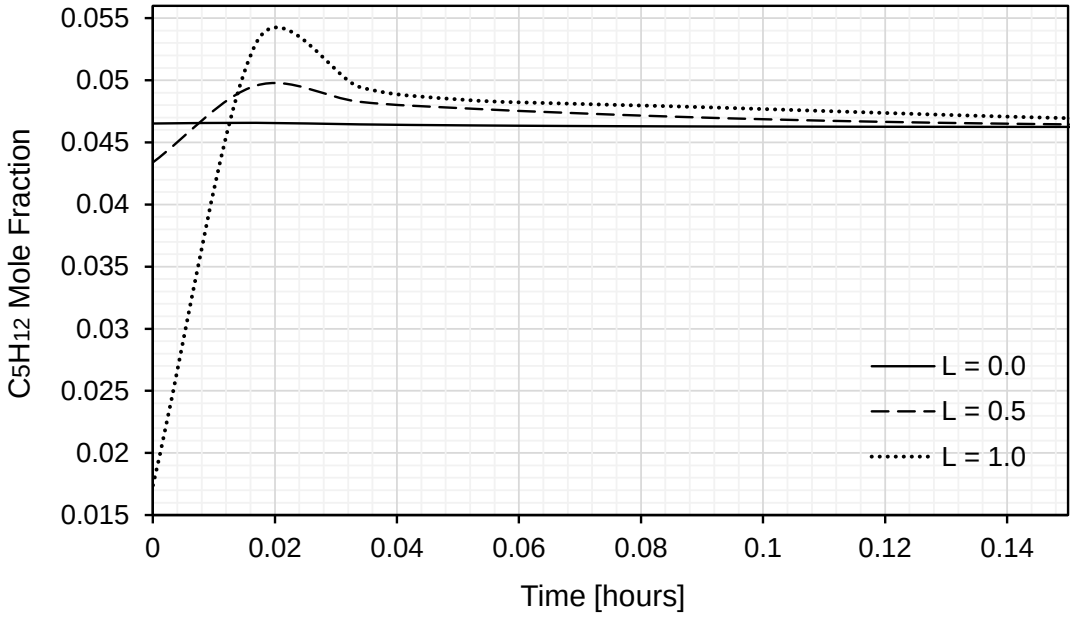

Figure 4.10: Pentane mole fraction on solid phase for different bed lengths during full adsorption cycle. L = 0 is the top of the bed and L = 1, the bottom.

Table 4.3: Feed stream composition, Y_f at the beginning of the adsorption phase (t = 0 hour) and product stream composition at the end of the adsorption phase (t = 12 hours).

Species	Feed Mole Fraction (Y_f)	Product Mole Fraction (Y_p)
H_2O	0.0008	2.64×10^{-5}
CH_4	0.4830	0.4834
CO_2	0.4700	0.4700
C_5H_{12}	0.0462	0.0462

4.1.5 Concentrations

The explanation for the concentration plots is similar to the plots for the molar fractions. However, since pressure and compressibility vary significantly with time, so does the total concentration of the gas. The relationship between the molar fraction Y_i of a component i and the concentration C_i of that same component is given by Equation 4.1, where Z is the compressibility factor of the mixture, T is the temperature, P is the pressure and R is the universal gas constant.

$$C = \frac{P}{Z \cdot R \cdot T}; \qquad C_i = Y_i \cdot C \tag{4.1}$$

As can be observed in Figure 4.11, Z varies very little with pressure and is approximately linear with temperature during the adsorption phase. Since the

feed pressure and temperature are 74 bar and 34°C, respectively, Z is approximately 0.7198. With this information, the feed concentration C_f is equal to 4.0245 kmol/m^3. Multiplying this value by the feed stream mole fractions yields the concentrations of the feed stream components: C_{H_2O} = 0.0032 kmol/m^3, C_{CH_4} = 1.9438 kmol/m^3, C_{CO_2} = 1.8915 kmol/m^3, and $C_{C_5H_{12}}$ = 0.1859 kmol/m^3.

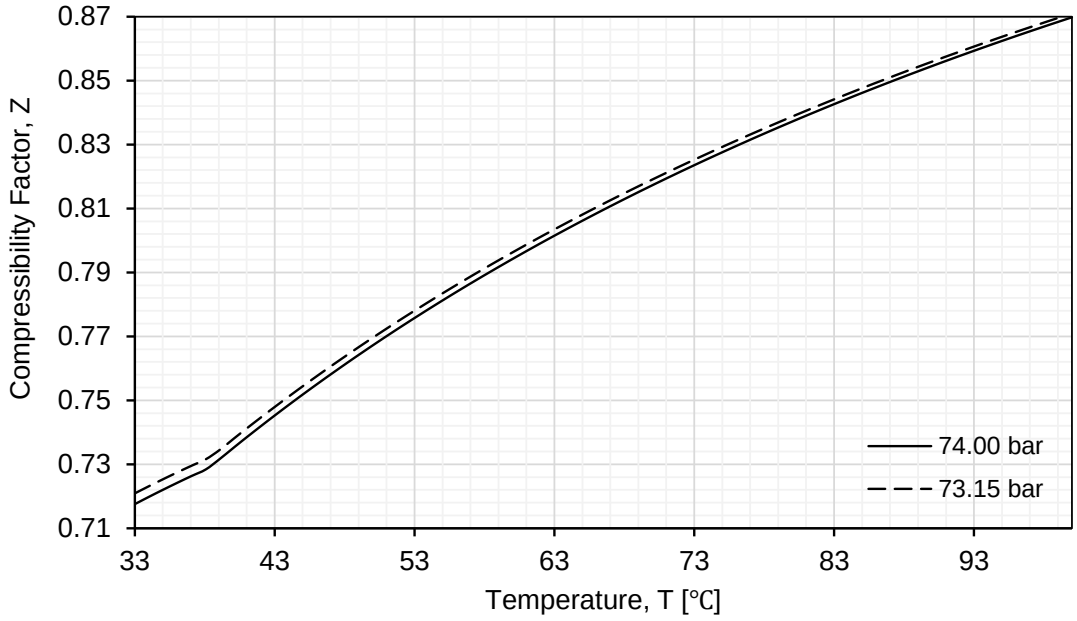

Figure 4.11: Dependence of the compressibility factor Z with temperature and pressure.

Figure 4.12 presents the concentration of water in the gas along the packed bed. Since the bed was initially filled with methane, there was no water along the bed and any water content was initially adsorbed as the feed gas entered. As the water loading of the initial portion of the bed increased, so does the concentration of water on the gas. After six hours, the initial portion of the bed is saturated and the gas stream at that point reaches a concentration of 0.0032 kmol/m^3, equal to the concentration of the feed stream. It can be observed that the mass transfer zone travels at approximately 0.1894 m/h. At the end of the adsorption phase, the concentration of water in the product stream is 2.87×10^{-14} kmol/m^3.

The methane concentration is presented in two plots. Figure 4.13 shows the methane concentration for different bed lengths during initial portion of the adsorption cycle (t < 0.4 hour), while Figure 4.14 presents the methane concentration for the whole adsorption phase (0 < t < 12 hours). Initially, the concentration inside the bed was completely methane. However, as soon as the simulation started, due to adsorption and to the feed concentration of adsorption being lower than the concentration inside the bed, C_{CH_4} drops. As the bed

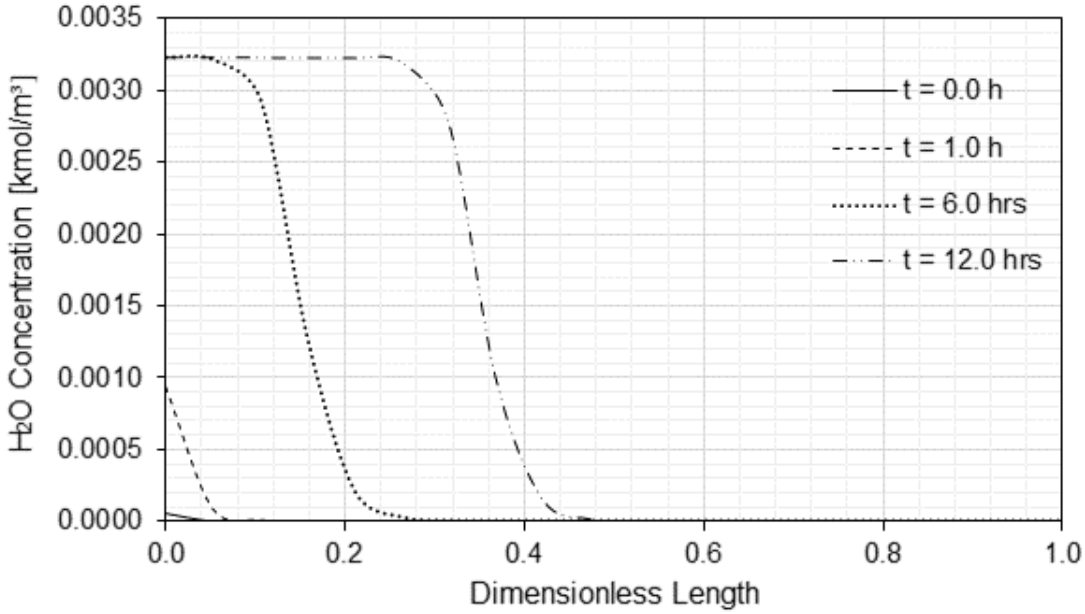

Figure 4.12: Water concentrations across packed bed. L = 0 is the top of the bed and L = 1, the bottom.

became loaded with CH_4, the concentration increased and returned to the feed gas concentration of about 1.94 kmol/m^3. From Equation 4.1, it can be observed that concentration is inversely proportional to temperature and the compression factor. From t = 0 hour to t = 0.3 hour, there is a peak in temperature, accompanied by the peak in the compressibility factor. Therefore, it explains the valley in the methane concentration. At the temperature peak (T = 100°C), where L = 1, time is approximately 0.05 hour. For that time and temperature, Z $\approx$ 0.87, and $Y_{CH_4} \approx 0.5248$ and the pressure is close to 73.08 bar. Replacing these values in Equation 4.1 yields C_{CH_4} = 1.42 kmol/m^3, which is the value observed at the CH_4 concentration valley in Figure 4.13.

Figure 4.14 shows the methane concentration for the rest of the adsorption phase. It can be observed that the values were different for each bed coordinate. At L = 0.0, the C_{CH_4} converged to 1.9495 kmol/m^3. At L = 0.5, C_{CH_4} converged to 1.9313 kmol/m^3. At the end of the bed (L = 1.0), C_{CH_4} converged to 1.9268 kmol/m^3. After 2.4 hours, the temperature varies very little and the difference in concentration along the bed is mainly due to the practically constant linear pressure drop.

Similarly, as was observed for the methane concentration, the carbon dioxide concentration does not reach a constant value until t = 2.4 hours, which is the time when the temperature peak due to initial adsorption disappears (see Figures 4.15 and 4.16). However, since there was initially no carbon dioxide in the bed, there is not the steep drop in the beginning as was observed for the CH_4.

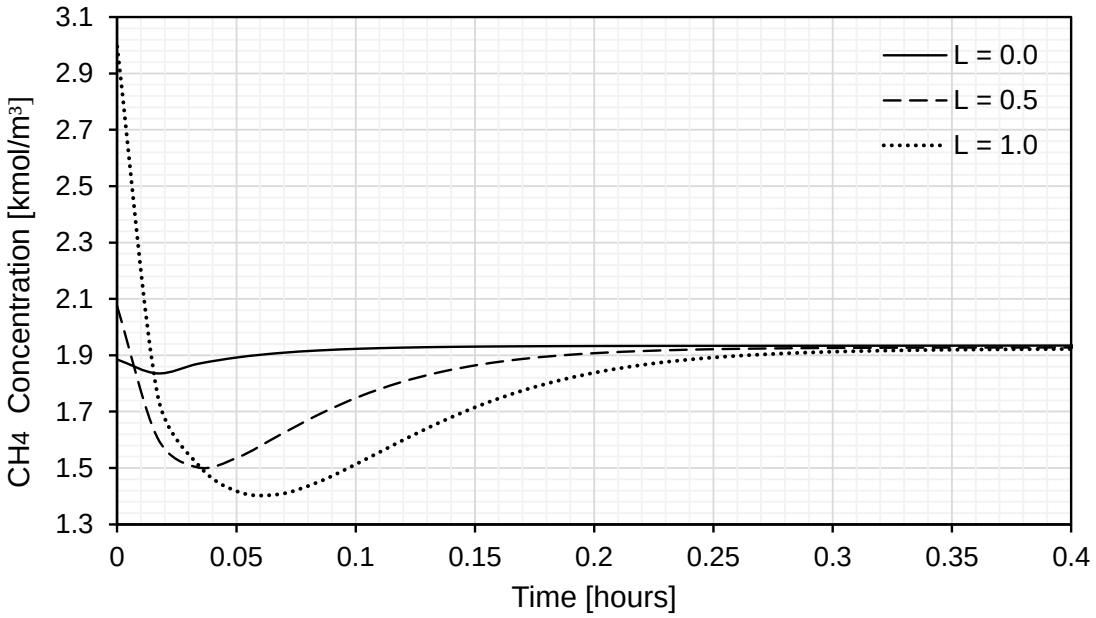

Figure 4.13: Methane concentration for different bed lengths during initial portion of the adsorption cycle (t < 0.4 hour). L = 0 is the top of the bed and L = 1, the bottom.

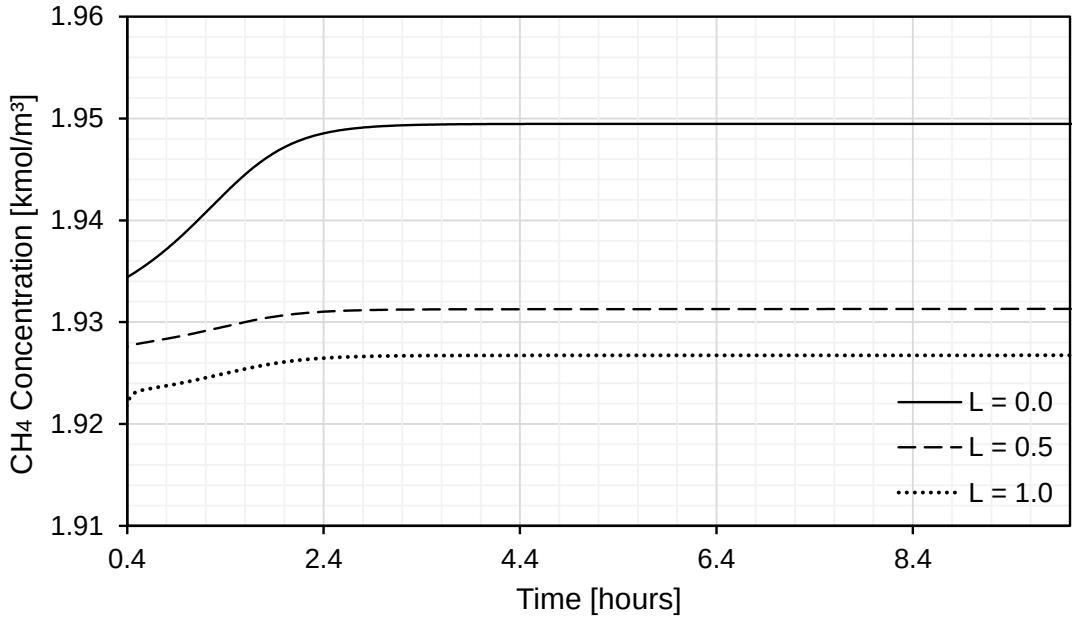

Figure 4.14: Methane concentration for different bed lengths during full adsorption cycle. L = 0 is the top of the bed and L = 1, the bottom.

At the beginning of the bed, the carbon dioxide concentration is a little smaller than in the feed stream, since some of it is initially adsorbed. In the middle of the bed, more carbon dioxide has been adsorbed so the concentration is lower. At the end of the bed, great part of the CO_2 is adsorbed, so the concentration is even lower. There is a small oscillation close to t = 0.05 hours due to the temperature variation and then the bed reaches its maximum loading value for carbon dioxide. At t = 2.4 hours, the bed no longer adsorbs CO_2 and the temperature has smaller variation. The concentrations reach the constant values of 1.8970 kmol/m^3 at L = 0.0, 1.8793 kmol/m^3 at L = 0.5 and 1.87489 kmol/m^3 at L = 1.0.

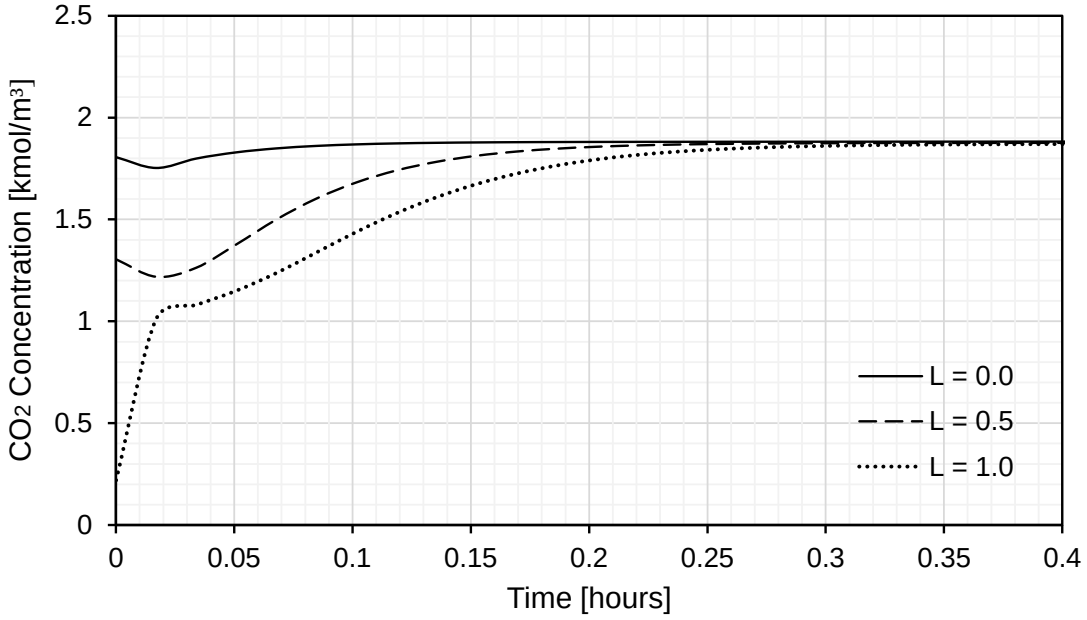

Figure 4.15: Carbon dioxide concentration for different bed lengths during initial portion of the adsorption phase (t < 0.4 hour). L = 0 is the top of the bed and L = 1, the bottom.

The pentane concentration analysis is similar to the analysis of the CO_2 and CH_4 concentrations (see Figures 4.17 and 4.18). Initially, there is no pentane at the bottom of the bed, so the concentration is very low for L = 1.0. As the other components get adsorbed, the pentane concentration increases. This varies also according to the temperature profile, so the constant concentration value for C_5H_{12} is also reached after 2.4 hours. The different concentrations along the bed are also due to linear pressure drop. The final values are: 0.1865 kmol/m^3 at L = 0.0, 0.1847 kmol/m^3 at L = 0.5 and 0.1843 kmol/m^3 at L = 1.0. Due to condensation, pentane concentration has decreased to a value lower than that of the feed concentration, even though the concentrations of the other components of the gas stream are decreasing. Table 4.4 summarizes the values for the feed concentration and the product concentration after 2.4 hours into the adsorption

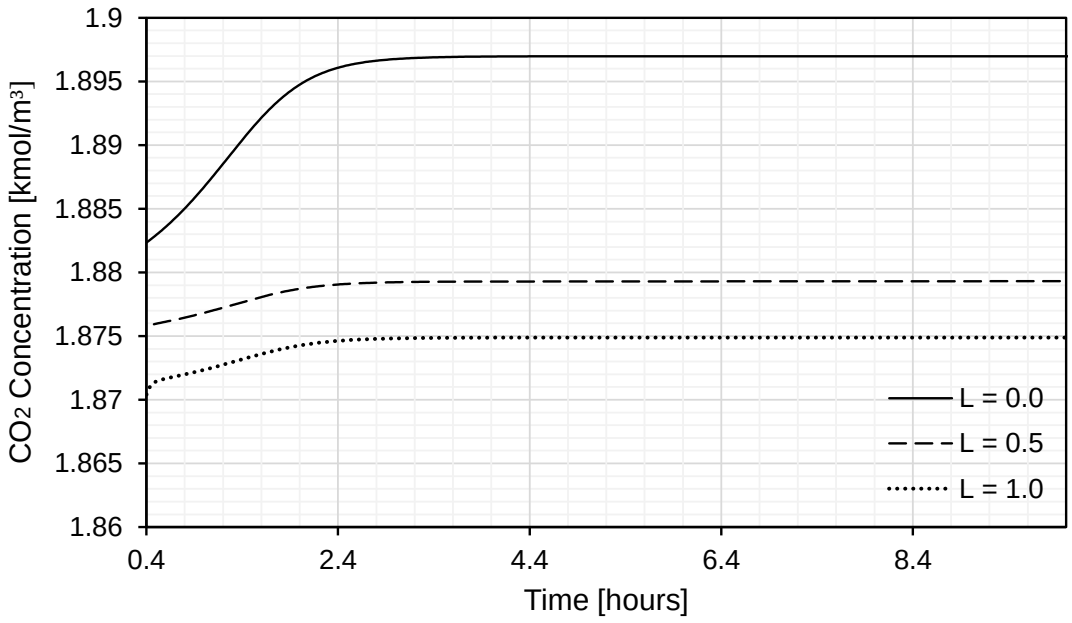

Figure 4.16: Carbon dioxide concentration for different bed lengths during final portion of the adsorption phase (0.4 < t < 12 hours). L = 0 is the top of the bed and L = 1, the bottom.

phase.

Table 4.4: Feed stream concentration and product stream concentration after 2.4 hours of the adsorption phase (2.4 < t < 12 hours).

Species	Feed Concentration [kmol/m^3]	Product Concentration [kmol/m^3]
H_2O	0.0032	2.87×10^{-14}
CH_4	1.9438	1.9268
CO_2	1.8915	1.8749
C_5H_{12}	0.1859	0.1843

4.1.6 Adsorbed Inventory

Figure 4.19 shows the total amount of each component that was adsorbed by the molecular sieves, i.e. the *adsorbed inventory*. As was observed in Chapter 3, the 4A zeolites have a smaller capacity for holding carbon dioxide and methane when compared to water. As can be observed in the figure, the bed saturates with CO_2 and CH_4 in less than one our, while it continues to adsorb water practically linearly. At the end of the adsorption phase, it can be observed that

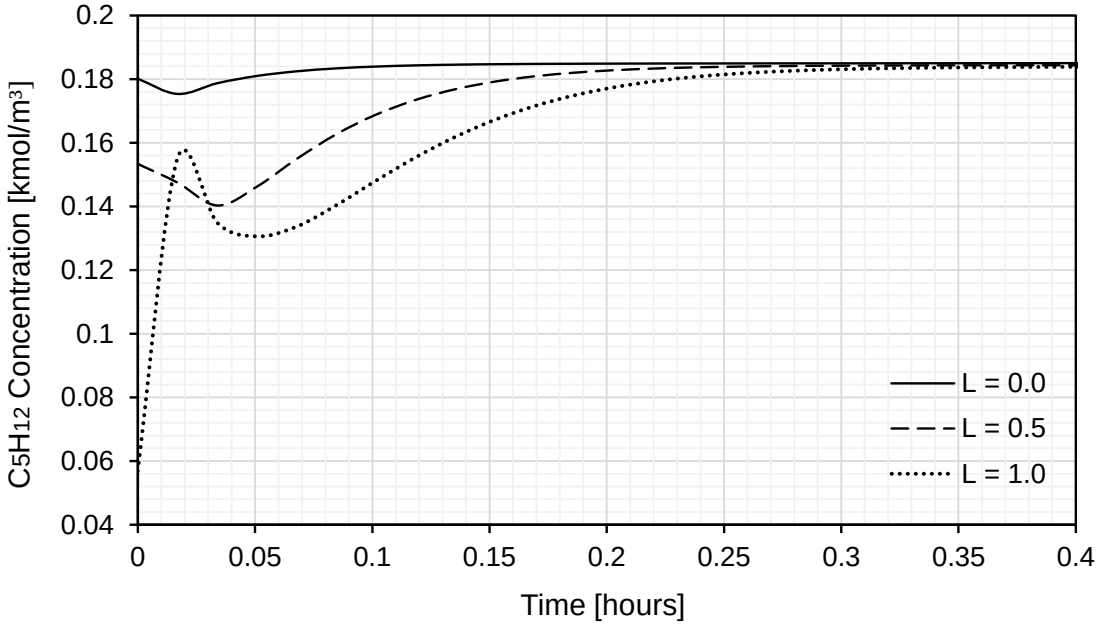

Figure 4.17: Pentane concentration for different bed lengths during initial portion of the adsorption phase (t < 0.4 hour). L = 0 is the top of the bed and L = 1, the bottom.

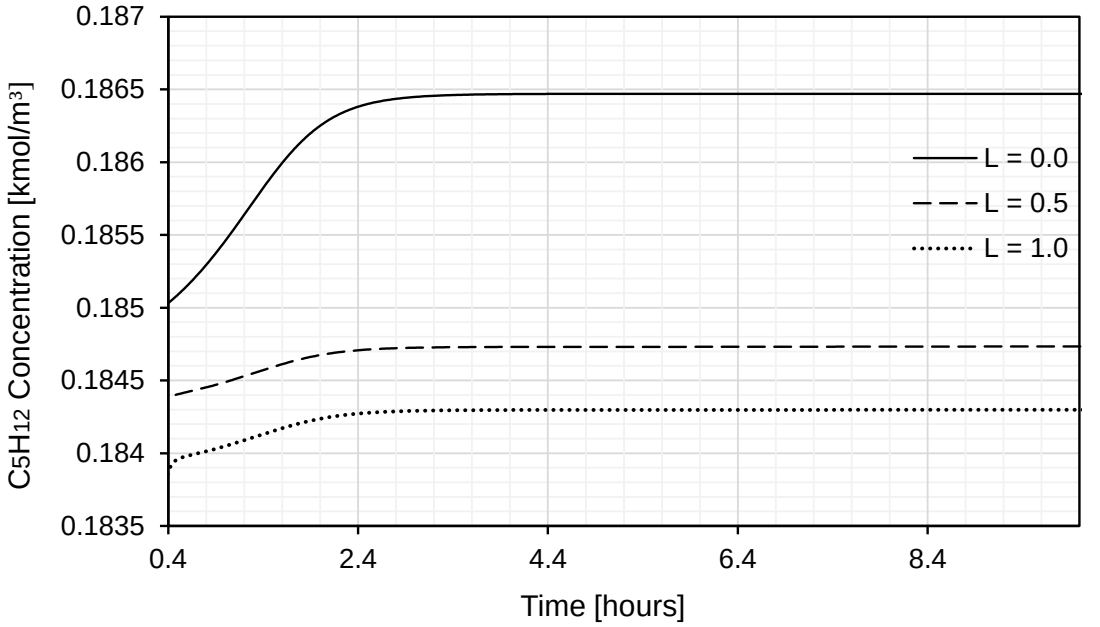

Figure 4.18: Pentane concentration for different bed lengths during final portion of the adsorption phase (0.4 < t < 12 hours). L = 0 is the top of the bed and L = 1, the bottom.

no pentane was adsorbed, 58.2271 kmol of methane were adsorbed, 65.5043 kmol of carbon dioxide and 123.085 kmol of water.

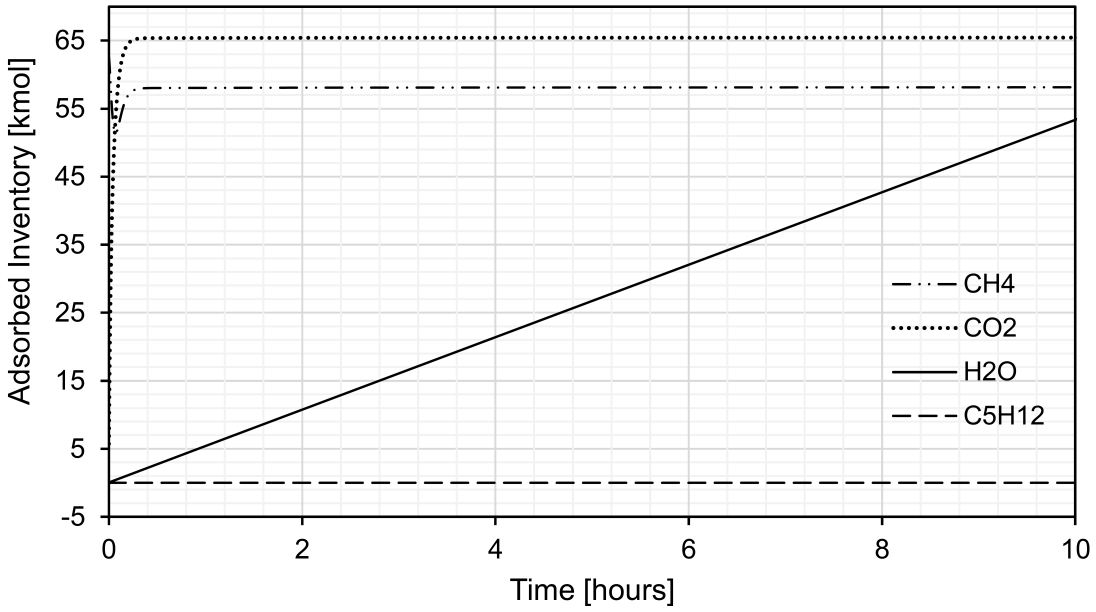

Figure 4.19: Inventory of components adsorbed by packed bed during the adsorption phase (0 hrs < t < 12 hrs). Final values (t = 12 hrs) of each component are, in kmol: N_{CH_4} = 58.2271; N_{CO_2} = 65.5043; N_{H_2O} = 123.085; and $N_{C_5H_{12}}$ = 1.07E-19.

4.1.7 Gas Inventory

The gas inventory is the quantity of moles in the total gas inside the molecular sieves vessel. This result is shown in Figure 4.20. The pentane concentration is practically constant, since no pentane is adsorbed throughout the adsorption cycle, this value remains constant and equal to 3.3500 kmol. Since the bed is still not saturated when the end of the adsorption phase is reached, the water content is 0.0052 kmol. Regarding carbon dioxide and methane, the bed saturates very quickly and in less than an hour the number of moles of these components on the gas becomes constant. The gas holds a total of 35.0228 kmol of methane and 34.0802 kmol of carbon dioxide during most of the adsorption phase.

4.1.8 Vapor-Liquid Equilibrium and Phase Behavior

As can be observed in Figure 4.21, in the working pressure interval of [73, 74] bar, the dew-point curve (dashed) is approximately a straight line. This means that, assuming that the composition variation is not significant inside the bed when compared to the feed stream, the dew-point temperature is approximately

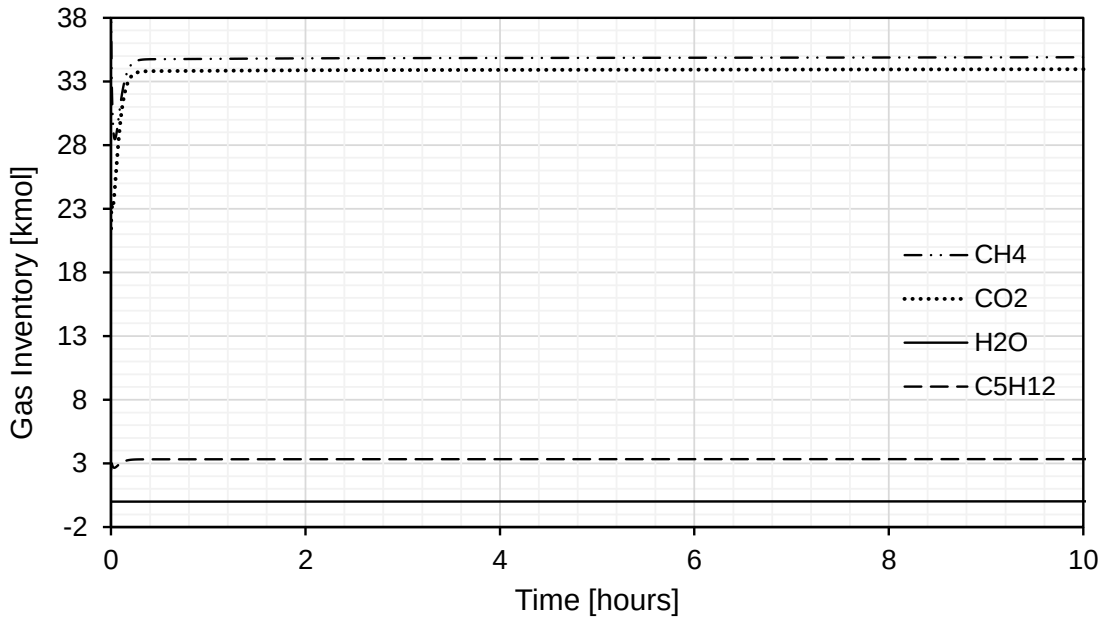

Figure 4.20: Gas phase inventory during regeneration phase (0 hrs < t < 12 hrs). Final values of each component are, in kmol: N_{CH_4} = 35.0228; N_{CO_2} = 34.0802; N_{H_2O} = 5.23E-02; and $N_{C_5H_{12}}$ = 3.3500.

constant and equal to 35.5°C. The bundle of lines on the plot represent the trajectories of the operating point with time. There is one line per discrete axial coordinate along the bed. The discretization was done using 40 points, but only 20 lines, evenly distributed along the bed, were plotted for convenience. However, it is not important to know which line corresponds to which bed coordinate, although this may be inferred by observing the temperature plots previously presented. The plot shall be interpreted as follows: any operating points to the left of the dashed line have entered the phase envelope, where both liquid and vapor phases are present, i.e. condensation happens; operating points to the right of the dashed line are in a pure gas state and represent no harm to the molecular sieves.

It is possible to observe, that some of the operating points lie in the left of the dew-point curve. Therefore, it may be inferred that condensation is happening. During the cycle, the minimum temperature inside the packed bed was found to be T_{MIN} = 33.5°C, which means that it is a ΔT of 2.0°C below the dew-point temperature. The solution recommended by TERRIGEOL (2012) of heating the feed stream by 3 to 5 °C would seem enough to bring all operating points out of the envelope. However, feed composition of the GDU is not constant throughout operation. Assume, for example, that a 10% increase occurred on the mole fractions of H_2O, CO_2 and C_5H_{12}. Consequently, the mole fraction of CH_4 would be reduced by 10.7%. The new compositions would be the following: Y_{H_2O} =

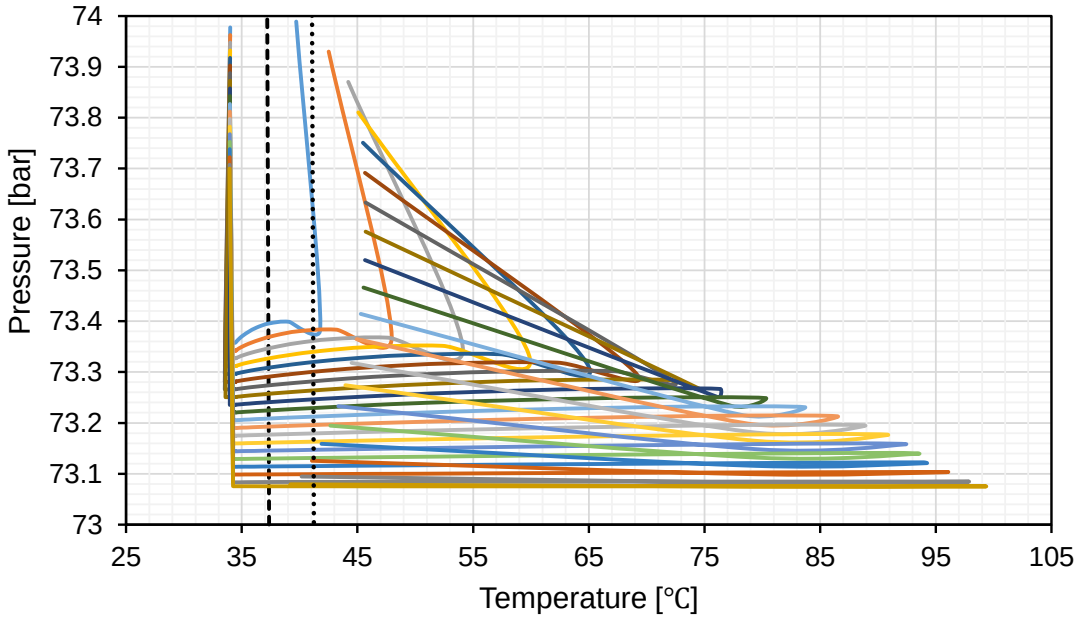

Figure 4.21: Operating point for different discrete axial coordinates during the initial TSA cycle (12 hours) and phase envelope. The dew-point temperature T_{DEW} is approximately constant and equal to 35.5°C (dashed line). The minimum temperature reached in the bed is 33.5°C. The dotted line represents the dew-point curve for the modified composition: Y_{H_2O} = 0.0009, Y_{CO_2} = 0.5170, Y_{CH_4} = 0.4313, and $Y_{C_5H_{12}}$ = 0.0508. In this case, T_{DEW} is approximately constant and equal to 39.49°C.

0.0009, Y_{CH_4} = 0.4313, Y_{CO_2} = 0.5170, and $Y_{C_5H_{12}}$ = 0.0508. In this case, T_{DEW} would increase to 39.5°C, for the same pressure range. This is represented by the dotted line in Figure 4.21. It is important to observe that the ΔT of 3°C or 5°C would no longer be enough to keep the operation points to the right of the new dew-point curve. The feed stream could be increased to an even greater temperature, but the feed stream could vary once again, bringing the dew-point curve even further to the right. Selecting a fixed high value of ΔT is also not the most efficient solution, since lower temperatures favor the adsorption process. It is therefore ideal to vary the ΔT according to the dew-point curve, which is the control strategy proposed in this work.

4.2 Simulation 2: Single Vessel Regeneration

The second simulation consists of a single vessel in the regeneration phase of the TSA cycle. Figure 4.22 shows the schematic used for the simulation. It can be observed that the regeneration gas is injected from the bottom of the adsorption vessel. In reality, this gas stream is part of the dehydrated gas product, but since the simulations were selected to increase progressively in complexity, a feed block with a fixed composition was used. The mole fractions of the product stream at the end of the adsorption cycle in simulation 1 (see Table 4.3) were used as the regeneration feed gas composition. Fixed values of pressure were defined for the regeneration gas feed and for the extract header. As was done in simulation 1, a control valve was used to ensure the adequate flow rate, which is 11% of the unit's product flow rate. Considering that there are two vessels in the adsorption phase and that the unit's product flow rate is equal to 3.7 kmol/s, the regeneration flow rate is equal to 0.407 kmol/s. The regeneration temperature is 230°C, which is adequate for the 4A zeolite, and the initial conditions within the packed bed are the values presented at the end of simulation 1. The operating conditions for simulation 2 are presented on Table 4.5.

Table 4.5: Operating conditions for simulation 2

Parameter	Value	Unit	Description
P_r	74.09	bar	Pressure at regeneration feed header
P_e	73.07	bar	Pressure at extract header
T_r	230	°C	Regeneration temperature
F_r	0.407	kmol/s	Regeneration flow rate
C_{v_i}	0.409	$\mathrm{kmol\,s^{-1}\,bar^{-1}}$	Valve's initial flow coefficient

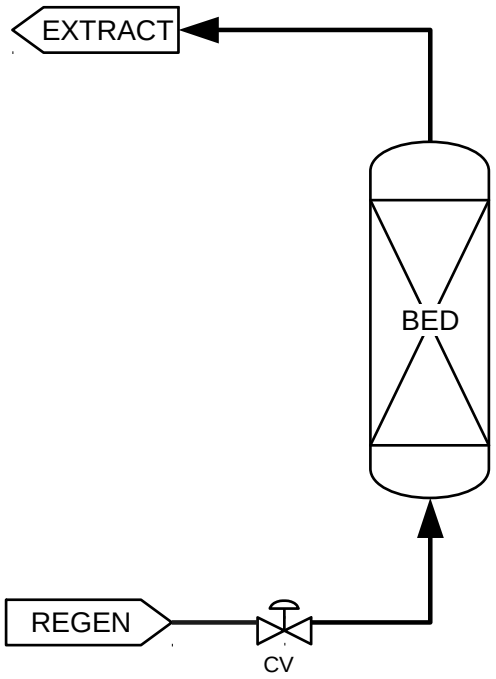

Figure 4.22: Molecular sieve bed regeneration schematic for simulation 2.

4.2.1 Temperature

At the end of the adsorption phase (t = 12 hours), the temperature at the bottom of the packed bed was approximately 34.3°C. As the feed gas stopped flowing and the regeneration gas was inserted, the temperature at L = 1.0 increased to 230°C. The temperature at this coordinate increases first because, as mentioned, the feed gas enters the packed bed from the bottom. Figure 4.23 shows the temperature at different bed lengths during the regeneration phase. From t = 12 hours to about t = 12.2 hours, a first phenomenon can be observed. During this time, the temperature rise is virtually completely due to sensible heat. This is the time that it takes to heat the bed from the adsorption temperature to about 80°C. At this time, desorption of water begins. From t = 12.2 hours to approximately t = 13 hours, a second phenomenon is observed. Most of the water is driven out of the zeolites. During this interval, enough heat has been supplied to desorb the water and break the attractive forces binding the water to the surface of the adsorbent. From t = 13 hours, the bulk of the water has been driven off the bed and heavy contaminants and residual water are removed. For t > 13.4 hours, the desorption has already happened. The temperature, therefore, remains constant and equal to the regeneration gas stream temperature until the end of the regeneration phase (t = 18 hours). The temperature behavior for simulation 2 is in accordance with what was described by CAMPBELL (2014).

It is important to observe that at the beginning of the regeneration phase

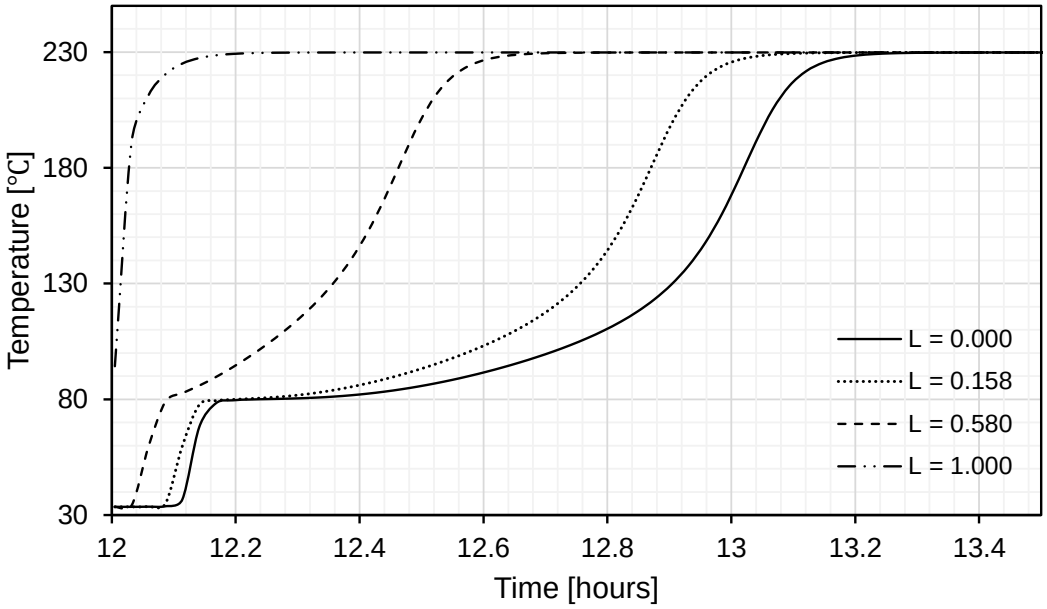

Figure 4.23: Temperature on different axial distances across packed bed during regeneration (t > 12 hours). L is the dimensionless length, being L = 0 the top of the packed bed and L = 1, the bottom of the packed bed. After t = 13.4 hours, the temperature remains constant and equal to 230°C.

(12 < t < 12.11 hours), the temperature of the bed is initially lower than T_{DEW} (35.5°C), which indicates the occurrence of condensation. The bed stays in this state for about 6.6 minutes and at t = 12.11 hours the temperature at the top of the bed reaches T_{DEW}. For t > 12.11 hours, the temperature only increases, so there is no risk of condensation during the rest of the regeneration phase.

4.2.2 Pressure

As was observed for simulation 1, the pressure drop across the packed bed is approximately linear for simulation 2. However, since gas flows from the bottom of the vessel to the top, the pressure is greater at the bottom. Figure 4.24 shows the pressure profile across the packed bed at different times into the regeneration phase. It can also be observed that the pressure drop increases with time from 0.02 bar to about 0.03 bar. As expected, the behavior of the pressure profile during regeneration is the opposite of the behavior observed during adsorption. While on the first the pressure drop decreased as the adsorbed inventory increased, on the second, the pressure drop increased as the adsorbed inventory decreased.

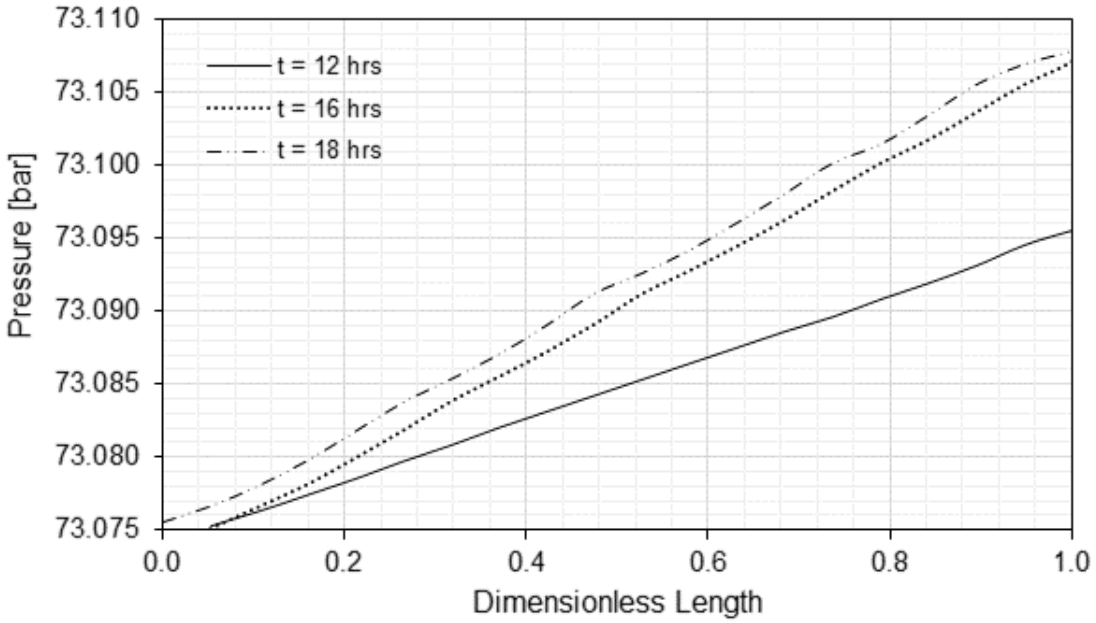

Figure 4.24: Pressure profile across packed bed during regeneration (t > 12 hours). L is the dimensionless length, being L = 0 the top of the packed bed and L = 1, the bottom of the packed bed.

4.2.3 Velocity

During the regeneration phase, gas is fed from the bottom of the adsorption vessel, so the flow direction is contrary to the axial coordinate system. Figure 4.25 presents how the absolute values of the gas velocity vary with time for three different dimensionless bed lengths: L 0.0, L = 0.5 and L = 1.0. It can be observed that the shapes of the curves resemble the shapes of the temperature curves. The temperature curve assumes its shape due to desorption. This resemblance shows that the gas velocity is directly influenced by these factors. The same explanation given to the temperature profiles can be applied to the velocity behavior.

For L = 1.0, at t = 12 hours, when the hot regeneration feed gas at 230°C meets the bottom of the packed bed, which is at about 34.25°C, the resulting temperature is about 94.3°C. Fort this temperature, regeneration composition and at the regeneration header pressure of 74.09 bar, the compressibility factor Z is 0.861619. The gas velocity v_g can be calculated using Equation 4.2, where Q_n is the molar flow rate in kmol/s. For the regeneration phase, Q_n = 0.407 kmol/s. This yields an initial gas velocity at L = 1.0 of about 0.027 m/s, which is approximately the value observed in Figure 4.25. The final values correspond to the regeneration gas composition at regeneration feed stream, 230°C and the 74.09 bar pressure. For these values, Z = 0.970308, which yields a final v_g of

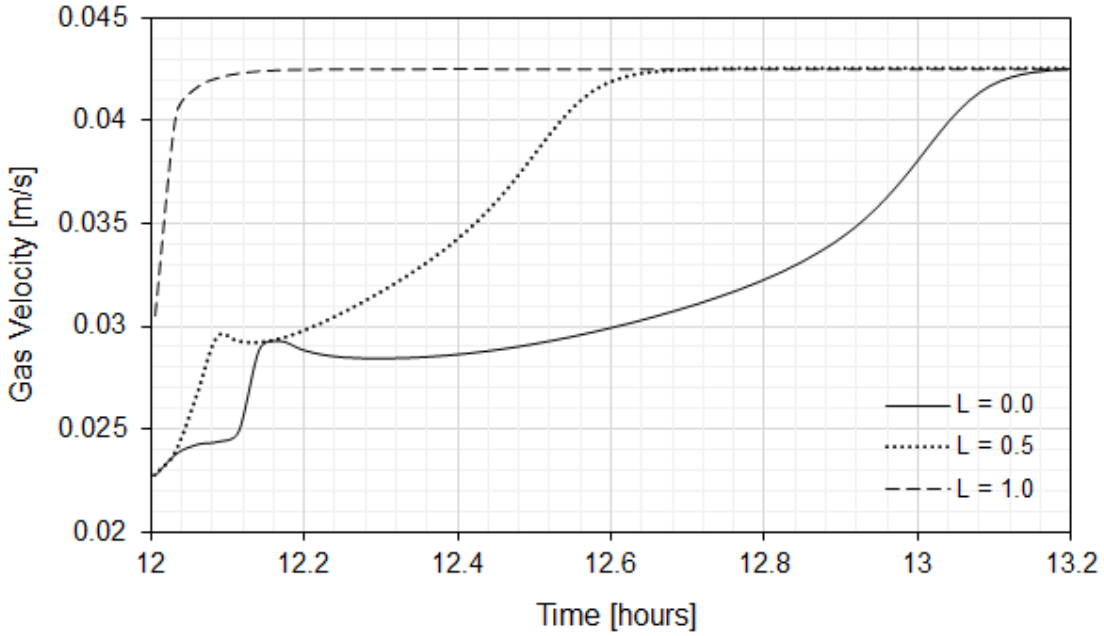

Figure 4.25: Gas velocity across packed bed during regeneration interval (t > 12 hours) for three different bed lengths. The direction is contrary to the axial coordinates (regeneration gas is fed from the bottom). L is the dimensionless length, being L = 0 the top of the packed bed and L = 1, the bottom of the packed bed.

0.042m/s. This can also be observed at Figure 4.25 for L = 1.0 and t > 12.2 hours.

$$v_g = \frac{4 \cdot Z \cdot Q_n \cdot R \cdot T}{P_r \cdot D_b^2} \tag{4.2}$$

4.2.4 Mole Fractions

During the regeneration phase, the adsorbed components are desorbed from the molecular sieves. As was explained for the temperature plots, up until t = 12.2 hours, the temperature rise is virtually completely due to sensible heat. The less strongly adsorbed components start desorbing, but water is still evaporating. This can be observed in Figure 4.26. As soon as the hot regeneration gas enters the packed bed at L = 1.0, there is a little peak indicating that all the water from that bed coordinate was desorbed. This water is carried upwards. The water at the middle of the bed (L = 0.5) only leaves the adsorbent a few minutes later. The peak is significantly higher, since water was carried from the bottom of the bed to the top and more water was adsorbed at the top of the bed than at the bottom. At t = 12.2 hours, the desorption process begins at the top of the bed (L = 0.0). The mole fraction reaches its highest value (since that portion of the bed was saturated during the adsorption phase) and remains desorbing for

approximately another hour. At t > 13.4 hours, all the water has been recovered.

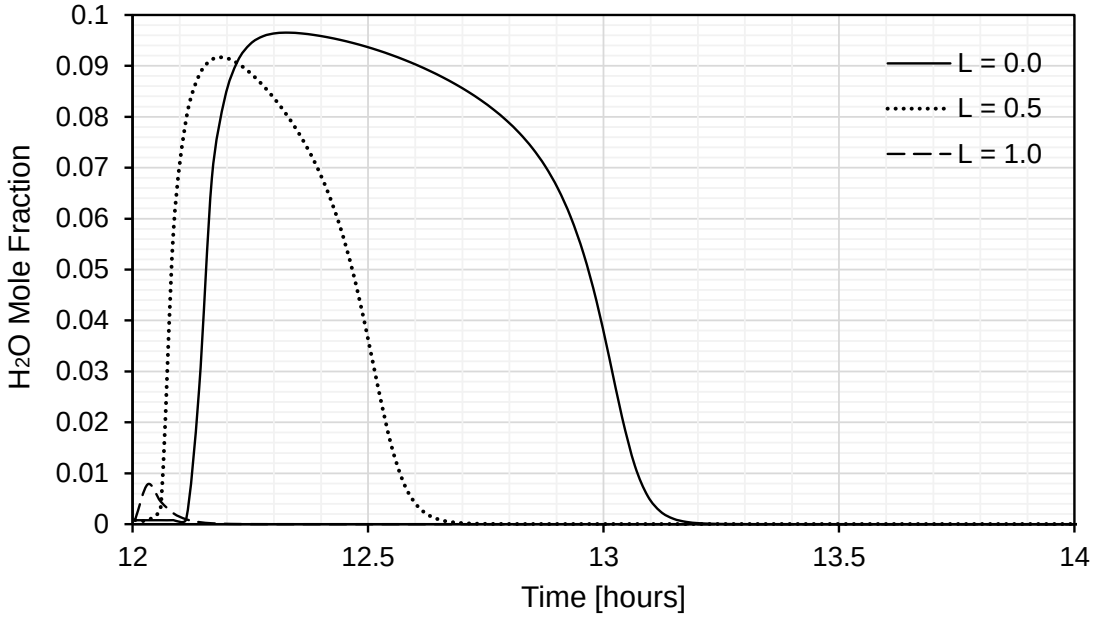

Figure 4.26: Mole fraction of water across packed bed during regeneration interval (t > 12 hours). L is the dimensionless length, being L = 0 the top of the packed bed and L = 1, the bottom of the packed bed. Regeneration temperature is 230°C. Mole fraction at the end of the regeneration phase is 2.6×10^{-5}.

Figure 4.27 shows how the mole fraction of CH_4 varies with time at different dimensionless bed lengths. The methane is quickly recovered from the bed. For this reason, when t = 12.2 hours, all the methane has already been recovered and a peak can be observed at each axial coordinate. As has happened to the water, the peak is highest at the top portion of the bed, which was saturated during the adsorption phase. At t = 12.2 hours, it was seen that water starts desorbing so the mole fraction of CH_4 decreases proportionately. The depression in the mole fraction of CH_4 is practically complementary to the increase in the mole fraction of water at each bed length. At the end of the regeneration phase, Y_{CH_4} is equal to 0.4834, which is the regeneration stream value.

Figure 4.28 shows how the mole fraction of carbon dioxide varies with time for different bed lengths. From the plot, it can be seen that no significant amount of CO_2 was recovered when compared to methane and water. For t < 12.2 hours, there is a decrease in the mole fraction of carbon dioxide due to methane desorption. After that, the mole fraction decreases even more due to water desorption. The mole fraction of CO_2 seems complementary to the methane mole fraction curve for t < 12.2 hours and to the H_2O curve for t > 12.2 hours. At the end of the regeneration phase, Y_{CO_2} is equal to 0.4704, which is approximately the regeneration gas value.

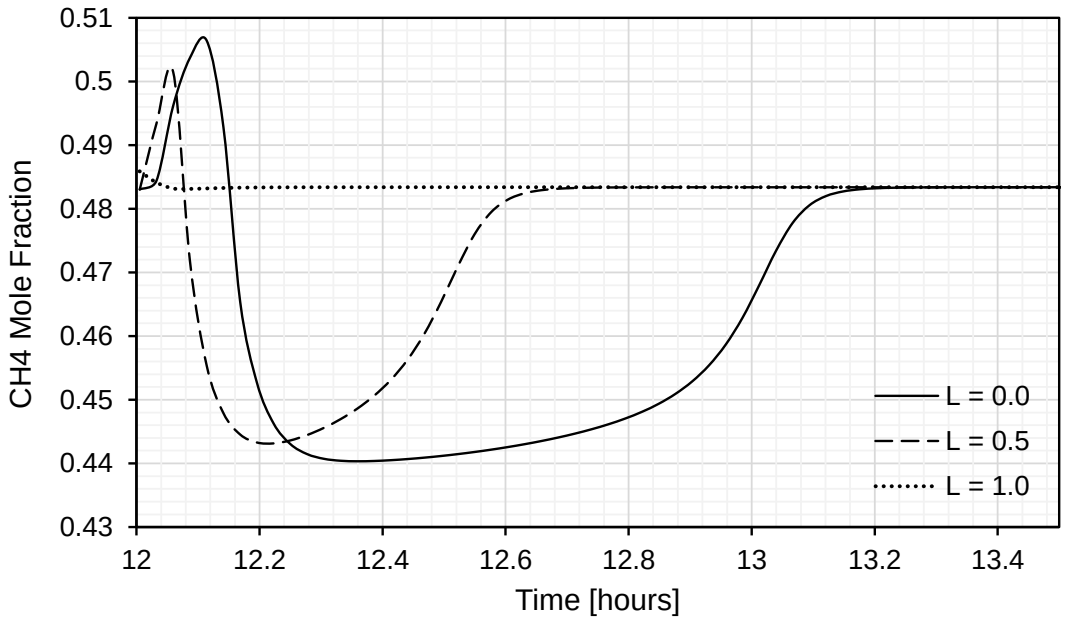

Figure 4.27: Mole fraction of methane across packed bed during regeneration interval (t >12 hours). L is the dimensionless length, being L = 0 the top of the packed bed and L =1, the bottom of the packed bed. Regeneration temperature is 230°C. Mole fraction at the end of the regeneration phase is 0.4834.

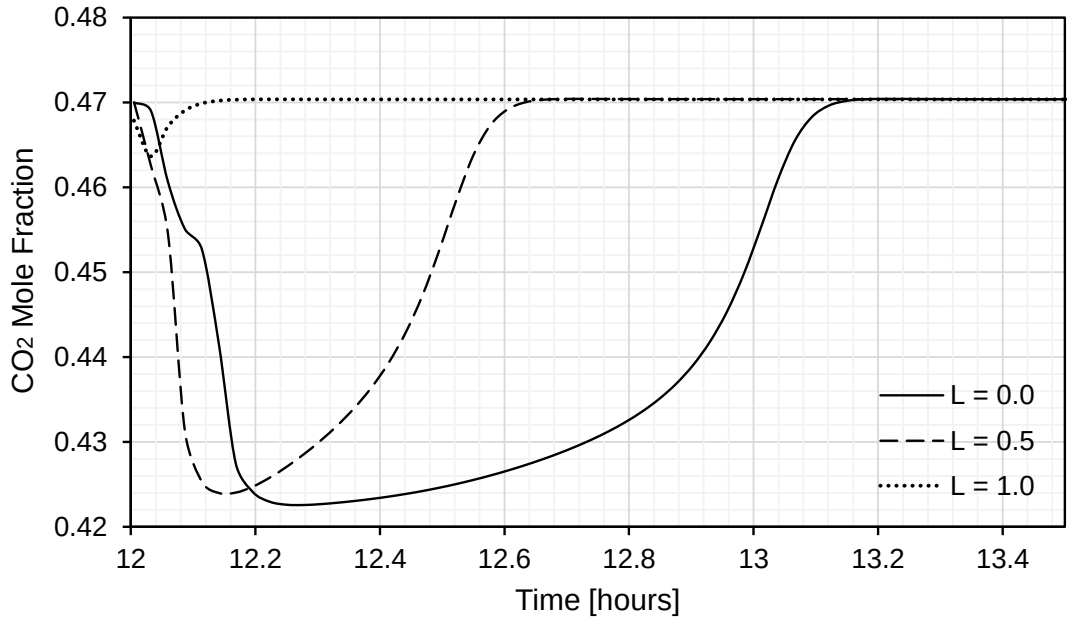

Figure 4.28: Mole fraction of carbon dioxide across packed bed during regeneration interval (t >12 hours). L is the dimensionless length, being L = 0 the top of the packed bed and L = 1, the bottom of the packed bed. Regeneration temperature is 230°C. Mole fraction at the end of the regeneration phase is 0.4704.

Figure 4.29 shows how the mole fraction of pentane varies with time for different bed lengths. Since pentane was not adsorbed by the molecular sieve,

it was not recovered during the regeneration phase. Therefore, the plot for the mole fraction of C_5H_{12} is complementary to all other plots. At the end of the regeneration phase, $Y_{C_5H_{12}}$ = 0.0462, which is approximately the value found in the regeneration feed stream.

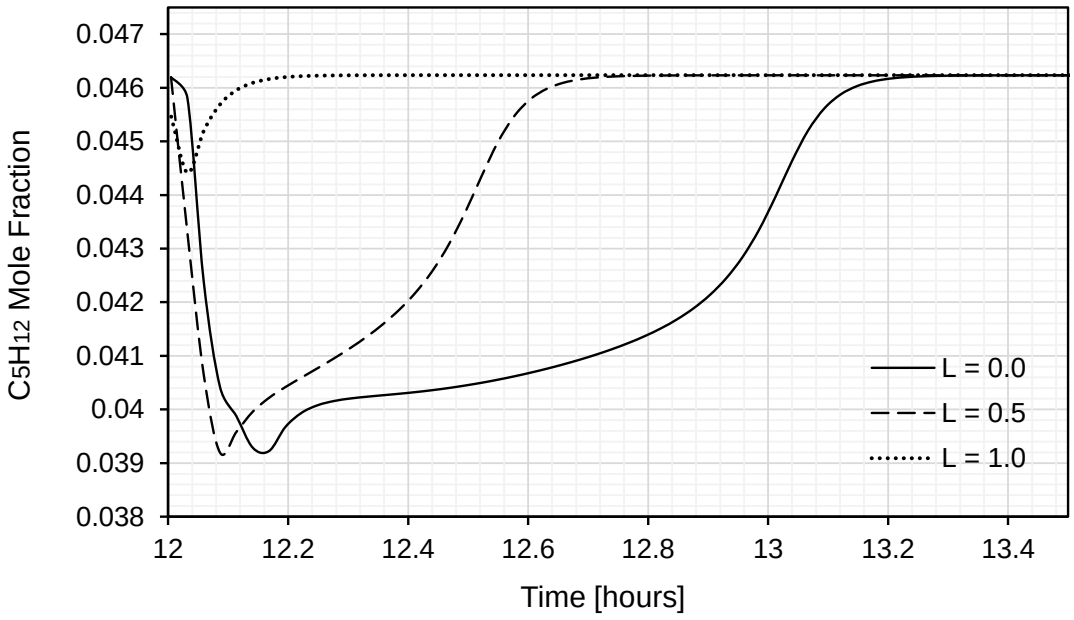

Figure 4.29: Mole fraction of pentane across packed bed during regeneration interval (t >12 hours). L is the dimensionless length, being L = 0 the top of the packed bed and L =1, the bottom of the packed bed. Regeneration temperature is 230°C. Pentane mole fraction at the end of the regeneration phase is 0.0462.

Although the regeneration phase lasts 6 hours, by t = 13.4 hours the regeneration of the bed is complete.

4.2.5 Concentrations

Figures 4.31, 4.32, 4.33 and 4.34 present how the concentration of each component varies with time, during the regeneration phase of the packed bed. The analysis of the concentration plots is similar to the analysis of the mole fraction plots. The difference lies in the relationship given by Equation 4.1, previously presented. For each time instant, the concentration of each component is the mole fraction of that component times the global concentration (see Figure 4.30). The global concentration varies mostly due to temperature and composition variation. For t < 12.2 hours, the heavier components are desorbed, while adsorbed water is still heating. Also, the temperature and the compressibility factor are lower when compared to the rest of the regeneration phase. This is true especially at the top of the bed, since the regeneration gas travels upwards. Due

to these factors, the concentration is the highest for t < 12.2 hours. After that, the heavier components have already been desorbed and water starts being recovered. This happens until about t = 13.2 hours. After that, regeneration is complete and the concentration remains constant and equal to the regeneration gas feed concentration.

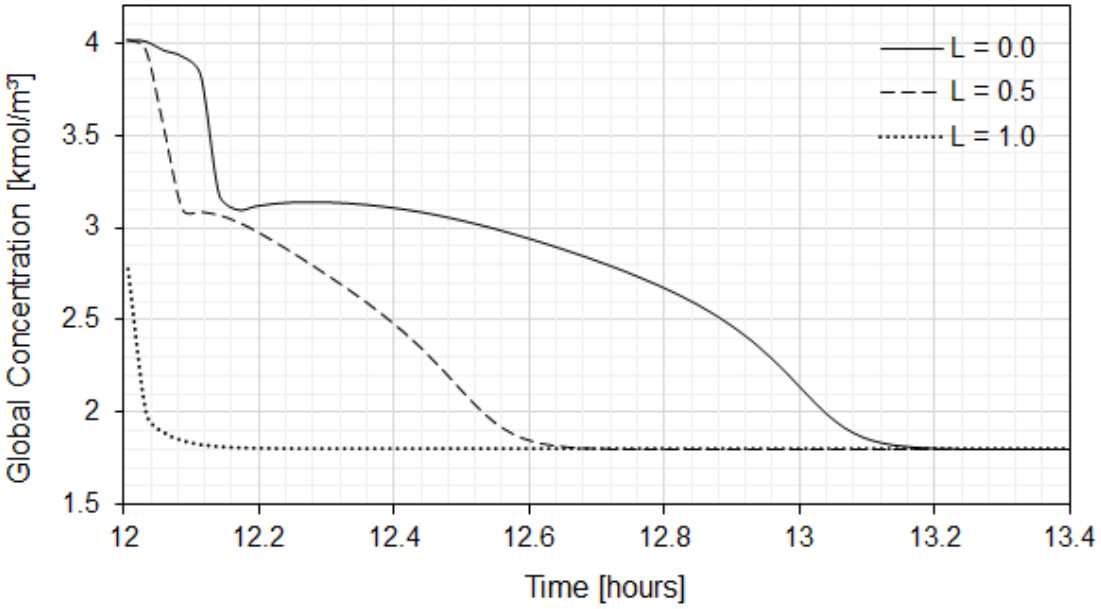

Figure 4.30: Global concentration of gas across packed bed during regeneration interval (t > 12 hours). L is the dimensionless length, being L = 0 the top of the packed bed and L = 1, the bottom of the packed bed. Regeneration temperature is 230°C.

What is observed is that the concentrations of methane, carbon dioxide and pentane closely resemble the global concentration plot. This is because the mole fraction variation of these components with regard to the regeneration gas mole fraction throughout the regeneration phase was quite modest: for methane, the greatest ΔY (maximum $|Y|$ minus Y_r) was less than 0.05, less than 0.05 for carbon dioxide and less than 0.01 for pentane. For water, the greatest ΔY was about 0.1 and Y_{H2O} was very low in the beginning (t < 12.2 hours). For this reason, the concentration of water is more similar to the mole fraction of water plot than to the global concentration plot.

Figure 4.32 is the concentration plot of methane. For t < 12.2 hours, the mole fraction of methane reached a peak of a little more than 0.5. This is why for t = 12.1 hours the concentration of methane reached a value of about 2 kmol/m^3 (half of the global concentration). Similar analysis can be done for the rest of the cycle and for the other components.

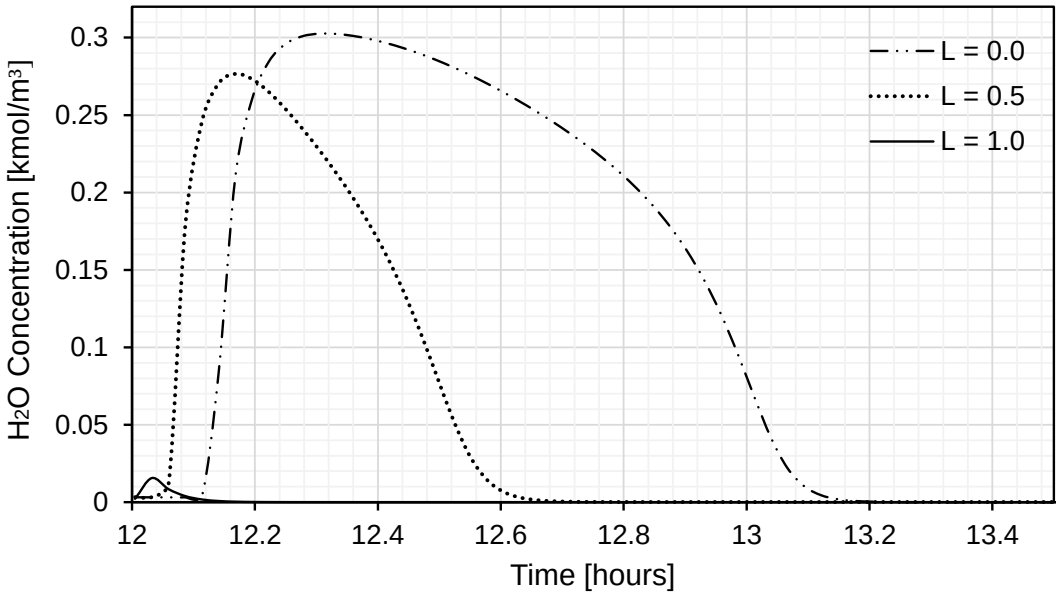

Figure 4.31: Concentration of water across packed bed during regeneration interval (t >12 hours). L is the dimensionless length, being L = 0 the top of the packed bed and L =1, the bottom of the packed bed. Regeneration temperature is 230°C. Water concentration at the end of the regeneration phase is 4.75×10^{-5} kmol m^{-3}.

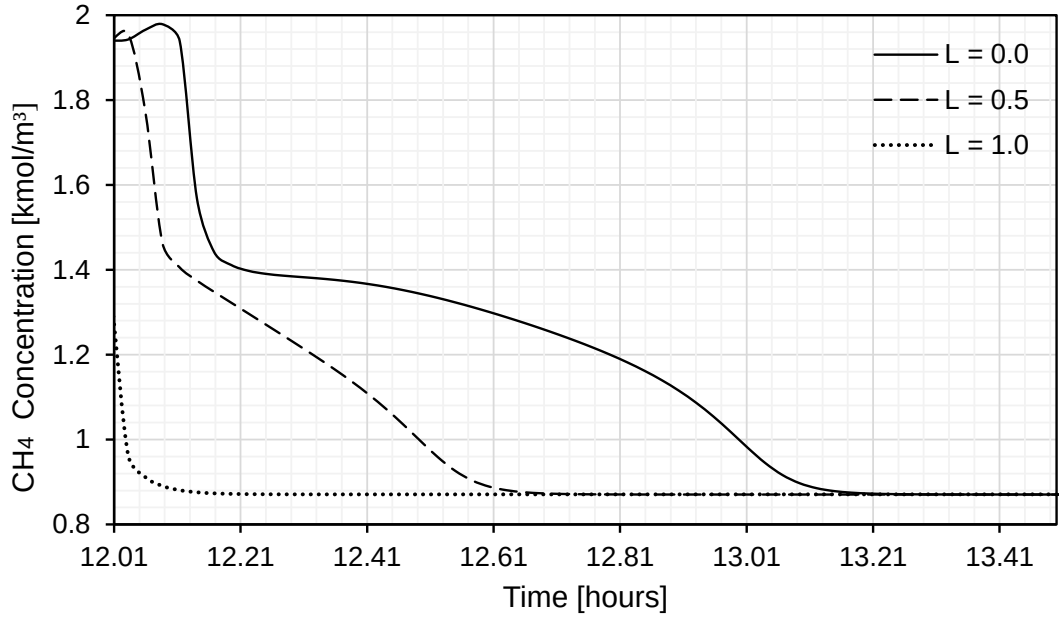

Figure 4.32: Concentration of methane for different axial packed bed axial coordinates during regeneration interval (t > 12 hours). L is the dimensionless length, being L = 0 the top of the packed bed and L =1, the bottom of the packed bed. Regeneration temperature is 230°C. CH_4 concentration at the end of the regeneration phase is 0.8706 kmol m^{-3}.

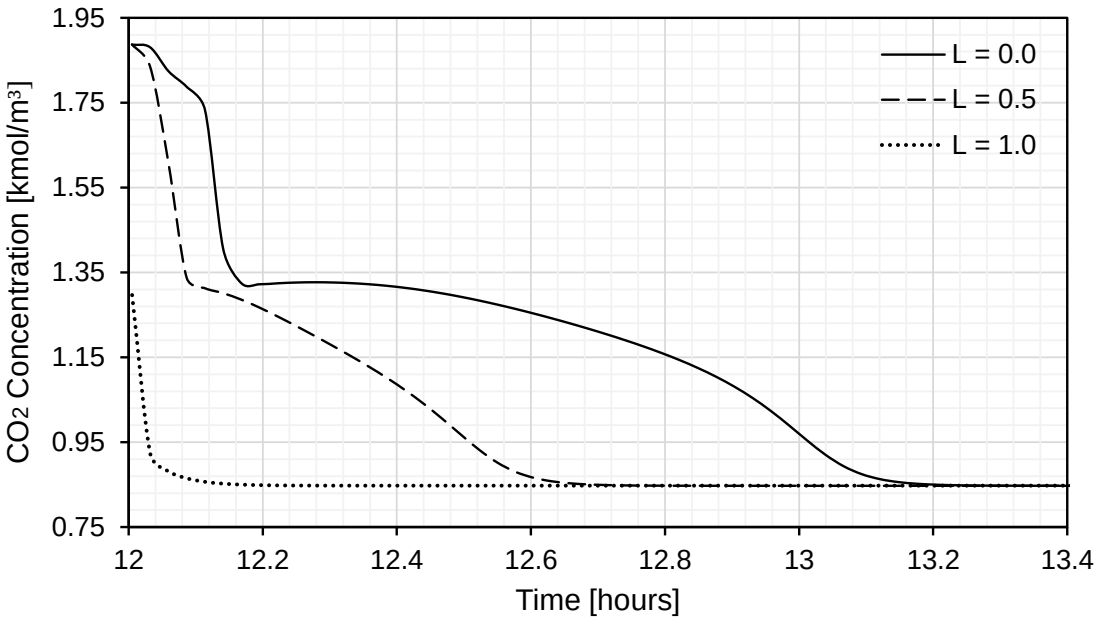

Figure 4.33: Concentration of carbon dioxide for different packed bed axial coordinates during regeneration interval (t > 12 hours). L is the dimensionless length, being L = 0 the top of the packed bed and L =1, the bottom of the packed bed. Regeneration temperature is 230°C. CO_2 concentration at the end of the regeneration phase is 0.8476 kmol m^{-3}.

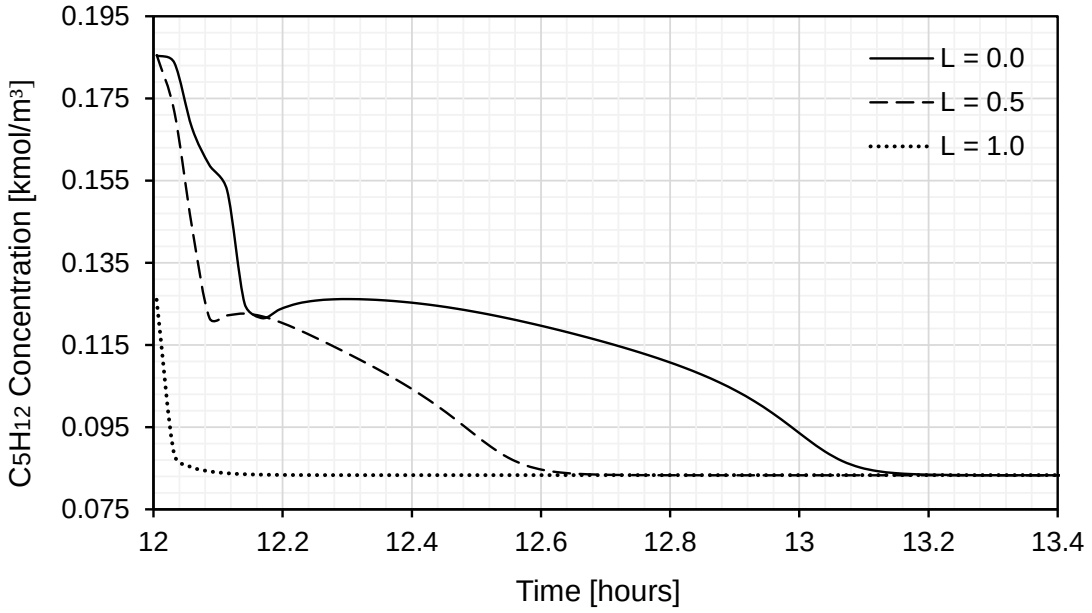

Figure 4.34: Concentration of pentane for different packed bed axial coordinates during regeneration interval (t > 12 hours). L is the dimensionless length, being L = 0 the top of the packed bed and L =1, the bottom of the packed bed. Regeneration temperature is 230°C. C_5H_{12} concentration at the end of the regeneration phase is 0.1855 kmol m^{-3}.

4.2.6 Adsorbed Inventory

Figure 4.35 presents the adsorbed inventory of the packed bed during the regeneration phase (t > 12 hours). The bed enters the regeneration phase (t = 12 hours) with 123.09 kmol of water, 65.50 kmol of carbon dioxide, 58.23 kmol of methane, and 1.07×10^{-19} kmol of pentane (no pentane was adsorbed). Although great part of the CO_2 and CH_4 are desorbed before t = 12.2 hours, Figure 4.35 shows that there is a modest decrease in the inventory of these components until t = 13.2 hours. The number of water moles decreases very slowly before t = 12.2 hours, and after that assumes a steeper, practically linear decrease. At t = 13.4 hours, the desorption process has ended.

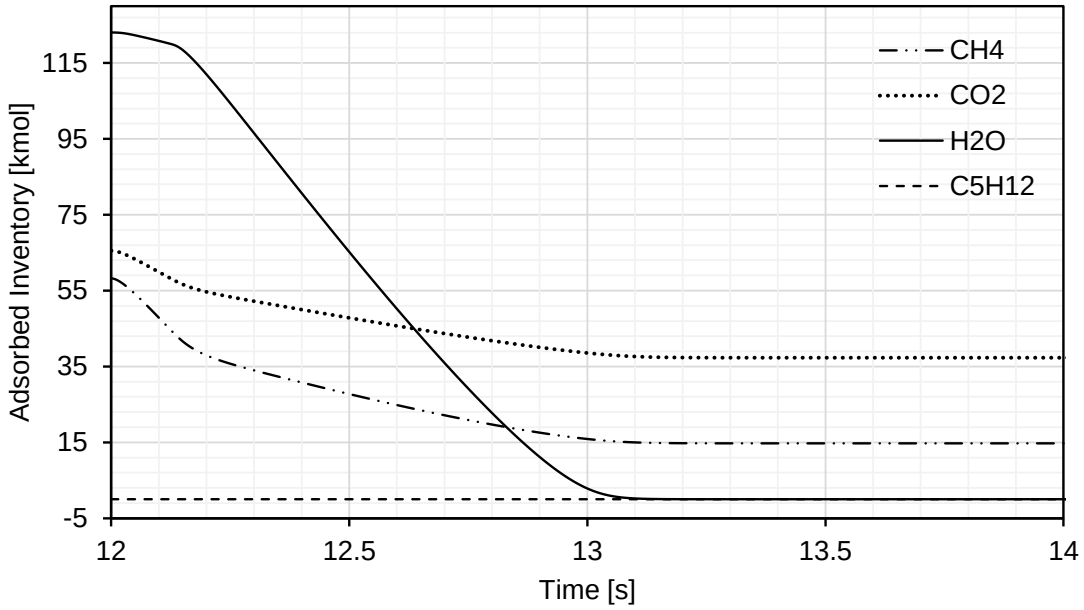

Figure 4.35: Inventory of components adsorbed by packed bed during regeneration phase (t > 12 hours). Final values of each component are, in kmol: N_{CH_4} = 14.748; N_{CO_2} = 37.326; N_{H_2O} = 0.0024; and $N_{C_5H_{12}} = 1.14\times10^{-26}$.

It is important to note that not all of the CH_4, CO_2 and H_2O were desorbed. The adsorbed inventory increases at the end of each TSA cycle so that inevitably a time will come when the molecular sieves have to be replaced. During the GDU's design process, this fact is considered, which is why, during the first cycle, the bed's length and regeneration phase duration seem oversized.

4.2.7 Gas Inventory

Figure 4.36 presents the gas inventory inside the packed bed during the regeneration phase (t > 12 hours). The gas has initially 35.02 kmol of methane, 34.08 kmol of carbon dioxide, 5.23×10^{-2} kmol of water and 3.35 kmol of pentane. The

amounts of CH_4 and CO_2 are initially high because the desorbed components are transferred from the solid phase to the fluid phase. Desorption occurs until t $\approx$ 13.2 hours. For 12.2 < t < 13.2 hours, the gas inventory decreases slowly. For t > 13.2 hours, no more desorption occurs and the gas inventory remains stationary at a value due to the constant regeneration feed flow rate and composition. During 12 < t < 12.2 hours the concentration of water increases because desorption is starting. For t > 12.2 hours, the amount of water decreases slowly as the lower portions of the bed are regenerated. At t $\approx$ 13.2 hours, most of the water has been removed from the bed and regeneration is complete, so the amount of water in the gas inside the packed bed remains constant at a value equal to the value of the regeneration feed stream.

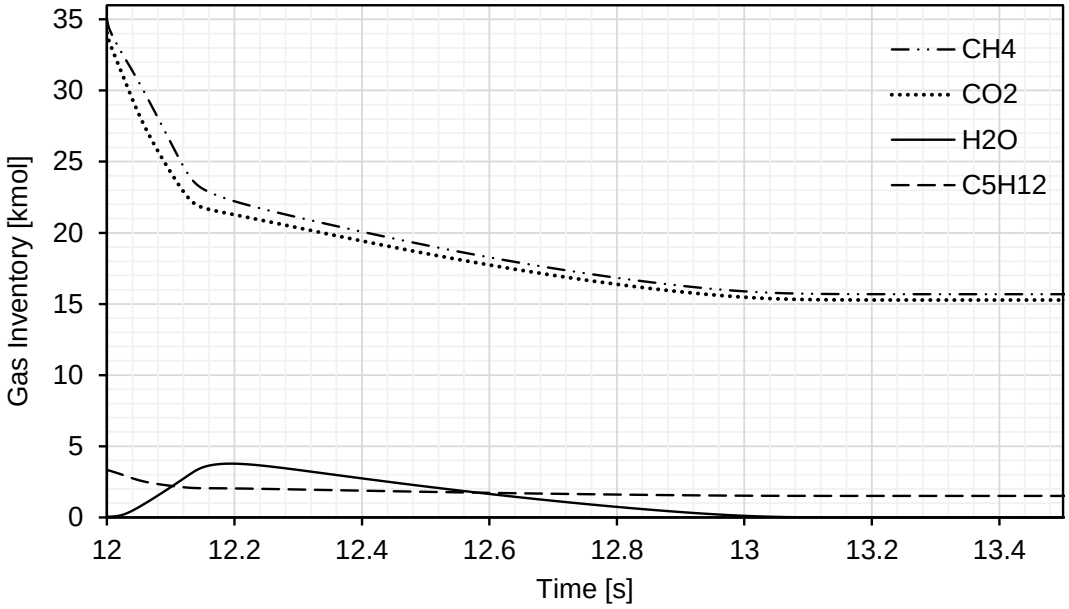

Figure 4.36: Gas phase inventory during regeneration phase (t > 12 hours). Final values of each component are, in kmol: N_{CH_4} = 15.6935; N_{CO_2} = 15.2711; N_{H_2O} = 8.57E-04; and $N_{C_5H_{12}}$ = 1.5011.

4.2.8 Vapor-Liquid Equilibrium and Phase Behavior

During the regeneration phase, since the regeneration gas is at 230°C, the operation point of the plant is drawn away from the phase envelope. This can be observed on Figure 4.37. Initially, the bed is at the temperature resulting from the adsorption phase, which is a little smaller than the feed temperature (as was observed on the results of simulation 1). During this time, condensation occurs. However, the temperature is quickly increased due to the hot regeneration gas being fed from the bottom of the vessel. For this reason, the regeneration

phase is of no concern when it comes to developing a control strategy for reducing condensation. It takes about 6 minutes for the operating point to leave the phase envelope. In a real unit, in which the regeneration gas temperature would take on the form presented in Figure 3.4, this time would be greater, since the temperature is slowly increased linearly.

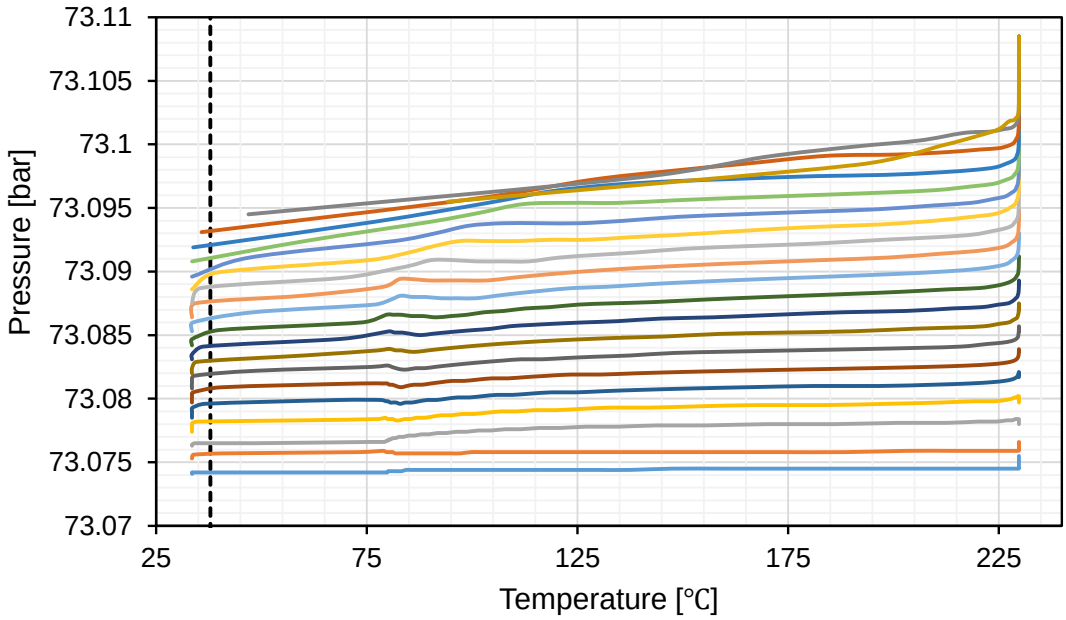

Figure 4.37: Phase behavior for 20 evenly distributed packed bed axial coordinates during regeneration phase (12 hrs < t < 18 hrs). For the process pressure range (73.07 bar < P < 73.11 bar), T_{DEW} is approximately constant and equal to 35.5°C.

4.3 Simulation 3: Two Vessel Adsorption

The complete GDU consists of two molecular sieve adsorption vessels adsorbing in parallel. Figure 4.38 shows the scheme for simulation 3. This simulation was one of the steps towards building the complete unit. The results were similar to those for simulation 1 and will therefore not be presented. The only difference with regard to simulation 1 is that the feed flow rate is 3.7 kmol/s. However, since there are two beds, half of the flow is directed to each.

Even though the results for simulation 3 will not be presented, it was an essential step in order to guarantee suitable initial conditions to simulation 4.

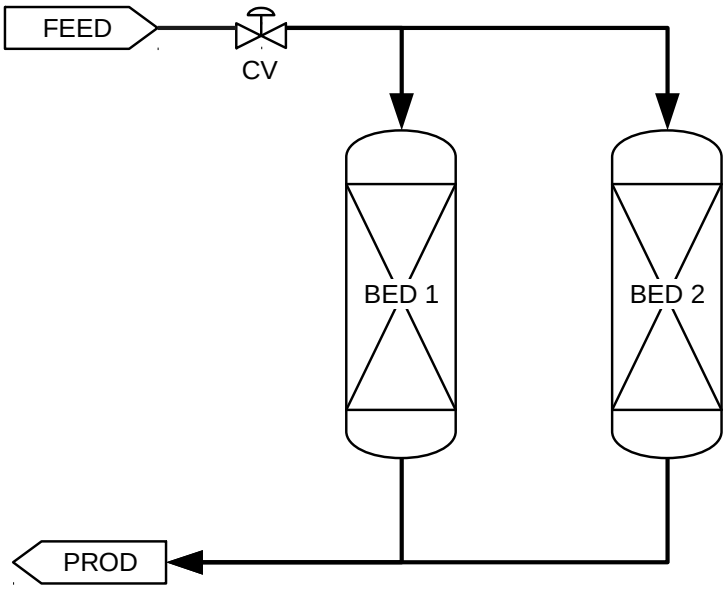

Figure 4.38: Molecular sieve bed regeneration schematic for simulation 3.

4.4 Simulation 4: TSA Cycle of Complete GDU with Typical Control Loops

As mentioned in Chapter 3, the fourth simulation consists of the complete GDU with the typical control loops and TSA cycles. Figure 4.39 shows the schematic used for simulation 4. It can be observed that the simulated unit is similar to the real GDU presented in Chapter 3. However, in Figure 4.39 the control loops of the regeneration feed stream are also presented. The GDU consists of three adsorption vessels (BED 1, BED 2 and BED 3) and a regeneration loop. The regeneration gas is a fraction (approximately 11%) of the dry gas. A flow control loop (FFIC-1) ensures that the flow rate of the regeneration stream will be the desired fraction of the dry gas and a temperature control loop (TIC-1) ensures that the regeneration temperature remains constant at approximately 230°C. The operating conditions for simulation 4 (see Table 4.6) are essentially the same as that of simulation 1.

Since there are two control loops in simulation 4 (FFIC-1 and TIC-1), there are two controllers, one for each loop. Each controller consists of a classical, ideal PI controller, adjusted by trial-and-error.

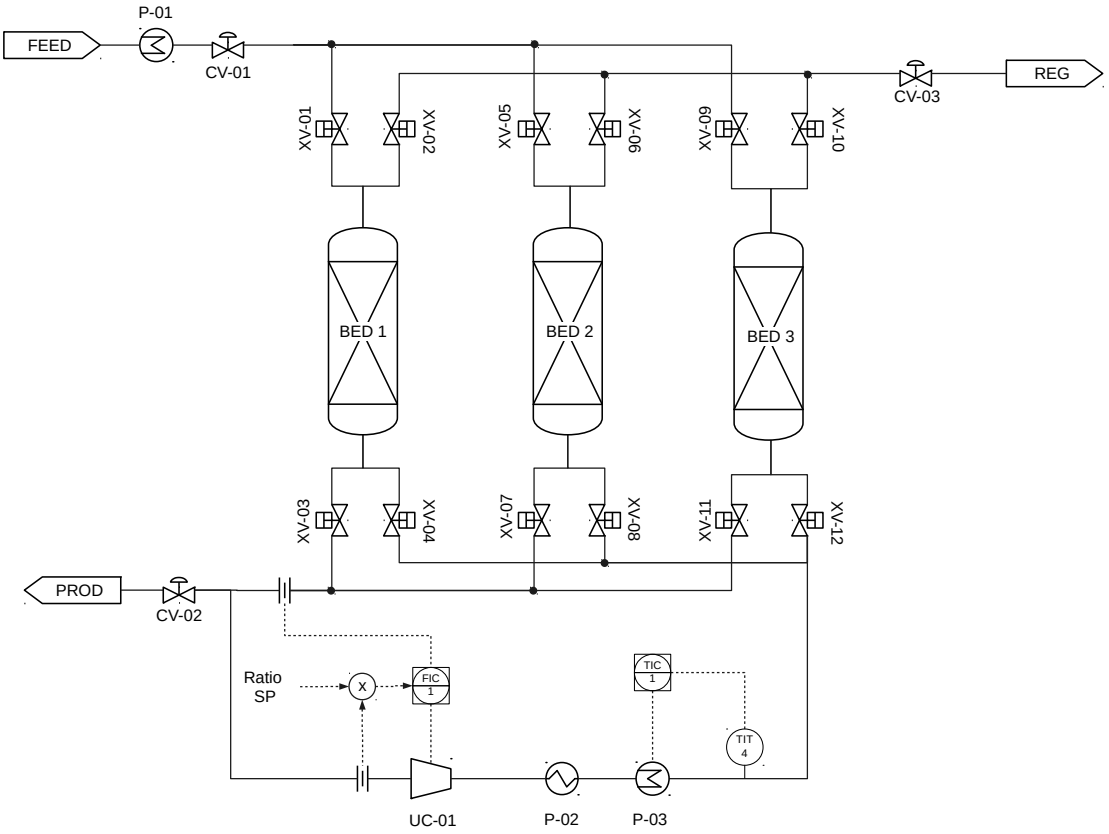

Figure 4.39: Schematic of GDU with typical control loops for simulation 4.

4.4.1 Valve Switching

The on-off valves were added for defining the phase of the cycle in which each bed is in (adsorption / regeneration). The state of the valves (on / off) were scheduled using ADSIM's cycle organizer. The cycle organizer is graphical user interface that generates a script using Task Language. The script contains the times at which each valve status will change and how many times the task is to be repeated, i.e. how many cycles to be simulated. Figures 4.40, 4.41 and 4.42 indicate the state of valves XV-01 through XV-12 for each instant of time.

Figure 4.40 shows the states of on-off valves XV-01, XV-02, XV-03 and XV-04. Each valve assumes the following states throughout the cycle: "1", indicating that the valve is "on" or open (pressure drop across the valve assumes it's smallest value); "0", indicating that the valve is "off" or shut (the pressure drop across the valve assumes it's maximum value). When XV-01/XV-03 are on and XV-02/XV-04 are off, BED 1 is in the adsorption phase. When XV-01/XV-03 are off and XV-02/XV-04 are on, BED 1 is in the regeneration phase. As can be observed, in the beginning of simulation 4 (t < 6 hours), BED 1 is in the adsorption phase. After 6 hours, the valve status switch and BED 1 reaches the regeneration phase (6 hours < t < 12 hours). Six hours later, the valve switches again and BED 1 starts

Table 4.6: Operating conditions for simulation 4

Parameter	Value	Unit	Description
P_f	74.09	bar	Feed stream pressure
P_p	73.07	bar	Product stream pressure
T_f	34.0	°C	Feed temperature
F_f	3.70	kmol/s	Feed stream flow rate
C_{v_i}	5.53	kmol/s/bar	Valve's initial flow coefficient
Y_{CH_4}	0.4830	mol / mol	Molar fraction of CH_4 at feed stream
Y_{CO_2}	0.4700	mol / mol	Molar fraction of CO_2 at feed stream
Y_{H_2O}	0.0008	mol / mol	Molar fraction of H_2O at feed stream
$Y_{C_5H_{12}}$	0.0462	mol / mol	Molar fraction of pentane at feed stream

adsorbing once again. Since adsorption phase takes 12 hours and regeneration, 6 hours, the TSA cycle takes a total of 18 hours. Therefore, Figure 4.40 shows a total of about 5.5 cycles.

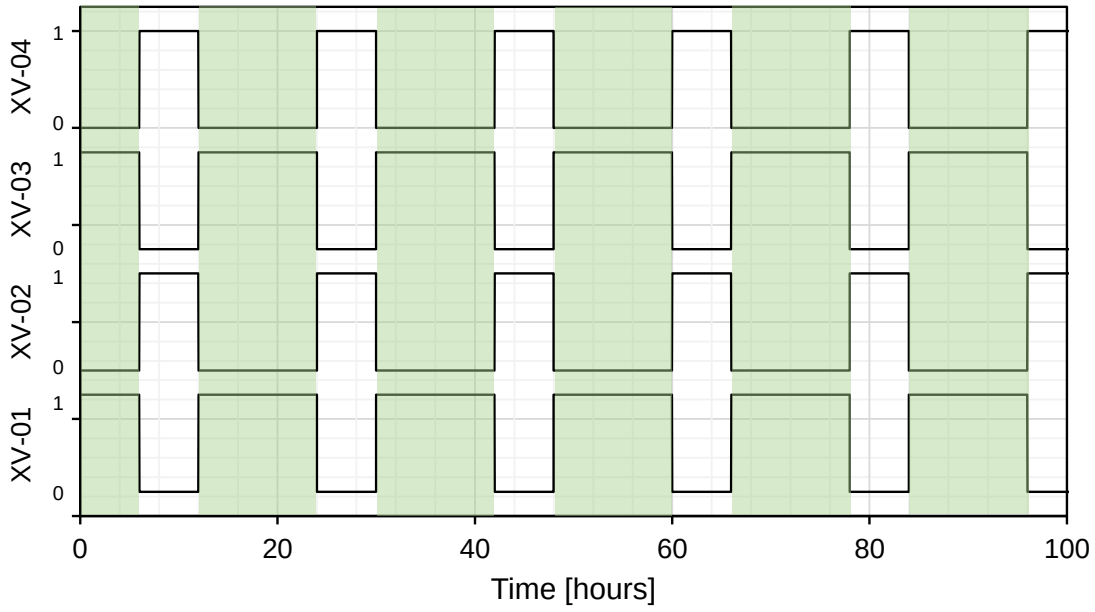

Figure 4.40: State of BED 1 valves: "1" – ON; "0" – OFF. Shaded areas indicate that the vessel is in regeneration mode.

Figure 4.41 shows the states of on-off valves XV-05, XV-06, XV-07, and XV-08. When XV-05/XV-07 are on and XV-06/XV-08 are off, BED 2 is in the adsorption phase. When XV-05/XV-07 are off and XV-06/XV-08 are on, BED 2 is in the regeneration phase. As can be observed, in the beginning of simulation 4 (t < 12 hours), BED 2 is in the adsorption phase. After 12 hours, the valve status switch and BED 2 reaches the regeneration phase (12 hours < t < 18 hours). Six hours later, the valve switches again and BED 2 starts adsorbing once again.

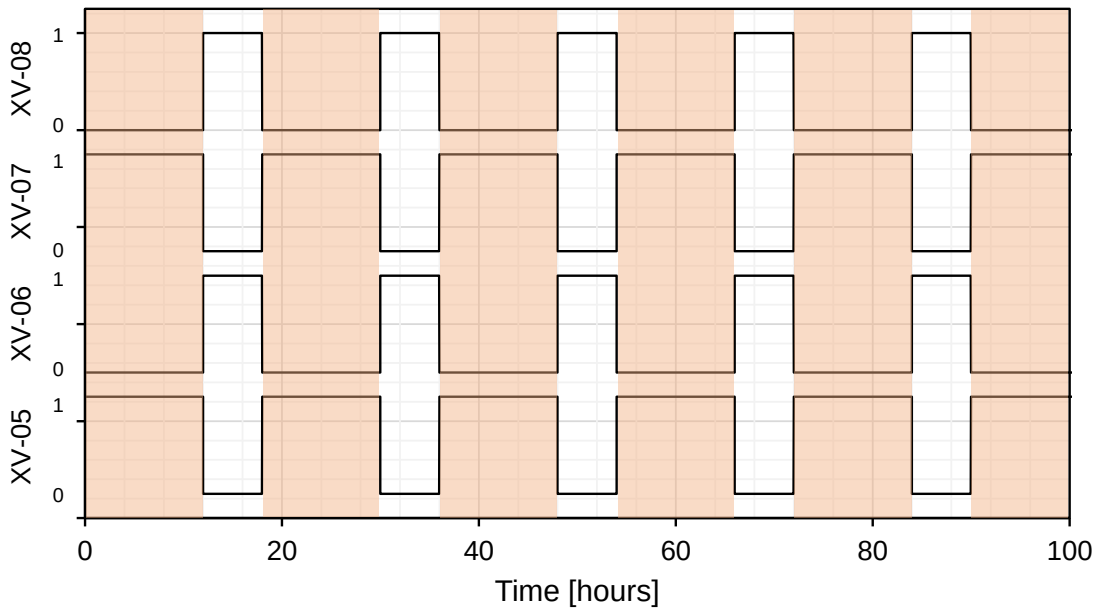

Figure 4.41: State of BED 2 valves: "1" – ON; "0" – OFF. Shaded areas indicate that the vessel is in regeneration mode.

Figure 4.42 shows the states of on-off valves XV-09, XV-10, XV-11, and XV-12, which belong to BED 3. When XV-09/XV-11 are on and XV-10/XV-12 are off, BED 3 is in the adsorption phase. When XV-09/XV-11 are off and XV-10/XV-12 are on, BED 3 is in the regeneration phase. As can be observed, in the beginning of simulation 4 (t < 6 hours), BED 3 is in the regeneration phase. After 6 hours, the valve status switch and BED 3 reaches the adsorption phase (6 hours < t < 18 hours). Twelve hours later, the valves switch again and BED 3 starts regenerating.

The same valve switching task will be used for simulation 5.

4.4.2 Temperature

Since during the TSA cycles each bed is either in adsorption phase or regeneration phase, it is expected that the temperature along each bed oscillates at 34°C or 230°C. The detailed behavior of the temperature along the bed throughout the adsorption and regeneration phase was already examined in simulations 1 and 2. Now, the overall behavior is studied for a whole TSA cycle. Figure 4.43 presents the temperature of gas at three bed lengths (L = 0.0, L = 0.5 and L = 1.0) for each bed during the first TSA cycle of Simulation 4. For t > 18 hours the behavior was periodic, so only the first cycle was shown for better viewing.

The first plot corresponds to the temperature of BED 3. As was noted by observing the valve status plot, BED 3 starts simulation 4 in the regeneration

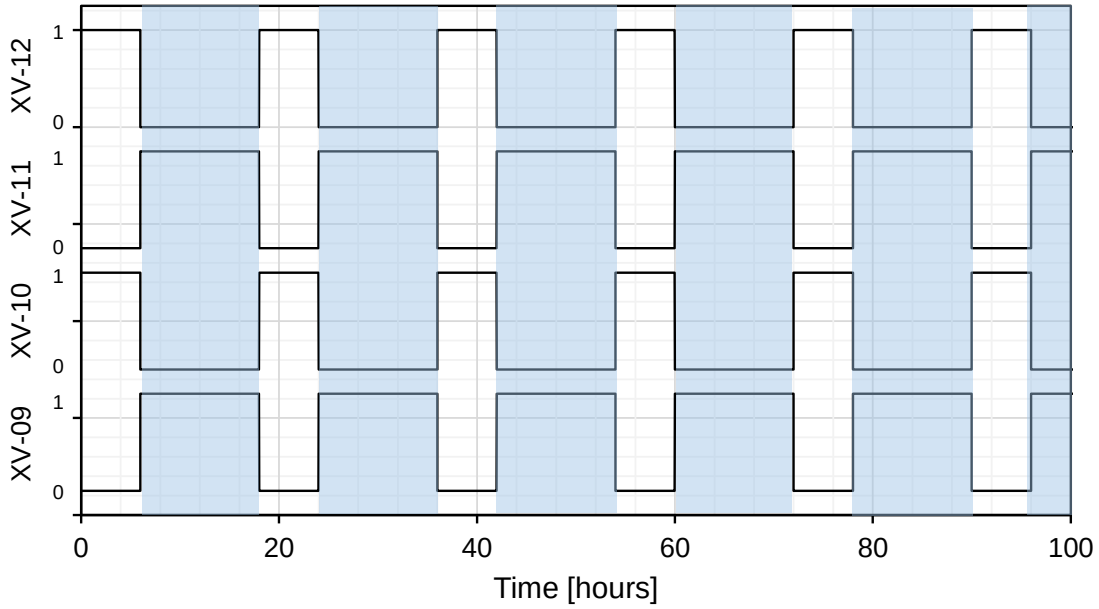

Figure 4.42: State of BED 3 valves: "1" – ON; "0" – OFF. Shaded areas indicate that the vessel is in regeneration mode.

phase. Throughout the first six hours, the bed's temperature is approximately constant and equal to 230.5°C, the regeneration temperature. At t = 6 hours, the valves switch and BED 3 enters the adsorption phase, where it remains until the end of the cycle (t < 18 hours). The temperature at L = 0.0 changes almost immediately to the adsorption feed stream temperature (34°C), since the feed stream enters the bed from the top. The cooling lakes longer to occur at L = 0.5 and even longer at the bottom of the bed (L = 1.0), as was expected. The whole bed takes about 20 minutes to be cooled. The temperature during most of the adsorption phase is approximately 33.6°C.

The second plot corresponds to the temperature of BED 1. It was noted that BED 1 starts simulation 4 in the adsorption phase, where it remains for the next six hours. During this time interval, the bed's temperature is approximately constant and equal to 33.6°C. At t = 6 hours, the valves switch and BED 1 enters the regeneration phase, where it remains for another six hours. As expected, the temperature rises first at the bottom of the bed, following L = 0.5 and L = 0.0. Since regeneration gas is fed from the bottom of the bed, the temperature at L = 1.0 changes almost immediately to the regeneration feed stream temperature. The heating lakes longer to occur at L = 0.5 and even longer at the top of the bed (L = 0.0). The heating of the whole bed from adsorption temperature to regeneration temperature takes about 40 minutes.

Finally, the third plot in Figure 4.43 is the temperature at BED 2. This bed also started the simulation in the adsorption phase. After 12 hours, the valves

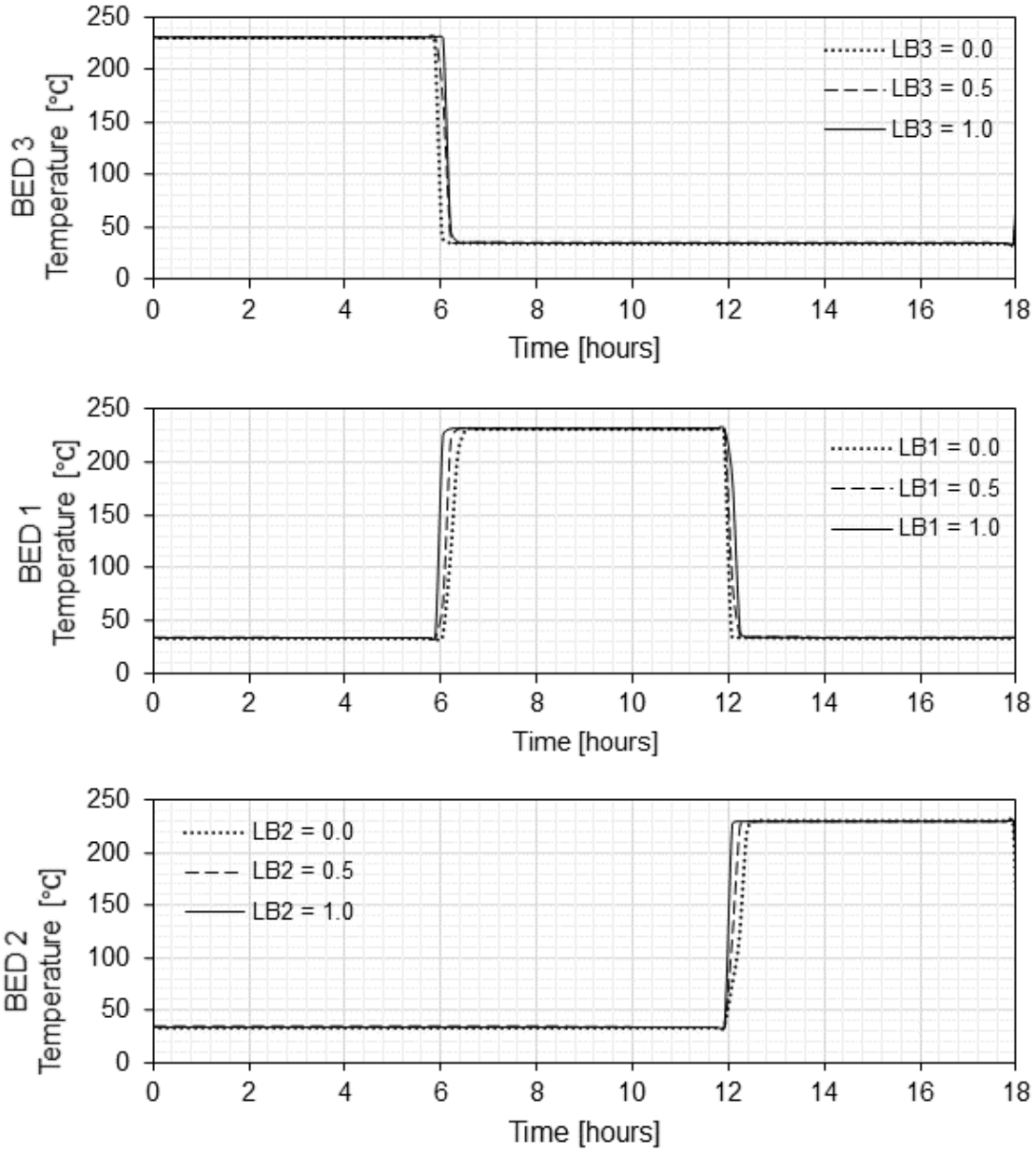

Figure 4.43: Temperature of gas along packed bed during the first TSA cycle of Simulation 4.

switch and BED 2 enters the regeneration phase. Since bed dynamics are the same, it takes about 40 minutes to heat the whole bed. The bottom of the bed (L = 1.0) is heated almost immediately, followed by L = 0.5 and L = 0.0.

4.4.3 Pressure

Figure 4.44 presents the pressure along the packed beds during the first TSA cycle of Simulation 4.

For t < 6 hours, BED 3 is regenerating while BED 1 and BED 2 are in the

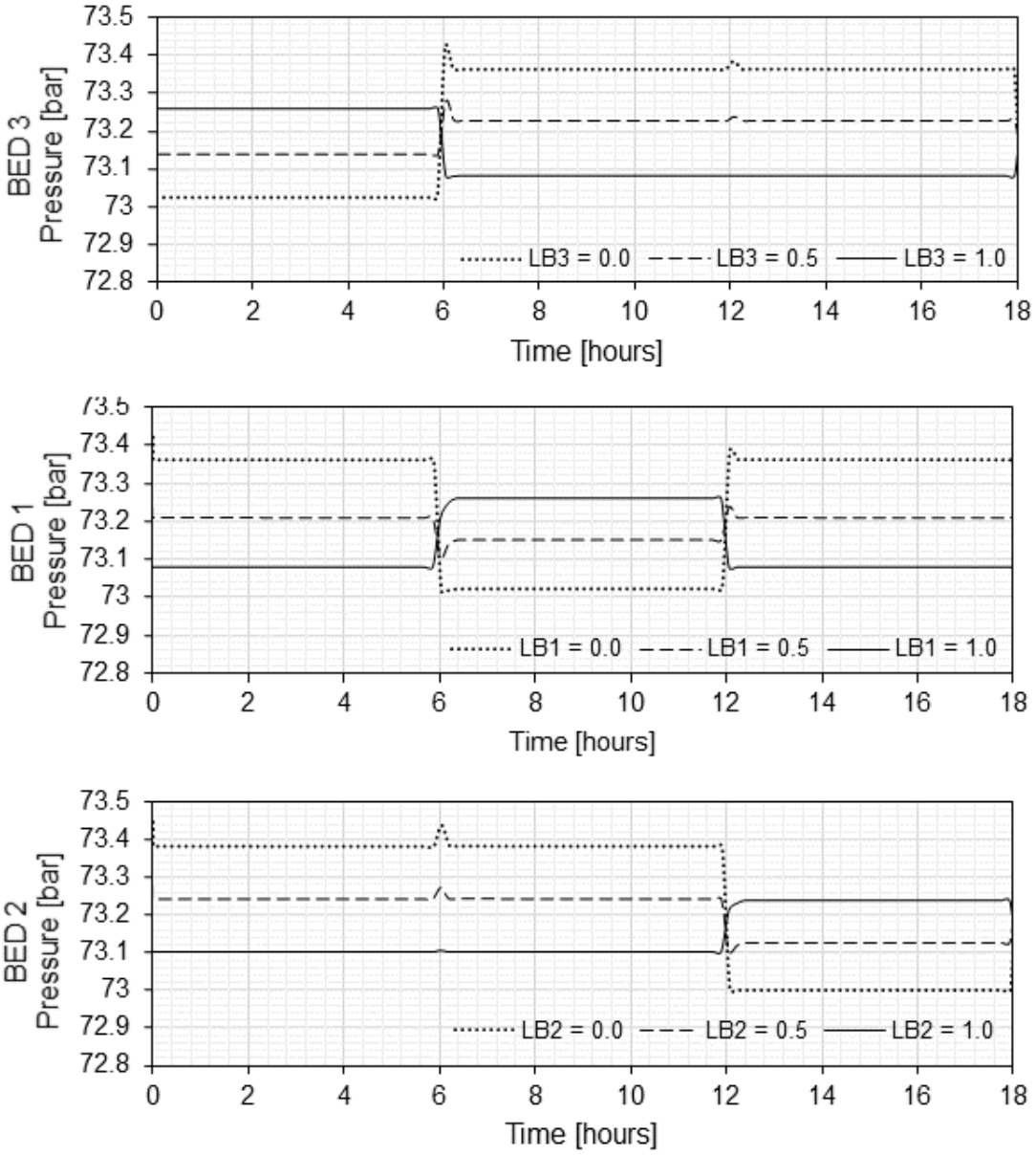

Figure 4.44: Pressure along packed bed during the first TSA cycle of Simulation 4.

adsorption phase. During adsorption, it was seen from the analysis of simulation 1 that the pressure is greater at the top of the bed and smaller at the bottom. For this reason, the gas flows from the top to the bottom. This can be observed from the plots for BED 1 and BED 2. During regeneration, gas flows from the bottom to the top of the bed, which means that the pressure is greater at the bottom than at the top. This can be observed on the first plot, corresponding to BED 3.

Since the pressure profile is linear along the bed and varies little during most of the cycle, the curves for L = 0.0, L = 0.5 and L = 1.0 are practically constant and similar during each phase. Small peaks appear at the top and middle of the

beds every six hours due to valve switching. Since the boundary condition of the Ergun equation is the pressure at the end of the bed, this is not observed for L = 1.0.

4.4.4 Gas Velocity

Figure 4.45 presents the velocity of gas along packed bed during the first TSA cycle of Simulation 4. Since from the adsorption phase to the regeneration phase the gas changes direction, the TSA cycle phase can be clearly identified from Figure 4.45, by observing the times when the gas velocity changes signal. Since gas velocity is related to the axial pressure gradient, when the bed switches between adsorption and regeneration phase, the pressure at the end of the bed L = 1.0 changes in from the product header pressure to the regeneration gas header pressure, almost instantly, in a step like manner. For this reason, a gas velocity peak appears at the bottom of the bed, similar to an impulse response. Since there is a small pressure variation every six ours even for the beds that do not switch, there is also a peak at the velocity at the same beds.

The first plot in Figure 4.45 corresponds to the gas velocity at BED 3. As is already known, this bed starts simulation 4 in the regeneration phase. It can be observed that the gas velocity is initially negative. During the regeneration phase, the absolute average values of the velocities at L = 0.0, L = 0.5 and L = 1.0 for BED 3 are, respectively, 0.118149 m/s, 0.117959 m/s, and 0.1178 m/s. After t = 6 hours, the gas velocity becomes positive, because gas starts flowing in from the top of the bed for adsorption. At t = 6.34 hours, a maximum value of 0.0869 m/s is reached at L = 1.0. At t = 6.03 hours, a maximum value of 0.1325 / is reached at L = 0.5. During the adsorption phase, the absolute average values of the velocities at L = 0.0, L = 0.5 and L = 1.0 for BED 3 are, respectively, 0.0864 m/s, 0.0871 m/s, and 0.0874 m/s.

The second plot corresponds to the gas velocity at BED 1. This bed starts simulation 4 in the adsorption phase. It can be observed that the gas velocity is initially positive, becomes negative after t = 6 hours (regeneration phase), and positive again, after t = 12 hours. During the adsorption phase, the absolute average values of the velocities at L = 0.0, L = 0.5 and L = 1.0 for BED 1 are, respectively, 0.0863 m/s, 0.0873 m/s, and 0.0874 m/s. During the regeneration phase, the absolute average values of the velocities at L = 0.0, L = 0.5 and L = 1.0 for BED 1 are, respectively, 0.1182 m/s, 0.1180 m/s, and 0.1178 m/s. After t = 12 hours, the gas velocity becomes positive after regeneration. At t = 12.07 hours, a maximum value of 0.1390 m/s is reached at L = 1.0. At the same time, a maximum value of 0.1038 / is reached at L = 0.5.

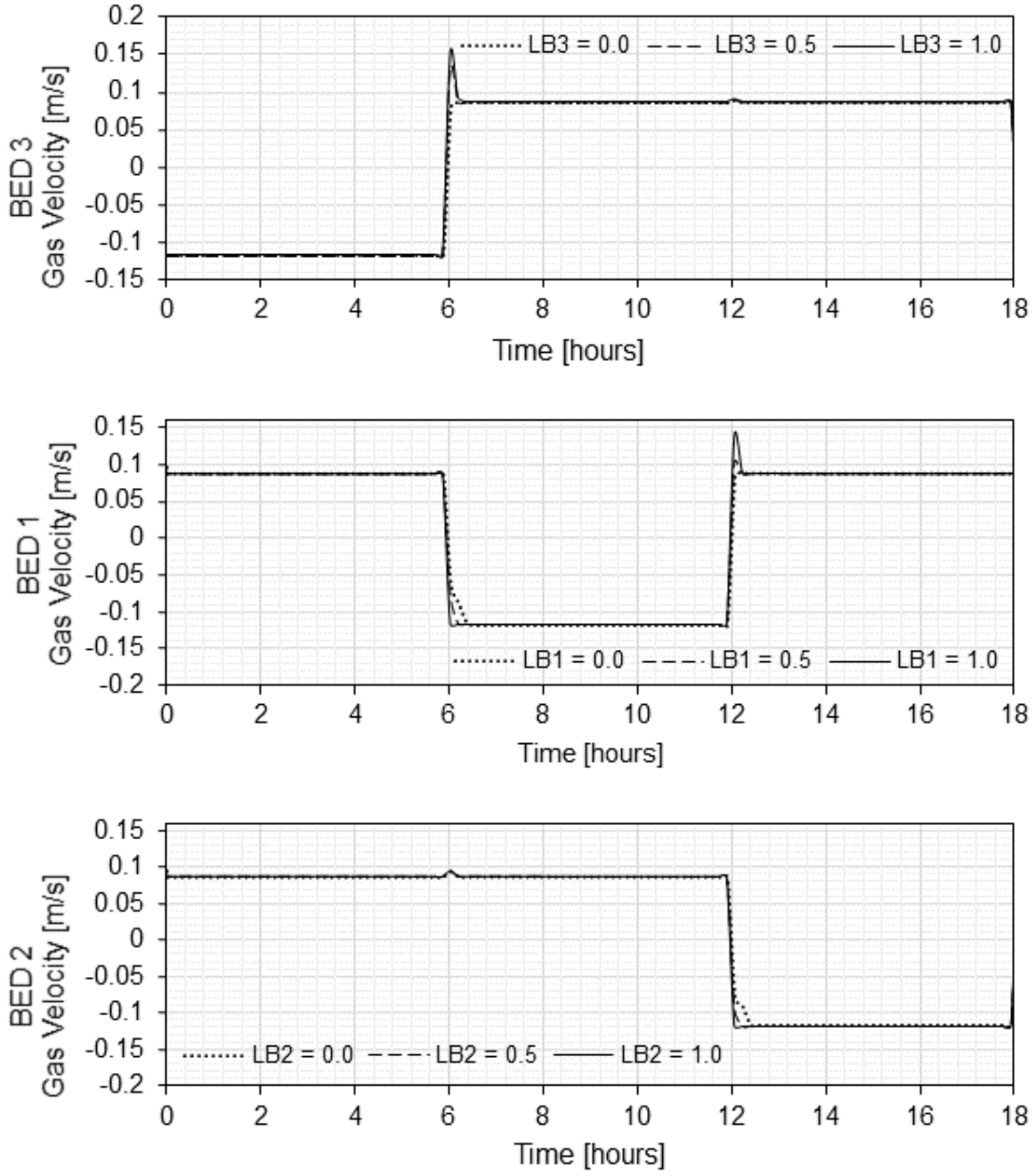

Figure 4.45: Gas velocity along packed bed during the first TSA cycle of Simulation 4.

The last plot corresponds to the gas velocity at BED 2. This bed starts simulation 4 in the adsorption phase. The gas velocity is positive until t = 12 hours, when it enters the regeneration phase. During the adsorption phase, the absolute average values of the velocities at L = 0.0, L = 0.5 and L = 1.0 for BED 2 are, respectively, 0.0863 m/s, 0.0871 m/s, and 0.0873 m/s. During the regeneration phase, the absolute average values of the velocities at L = 0.0, L = 0.5 and L = 1.0 for BED 2 are, respectively, 0.1182 m/s, 0.1180 m/s, and 0.1178 m/s.

4.4.5 Mole Fractions

Figure 4.46 presents the mole fraction of water along each packed bed during the first TSA cycle of Simulation 4.

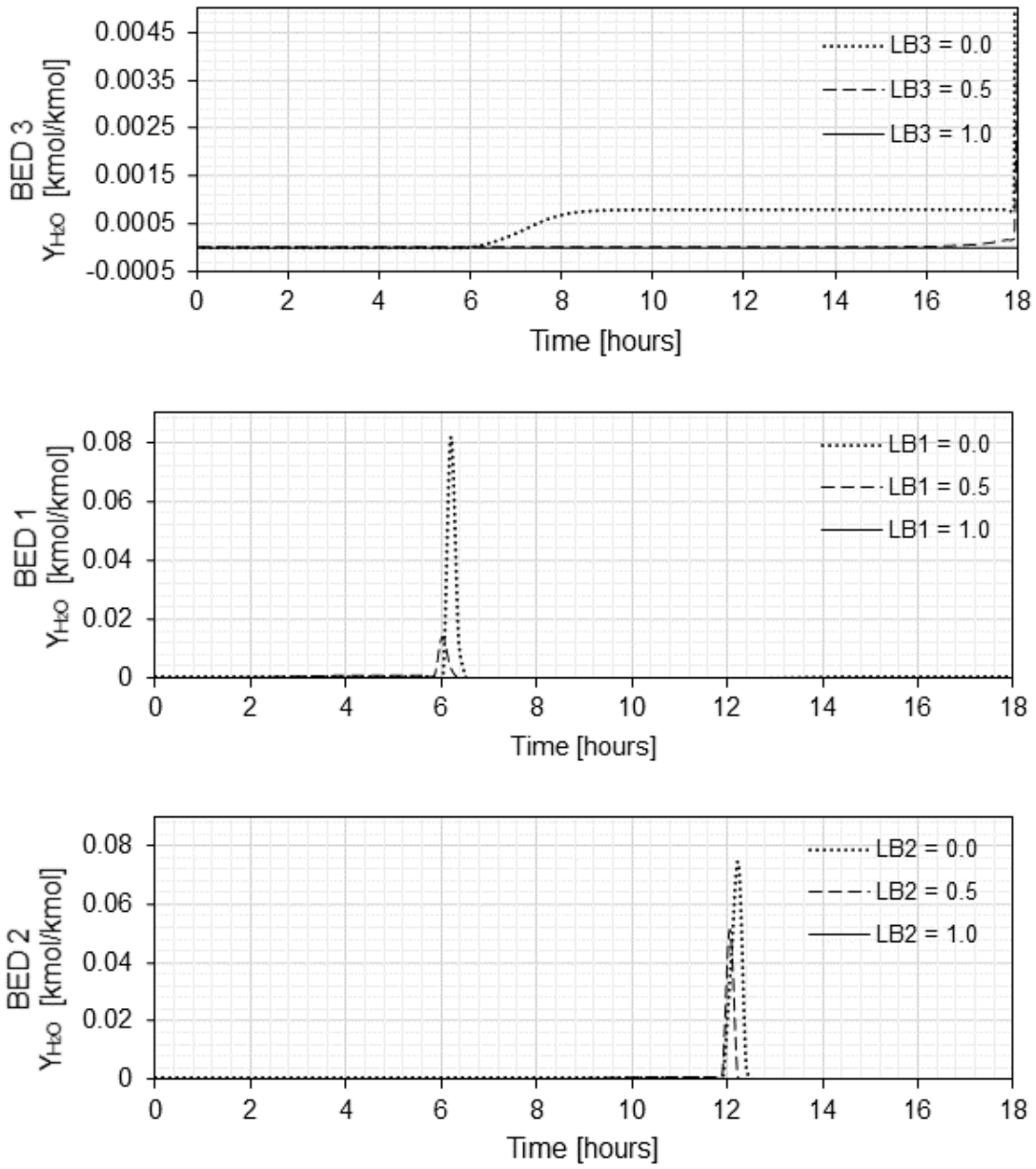

Figure 4.46: Mole fraction of water along packed beds during the first TSA cycle of Simulation 4.

The first plot presented on Figure 4.46 is the mole fraction of water on the gas inside BED 3. Since initially the composition of the gas inside the bed was only methane and it started the TSA cycle in the regeneration phase, the mole fraction of water is 1.7065×10^{-9} throughout the whole bed, which was the initial composition of the regeneration header. This is considered dry gas, since the mole fraction of water is below the cut (1.0×10^{-4}). At t = 6 hours, the valves

switch and BED 3 enters the adsorption phase. The mole fraction of water starts to increase. Since gas is fed from the top, this portion of the bed (L = 0.0) saturates first (after 8.5 hours) at a value of 0.0008, which is the feed stream composition. The mole fraction of H_2O takes longer to increase at the rest of the bed, as can be observed at L = 0.5 and L = 1.0. At the end of the adsorption phase, the mole fraction of water in the gas at L = 0.5 is 0.0002 and at L = 1.0 is L = 1.71×10^{-9}. This means that the at the end of the adsorption phase, the mass transfer zone (MTZ) still has not reached the end of the bed.

The second plot on Figure 4.46 is the mole fraction of water on the gas inside BED 1. BED 1 started the TSA cycle in the adsorption phase. The mole fraction of water is initially 0, but as soon as the simulation starts it rises to 0.0008 at L = 0.0 (top of the bed), which is the composition of the feed stream. At the end of the adsorption phase, the mole fractions at L = 0.0, L = 0.5 and L = 1.0 are, respectively, 0.0008, 0.0008 and 2.7491 $\times 10^{-9}$. At t = 6 hours, BED 1 enters the regeneration phase, so peaks of water can be observed at L = 0.5 (Y_{H_2O} = 0.0139) and at L = 0.0 (Y_{H_2O} = 0.0819) for t = 6.20 hours. These peaks are smaller than the peaks presented for the mole fraction of water in Figure 4.26, for simulation 2. This is because in simulation 2, the bed started with an adsorbed inventory of 23.09 kmol of water, while in this case, BED 1 has started with 58.70kmol. At t = 7.01 hours, it can be considered that the whole bed has been regenerated, since Y_{H_2O} = 1.5918 $\times 10^{-9}$ for L = 0.0, L = 0.5 and L = 1.0. The regeneration phase ends at t = 12 hours and BED 1 enters, once again, the adsorption phase.

The last plot on Figure 4.46 is the mole fraction of water on the gas inside BED 2. BED 2 started the TSA cycle in the adsorption phase and remained in it for 12 hours (one full adsorption phase). The mole fraction of water is initially 0, but as soon as the simulation starts it rises to 0.0008 at L = 0.0 (top of the bed), which is the composition of the feed stream. At the end of the adsorption phase, the mole fractions at L = 0.0, L = 0.5 and L = 1.0 are, respectively, 0.0008, 0.0008 and 2.31 $\times 10^{-9}$. At t = 12 hours, BED 2 enters the regeneration phase, so peaks of water can be observed at L = 0.5 (Y_{H_2O} = 0.0511) and at L = 0.0 (Y_{H_2O} = 0.0740) for t = 12.23 hours. Although BED 2 has remained in the adsorption phase for twice the time of BED 1, the peaks have approximately the same sizes because BED 2 started with an adsorbed inventory of 23.50 kmol of water. At t = 13.04 hours, it can be considered that the whole bed has been regenerated, since Y_{H_2O} = 1.44×10^{-9} for L = 0.0, L = 0.5 and L = 1.0.

Figure 4.47 is the mole fraction of methane along each packed bed during the first TSA cycle of Simulation 4.

The first plot presented on Figure 4.47 is the mole fraction of methane on the gas inside BED 3. The initial mole fraction of CH_4 in BED 3 is 0.4834 throughout

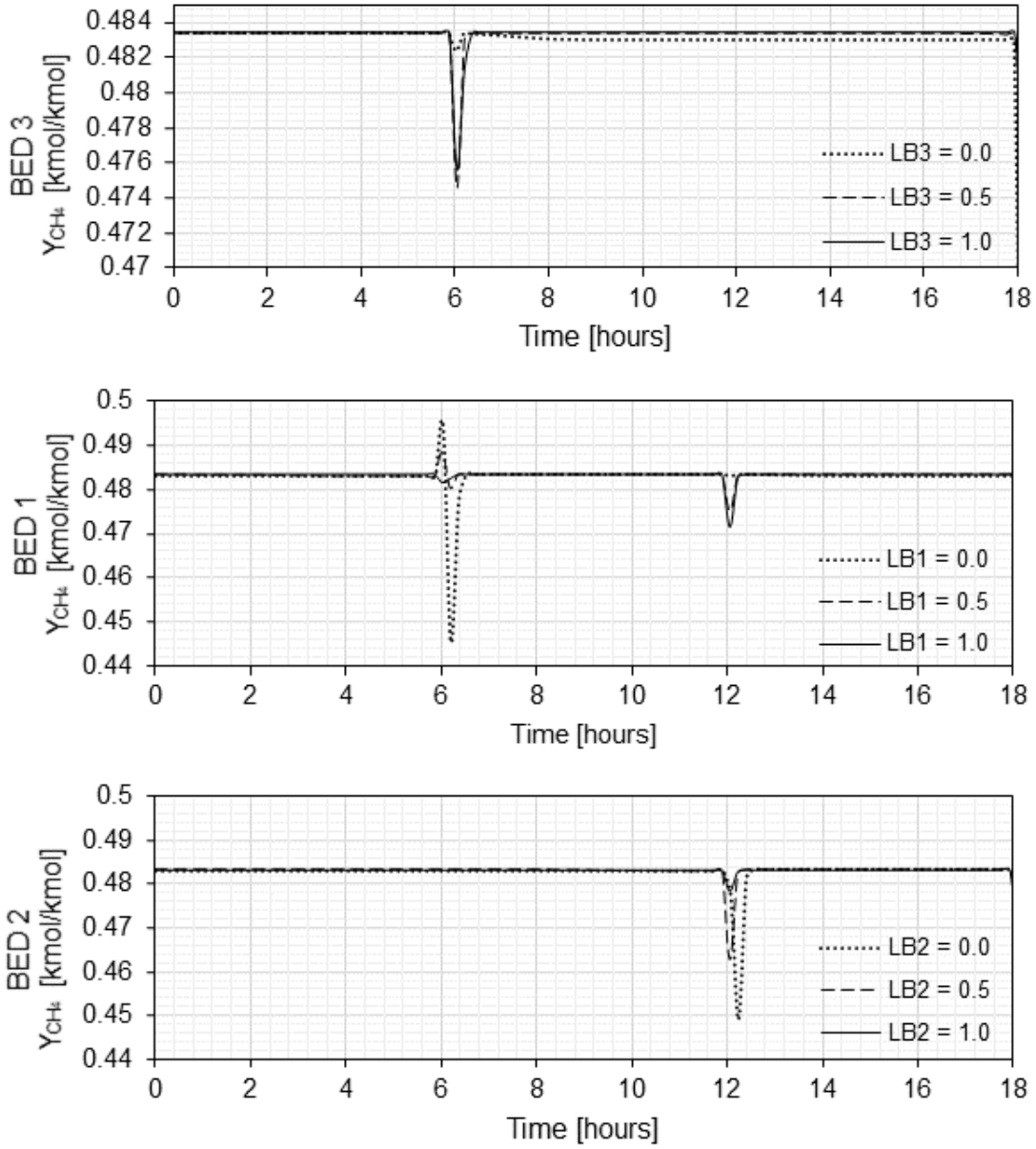

Figure 4.47: Mole fraction of methane along packed bed during the first TSA cycle of Simulation 4.

the whole bed, which was the initial composition of the regeneration header. At t = 6 hours, the valves switch and BED 3 enters the adsorption phase. There is a quick adsorption of methane, which causes a reduction of the mole fraction of this component in the gas. However, the bed becomes saturated with CH_4 in less than half an hour, so Y_{CH_4} rapidly returns to the feed stream composition value. At t = 6.03 hours, the mole fraction of methane at L = 0.5 drops to 0.4746 and at L = 1.0, to 0.4755. For 6 hours < t < 8 hours, the there is an increase in the adsorption of water at the beginning of the bed (L = 0.0). For this reason, there is also a decrease in the mole fraction of methane. After t = 8 hours, the water

adsorption rate becomes constant and the mole fraction of methane stabilizes at a value slightly lower than the feed stream value (Y_{CH_4} = 0.4830) at the beginning of the bed.

The second plot on Figure 4.47 is the mole fraction of methane on the gas inside BED 1. BED 1 started the TSA cycle in the adsorption phase. The mole fraction of methane is initially 0.4834, but as soon as the simulation starts it is reduced to 0.483 at L = 0.0 (top of the bed), due to the quick adsorption of this component. At t = 6 hours, when the bed enters regeneration, the mole fraction for this component suddenly rises due to the recovery of methane and then lowers due to the recovery of water. The peak values reached during regeneration are, for L = 0.0 and L = 0.5, respectively, 0.4944 and 0.4885. No peak was observed for L = 1.0, since the adsorption at that point is very fast. The peak values reached during regeneration for t = 6.03 hours are, for L = 0.0 and L = 0.5, respectively, 0.4944 and 0.4885. No peak was observed for L = 1.0, since the adsorption at that point is very fast. The valley values reached during regeneration at t = 6.36 hours for L = 0.0, L = 0.5 and L = 1.0 are, respectively, 0.4774, 0.4833 and 0.4834. At t = 12 hours, BED 1 enters, once again, the adsorption phase. The mole fraction of methane in the gas drops to 0.4830, 0.4750 and 0.4713 at L = 0.0, L = 0.5 and L = 1.0, due to the fast adsorption of these components.

The last plot on Figure 4.47 is the mole fraction of methane on the gas inside BED 2. BED 2 started the TSA cycle in the adsorption phase and remained in it for 12 hours (one full adsorption phase). At t = 12 hours, BED 2 enters the regeneration phase and valleys of Y_{CH_4} can be observed at t = 12.23 hours for L = 1.0 (Y_{CH_4} = 0.4829), L = 0.5 (Y_{CH_4} = 0.4823) and L = 0.0 (Y_{H_2O} = 0.4491), which happens due to the fast adsorption of this component. The values soon return to feed gas composition since the bed gets saturated.

Figure 4.48 is the mole fraction of carbon dioxide along each packed bed during the first TSA cycle of Simulation 4.

The first plot presented on Figure 4.48 is the mole fraction of carbon dioxide on the gas inside BED 3. The initial mole fraction of CO_2 in BED 3 is 0.4704 throughout the whole bed, which was the initial composition of the regeneration header. At t = 6 hours, the valves switch and BED 3 enters the adsorption phase. There is a quick adsorption of carbon dioxide, but due to the co-adsorption of methane, there is an increase in the mole fraction of this component in the gas. However, the bed becomes saturated with CO_2 and CH_4 in less than half an hour, so Y_{CO_2} rapidly returns to the feed stream composition value. At t = 6.03 hours, the mole fraction of carbon dioxide at L = 0.0 rises to 0.4710, at L = 0.5 to 0.4754, and at L = 1.0, to 0.4743. After t = 8 hours, due to the higher pressure at the top of the bed due to the adsorption phase, the mole fraction of carbon

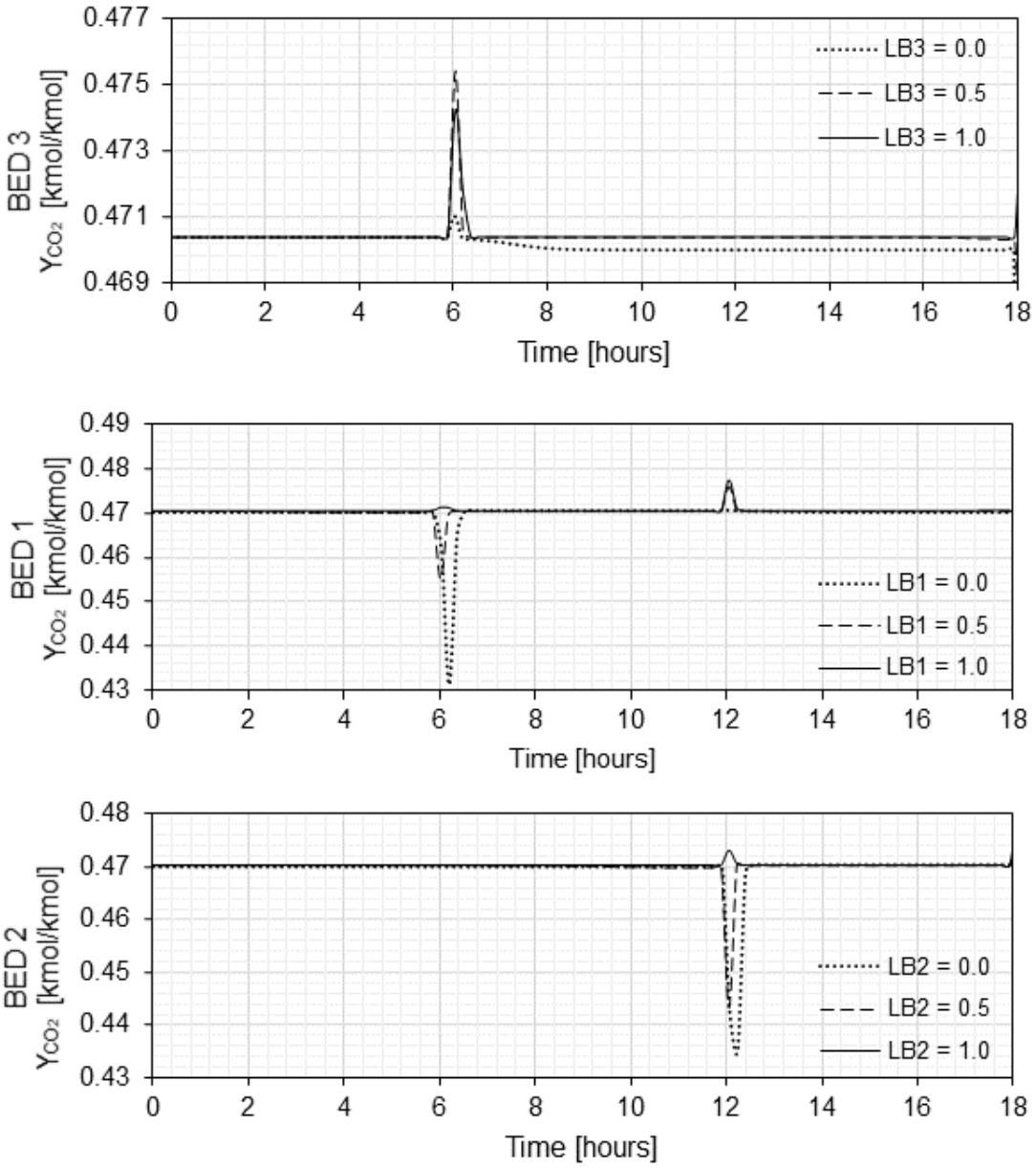

Figure 4.48: Mole fraction of carbon dioxide along packed bed during the first TSA cycle of Simulation 4.

dioxide reduces to 0.4700.

The second plot on Figure 4.48 is the mole fraction of carbon dioxide on the gas inside BED 1. When BED 1 switched from the adsorption phase to the regeneration phase at t = 6 hours, there is a valley in the molar fraction of carbon dioxide due to the increase in the mole water fraction and methane fraction. At t = 6 hours, when the bed enters regeneration, the mole fraction for this component suddenly drops due to the recovery of methane and water. The valley values reached during regeneration are, for L = 0.0 and L = 0.5, respectively, 0.4312 (at t = 6.20 hours) and 0.4550 (at t = 6.03 hours). A small

peak was observed for L = 1.0, since the recovery of CO_2 at that point is very fast (Y_{CO_2} = 0.4711 at t = 6.03 hours). At t = 12 hours, there is an increase in the mole fraction of CO_2 due to the adsorption of methane (Y_{CO_2} = 0.4706 at L = 0.0, 0.4759 at L = 0.5, and L = 0.4774 at L = 1.0, for t = 12.07 hours).

The last plot on Figure 4.47 is the mole fraction of carbon dioxide on the gas inside BED 2. BED 2 started the TSA cycle in the adsorption phase and remained in it for 12 hours (one full adsorption phase). At t = 12 hours, BED 2 enters the regeneration phase and valleys of Y_{CO_2} can be observed at t = 12.23 hours for L = 0.0 (Y_{CO_2} = 0.4351) and at t = 12.07 hours, for L = 0.5 (Y_{CO_2} = 0.4433), which happens due to desorption of methane. At t = 12.07 hours, the regeneration of CO_2 was significant when compared to the other components, so a small peak can be observed (Y_{CO_2} = 0.4732).

Figure 4.49 is the mole fraction of pentane along each packed bed during the first TSA cycle of Simulation 4.

The first plot presented on Figure 4.49 is the mole fraction of pentane on the gas inside BED 3. The initial mole fraction of C_5H_{12} in BED 3 is 0.0462 throughout the whole bed, which was the initial composition of the regeneration header. At t = 6 hours, the valves switch and BED 3 enters the adsorption phase. There is a quick adsorption of carbon dioxide and methane, so the mole fraction of pentane increases. However, the bed becomes saturated with CO_2 and CH_4 in less than half an hour, so $Y_{C_5H_{12}}$ rapidly returns to the feed stream composition value. At t = 6.03 hours, the mole fraction of pentane at L = 0.0 rises to 0.0466, at L = 0.5 to 0.0500, and at L = 1.0, to 0.0502.

The second plot on Figure 4.49 is the mole fraction of pentane on the gas inside BED 1. When BED 1 switched from the adsorption phase to the regeneration phase at t = 6 hours, there is a valley in the mole fraction of pentane due to the increase in the mole fraction of methane. At t = 6 hours, when the bed enters regeneration, the mole fraction for this component suddenly drops due to the recovery of methane and water. The valley values reached during regeneration are, for L = 0.0 and L = 0.5, respectively, 0.0414 (at t = 6.20 hours) and 0.0426 (at t = 6.03 hours). After the phase switching, a peak can be observed for L = 1.0 ($Y_{C_5H_{12}}$ = 0.0473 at t = 6.03 hours). Six hours later, the regeneration phase is over and at t = 12 hours, BED 1 starts adsorbing again. The peaks formed on the mole fraction of pentane (t = 12.07 hours) due to the adsorption of the other components has the following values at L = 0.0, L = 0.5 and L = 1.0, respectively: 0.0464, 0.0491 and 0.0513.

The last plot on Figure 4.49 is the mole fraction of pentane on the gas inside BED 2. BED 2 started the TSA cycle in the adsorption phase and remained in it for 12 hours (one full adsorption phase). At t = 12 hours, BED 2 enters the

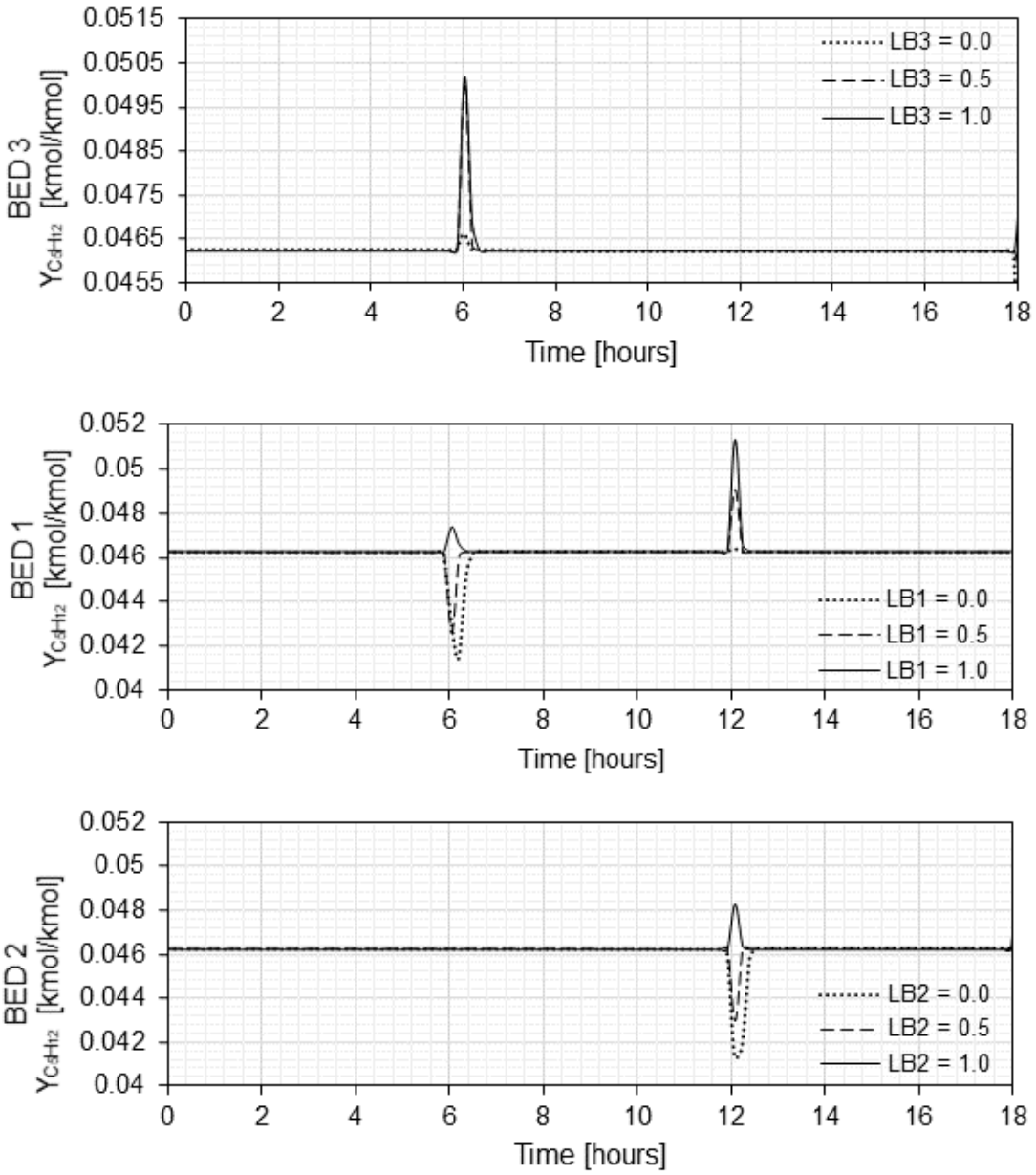

Figure 4.49: Mole fraction of pentane along packed bed during the first TSA cycle of Simulation 4.

regeneration phase and valleys of $Y_{C_5H_{12}}$ can be observed at t = 12.07 hours for L = 0.0 ($Y_{C_5H_{12}}$ = 0.0413) and for L = 0.5 ($Y_{C_5H_{12}}$ = 0.0429), which happens due to desorption of methane. During that same period, a small peak can be observed for L = 1.0 ($Y_{C_5H_{12}}$ = 0.0483).

4.4.6 Concentrations

This section presents how the concentration of each species varies with time along BED 1, BED 2 and BED 3. As mentioned during the analysis of simulation

2, the concentration is related to the mole fraction. The concentration of each component is the global concentration multiplied by the mole fraction of the component. For this reason, the concentration plots assume a shape similar to that of the molar fraction plots.

Figure 4.50 presents the concentration of water along the packed beds during the first TSA cycle of Simulation 4.

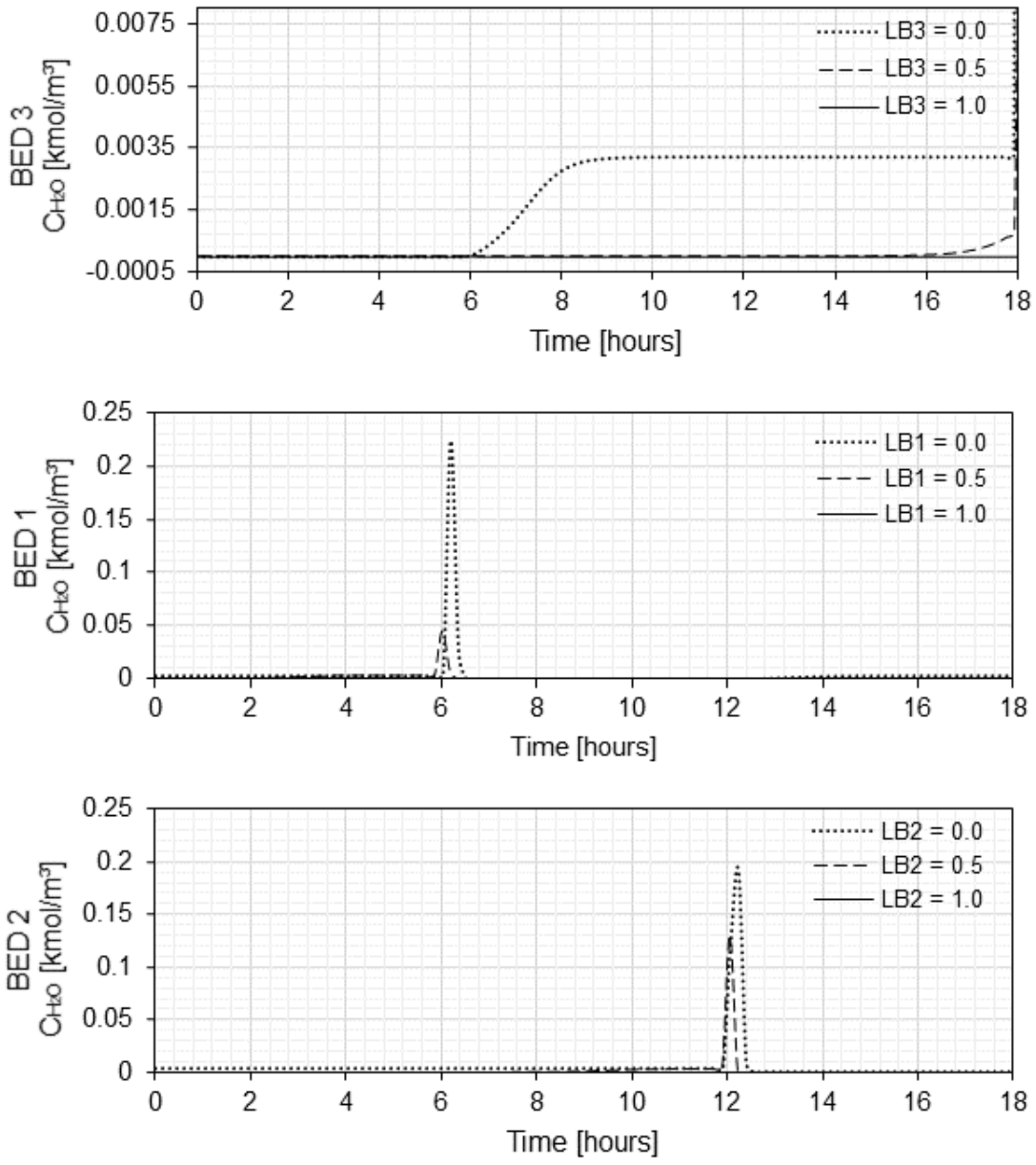

Figure 4.50: Concentration of water along packed beds during the first TSA cycle of Simulation 4.

The first plot in Figure 4.50 is the concentration of water along BED 3. Its value is initially 3.0638×10^{-9} kmol/m^3. At t = 6 hours, the regeneration phase ends and BED 3 starts adsorption. For 6 hours < t < 8 hours, the concentra-

tion of water increases at the top of the bed since that part of the bed saturates first. It then remains constant and equal to the feed stream concentration (C_{H_2O} = 0.0032 kmol/m^3). The half of the bed (L = 0.5) only starts saturating at about t = 16 hours. At the end of the adsorption cycle, the C_{H_2O} increases to 0.0008 kmol/m^3 at L = 0.5. The concentration at the bottom of the bed remains unchanged throughout the TSA cycle.

The second plot in Figure 4.50 is the concentration of water along BED 1. Since in the adsorption phase, the concentration of water rapidly rises to 0.0032 kmol/m^3 at the top of the bed (L = 0.0). At t = 6 hours, BED 1 enters the regeneration phase. Since water is removed from the adsorbent, C_{H_2O} increases until the whole bed is recovered. Since there the MTZ had not reached the bottom of the bed at the end of the adsorption phase, the concentration of water remains constant for L = 1.0 throughout the whole recovery phase. However, the middle of the bed was already saturated, so peaks can be observed in the concentrations at L = 0.0 and L = 0.5 (C_{H_2O} = 0.2240 kmol/m^3 at t = 6.2 hours, and C_{H_2O} = 0.0442 kmol/m^3 at t = 6.03 hours).The regeneration ends at t = 12 hours, when the concentration of water starts to rise again, first at L = 0.0 and afterwards at L = 0.5.

The third plot in Figure 4.50 is the concentration of water along BED2, which stays in the adsorption phase during the next 12 hours in the simulation. As explained for BED 1, peaks can be observed in the concentrations at L = 0.0, L = 0.5 and at L = 1.0: C_{H_2O} = 0.1906 kmol/m^3 at t = 12.2 hours, L = 0.5 C_{H_2O} = 0.1298 kmol/m^3 at t = 12.1 hours, and C_{H_2O} = 2.0458 $\times 10^{-6}$ kmol/m^3 at t = 12.1 hours, respectively.

Figure 4.51 presents the concentration of methane along the packed beds during the first TSA cycle of Simulation 4. The first plot in Figure 4.51 corresponds to the concentration of methane along BED 3. During the regeneration phase, the concentration is approximately 0.8685 kmol/m^3 throughout the bed. At t = 6 hours, regeneration phase ends and adsorption starts. The concentration of methane increases first at the top of the bed, since that is where the the feed gas enters and where the bed saturates first with regard to the adsorption of CH_4. It is then followed by L = 0.5 and L = 1.0. At the end of the adsorption phase, the concentrations are as follows: for L = 0.0, C_{CH_4} = 1.9496 kmol/m^3, for L = 0.5, C_{CH_4} = 1.9344 kmol/m^3, and for L = 1.0, C_{CH_4} = 1.9269 kmol/m^3.

The second plot in Figure 4.51 corresponds to the concentration of methane along BED 1. During the adsorption phase, 0 < t < 6 hours and 12 < t < 18 hours, the concentrations for L = 0.0, L = 0.5 and L = 1.0 are as follows: 1.9496 kmol/m^3, 1.9445 kmol/m^3, and 1.9269 kmol/m^3. During the regeneration phase (6 hours < t < 12 hours), the concentrations for L = 0.0, L = 0.5 and L = 1.0 are as follows:

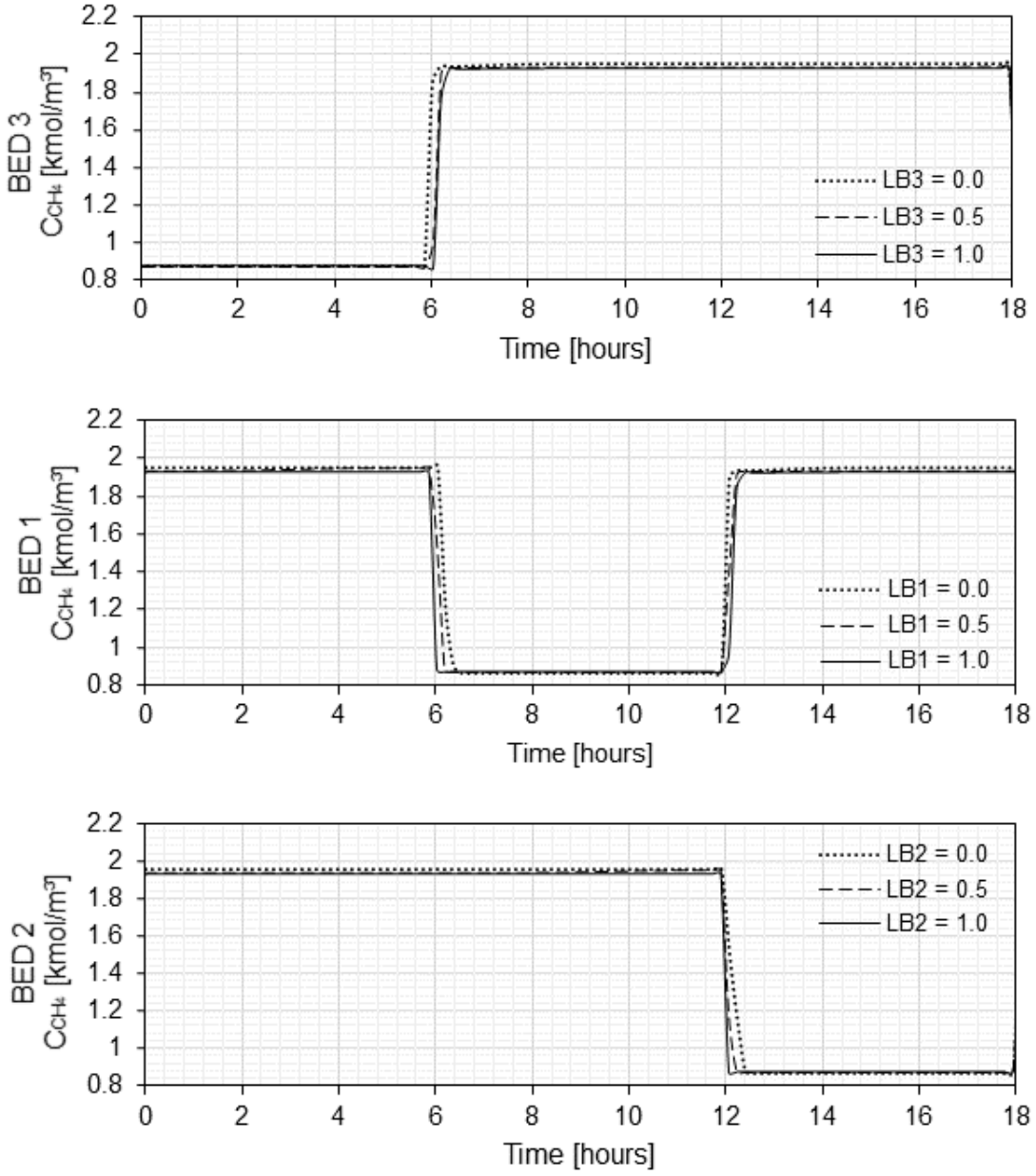

Figure 4.51: Concentration of methane along packed bed during the first TSA cycle of Simulation 4.

0.8684 kmol/m^3, 0.8700 kmol/m^3, and 0.8714 kmol/m^3.

The third plot in Figure 4.51 corresponds to the concentration of methane along BED 2. During the regeneration phase, the adsorption phase ($0 < t < 12$ hours), the concentrations for L = 0.0, L = 0.5 and L = 1.0 are as follows: 1.9496 kmol/m^3, 1.9444 kmol/m^3, and 1.9269 kmol/m^3. During the regeneration phase ($12 < t < 18$ hours), the concentrations for L = 0.0, L = 0.5 and L = 1.0 are as follows: 0.8685 kmol/m^3, 0.8700 kmol/m^3, and 0.8714 kmol/m^3.

Figure 4.52 presents the concentration of carbon dioxide along packed bed during the first TSA cycle of Simulation 4.

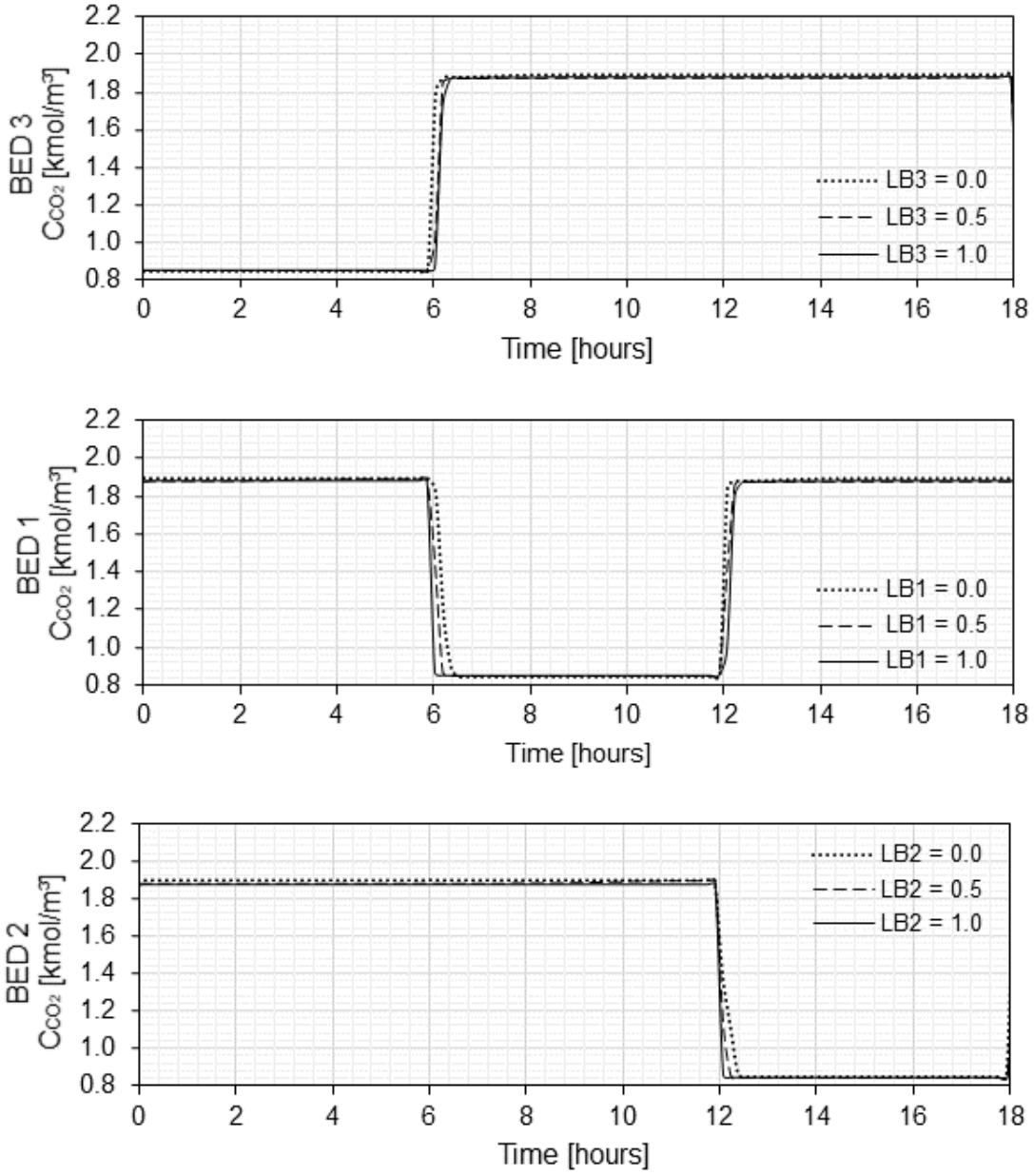

Figure 4.52: Concentration of carbon dioxide along packed bed during the first TSA cycle of Simulation 4.

The first plot in Figure 4.52 corresponds to the concentration of carbon dioxide along BED 3. During the regeneration phase, $0 < t < 6$ hours, the concentrations for L = 0.0, L = 0.5 and L = 1.0 are as follows: 0.8451 kmol/m^3, 0.8464 kmol/m^3, and 0.8480 kmol/m^3. During the adsorption phase ($6 < t < 18$ hours), the concentrations for L = 0.0, L = 0.5 and L = 1.0 are as follows: 1.8750 kmol/m^3, 1.8800 kmol/m^3, and 0.8714 kmol/m^3.

The second plot in Figure 4.52 corresponds to the concentration of carbon dioxide along BED 1. During the adsorption phase, $0 < t < 6$ hours and 12 hours $< t < 18$ hours, the concentrations for L = 0.0, L = 0.5 and L = 1.0 are as

follows: 1.8971 kmol/m^3, 1.8919 kmol/m^3, and 1.8750 kmol/m^3. During the regeneration phase (6 hours < t < 12 hours), the concentrations for L = 0.0, L = 0.5 and L = 1.0 are as follows: 0.8451 kmol/m^3, 0.8466 kmol/m^3, and 0.8480 kmol/m^3.

The third plot in Figure 4.52 corresponds to the concentration of carbon dioxide along BED 2. During the adsorption phase, 0 < t < 12 hours, the concentrations for L = 0.0, L = 0.5 and L = 1.0 are as follows: 1.8971 kmol/m^3, 1.8907 kmol/m^3, and 1.8750 kmol/m^3. During the regeneration phase (12 hours < t < 18 hours), the concentrations for L = 0.0, L = 0.5 and L = 1.0 are as follows: 0.8451 kmol/m^3, 0.8466 kmol/m^3, and 0.8480kmol/m^3.

Figure 4.53 presents the concentration of pentane along packed bed during the first TSA cycle of Simulation 4. These figures are similar o the concentration plots for methane, as happened with simulation 2.

The first plot in Figure 4.53 corresponds to the concentration of pentane along BED 3. BED 3 starts simulation 4 in the regeneration phase. During the regeneration phase, 0 < t < 6 hours, the concentrations for L = 0.0, L = 0.5 and L = 1.0 are as follows: 0.0831 kmol/m^3, 0.0832 kmol/m^3, and 0.0834 kmol/m^3. During the adsorption phase (6 < t < 18 hours), the concentrations for L = 0.0, L = 0.5 and L = 1.0 are as follows: 0.1865 kmol/m^3, 0.1848 kmol/m^3, and 0.1843 kmol/m^3.

The second plot in Figure 4.53 corresponds to the concentration of pentane along BED 1. BED 1 starts simulation 4 during the adsorption phase. During the adsorption phase, 0 < t < 6 hours and 12 hours < t < 18 hours, the concentrations for L = 0.0, L = 0.5 and L = 1.0 are as follows: 0.1865 kmol/m^3, 0.1858 kmol/m^3, and 0.1843 kmol/m^3. During the regeneration phase (6 < t < 12 hours), the concentrations for L = 0.0, L = 0.5 and L = 1.0 are as follows: 0.0831 kmol/m^3, 0.0832 kmol/m^3, and 0.0834 kmol/m^3.

The third plot in Figure 4.53 corresponds to the concentration of pentane along BED 2. BED 2 starts simulation 4 during the adsorption phase. During the adsorption phase, 0 < t < 12 hours, the concentrations for L = 0.0, L = 0.5 and L = 1.0 are as follows: 0.1865 kmol/m^3, 0.1853 kmol/m^3, and 0.1843 kmol/m^3. During the regeneration phase (12 < t < 18 hours), the concentrations for L = 0.0, L = 0.5 and L = 1.0 are as follows: 0.0831 kmol/m^3, 0.0832 kmol/m^3, and 0.0834kmol/m^3.

4.4.7 Adsorbed Inventory

Figures 4.54, 4.55 and 4.56 present the number of moles of each component adsorbed in BED 1, BED 2 and BED 3, respectively. By looking at Figure 4.54, it can be observed that BED 1 started simulation 4 with an initial 58.1457 kmol of

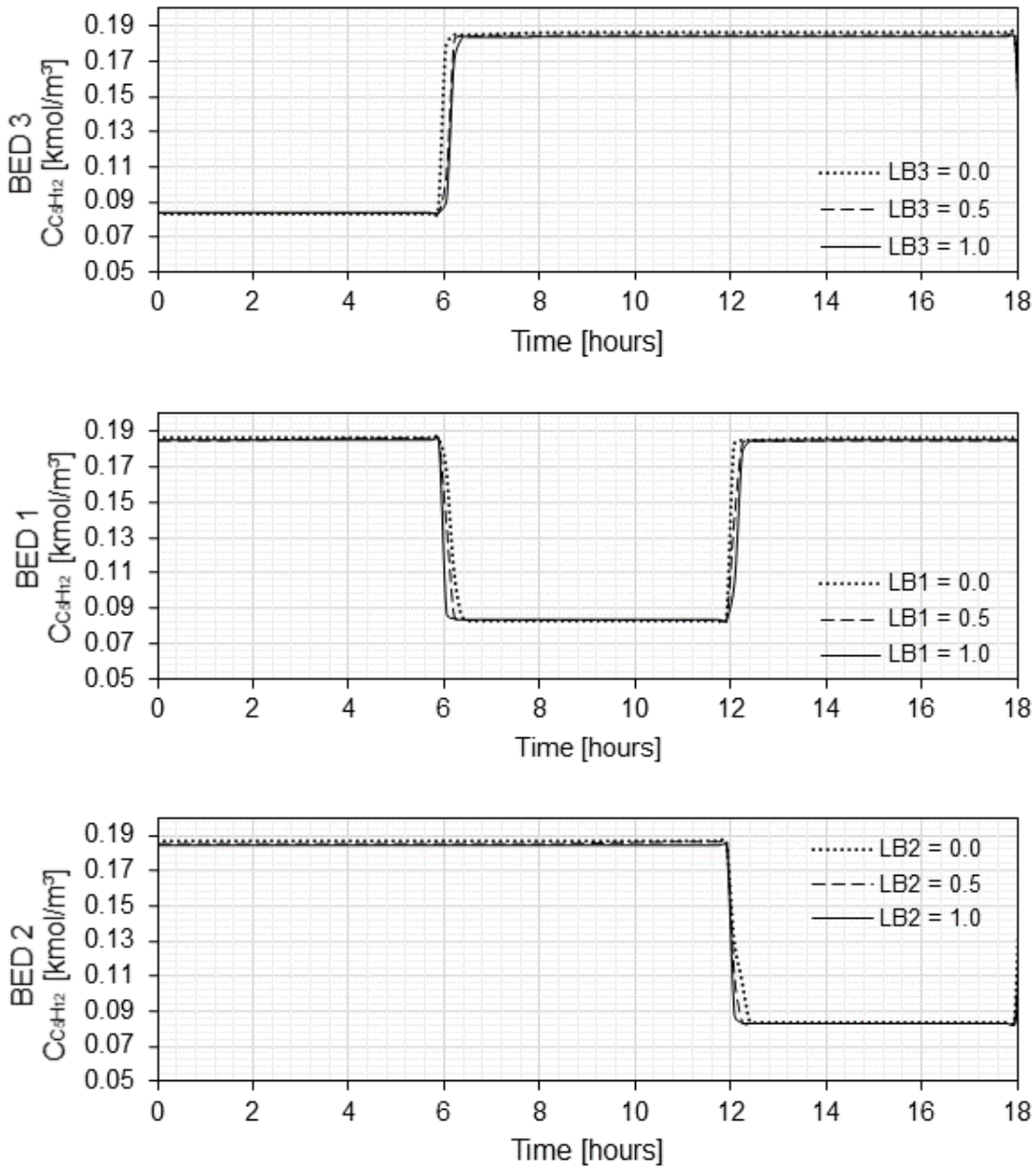

Figure 4.53: Concentration of pentane along packed bed during the first TSA cycle of Simulation 4.

methane, 65.4485 kmol or carbon dioxide, 58.7037 kmol of water and 7.85×10^{-20} kmol of pentane.

For 0 < t < 6 hours, since the bed was already saturated in CH_4 and CO_2, the number of kmol for these components remained the same, while the number o kmol of water increased linearly to 90.6618 kmol. After the bed entered the regeneration phase, in less than an hour the amounts of each component dropped and became constant (14.6825 kmol of methane, 37.2281 kmol of carbon dioxide, 1.9426 $\times 10^{-7}$ kmol of water, and 9.74×10^{-19} kmol of pentane). It is important to observe that while practically all of the water was removed, some of the

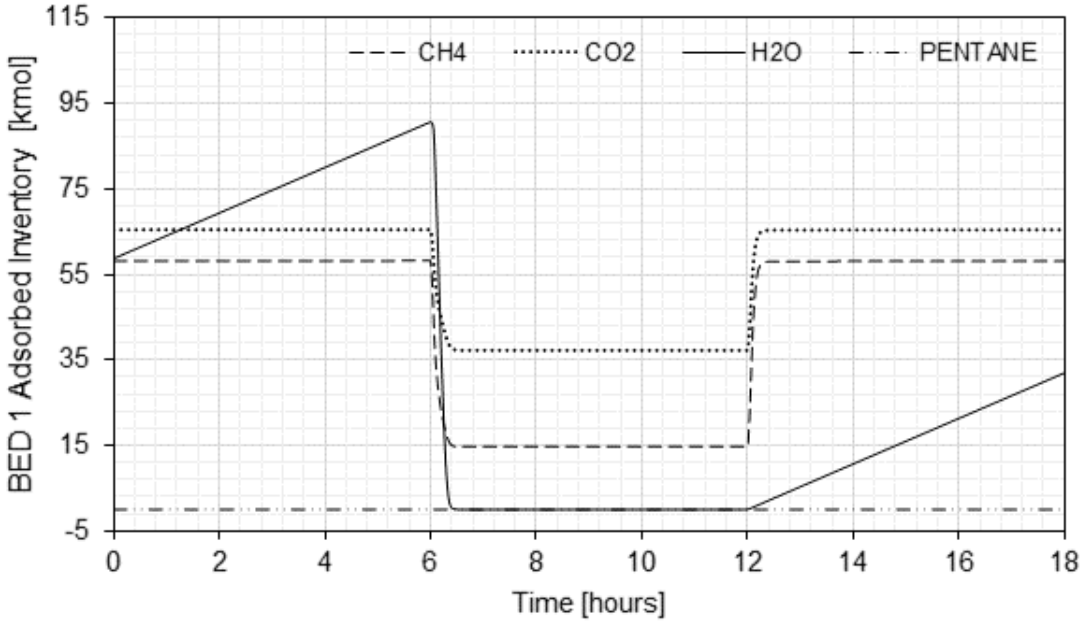

Figure 4.54: Adsorbed inventory of BED 1 during the first TSA cycle of Simulation 4.

methane and carbon dioxide still remained in the bed. At t = 12 hours, BED 1 entered the adsorption phase once again. The amounts of CH_4 and CO_2 quickly stabilized at 58.1177 kmol and 65.4320 kmol, respectively, while the amount of H_2O increased linearly from 1.9426 $\times 10^{-7}$ kmol to 31.9944 kmol. The amount of pentane remained constant and close to zero (1.96×10^{-19}).

Figure 4.55 shows the adsorbed inventory of BED 2. The vessel started simulation 4 in the adsorption phase, with an initial inventory of 58.1037 kmol of methane, 23.4992 kmol of water, 65.4211 kmol of carbon dioxide, and 2.13 $\times 10^{-18}$ kmol of pentane.

During that time, the bed was saturated in CO_2 and CH_4, so the amounts of these components remained the same, while the amount of water increased linearly to 87.4504 kmol at t = 12 hours. At this time, BED 2 entered the regeneration phase and in less than an hour the amounts of each component dropped to constant values (14.6825 kmol of methane, 3.7581 $\times 10^{-7}$ kmol of water, 37.2281 kmol of carbon dioxide, and 7.21 $\times 10^{-18}$ kmol of pentane.

Figure 4.56 shows the adsorbed inventory of BED 3.

The vessel started simulation 4 in the regeneration phase, with an initial inventory of 14.6825 kmol of methane, 1.5530 $\times 10^{-7}$ kmol of water, 37.2281 kmol of carbon dioxide, and 5.32 $\times 10^{-20}$ kmol of pentane. Since the bed had not been adsorbing before, the amounts of each component remained constant during the regeneration phase. At t = 6 hours, BED 3 entered the adsorption phase. The amounts of methane and carbon dioxide quickly increase to constant values

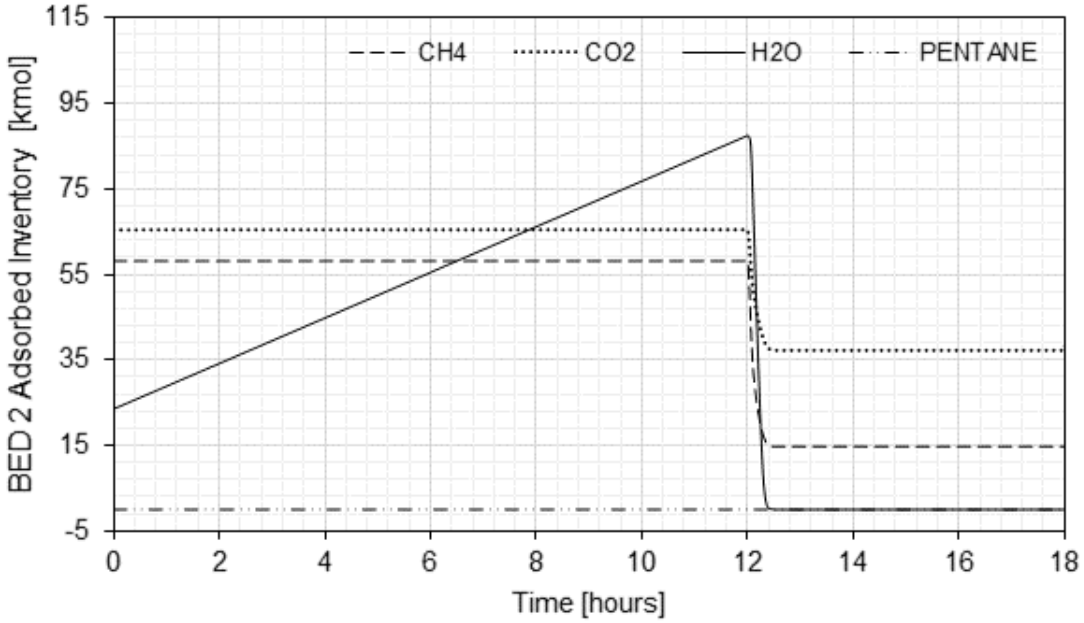

Figure 4.55: Adsorbed inventory of BED 2 during the first TSA cycle of Simulation 4.

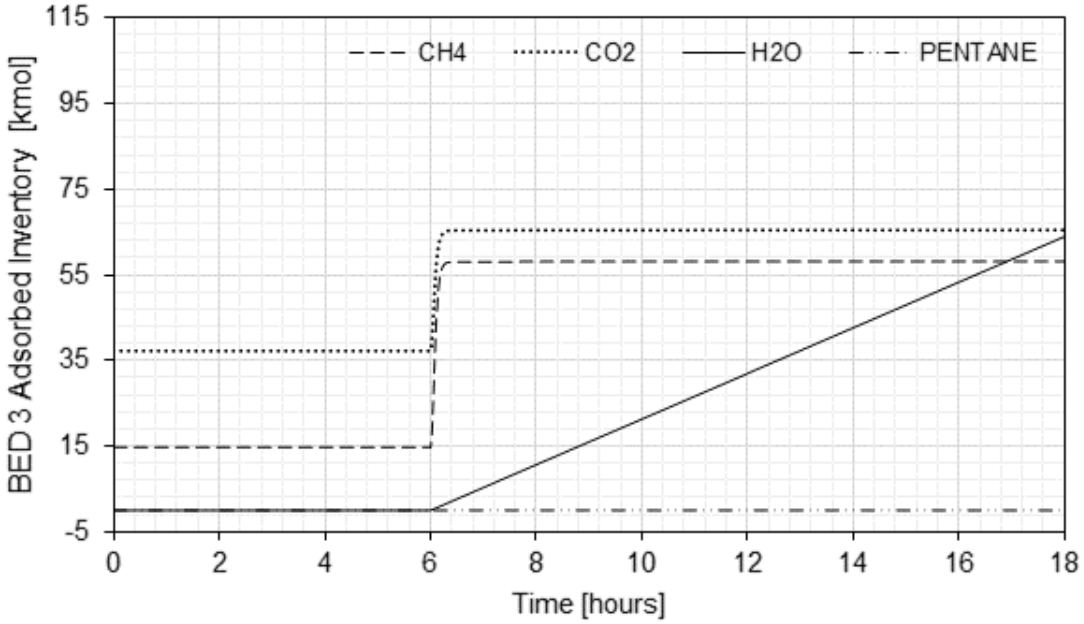

Figure 4.56: Adsorbed inventory of BED 3 during the first TSA cycle of Simulation 4.

(58.0866 kmol and 65.4125 kmol, respectively). Since no pentane is adsorbed, the number of moles remained approximately constant for this component throughout the whole TSA cycle. The amount of water increased linearly to 63.9025 kmol at t = 18 hours.

4.4.8 Product Composition

Figures 4.57, 4.58, 4.59 and 4.60 present the mole fractions of water, methane, carbon dioxide and pentane of the product stream for simulation 4. Although it is interesting to look at the mole fraction for all the components in the product stream, the mole fraction of water is the most critical, since it has a restriction of being less than 0.0001. It can be observed in Figure 4.57, that the mole fraction of water remained within specification limit (less than 0.0001) throughout the whole simulation. The mole fractions of water remained mostly constant with a value of 1.71 $\times 10^{-9}$, with spikes being observed during every six hours (every valve switch). The highest value observed during the six cycles was 8.17 $\times 10^{-5}$, which is still lower than the product cut. By observing Figure 4.57, it can be observed that although there is a pattern in the peaks, the values do not seem periodic (e.g. not all of the highest peaks present the same size). It would seem that the cyclic steady state was not achieved. However, this only happens for the water mole fractions. The difference in response for the TSA cycles can be due to the values being very small. It can be observed that the mole fractions of water are multiplied by 10^{-5}, which is the same order of magnitude of the tolerances set for the solver.

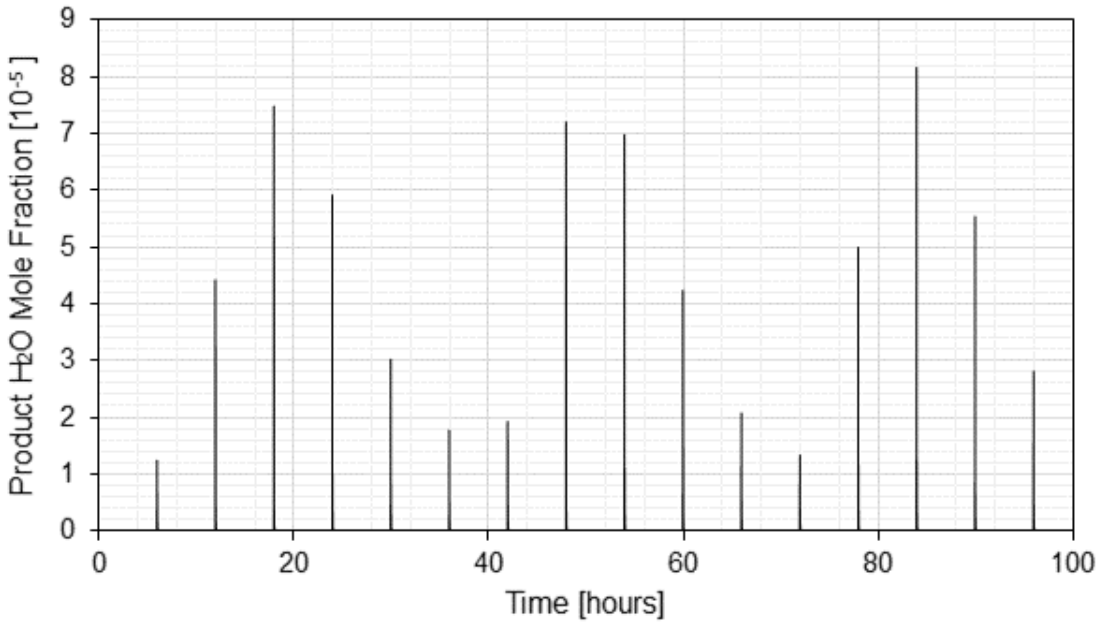

Figure 4.57: Mole fraction of water in the product stream during approximately six TSA cycles for simulation 4. The water cut is at 0.0001 kmol/kmol.

Figure 4.58 is the mole fraction of carbon dioxide observed in the product. The value remained mostly constant and equal to 0.4834 throughout the cycle, with valleys every six hours (valve switching). The size of the valleys were quite

uniform. The lowest value observed was 0.4778.

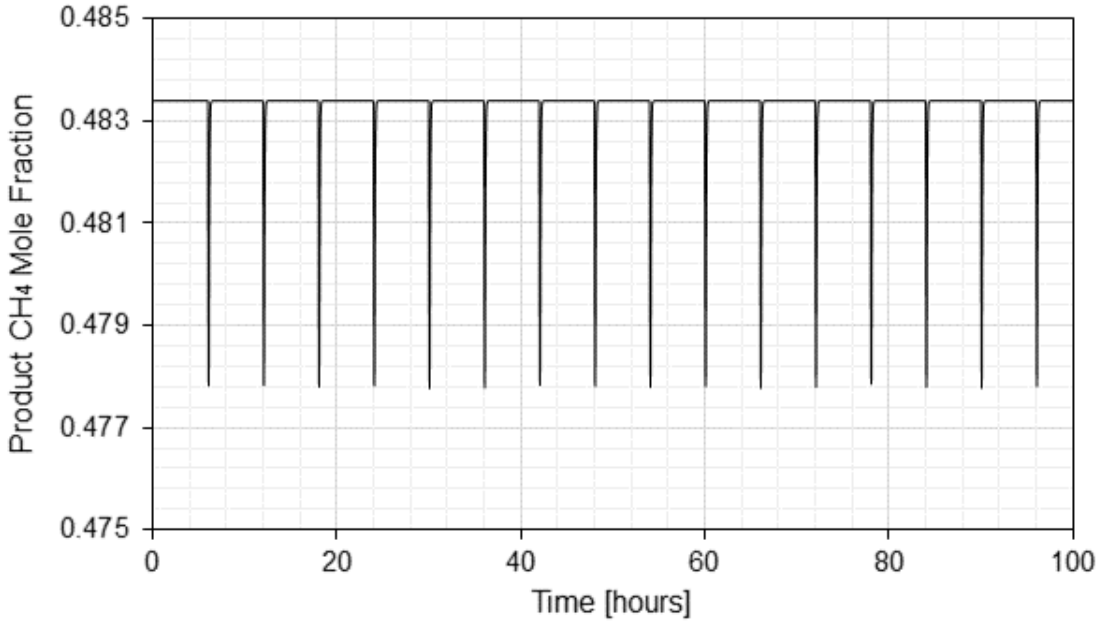

Figure 4.58: Mole fraction of methane in the product stream during approximately six TSA cycles for simulation 4.

Figure 4.59 is the mole fraction of carbon dioxide observed in the product. Similar to the other species, the value remained mostly constant throughout the cycle, but with approximately uniform peaks every six hours (valve switching). During the periods where the value remained constant, it was equal to 0.4704. The highest value observed was 0.4739.

Figure 4.60 is the mole fraction of pentane observed in the product. The value remained mostly constant throughout the cycle, but with approximately uniform peaks every six hours (valve switching). The plot is quite similar to that of the carbon dioxide mole fraction. During the periods where the value remained constant, the mole fraction of pentane was equal to 0.0462. The highest value observed was 0.0485.

4.4.9 Control Loops

In this section, the control loop responses of FFIC-1 and TIC-1 during the beginning of the simulation and after the first valve switching event (t = 6 hours) of the TSA cycle of simulation 4 are analyzed. For both of these control loops, a PI controller was used.

For the FFIC-1 control loop, the PI controller tuning parameters were: direct controller action, 20 %/% gain and 0.15 min integral time. Figures 4.61 and 4.62 show the control loop response. The process variable is given in kmol/s, the

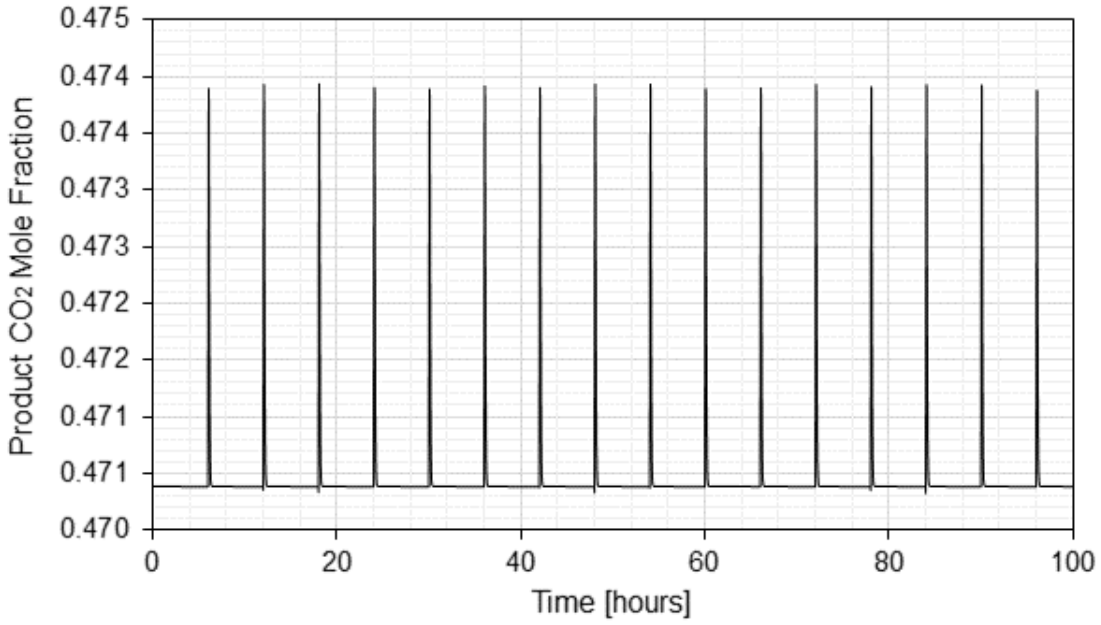

Figure 4.59: Mole fraction of carbon dioxide in the product stream during approximately six TSA cycles for simulation 4.

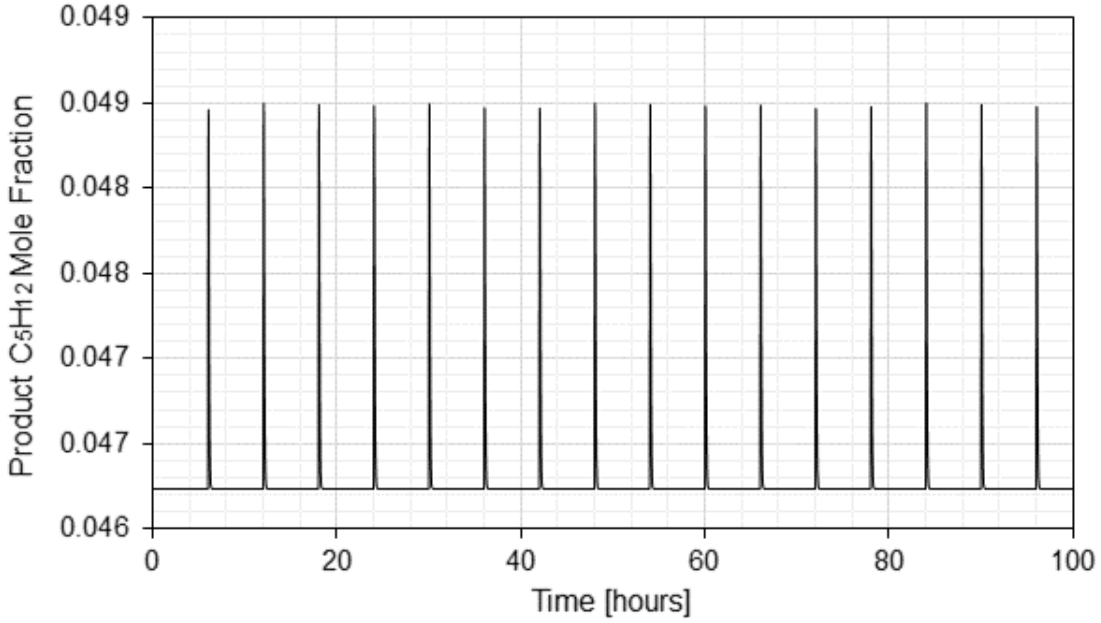

Figure 4.60: Mole fraction of pentane in the product stream during approximately six TSA cycles for simulation 4.

set-point in kmol/s, and the manipulated variable (OP), m^3/s For the implementation in simulation 4, the SP was assumed to be the molar flow rate of the gas stream that leaves both beds in adsorption phase. The process variable is the molar flow rate of the regeneration phase divided by 0.11. The output of the controller is the volumetric flow rate at the compressor (UC-01) inlet. Due

to the initial conditions, the feed gas stream molar flow rate started very high (about 10.4 kmol/s) and was reduced to the desired value of 3.7 kmol/s. This can be observed in Figure 4.61 as the behavior of the SP curve (assuming that the product stream molar flow rate is equal to the feed stream molar flow rate). The process variable and the manipulated variable both accompanied this change. It took about 15 seconds for the process variable to reach 90% of the set-point.

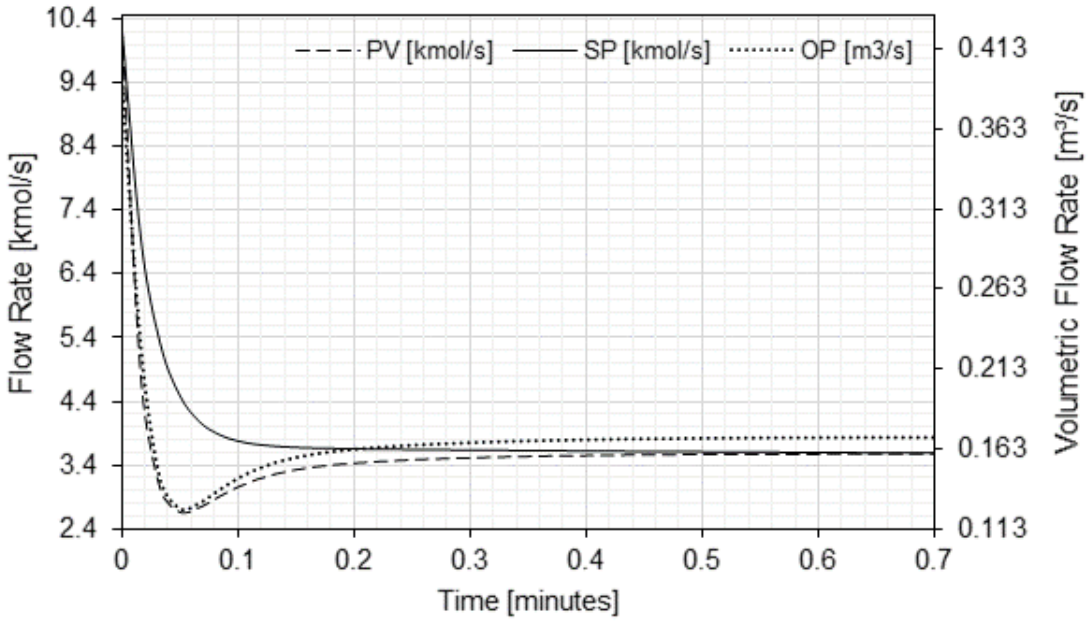

Figure 4.61: Flow Control Loop for Simulation 4. Controller action: direct. Gain: 20 %/%. Integral time: 0.15 min.

The importance of this flow control loop is so that the regeneration gas stream molar flow rate may be proportional to the molar flow rate of the GDU feed stream. This behavior can be observed in Figure 4.62. At t = 6 hours, the switching of on-off valves introduced disturbance to the process. In this case, a drop in the molar flow rate of the product stream was observed. However, the regeneration stream molar flow rate was able to accompany this change. At t = 6.5 hours, the process stabilized.

For the TIC-1 control loop, the PI controller tuning parameters were: reverse controller action, 10 %/% gain and 0.2 min integral time. Figures 4.63 and 4.64 show the control loop response. The importance of this temperature control loop is to keep the regeneration stream temperature fixed at about 230°C, which is the ideal temperature for the specific 4A molecular sieve used in this unit. For this control loop, the process variable is the regeneration feed stream temperature in °C, the set-point is fixed at 230.5°C, and the manipulated variable is the heat exchanger duty in MW.

Figure 4.63 shows the control loop performance at the beginning of simula-

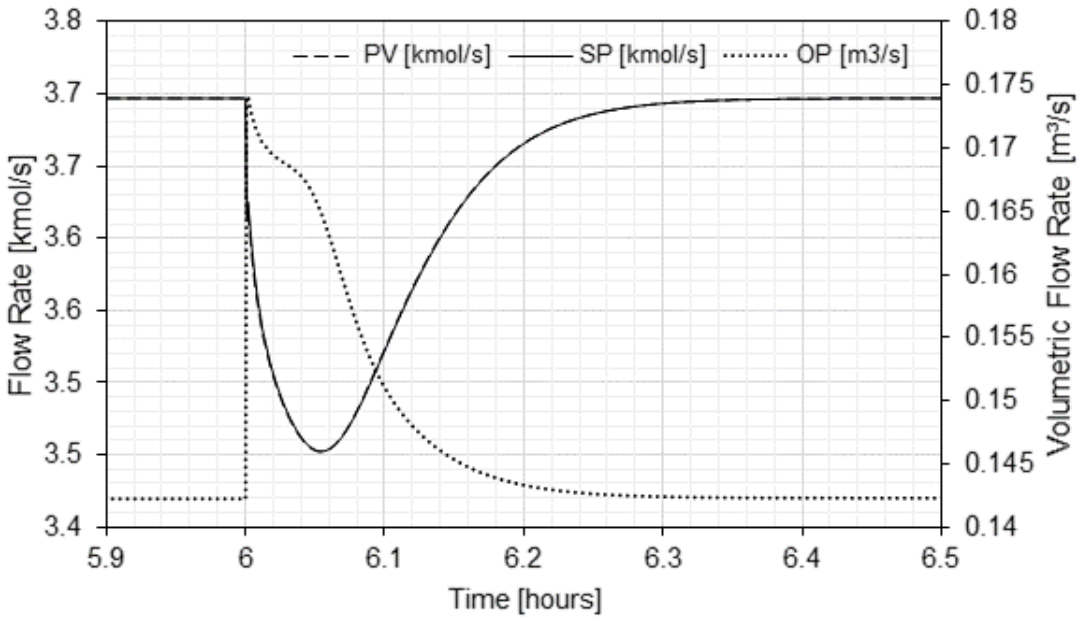

Figure 4.62: Flow Control Loop for Simulation 4 during first switching event. Controller action: direct. Gain: 20 %/%. Integral time: 0.15 min.

tion 4. There is an initial temperature rise in which the regeneration temperature reaches a maximum of 242.6 °C. This is accompanied by a drop in the manipulated variable, which reached a minimum of -2.9277 MW. It takes less than one minute for the regeneration temperature to be within a 10% range of the set-point.

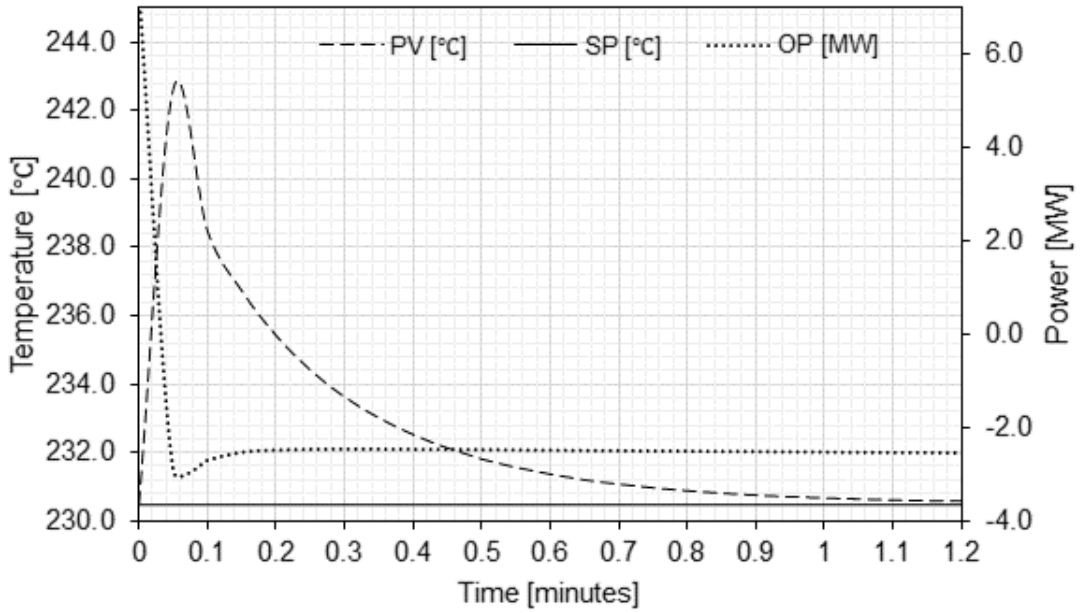

Figure 4.63: Temperature control Loop for Simulation 4 for t < 1.2 minutes. Controller action: reverse. Gain: 10 %/%. Integral time: 0.2 min.

Figure 4.64 shows the control loop performance of TIC-1 for the first on-off valve switching event (t = 6.0 hours) of the TSA cycle. As mentioned before, the valve switching introduces a disturbance to the process. The regeneration stream which was initially at 230.5°C spikes up to a maximum value of 232.3°C. This causes the manipulated variable to drop to -2.5736 MW. The temperature returns to the set-point value in about 20 minutes.

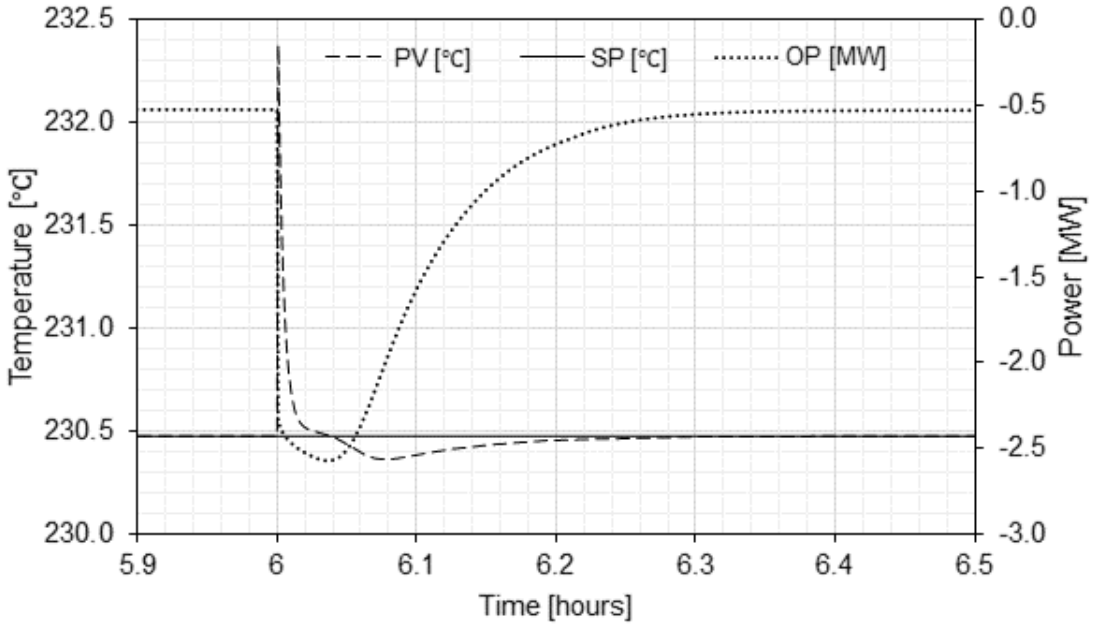

Figure 4.64: Temperature control Loop for Simulation 4 during first switching event. Controller action: reverse. Gain: 10 %/%. Integral time: 0.2 min.

4.4.10 Vapor-Liquid Equilibrium and Phase Behaviour

Figures 4.65, 4.66 and 4.67 show the operating points and phase envelopes for beds 1, 2 and 3, respectively, during six TSA cycles of simulation 4. For each figure, a plot for the whole temperature range, (a), was presented along with a second plot, (b), for the reduced temperature range 32.0°C < T < 40.0°C, so that the behavior of the GDU close to the phase envelope (dashed line) can be studied. Although the bed was divided into 40 discretization nodes, only 20 evenly distributed data series were plotted for convenience. As mentioned during the analysis of the results of simulations 1 and 2, the pressure does not vary significantly. As can be seen on Figures 4.65, 4.66 and 4.67, for the operating point pressure range, the dew-point temperature T_{DEW} remained approximately constant and equal to 38.5°C. For all three beds, many operating points are located to the left of the dashed line, i.e., the temperature is lower than T_{DEW} and the phase envelope is entered. In this condition, there is condensation. For all

of the beds, the minimum temperature observed was 33.5°C and the maximum temperature was 230.5°C. It was verified that the operating points remained inside the phase envelope for 60% of the simulated time interval (65 out of the 108 hours, which correspond to six 18 hour TSA cycles).

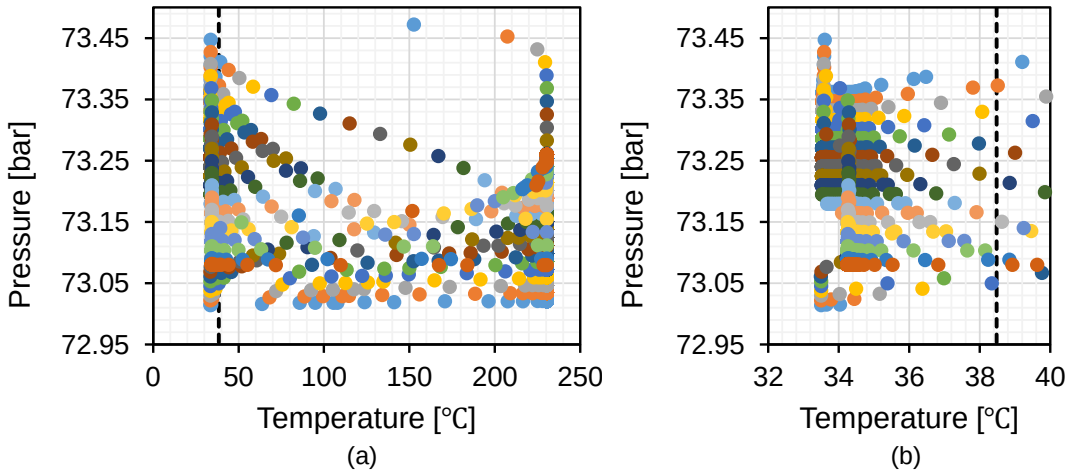

Figure 4.65: Operating points and phase envelope for BED 1 during six TSA cycles for Simulation 4 (a) for the whole temperature range of the six TSA cycles and (b) zoom close to T_{DEW} (dashed line). For the process pressure range (72.95 bar < P < 73.50 bar), T_{DEW} is approximately constant and equal to 38.5°C.

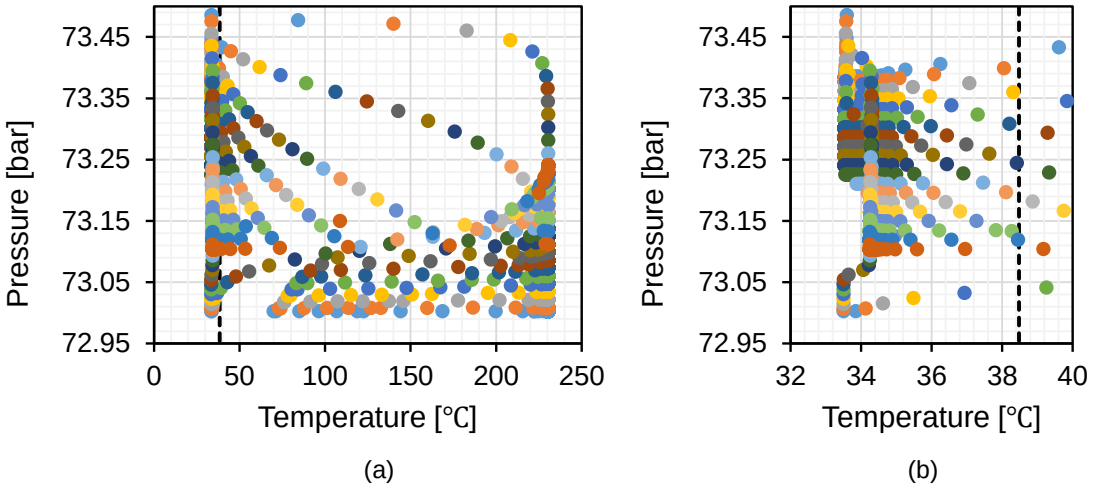

Figure 4.66: Operating points and phase envelope for BED 2 during six TSA cycles for Simulation 4 (a) for the whole temperature range of the six TSA cycles and (b) zoom close to T_{DEW} (dashed line). For the process pressure range (72.95 bar < P < 73.50 bar), T_{DEW} is approximately constant and equal to 38.5°C.

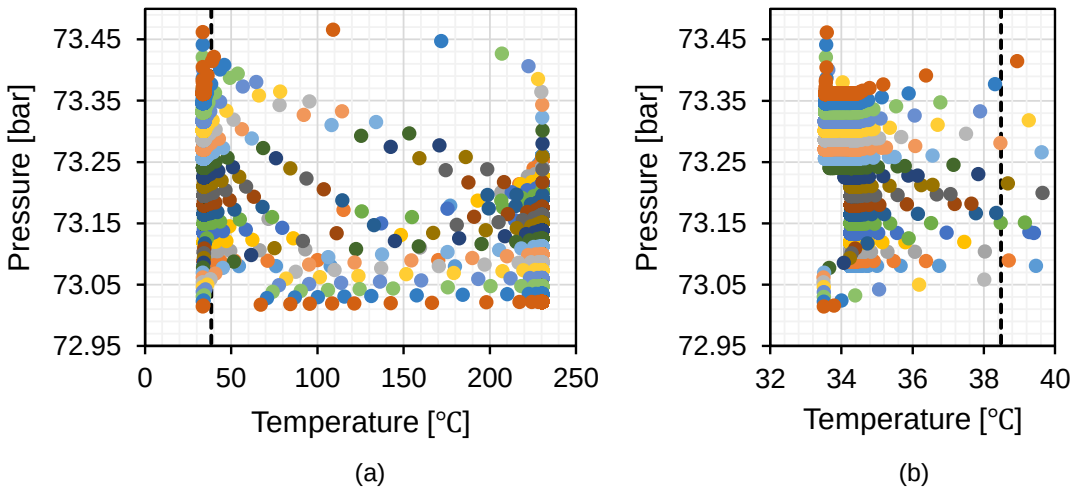

Figure 4.67: Operating points and phase envelope for BED 3 during six TSA cycles for Simulation 4 (a) for the whole temperature range of the six TSA cycles and (b) zoom close to T_{DEW} (dashed line). For the process pressure range (72.95 bar < P < 73.50 bar), T_{DEW} is approximately constant and equal to 38.5°C.

4.5 Simulation 5 Results: TSA Cycles of Complete GDU with Feed Temperature Control Loop

Simulation 5 corresponds to the process plant schematic presented in Figure 3.10. Besides the typical control loops presented in simulation 4, it also includes the TIC-2 control loop, which is responsible for controlling the feed stream temperature in order to drive the operating points of the unit out of the phase envelope. The operating conditions for simulation 5 are the same as those for simulation 4 (see Table 4.6).

4.5.1 Temperature

Figure 4.68 presents the temperature of gas at three bed lengths (L = 0.0, L = 0.5 and L = 1.0) for each bed during the first TSA cycle of Simulation 5. For t > 18 hours the behavior was periodic, so only the first cycle was shown for better viewing.

The first plot corresponds to the temperature of BED 3, which is just entering the regeneration phase when simulation 5 starts. Throughout the first six hours, the bed's temperature is approximately constant and equal to 230.5°C, the regeneration temperature. At t = 6 hours, the valves switch and BED 3 enters the adsorption phase, where it remains until the end of the cycle (t < 18 hours). The temperature at L = 0.0 changes almost immediately to the adsorption feed stream temperature (34.0°C), since the feed stream enters the bed from the top.

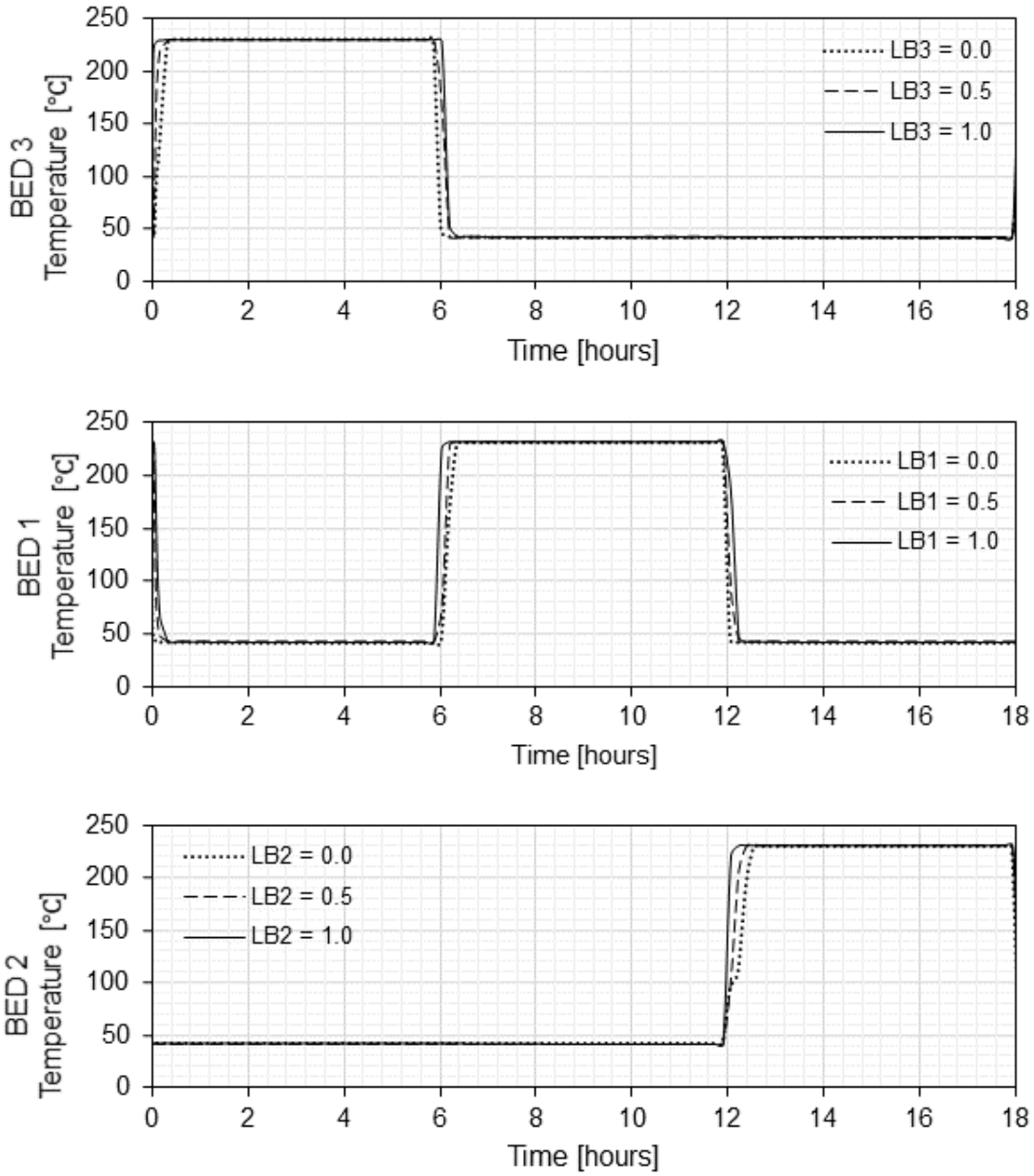

Figure 4.68: Temperature of gas along packed bed during the first TSA cycle of Simulation 5.

The cooling lakes longer to occur at L = 0.5 and even longer at the bottom of the bed (L = 1.0), as was expected. The whole bed takes about 40 minutes to be cooled. The temperature during most of the adsorption phase is approximately 42.1°C. It important to observe, that although the shape of the curve is similar to that obtained for simulation 4 (see Figure 4.43), during the adsorption phase the temperature is higher for simulation 5 (for simulation 4 it was 33.6°C). This is due to the head exchanger and the control loop TIC-2 at the feed stream working to keep the temperature throughout the packed beds higher than T_{DEW}.

The second plot corresponds to the temperature of BED 1. At the beginning

of simulation 5, BED 1 is just entering the adsorption phase, where it remains for the next six hours. During this time interval, the bed's temperature is approximately constant and equal to 42.2°C. At t = 6 hours, the valves switch and BED 1 enters the regeneration phase, where it remains for another six hours.The temperature rises first at the bottom of the bed, following L = 0.5 and L = 0.0. The heating of the whole bed from adsorption temperature to regeneration temperature (230.5°C) takes about 50 minutes.

Finally, the third plot in Figure 4.43 is the temperature at BED 2. This bed also started the simulation 5 entering the adsorption phase. After 12 hours, the valves switch and BED 2 enters the regeneration phase. It took about 1.2 hours to heat the whole bed.

It can be observed that after including the feed temperature control, it took longer to heat the bed than it did for simulation 4.

4.5.2 Pressure

Figure 4.69 presents the pressure along the packed beds during the first TSA cycle of Simulation 5. The overall shapes of the curves was already explained for simulation 4. For simulation 5, it is quite similar. However, the values will be presented for comparison purpose.

The first plot on Figure 4.69 is the pressure across BED 3. For 0 < t < 6 hours, BED 3 is in the regeneration phase, so the pressure at the bottom of the bed is greater than the pressure at the top. During this period, the pressures at L = 0.0, L = 0.5 and L = 1.0 are, respectively, 73.02 bar, 73.14 bar and 73.26 bar. A total drop of 0.24 bar was observed. At t = 6 hours, BED 3 enters the adsorption phase. The pressure remains mostly constant at 73.38 bar for L = 0.0, 73.23 bar at L = 0.5, and 73.08 bar at L = 1.0. A total pressure drop of 0.15 bar was observed during the adsorption phase.

The second plot on Figure 4.69 is the pressure across BED 1. For 0 < t < 6 hours, BED 1 is in the adsorption phase, so the pressure at the top of the bed is greater than the pressure at the bottom. During this period, the pressures at L = 0.0, L = 0.5 and L = 1.0 are, respectively, 73.39 bar, 73.23 bar and 73.08 bar. A total pressure drop of 0.31 bar was observed. At t = 6 hours, BED 1 enters the regeneration phase. The pressure remains mostly constant at 73.02 bar for L = 0.0, 73.15 bar at L = 0.5, and 73.26 bar at L = 1.0. A total pressure drop of 0.24 bar was observed during the regeneration phase. At t = 12 hours, BED 1 enters the adsorption phase once again. During this time, the values are constant at 73.38 bar for L = 0.0, 73.22 bar for L = 0.5, and 73.08 bar for L = 1.0. A total pressure drop of 0.3 bar was observed during this second adsorption phase.

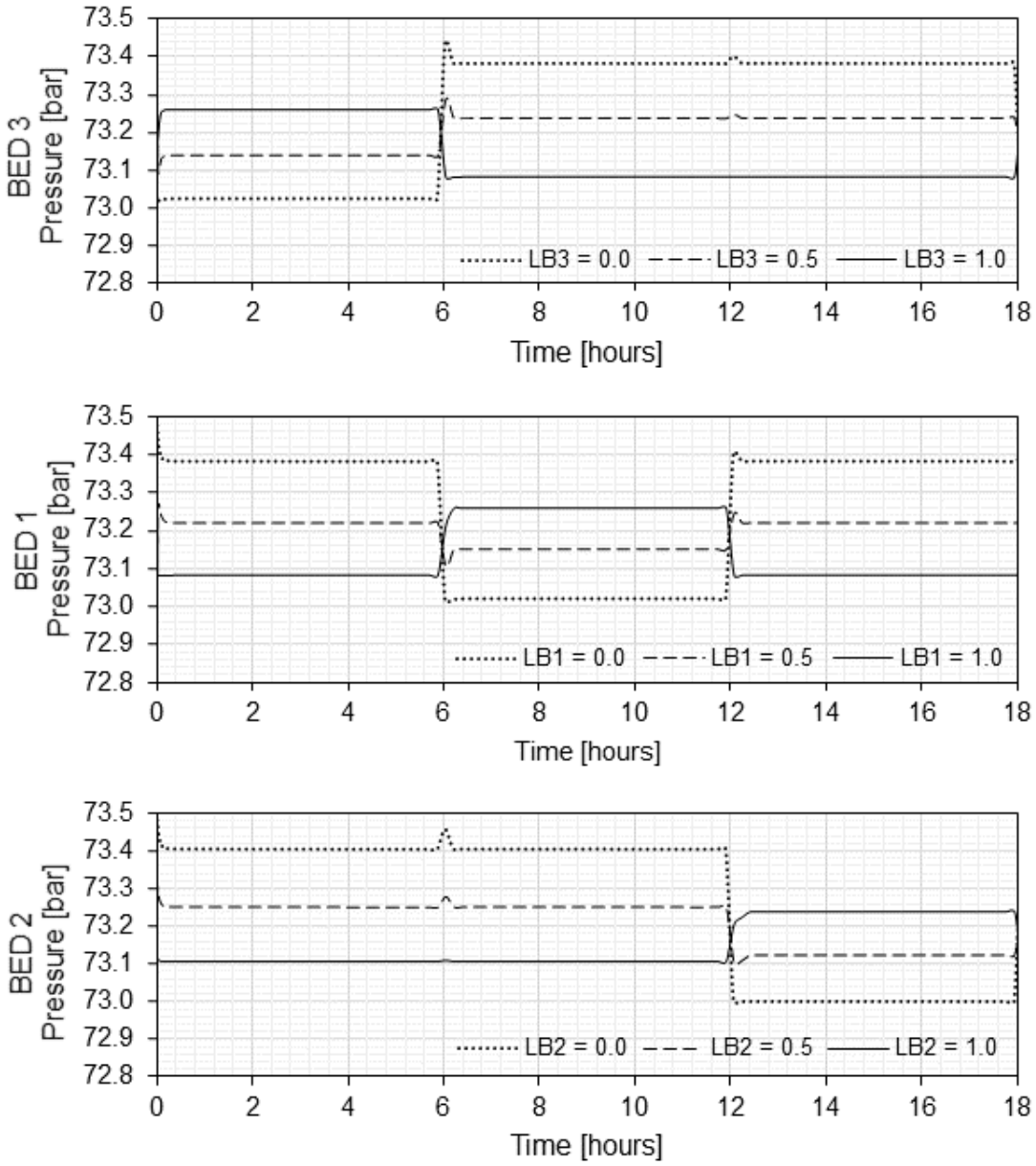

Figure 4.69: Pressure along packed bed during the first TSA cycle of simulation 5.

The third plot on Figure 4.69 is the pressure across BED 2. For $0 < t < 12$ hours, BED 2 is in the adsorption phase. During this period, the pressures at L = 0.0, L = 0.5 and L = 1.0 are, respectively, 73.40 bar, 73.25 bar and 73.10 bar. A total pressure drop of 0.30 bar was observed. At t = 12 hours, BED 2 enters the regeneration phase. The pressure remains mostly constant at 73.00 bar for L = 0.0, 73.12 bar at L = 0.5, and 73.24 bar at L = 1.0. A total pressure drop of 0.24 bar was observed during the regeneration phase.

4.5.3 Gas Velocity

Figure 4.70 presents the velocity of gas along the packed beds during the first TSA cycle of simulation 5. The plot looks identical to the one obtained for simulation 4.

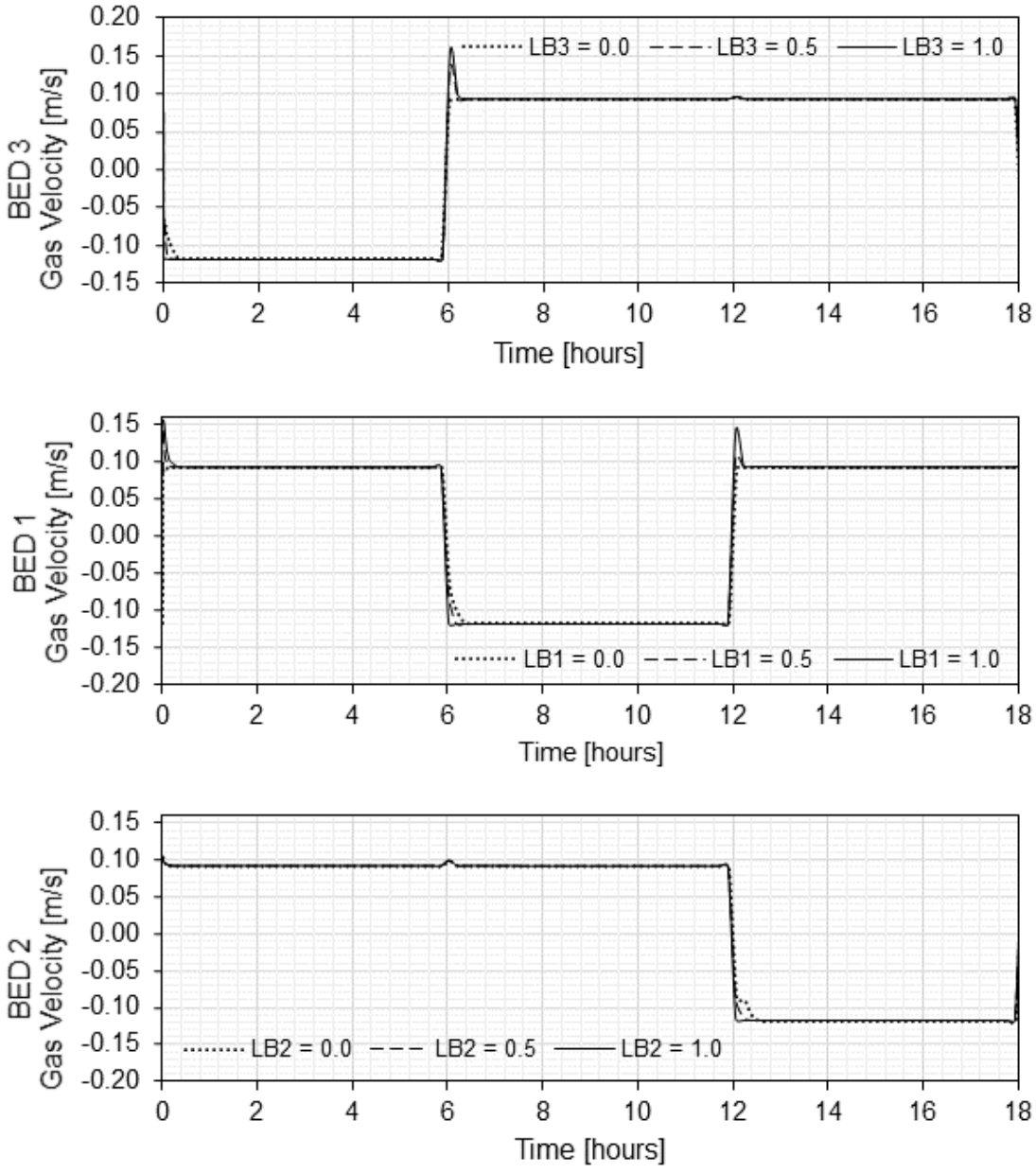

Figure 4.70: Gas velocity along packed bed during the first TSA cycle of simulation 5.

The first plot in Figure 4.70 corresponds to the gas velocity at BED 3. This bed starts simulation 5 entering the regeneration phase. It can be observed that the gas velocity is initially negative. During the regeneration phase, the absolute values of the velocities at L = 0.0, L = 0.5 and L = 1.0 for BED 3 are, respectively, 0.1182 m/s, 0.1180 m/s, and 0.1178 m/s. After t = 6 hours, the gas

velocity becomes positive, because gas starts flowing in from the top of the bed for adsorption. At t = 6.33 hours, a maximum value of 0.1550 m/s is reached at L = 1.0 and of 0.1347 m/s at L = 0.5. During the adsorption phase, the absolute values of the velocities at L = 0.0, L = 0.5 and L = 1.0 for BED 3 are, respectively, 0.0921 m/s, 0.0926 m/s, and 0.0931 m/s.

The second plot corresponds to the gas velocity at BED 1. This bed starts simulation 5 entering the adsorption phase. It can be observed that the gas velocity is initially positive, becomes negative after t = 6 hours (regeneration phase), and positive again, after t = 12 hours. During the adsorption phase, the absolute values of the velocities at L = 0.0, L = 0.5 and L = 1.0 for BED 1 are, respectively, 0.0920 m/s, 0.0928 m/s, and 0.0930 m/s. During the regeneration phase, the absolute average values of the velocities at L = 0.0, L = 0.5 and L = 1.0 for BED 1 are, respectively, 0.1182 m/s, 0.1180 m/s, and 0.1178 m/s. After t = 12 hours, the gas velocity becomes positive after regeneration. At t = 12.39 hours, a maximum value of 0.0924 m/s is reached at L = 1.0 and at t = 12.23 hours, a value of 0.0932 / is reached at L = 0.5.

The last plot corresponds to the gas velocity at BED 2. This bed starts simulation 5 also entering the adsorption phase. The gas velocity is positive until t = 12 hours, when it enters the regeneration phase. During the adsorption phase, the absolute values of the velocities at L = 0.0, L = 0.5 and L = 1.0 for BED 2 are, respectively, 0.0922 m/s, 0.0924 m/s, and 0.0927 m/s. During the regeneration phase, the absolute values of the velocities at L = 0.0, L = 0.5 and L = 1.0 for BED 2 are, respectively, 0.1182 m/s, 0.1180 m/s, and 0.1178 m/s.

4.5.4 Mole Fractions

Figure 4.71 presents the mole fraction of water along each packed bed during the first TSA cycle of Simulation 5.

The first plot presented on Figure 4.71 is the mole fraction of water on the gas inside BED 3. It seems that at the beginning of simulation 5, BED 3 was finishing a previous adsorption cycle. During most part of the regeneration phase of simulation 5, the water mole fraction of the gas inside BED 3 is 2.2×10^{-8} throughout the whole bed. This is considered dry gas, since the mole fraction of water is below the cut (1.0×10^{-4}). At t = 6 hours, the valves switch and BED 3 enters the adsorption phase. The mole fraction of water starts to increase. Since gas is fed from the top, this portion of the bed (L = 0.0) saturates first (after 8.5 hours) at a value of 0.0008, which is the feed stream composition. The mole fraction of H_2O takes longer to increase at the rest of the bed, as can be observed at L = 0.5 and L = 1.0. At the end of the adsorption phase, the mole fraction of

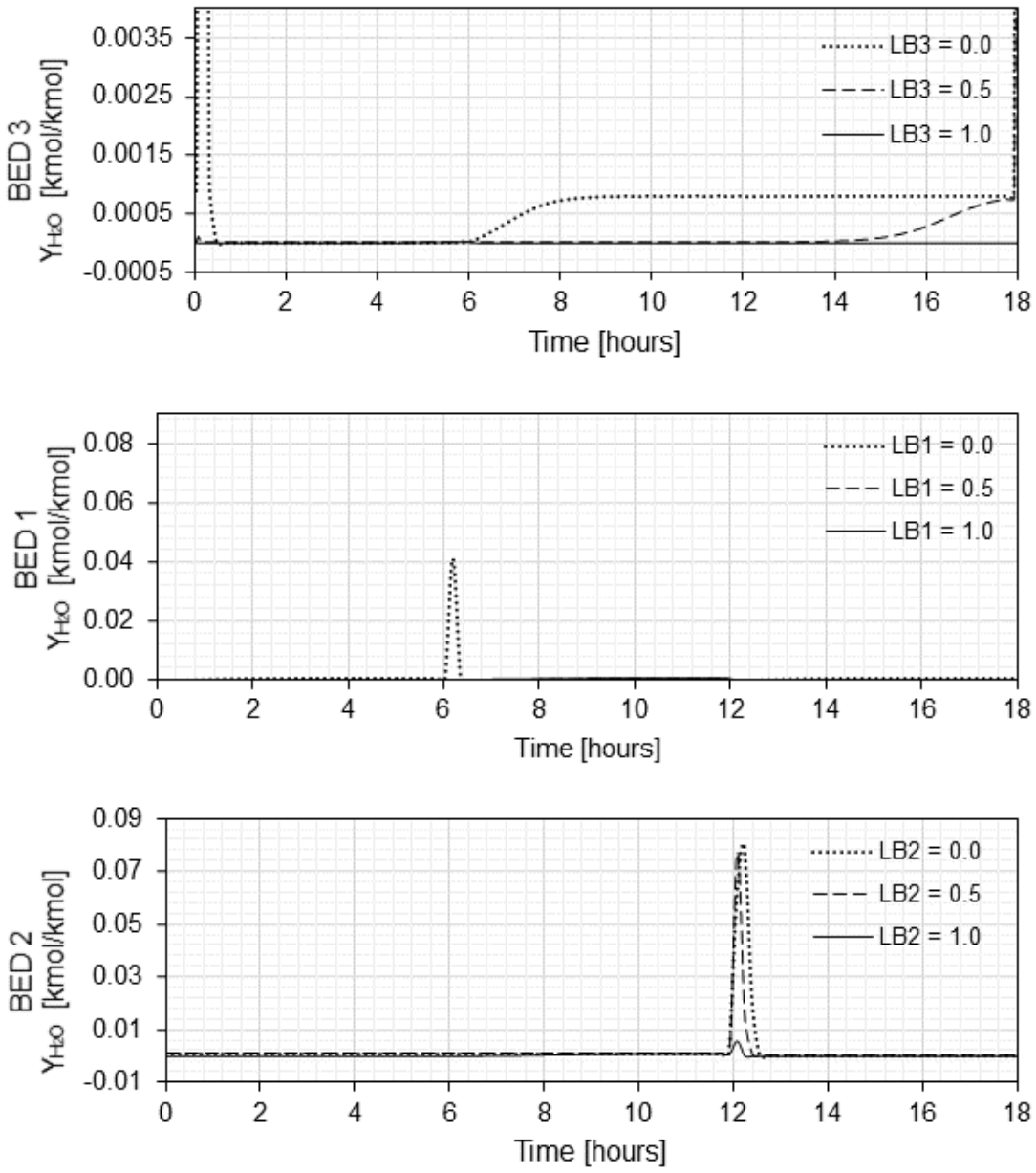

Figure 4.71: Mole fraction of water along packed beds during the first TSA cycle of simulation 5.

water in the gas at L = 1.0 is 5.5607×10^{-9}. This means that the at the end of the adsorption phase, the mass transfer zone (MTZ) still has not reached the end of the bed. At t = 14 hours, the mole fraction of water at L = 0.5 starts to increase more rapidly and at the end of the adsorption phase, the half of the bed is also saturated.

The second plot on Figure 4.71 is the mole fraction of water on the gas inside BED 1. BED 1 started the TSA cycle in the adsorption phase. The mole fraction of water is initially 5.6442×10^{-9}. At the end of the adsorption phase, the mole fractions at L = 0.0, L = 0.5 and L = 1.0 are, respectively, 0.0008, 8.4640×10^{-7}

and 3.0 $\times 10^{-5}$. At t = 6 hours, BED 1 enters the regeneration phase, so a peak of water can be observed at L = 0.0 (Y_{H_2O} = 0.0410) for t = 6.03 hours. The regeneration phase ends at t = 12 hours and BED 1 enters, once again, the adsorption phase. At the end of the regeneration phase, the mole fraction of H_2O is 0.0004 throughout the whole bed.

The last plot on Figure 4.71 is the mole fraction of water on the gas inside BED 2. BED 2 started the TSA cycle in the adsorption phase and remained in it for 12 hours (one full adsorption phase). The mole fraction of water is initially 0.0008 at L = 0.0 (top of the bed), 0.0007 at L = 0.5, and 8.2 $\times 10^{-9}$ at L = 1.0. At the end of the adsorption phase, the mole fraction of water is 0.0008 throughout the whole bed. This means that BED 2 became saturated during this first cycle and the product composition was above the specification (0.0001). Since a lot of water was adsorbed, when BED 2 entered the regeneration phase (t = 12 hours), large peaks of water can be observed at L = 1.0 (Y_{H_2O} = 0.0057, for t = 12.07 hours), L = 0.5 (Y_{H_2O} = 0.0775, for t = 12.07 hours) and at L = 0.0 (Y_{H_2O} = 0.0795, for t = 12.23 hours). At the end of the regeneration phase, the mole fraction of water is 1.4 $\times 10^{-8}$, which is less than the product cut, so the bed has been completely regenerated. The saturation of BED 2 is something that happened only during the first cycle due to the initial conditions of the bed. Figure 4.72 shows the mole fraction of water for the second TSA cycle (18 < t < 36 hours). It can be observed that there is no peak at L = 1.0 during regeneration and that the peak at L = 0.5 is a lot smaller at t = 30.17 hours (Y_{H_2O} = 0.0020).

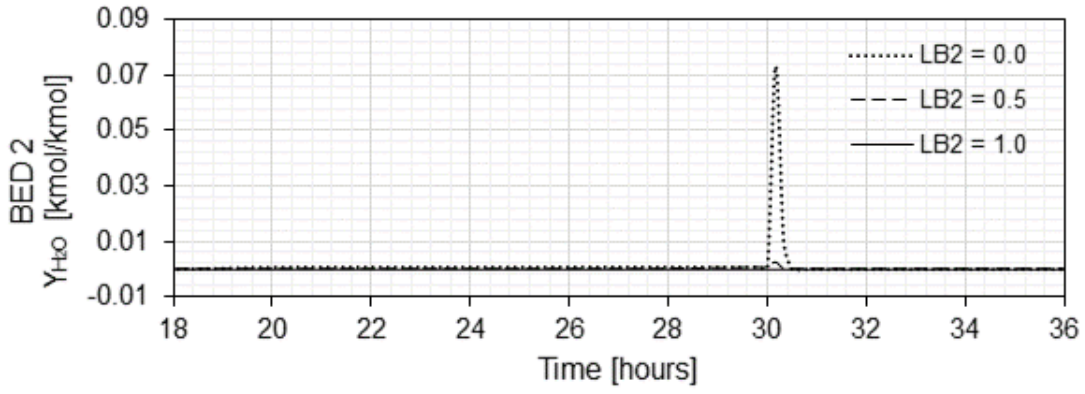

Figure 4.72: Mole fraction of water along BED 2 during the second TSA cycle of simulation 5.

4.5.5 Product Composition

Figure 4.73 presents the mole fraction of water in the product stream during simulation 5. Although it is interesting to look at the mole fraction for all the

components in the product stream, the mole fraction of water is the most critical, since it has a restriction of being less than 0.0001. It is important to note if the control strategy for reducing condensation did not cause the product to become unspecified. It can be observed in Figure 4.73, that the mole fraction of water exceeded the specification limit (greater than 0.0001) during the first cycle (0 < t < 18 hours) of the simulation, when it reached a maximum value of 40.7×10^{-5} at t = 12 hours. This did not happen because of the feed stream temperature control loop. It was actually due to the initial composition of water being high in the bed, as will be shown in the Adsorbed Inventory plots (see Figures 4.78 and 4.79). After the first cycle, the mole fraction of water remained mostly constant at a value of 1.44×10^{-8}, with spikes being observed during every six hours (every valve switch). The highest value observed during the other five cycles was 8.33×10^{-5}, which is still lower than the product cut.

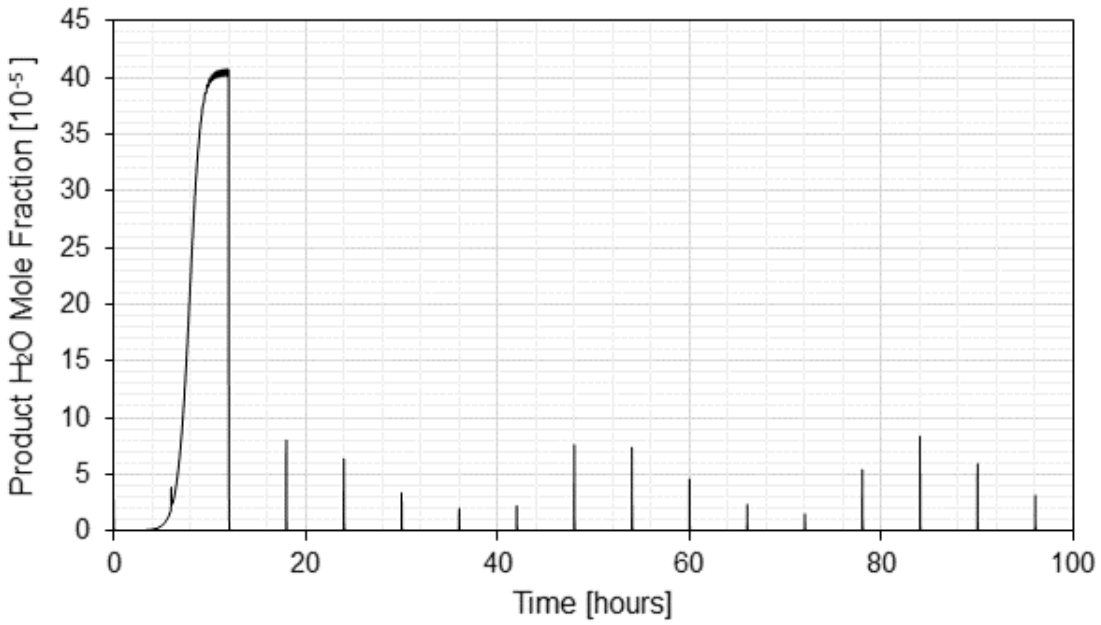

Figure 4.73: Mole fraction of water in the product stream during approximately six TSA cycles for simulation 5. The water cut is at 0.0001 kmol/kmol.

4.5.6 Control Loop

In this section, the control loop responses of TIC-2 during the beginning of the simulation and after the first valve switching event (t = 6 hours) of the TSA cycle of simulation 5 are analyzed. A PI controller was used. The tuning parameters were: reverse controller action, 1 %/% gain and 0.2 min integral time.

Figures 4.74, 4.75 and 4.76 show the control loop response. The process variable and the set-point are given in °C. The manipulated variable (OP) is given in

MW. The SP was assumed to be 3 °C, as recommended by TERRIGEOL (2012). It can be observed in Figure 4.74 that the set-point was reached by the process variable in less than 11 minutes. After that time, the manipulated variable remained constant at 1.869 MW. In Figure 4.75 some oscillation can be observed for the process variable. However, this only happened for the first cycle, which suggests that the abnormal behavior was due to the initial conditions of BED 2. In Figure 4.76 it can be observed that for the rest of the simulation, no oscillation was observed at the switching events.

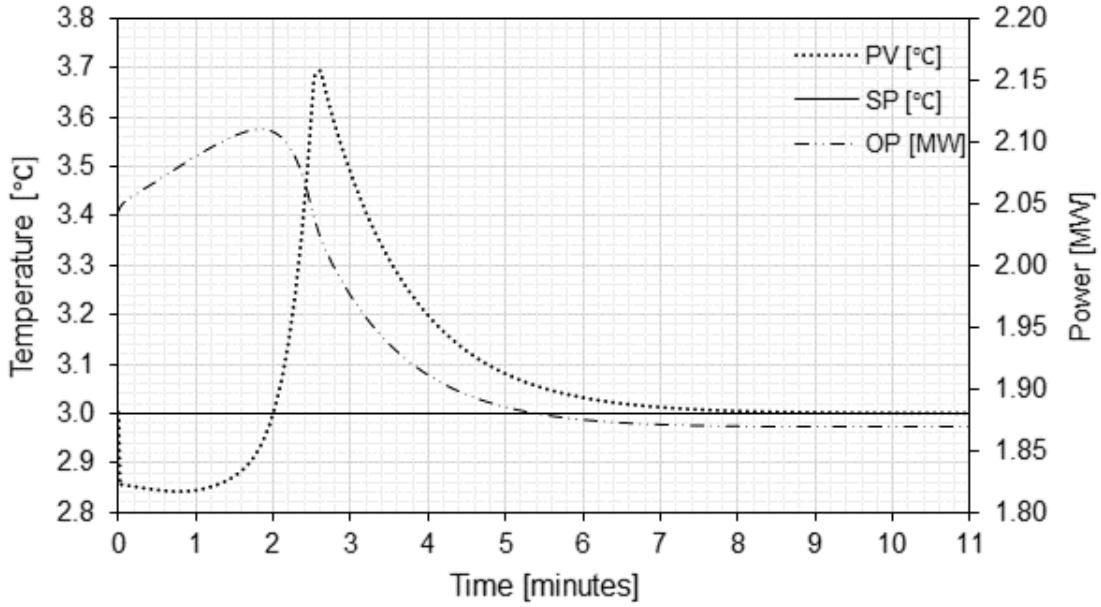

Figure 4.74: Feed stream temperature control loop TIC-2 for simulation 5. Controller action: reverse. Gain: 1 %/%. Integral time: 0.2 min.

4.5.7 Adsorbed Inventory

Figures 4.77, 4.78, 4.79 and 4.80 present the number of moles of each component adsorbed in BED 1, BED 2 and BED 3, respectively, during simulation 5. By looking at Figure 4.77, it can be observed that BED 1 started the adsorption phase in simulation 5 with 56.2451 kmol of methane, 64.3098 kmol of carbon dioxide, 5.1066 $\times 10^{-7}$kmol of water and 8.40×10^{-20} kmol of pentane.

For 0 < t < 6 hours, since the bed was saturated in CH_4 and CO_2, the number of kmol for these components remained constant, while the number of kmol of water increased linearly to 31.9118 kmol. After the bed entered the regeneration phase (t = 6 hours), in less than an hour the amounts of each component dropped and became constant (14,6788 kmol of methane, 37.2277 kmol of carbon dioxide, 0.0283 kmol of water, and 3.66×10^{-20} kmol of pentane). It is important

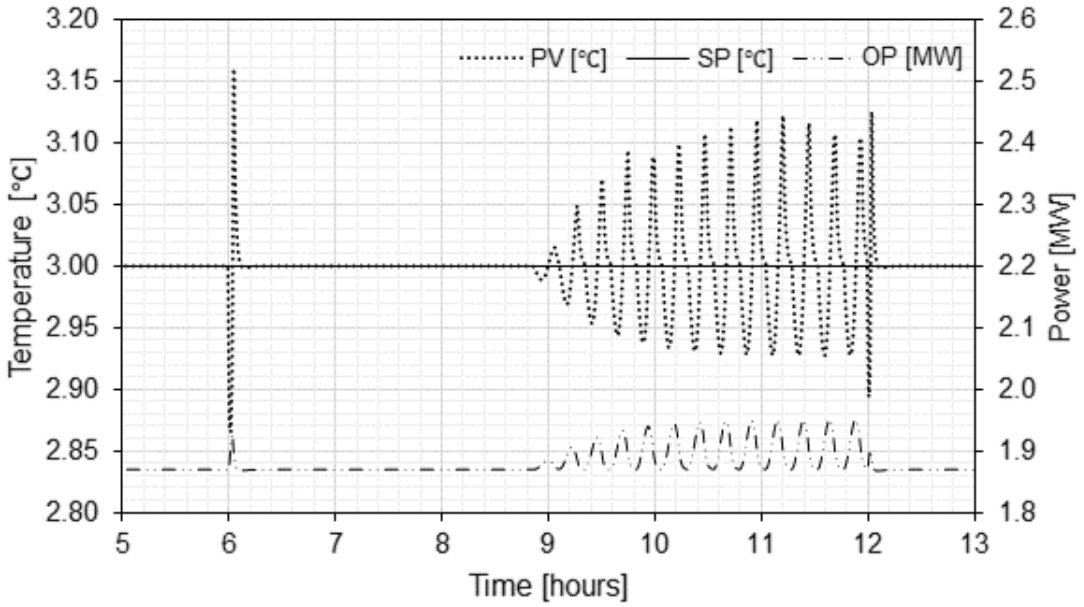

Figure 4.75: Feed stream temperature control loop TIC-2 for simulation 5 during the first valve switching event (t = 6 hours). Controller action: reverse. Gain: 1 %/%. Integral time: 0.2 min.

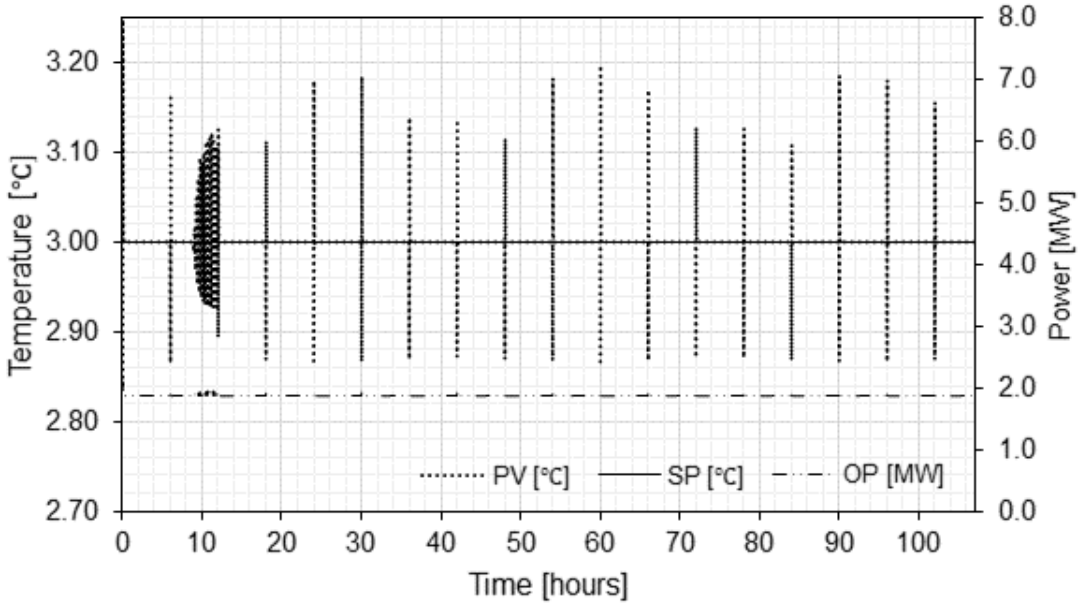

Figure 4.76: Feed stream temperature control loop TIC-2 for six TSA cycles of simulation 5. Controller action: reverse. Gain: 1 %/%. Integral time: 0.2 min.

to observe that not all of the water was removed and some of the methane and carbon dioxide still remained in the bed. At t = 12 hours, BED 1 entered the adsorption phase once again. The amounts of CH_4 and CO_2 quickly stabilized at 56.2422 kmol and 64.3081 kmol, respectively, while the amount of H_2O in-

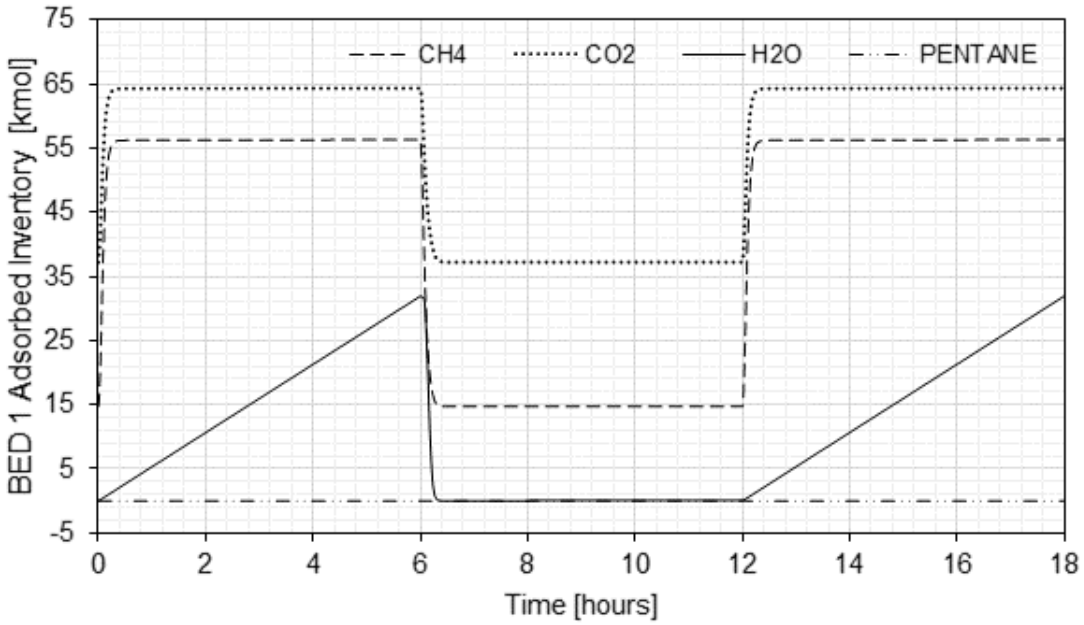

Figure 4.77: Adsorbed inventory of BED 1 during the first TSA cycle of simulation 5.

creased linearly to 31.9992 kmol at t = 18 hours. The amount of C_5H_{12} remained approximately constant and close to zero (1.53×10^{-19} kmol).

Figure 4.78 shows the adsorbed inventory of BED 2 during the first TSA cycle of simulation 5.

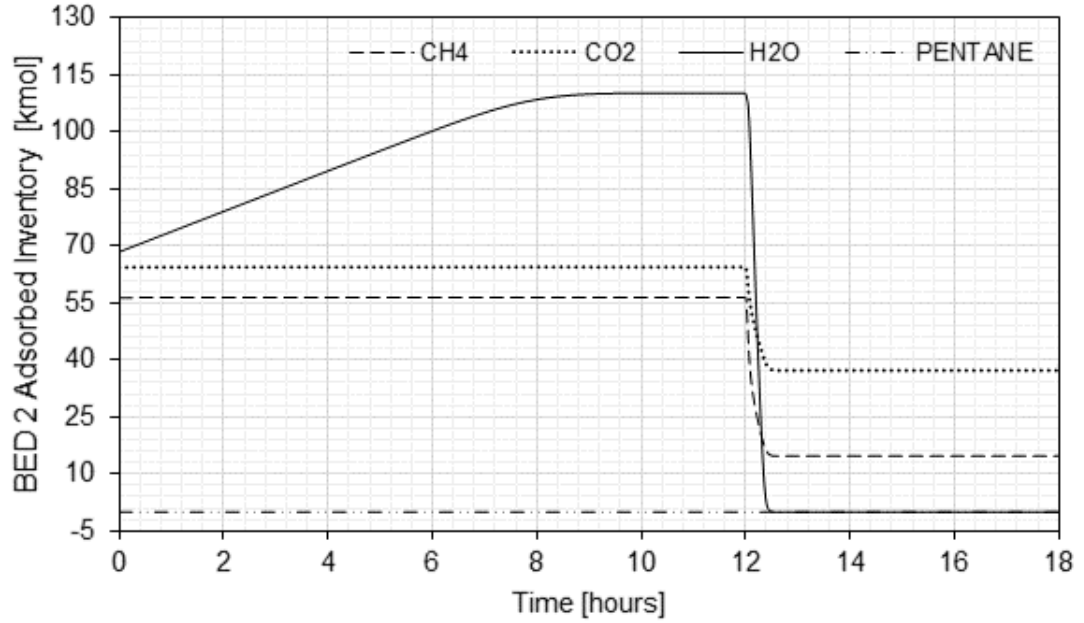

Figure 4.78: Adsorbed inventory of BED 2 during the first TSA cycle of simulation 5.

The vessel started the simulation entering the adsorption phase, which it

started with an inventory of 56.3870 kmol of methane, 68.3816 kmol of water, 64.3950 kmol of carbon dioxide, and 8.09 $\times 10^{-21}$ kmol of pentane. During that time, the bed was saturated in CO_2 and CH_4, so the amounts of these components remained the same, while the amount of water increased linearly to 108.5260 kmol at t = 8 hours, when the be became saturated with a constant value of 109.7390 kmol of water. At this time, BED 2 entered the regeneration phase and in less than an hour the amounts of each component dropped to constant values (14.6825 kmol of methane, 1.0750 $\times 10^{-6}$ kmol of water, 37.2281 kmol of carbon dioxide, and 3.61 $\times 10^{-19}$ kmol of pentane.

The saturation of BED 2 only happened during the first cycle due to the bed containing initially a great amount of water at the beginning of the simulation. Figure 4.79 shows the adsorption inventory for BED 2 during the second TSA cycle of simulation 5. In this plot, it can be observed that the bed did not saturate.

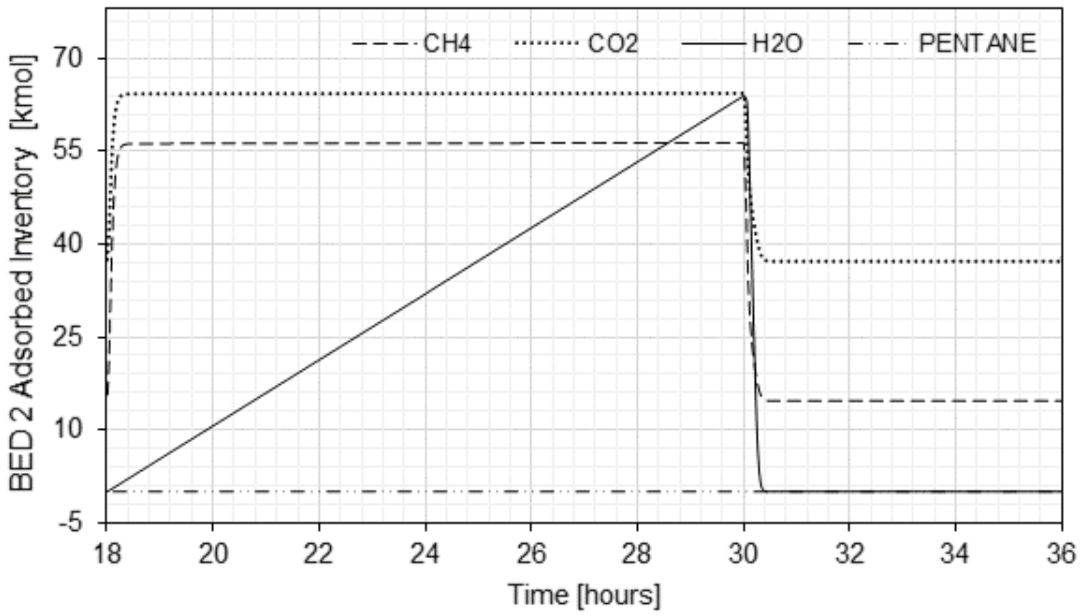

Figure 4.79: Adsorbed inventory of BED 2 during the second TSA cycle of simulation 5.

Figure 4.80 shows the adsorbed inventory of BED 3. The vessel began simulation 5 entering the regeneration phase, which it started with an inventory of 14.6825 kmol of methane, 1.2247$\times 10^{-6}$ kmol of water, 37.2281 kmol of carbon dioxide, and 3.04$\times 10^{-20}$ kmol of pentane. The amounts of each component remained constant during the regeneration phase. At t = 6 hours, BED 3 entered the adsorption phase. The amounts of methane and carbon dioxide quickly increased to constant values (56.2690 kmol and 64.3238 kmol, respectively). Since no pentane is adsorbed, the number of moles remained approximately constant for this component throughout the whole TSA cycle. The amount of water in-

creased linearly to 63.8750 kmol at t = 18 hours.

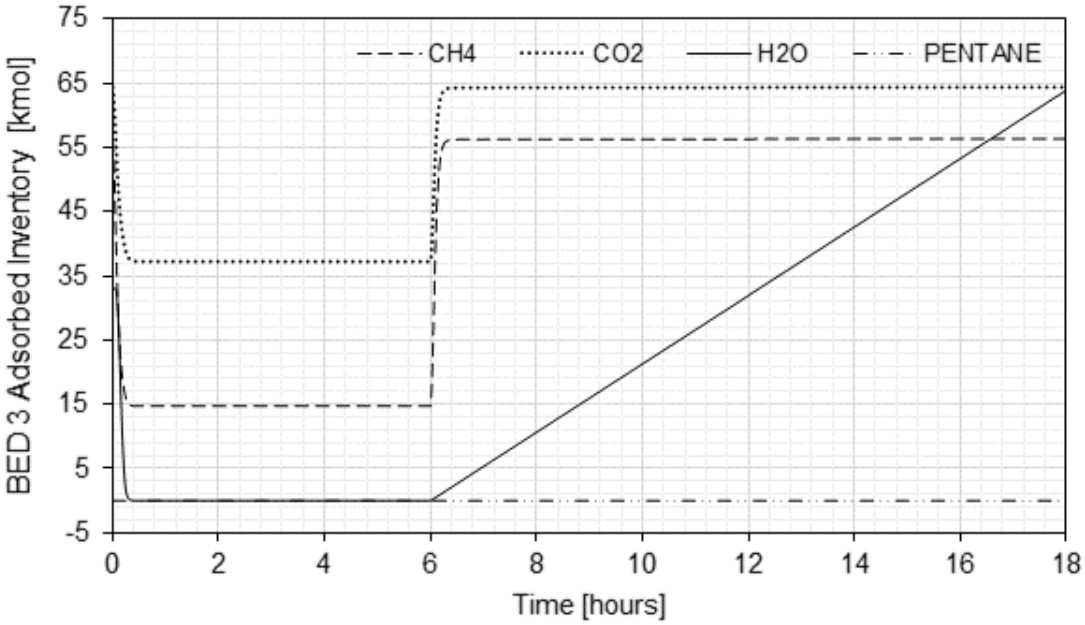

Figure 4.80: Adsorbed inventory of BED 3 during the first TSA cycle of simulation 5.

4.5.8 Vapor-Liquid Equilibrium and Phase Behaviour

Figures 4.81, 4.82 and 4.83 show the operating points and phase envelopes for beds 1, 2 and 3, respectively, during six TSA cycles of simulation 5. For each figure, a plot for the whole temperature range, (a), was presented along with a second plot, (b), for the reduced temperature range 37°C < T < 47°C, so that the behavior of the GDU close to the phase envelope (dashed line) can be studied.

Although the bed was divided into 40 discretization nodes, only 20 evenly distributed data series were plotted for convenience. As mentioned during the analysis of the results of simulations 1 and 2, the pressure does not vary significantly. As can be seen on Figures 4.81, 4.82 and 4.83, for the operating point pressure range, the dew-point temperature T_{DEW} remained approximately constant and equal to 38.5°C. For all three beds, all of the operating points are located to the right of the dashed line, i.e., the temperature is higher than T_{DEW} and the phase envelope is not entered. In this condition, there is no condensation. The dotted line corresponds to T_{DEW} plus TIC-2 controller set-point, ΔT = 3°C (T = 41.5°C). It can be observed that all the points remained to the right of the dotted line, at a safe distance (ΔT) from the phase envelope. For all of the beds, the minimum temperature observed was 41.3°C and the maximum temperature was 230.5°C. It was verified that the operating points remained outside

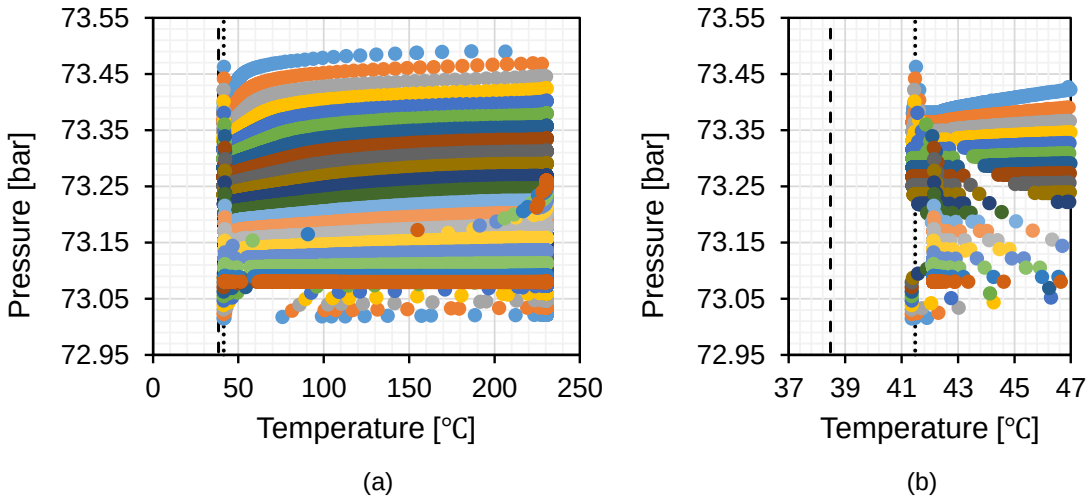

Figure 4.81: Operating points and phase envelope for BED 1 during six TSA cycles for Simulation 5 (a) for the whole temperature range of the six TSA cycles and (b) zoom close to T_{DEW} (dashed line). For the process pressure range (72.95 bar < P < 73.55 bar), T_{DEW} is approximately constant and equal to 38.5°C. The controller set-point (ΔT = 3°C) plus T_{DEW} is also approximately constant and equal to 41.5°C.

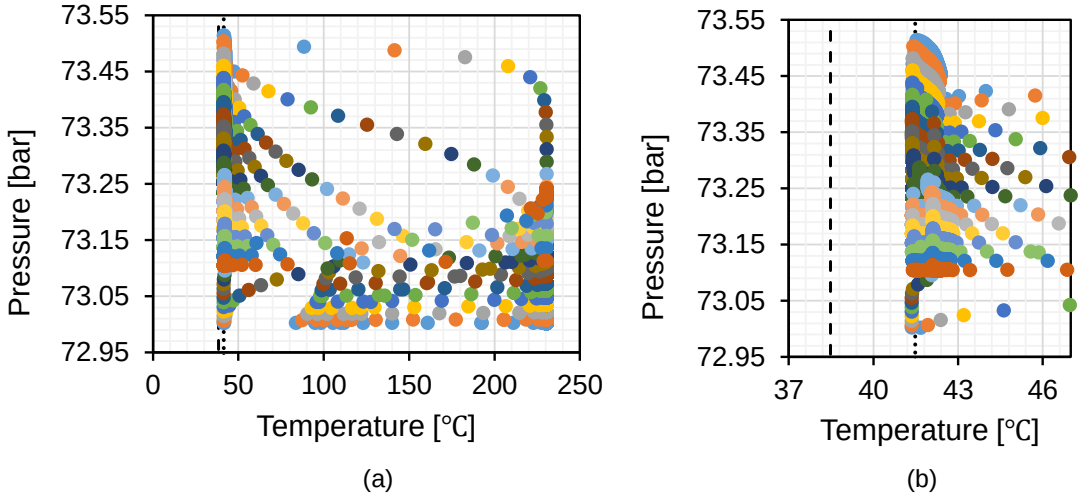

Figure 4.82: Operating points and phase envelope for BED 2 during six TSA cycles for Simulation 5 (a) for the whole temperature range of the six TSA cycles and (b) zoom close to T_{DEW} (dashed line). For the process pressure range (72.95 bar < P < 73.55 bar), T_{DEW} is approximately constant and equal to 38.5°C. The controller set-point (ΔT = 3°C) plus T_{DEW} is also approximately constant and equal to 41.5°C.

of the phase envelope during all of the TSA cycles.

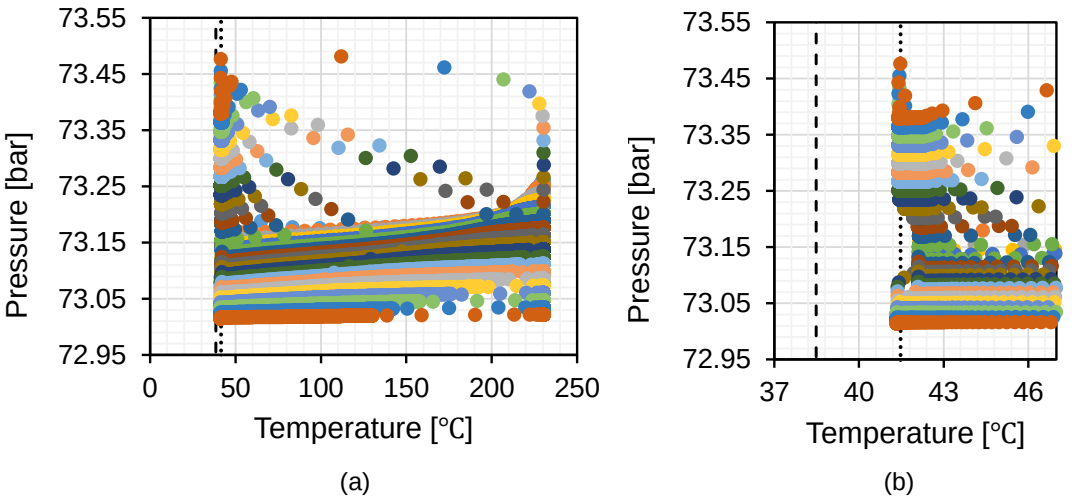

Figure 4.83: Operating points and phase envelope for BED 3 during six TSA cycles for Simulation 5 (a) for the whole temperature range of the six TSA cycles and (b) zoom close to T_{DEW} (dashed line). For the process pressure range (72.95 bar < P < 73.55 bar), T_{DEW} is approximately constant and equal to 38.5°C. The controller set-point (ΔT = 3°C) plus T_{DEW} is also approximately constant and equal to 41.5°C.

4.5.9 Feed Composition Variation

One of the advantages of including the control strategy presented for preventing condensation in the packed beds is that it should work even if there is a change in the feed stream composition, i.e., even if T_{DEW} changes. In order to verify the effectiveness of TIC-2 in this case, a 10% increase was applied to the mole fractions of H_2O, CO_2 and C_5H_{12} in the GDU feed stream. This 10% increase on the previously mentioned mole fractions was arbitrarily chosen. Table 4.7 presents the operating conditions for simulation 5 with a variation in feed stream composition. The simulation time was reset to t = 0 hours for the moment when the step changes in composition were applied.

Figure 4.84 presents the TIC-2 loop performance once the feed composition changes. As will be shown, for the new composition T_{DEW} = 39.5°C. This creates a drop in the process variable, which is accompanied by a rise in the manipulated variable. In less than 15 minutes the set-point is once again reached by the process variable. The manipulated variable stabilized at a value of 3.2163 MW. It is important to observe that initially, for 0 < t < 200 seconds there is condensation, since the point of lowest temperature on the bed is about 1°C smaller than T_{DEW} (PV negative). However, for the rest of the simulation the simulation, PV remains positive, indicating that there is no more condensation. Figure 4.85

Table 4.7: Operating conditions for simulation 5 with a 10% increase in the mole fractions of H_2O, CO_2 and C_5H_{12} in the GDU feed stream

Parameter	Value	Unit	Description
P_f	74.09	bar	Feed stream pressure
P_p	73.07	bar	Product stream pressure
T_f	34.0	°C	Feed temperature
F_f	3.7	kmol/s	Initial flow rate
Y_{CH_4}	0.4313	mol/mol	Molar fraction of methane at feed stream
Y_{CO_2}	0.5170	mol/mol	Molar fraction of carbon dioxide at feed stream
Y_{H_2O}	0.0009	mol/mol	Molar fraction of water at feed stream
$Y_{C_5H_{12}}$	0.0508	mol/mol	Molar fraction of N-PENTANE at feed stream

shows the control loop performance for the next switching event (t = 6 hours). The process variable remains positive at all times, which indicates that there is no condensation.

Figure 4.86 presents the mole fraction of water in the product stream. It can be observed that the product remained inside specification (1.0×10^{-4}) for all of the cycles.

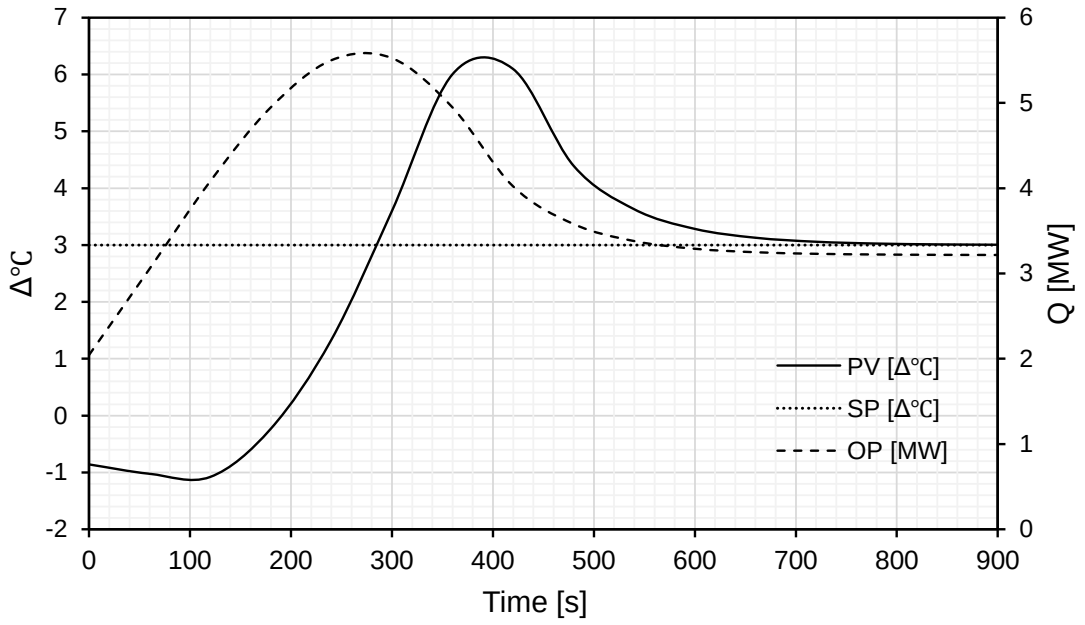

Figure 4.84: Feed temperature controller (TIC-2) performance during simulation 5, on first cycle after 10% composition increase on the mole fractions of H_2O, CO_2 and C_5H_{12}. PI parameters: controller action = reverse, gain = 1%/%, integral time = 0.2 min. Performance: $\tau_{10\%} \approx 600$ s, overshoot = 3.1°C. Maximum OP = 5.5 MW.

Figure 4.87 presents the operation points along BED 1 during 7.3 TSA cycles. At the [73, 73.6] bar pressure range, the new dew-point temperature remained

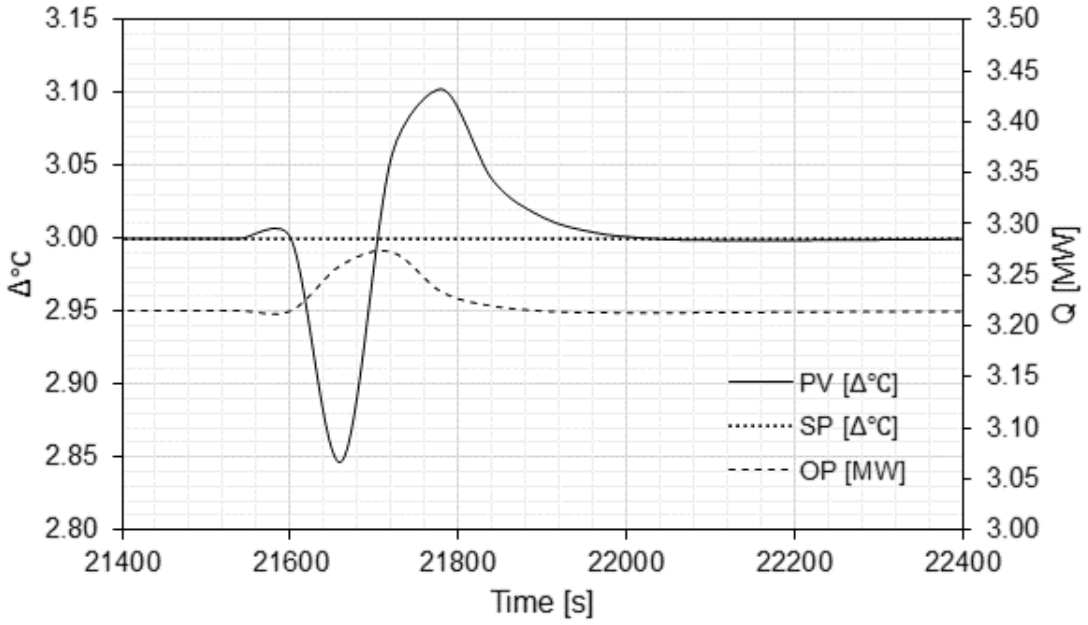

Figure 4.85: Feed temperature controller (TIC-2) cyclic performance during simulation 5, after 10% composition increase on the mole fractions of H_2O, CO_2 and C_5H_{12}. PI parameters: controller action = reverse, gain = 1%/%, integral time = 0.2 min.

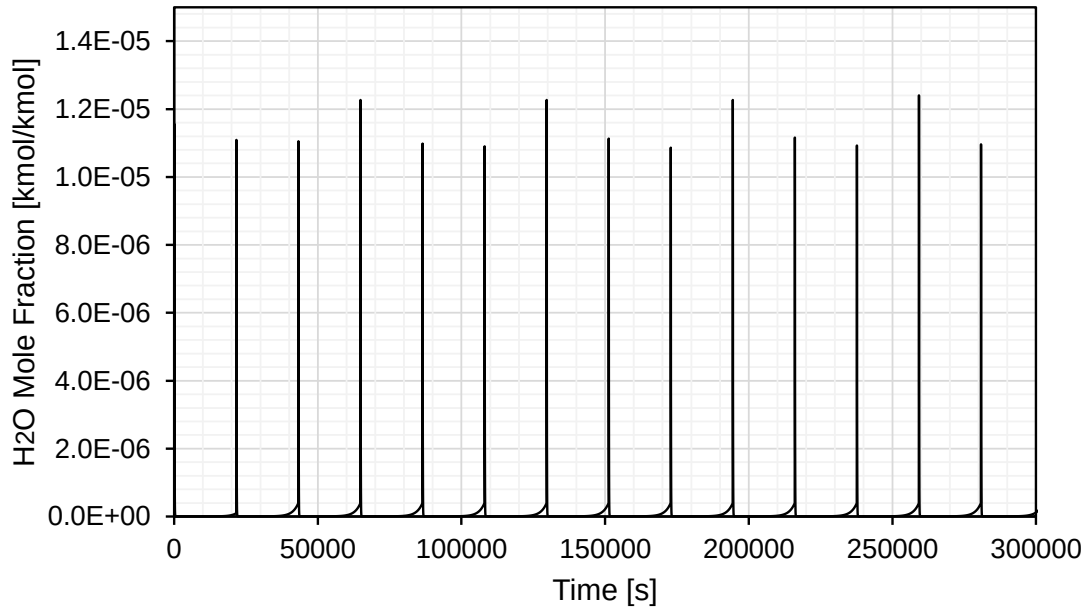

Figure 4.86: Mole fraction of water on product stream after 10% composition increase on the mole fractions of H_2O, CO_2 and C_5H_{12}. Product cut is at 1.0×10^{-4}.

practically constant at 39.5 °C. Only the plot for BED 1 was shown, since the plots for the other beds are very similar. It is important to note that although the points started initially to the left of the T_{DEW} + ΔT (T = 42.5°C), the control later drove them to the right, where it remained until the rest of the simulation.

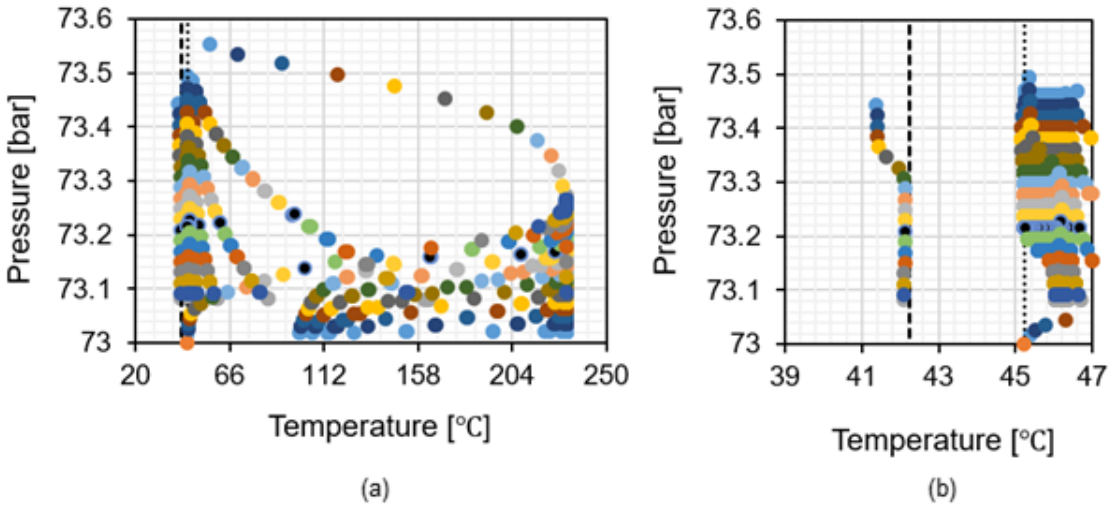

Figure 4.87: Operating points along BED 1 during 7.3 TSA cycles of simulation 5 after feed stream composition variation. For P $\in$ [73, 73.6] bar, the dew-point temperature remained practically constant at approximately 42.2°C (dashed line) and $T_{DEW} + \Delta T \approx$ 45.2°C (dotted line). (a) is presents the plot for the whole temperature range. (b) is the plot close to T_{DEW}. ΔT = 3°C.

Chapter 5

Conclusion

This chapter presents the conclusions of this work and a list with proposed future works that were not executed either due to lack of time or for being out of the scope of this research.

5.1 Conclusions

The simulation results for the adopted model were coherent, but indicated that a more simplified model could have been chosen using a fixed pressure profile along the bed. This would reduce computational time.

It was shown that condensation occurs on a packed bed being fed with saturated gas, since temperature drops to a value lower than the feed temperature during the adsorption phase of a TSA cycle.

It was also shown that preheating the feed stream with a fixed temperature above the fixed dew-point temperature for the design composition is not adequate since feed stream component mole fractions vary with time, which causes the dew-point temperature to also vary with time.

Simulations using the proposed PI controller with a variable set-point (a fixed ΔT from T_{DEW}) were able to reduce the time that the plant operated within the phase envelope without compromising product specification.

With the same control loop parameters, the simulated process plant managed to reduce its time inside the envelope after a 10% increase in the compositions of water, carbon dioxide and pentane.

For the proposed control strategy, a better evaluation is necessary to determine the exact amount of time in which all of the operating points remained outside of the phase envelope. This is necessary because this work considered that the variation of the composition inside the bed is very small, so that the phase envelope would remain the same throughout the packed bed. However,

this is actually not the case due to co-adsorption of other components that are present in elevated quantities in the feed stream. It is necessary to determine the phase envelope at each bed coordinate according to the gas composition at the particular coordinate. The difference between the T_{DEW} of the envelope with the highest dew-point temperature and T_{DEW} of the feed gas envelope at the operating pressure range can be used to determine a more conservative and more effective value of T for the TIC-2 controller.

5.2 Future Work Proposals

This section contains a series of actions that would enhance this work contributing to its conclusion and further expanding the investigation on the improvements that control could bring to the GDU, but were considered beyond the scope of this work:

- Perform experimental tests to obtain isotherms for the adsorption of CH_4, CO_2, H_2S and H_2O on different samples (pellets and beads) of 3A and 4A zeolites from various manufacturers under high temperature (200 °C - 300 °C) and pressure (60 bar - 80 bar), since open access scientific literature lacks this information.

- Redo the simulations considering variable bed parameters. Since some of the parameters vary with temperature and pressure, a weighted average was used so a single parameter could be adopted throughout the whole cycle. However, Aspen Adsorption allows parameters to be defined according to cycle times. This functionality could have been used and would have brought greater accuracy to the model.

- Remodel the regeneration loop including the ramped temperature heating, in order to represent more accurately the actual process.

- Perform a control strategy using the process variables that were already adopted, but with a multi-variable predictive controller. Constraints to velocity and product specification should be incorporated. Analyze the limits of feed stream composition variation for which the product remains under the desired specification and outside of the phase envelope.

- Analyze the impacts of H_2S co-adsorption and accumulation on the primary processing plant due to the cyclic behavior of the GDU.

- Develop a control strategy to define the optimum cycle time for each cycle according to process conditions.

- Develop a control strategy to define the optimum regeneration conditions (temperature and flow rate) for each cycle according to process conditions.

Appendix A

Desiccant Material Parameters

Table A.1 was obtained from AMBRÓSIO (2014).

Figure A.1: Parameters

Dessecante	Massa específica (kg/m³)	Calor Específico (kJ/kg°C)	Capacidade de Adsorção (adimensional)	Temperatura de Regeneração (°C)	Conteúdo de Água na Corrente de Saída
Alumina Ativada	820	1,005	0,07	177-316	-68 °C (ponto de orvalho)
Alumina Ativa Alcoa F200	770	1,000	0,07	177-316	-68 °C (ponto de orvalho)
Alumina Ativa UOP A-201	735	0,921	0,07	177-316	5 a 10 ppmv
Alumina Gel H-151	836	1,050	0,07	177-316	-68 °C (ponto de orvalho)
Sílica Gel	725	0,921	0,07	177	-51°C (ponto de orvalho)
Sílica Gel Sorbead-R	785	1,050	0,07	149	-51°C (ponto de orvalho)
Sílica Gel Sorbead-H	720	1,050	0,07	149	-51°C (ponto de orvalho)
Sílica Gel Sorbead-WS	720	1,050	0,07	149	-51°C (ponto de orvalho)
Sorbead Mobil	789	1,050	0,07	149-260	Não informado
Fluorita	805	1,005	0,045	177+	Não informado
Peneiras Moleculares (3A)	756	1,047	0,10	232-288	Não informado
Peneiras Moleculares (4A)	725	1,050	0,10	232-288	0,1 ppm
Peneiras Moleculares (4A) Davison	720	0,961	0,10	232-288	0,1 ppm (equivalente a -101 °C)
Peneiras Moleculares (4A) UPO - DG	705	1,005	0,10	232-288	0,1 ppm
Peneiras Moleculares (4A) Zeochen	735	1,005	0,10	232-288	0,1 ppm

Appendix B

Polynomial Interpolation of the Phase Diagram (Pressure - Temperature Curve)

Although the Phase Envelopes for both the simplified composition and the actual expected composition (see Table 3.3) have a rather complex form (see Figure B.1), these curves resemble a parabola on the interval of temperature and pressure involved in the GDU process (see Figure B.2). This suggests that a Polynomial Interpolation may be used to obtain a simple mathematical expression (polynomial) to describe the phase behaviour of the stream in the pressure-temperature interval of interest.

B.1 Obtaining a Simplified Composition

In order to reduce model complexity and increase simulation speed, a simplified composition was obtained. The simplified composition has a phase envelope similar to the original composition in both shape and cricondentherm value. Although the cricondenbar was a bit different, it was considered a good enough approximation in order to evaluate qualitatively the stream behavior regarding retrograde condensation.

B.2 Obtaining a Polynomial

In the interval $P(bar) \in [40, 106]$ and $T(^{\circ}C) \in [25, 40]$, the curve is as shown in Figure B.2.

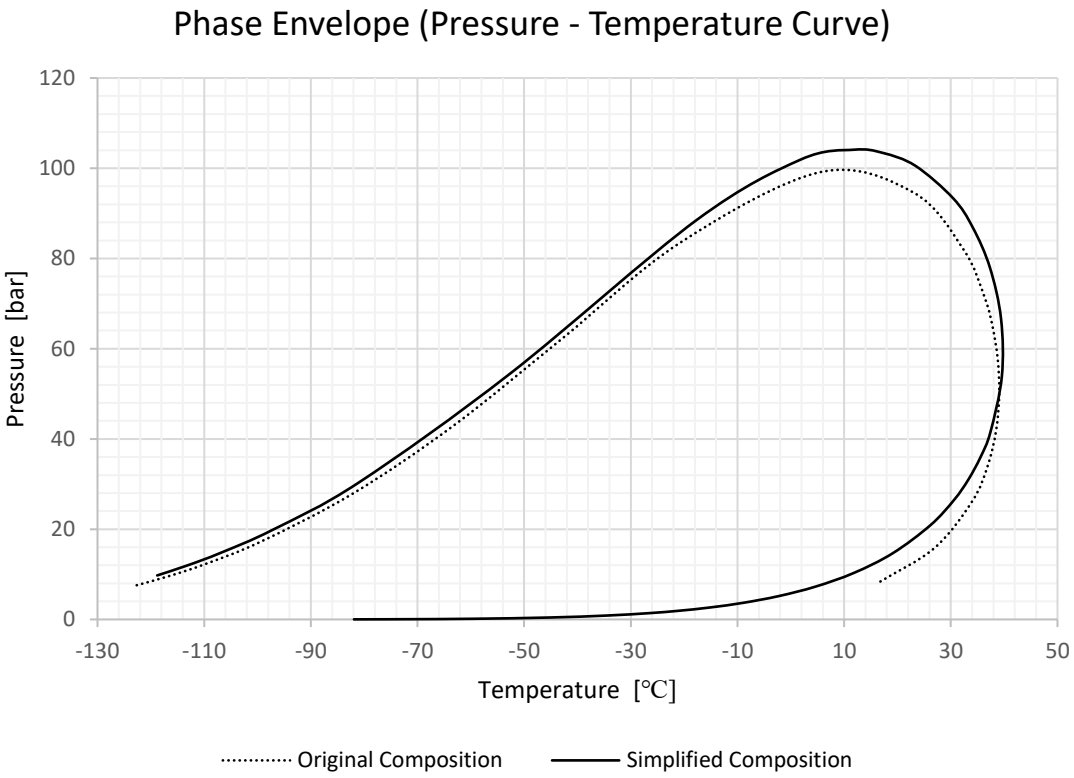

Figure B.1: Phase diagram.

Table B.1: Data points from the simplified composition's phase envelope

i	$T(^{\circ}C)$	$P(bar)$
0	37.42546	41.52103
1	39.57313	53.90402
2	39.41712	66.62534
3	37.33621	77.96777
4	34.10333	86.90816
5	30.43473	93.34444

Coefficient	**Value**
c_0	35.768838
c_1	-1.132463071
c_2	0.064786585
c_3	-0.001274913
c_4	$1.10733E-05$
c_5	$-3.78009E-08$

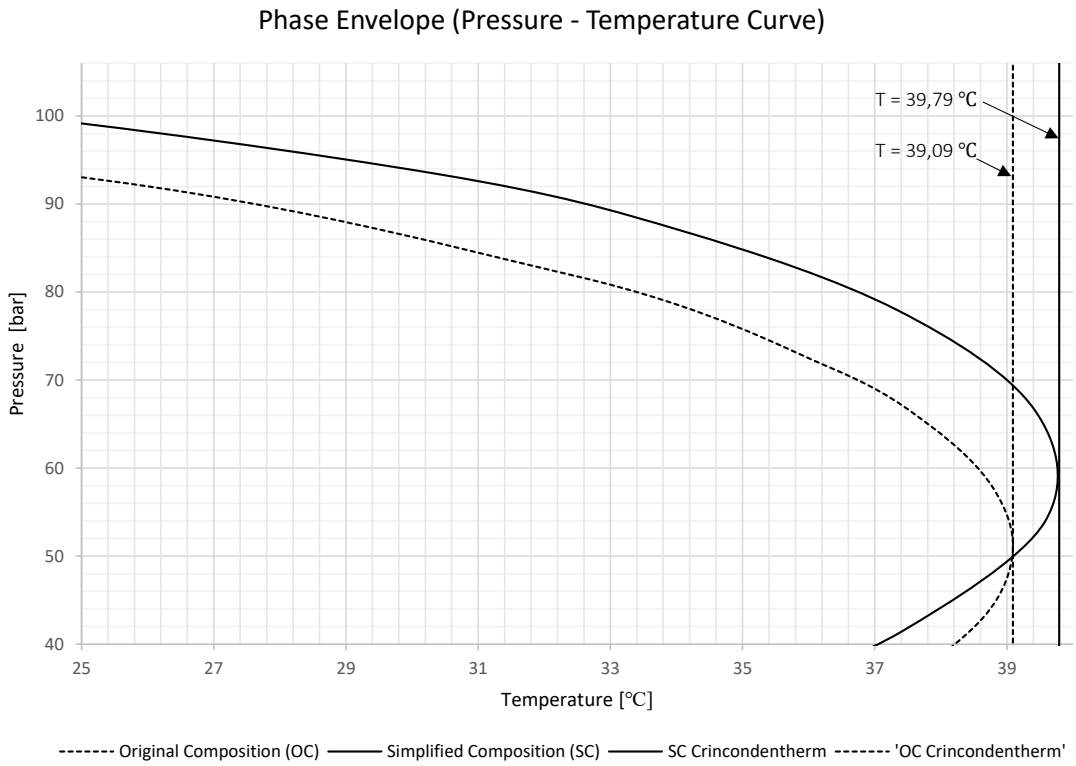

Figure B.2: Phase diagram.

$$\begin{cases} c_0 + c_1 \cdot P_1(bar) + c_2 \cdot P_1(bar)^2 + c_3 \cdot P_1(bar)^3 + c_4 \cdot P_1(bar)^4 + c_5 \cdot P_1(bar)^5 = T_1(^\circ C) \\ c_0 + c_1 \cdot P_2(bar) + c_2 \cdot P_2(bar)^2 + c_3 \cdot P_2(bar)^3 + c_4 \cdot P_2(bar)^4 + c_5 \cdot P_2(bar)^5 = T_2(^\circ C) \\ c_0 + c_1 \cdot P_3(bar) + c_2 \cdot P_3(bar)^2 + c_3 \cdot P_3(bar)^3 + c_4 \cdot P_3(bar)^4 + c_5 \cdot P_3(bar)^5 = T_3(^\circ C) \\ c_0 + c_1 \cdot P_4(bar) + c_2 \cdot P_4(bar)^2 + c_3 \cdot P_4(bar)^3 + c_4 \cdot P_4(bar)^4 + c_5 \cdot P_4(bar)^5 = T_4(^\circ C) \\ c_0 + c_1 \cdot P_5(bar) + c_2 \cdot P_5(bar)^2 + c_3 \cdot P_5(bar)^3 + c_4 \cdot P_5(bar)^4 + c_5 \cdot P_5(bar)^5 = T_5(^\circ C) \\ c_0 + c_1 \cdot P_6(bar) + c_2 \cdot P_6(bar)^2 + c_3 \cdot P_6(bar)^3 + c_4 \cdot P_6(bar)^4 + c_5 \cdot P_6(bar)^5 = T_6(^\circ C) \end{cases}$$

$$\begin{bmatrix} 1 & P_1 & P_1^2 & P_1^3 & P_1^4 & P_1^5 \\ 1 & P_2 & P_2^2 & P_2^3 & P_2^4 & P_2^5 \\ 1 & P_3 & P_3^2 & P_3^3 & P_3^4 & P_3^5 \\ 1 & P_4 & P_4^2 & P_4^3 & P_4^4 & P_4^5 \\ 1 & P_5 & P_5^2 & P_5^3 & P_5^4 & P_5^5 \\ 1 & P_6 & P_6^2 & P_6^3 & P_6^4 & P_6^5 \end{bmatrix} \times \begin{bmatrix} c_0 \\ c_1 \\ c_2 \\ c_3 \\ c_4 \\ c_5 \end{bmatrix} = \begin{bmatrix} T_1 \\ T_2 \\ T_3 \\ T_4 \\ T_5 \\ T_6 \end{bmatrix}$$

$$\begin{bmatrix} c_0 \\ c_1 \\ c_2 \\ c_3 \\ c_4 \\ c_5 \end{bmatrix} = \begin{bmatrix} 1 & P_1 & P_1^2 & P_1^3 & P_1^4 & P_1^5 \\ 1 & P_2 & P_2^2 & P_2^3 & P_2^4 & P_2^5 \\ 1 & P_3 & P_3^2 & P_3^3 & P_3^4 & P_3^5 \\ 1 & P_4 & P_4^2 & P_4^3 & P_4^4 & P_4^5 \\ 1 & P_5 & P_5^2 & P_5^3 & P_5^4 & P_5^5 \\ 1 & P_6 & P_6^2 & P_6^3 & P_6^4 & P_6^5 \end{bmatrix}^{-1} \times \begin{bmatrix} T_1 \\ T_2 \\ T_3 \\ T_4 \\ T_5 \\ T_6 \end{bmatrix} \tag{B.1}$$

$$\begin{aligned} T(^\circ C) \approx\ & 35.768838 - 1.132463071 \cdot P(bar) + 0.064786585 \cdot P(bar)^2 \\ & - 0.001274913 \cdot P(bar)^3 + 1.10733 \times 10^{-5} \cdot P(bar)^4 \\ & - 3.78 \times 10^{-8} \cdot P(bar)^5, \quad T \in [25, 40]^\circ C, P \in [40, 106] bar \end{aligned} \tag{B.2}$$

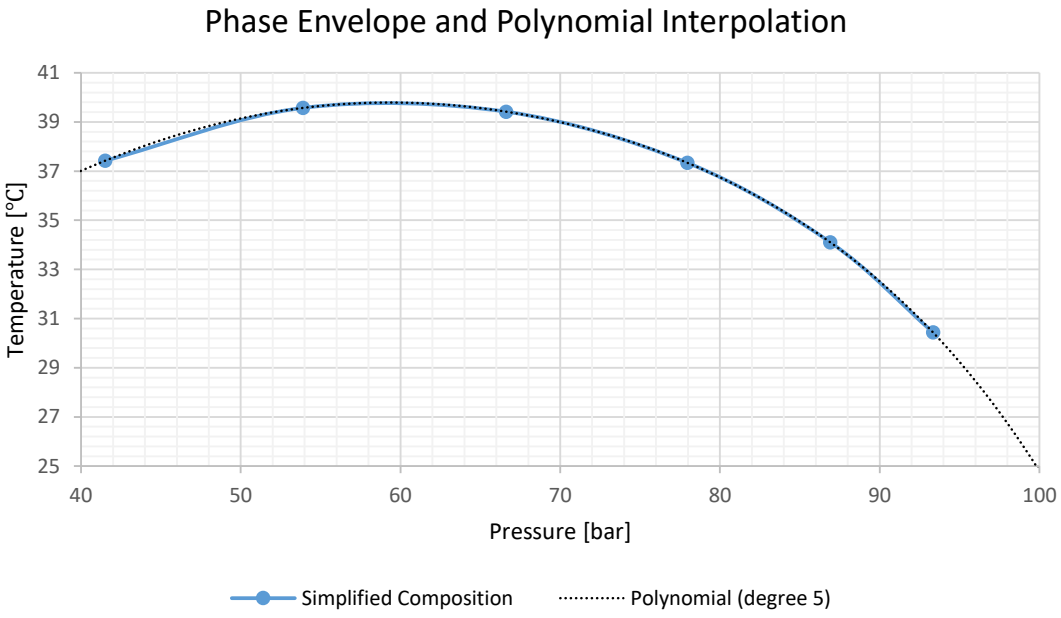

Figure B.3: Phase diagram.

Appendix C

CH_4 Adsorption Isotherm on 4A Zeolite

Literature data listed on Table C.1 was used to obtain the Langmuir 3 isotherm parameters for CH_4 adsorption on 4A zeolite.

302 K			273 K			248 K		
i	Pressure P (bar)	Loading q (kmol/kg)	i	Pressure P (bar)	Loading q (kmol/kg)	i	Pressure P (bar)	Loading q (kmol/kg)
01	0.13050847458	7.3286661754E-05	15	0.12516556291	0.00013742426377	31	0.053105045159	0.00016485934534
02	0.17796610169	9.1635961680E-05	16	0.23178807947	0.00028001409046	32	0.069303342346	0.00019959155497
03	0.29661016949	0.00016229182019	17	0.28741721854	0.00034108778357	33	0.101659667490	0.00028637174251
04	0.37016949153	0.00019373323508	18	0.36390728477	0.00042251092011	34	0.129385031350	0.00036446528217
05	0.47932203390	0.00024871923360	19	0.41490066225	0.00046828237283	35	0.159456077780	0.00043391531957
06	0.53864406780	0.00027230803242	20	0.47516556291	0.00052933915739	36	0.189527124200	0.00050336535696
07	0.60271186441	0.00030373176124	21	0.53774834437	0.00058528110469	37	0.242773111660	0.00060759074958
08	0.71186440678	0.00035871775976	22	0.63278145695	0.00067174299000	38	0.291368003220	0.00071178737847
09	0.84000000000	0.00040330434783	23	0.71158940397	0.00072762575736	39	0.321519588100	0.00074660587931
10	0.95864406780	0.00044787324982	24	0.83675496689	0.00082929688601	40	0.351610769140	0.00080739803256
11	1.04169491530	0.00048194104643	25	0.95728476821	0.00090545300831	41	0.437253350980	0.00098108784445
12	1.07966101690	0.00051853352985	26	0.98973509934	0.00093086656334	42	0.539255306910	0.00112024679280
13	1.14372881360	0.00053430508475	27	1.03145695360	0.00096645906721	43	0.564755795890	0.00115503652990
14	1.19355932200	0.00055787619749	28	1.08013245030	0.00099691982528	44	0.613451360520	0.00121594373810
			29	1.14039735100	0.00103244469490	45	0.650579589250	0.00125080538460
			30	1.19602649010	0.00106798647320	46	0.803703330840	0.00140759650230
						47	0.838485877010	0.00145110165100
						48	0.875634240350	0.00147730541330
						49	0.919718978310	0.00152086808950
						50	0.954521659090	0.00155571535410
						51	0.989344474490	0.00158190473450
						52	1.193751078600	0.00168706494850

Table C.1: Literature data as presented on SANTOS (2016) for the adsorption of methane on 4A zeolite.

Isotherm parameters were obtained by minimizing the Sum of the Estimated

Square Errors (SSE) with the restrictions that $IP_2 = 0$.

$$\hat{q}_i = \frac{(IP_1 - IP_2 \cdot T_i) \cdot IP_3 \cdot e^{IP_4/T_i} \cdot P_i}{1 + IP_3 \cdot e^{IP_4/T_i} \cdot P_i} \tag{C.1}$$

$$\sigma_i^2 = (q_i - \hat{q}_i)^2 \tag{C.2}$$

$$SSE = \sum_{i=1}^{52} \sigma_i^2 \tag{C.3}$$

$$\begin{aligned} \min_{IP_1, IP_2, IP_3 \in \mathbb{R}_{\geq 0}} \quad & \sum_{i=1}^{52} \left(q_i - \frac{(IP_1 - IP_2 \cdot T_i) \cdot IP_3 \cdot e^{IP_4/T_i} \cdot P_i}{1 + IP_3 \cdot e^{IP_4/T_i} \cdot P_i} \right)^2 \\ \text{s.t.} \quad & IP_2 = 0 \end{aligned} \tag{C.4}$$

A Differential Evolution and Particle Swarm (DEPS) Evolutionary Algorithm was used so solve Equation C.4, with the following parameters:

- Agent Switch Rate (DE Probability): 0.5
- Negative Variables Allowed
- DE: Crossover Probability: 0.9
- DE: Scaling Factor: 0.5
- Learning Cycles: 2000
- PS: Cognitive Constant: 1.494
- PS: Constriction Coefficient: 0.729
- PS: Mutation Probability: 0
- PS: Social Constant: 1.494
- Size of Swarm: 70
- Stagnation Limit: 70
- Stagnation Tolerance: 0.000001

- Variable Bounds Guessing Enabled
- Variable Bounds Threshold: 3

The LibreOffice Calc extension Solver for Nonlinear Programming (NLP-Solver) contains the DEPS Evolutionary Algorithm. This extension was used in order to solve the optimization problem.

After 175 learning cycles, which took a total of 20.51 seconds, a solution which provide a sum of squared errors of $6.14515340794823E-09$ was obtained. The parameters presented on Table C.2 obtained by SANTOS (2016) were used as initial conditions. The third column shows the parameters obtain by the DEPS Evolutionary Algorithm.

Table C.2: Langmuir 3 isotherm parameters for the adsorption of methane on 4A zeolite.

Parameter	SANTOS (2016)	DEPS
IP_1	0.007749408	0.003152522
IP_2	-1.77E-05	0.00E+00
IP_3	0.29661016949	6.82223E-05
IP_4	0.000827069	2381.605255

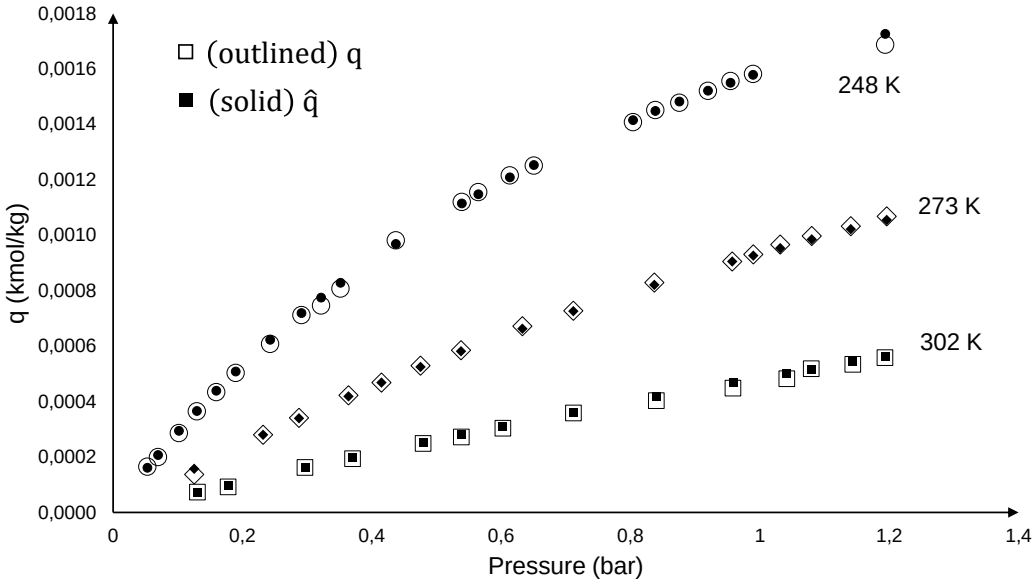

Figure C.1: Estimated isotherm data points for methane on 4A zeolite ($\widehat{q}$) compared with literature data presented in SANTOS (2016) (q).

Bibliography

ADSIM, 2017. "Aspen Adsorption's User Manual (software version 10)". .

AHN, H., MOON, J.-H., HYUN, S.-H., et al., 2004, "Diffusion Mechanism of Carbon Dioxide in Zeolite 4A and CaX Pellets", *Adsorption*, v. 10 (06), pp. 111–128. doi: <10.1023/B:ADSO.0000039867.14756.ac>.

AMBROZEK, B., 2008, "Removal and recovery of volatile organic compounds (VOCs) from waste air streams in thermal swing adsorption (TSA) system with closed-loop regeneration of adsorbent", *Environment Protection Engineering*, v. 34 (01), pp. 27–32.

AMBROŻEK, B., 2009, "The Simulation of Cyclic Thermal Swing Adsorption (TSA) Process". In: *Modelling Dynamics in Processes and Systems*, Springer Berlin Heidelberg, pp. 165–178. Availability: <https://doi.org/10.1007/978-3-540-92203-2_12>.

AMBRÓSIO, A. A. P. G. D. O., 2014, *Análise de Desempenho de Gás Natural por Adsorção em Peneiras Moleculares*. Master thesis, EQ/UFRJ, Rio de Janeiro, RJ, Brazil.

ANP, 2019. "Oil, Natural Gas and Biofuels Statistical Yearbook 2019". Availability: <http://www.anp.gov.br/publicacoes/anuario-estatistico/5237-anuario-estatistico-2019>.

API, 2011, "Robust Summary of Information on Crude Oil", *Industrial & Engineering Chemistry*.

ATUONWU, J. C., VAN STRATEN, G., VAN DEVENTER, H. C., et al., 2011a, "Model-Based Energy Efficiency Optimization of a Low-Temperature Adsorption Dryer", *Chemical Engineering & Technology*, v. 34, n. 10, pp. 1723–1732. doi: <10.1002/ceat.201100145>. Availability: <https://doi.org/10.1002/ceat.201100145>.

ATUONWU, J. C., VAN STRATEN, G., VAN DEVENTER, H. C., et al., 2011b, "Improving Adsorption Dryer Energy Efficiency by Simultaneous Op-

timization and Heat Integration", *Drying Technology*, v. 29, n. 12 (set.), pp. 1459–1471. doi: <10.1080/07373937.2011.591516>. Availability: <https://doi.org/10.1080/07373937.2011.591516>.

ATUONWU, J. C., VAN STRATEN, G., VAN DEVENTER, H. C., et al., 2012, "On the controllability and energy sensitivity of heat-integrated desiccant adsorption dryers", *Chemical Engineering Science*, v. 80, pp. 134–147. doi: <10.1016/j.ces.2012.06.006>. Availability: <http://dx.doi.org/10.1016/j.ces.2012.06.006>.

BASMADJIAN, D., 1975, "On the possibility of omitting the cooling step in thermal gas adsorption cycles", *The Canadian Journal of Chemical Engineering*, v. 53, n. 2 (abr.), pp. 234–238. doi: <10.1002/cjce.5450530216>. Availability: <https://doi.org/10.1002/cjce.5450530216>.

BENYAHIA, F., O'NEILL, K. E., 2005, "Enhanced Voidage Correlations for Packed Beds of Various Particle Shapes and Sizes", *Particulate Science and Technology*, v. 23, n. 2 (abr.), pp. 169–177. doi: <10.1080/02726350590922242>. Availability: <https://doi.org/10.1080/02726350590922242>.

BERCHE, B., HENKEL, M., KENNA, R., 2009, "Fenômenos críticos: 150 anos desde Cagniard de la Tour", *Revista Brasileira de Ensino de Física*, v. 31, n. 2 (jun.), pp. 2602.1–2602.4. doi: <10.1590/s1806-11172009000200015>. Availability: <https://doi.org/10.1590/s1806-11172009000200015>.

BERG, F., PASEL, C., ECKARDT, T., et al., 2019, "Temperature Swing Adsorption in Natural Gas Processing: A Concise Overview", *ChemBioEng Reviews*, (abr.). doi: <10.1002/cben.201900005>. Availability: <https://doi.org/10.1002/cben.201900005>.

BONJOUR, J., CHALFEN, J.-B., MEUNIER, F., 2002, "Temperature Swing Adsorption Process with Indirect Cooling and Heating", *Industrial & Engineering Chemistry Research*, v. 41, n. 23 (nov.), pp. 5802–5811. doi: <10.1021/ie011011j>. Availability: <https://doi.org/10.1021/ie011011j>.

BONNISSEL, M. P., LUO, L., TONDEUR, D., 2001, "Rapid Thermal Swing Adsorption", *Industrial & Engineering Chemistry Research*, v. 40, n. 10 (maio), pp. 2322–2334. doi: <10.1021/ie000809k>. Availability: <https://doi.org/10.1021/ie000809k>.

BRAUN, F., 2018, *Modeling and Optimization of Adsorption Natural Gas Dehydration Units*. Master thesis, PEQ/COPPE, Rio de Janeiro, RJ, Brazil.

BURKE, S. P., PLUMMER, W. B., 1928, "Gas Flow through Packed Columns1", *Industrial & Engineering Chemistry*, v. 20, n. 11 (nov.), pp. 1196–1200. doi: <10.1021/ie50227a025>. Availability: <https://doi.org/10.1021/ie50227a025>.

CAMPBELL, J. M., 2014, *Gas conditioning and processing: Volume 2: The equipment modules*. Norman, Oklahoma, John M. Campbell, PetroSkills. ISBN: 9780970344953. 9943198002346.

CLAUSSE, M., BONJOUR, J., MEUNIER, F., 2003, "Influence of the Presence of CO2 in the Feed of an Indirect Heating TSA Process for VOC Removal", *Adsorption*, v. 9, n. 1 (Mar), pp. 77–85. doi: <10.1023/A:1023819431640>. Availability: <https://doi.org/10.1023/A:1023819431640>.

CLAUSSE, M., BONJOUR, J., MEUNIER, F., 2004, "Adsorption of gas mixtures in TSA adsorbers under various heat removal conditions", *Chemical Engineering Science*, v. 59, n. 17 (set.), pp. 3657–3670. doi: <10.1016/j.ces.2004.05.027>. Availability: <https://doi.org/10.1016/j.ces.2004.05.027>.

DANNER, R., DAUBERT, T., OF REFINING, A. D., 1983, *API Technical Data Book - Petroleum Refining*. Washington, D.C.: The Dept.

DE CAMPOS, M. C. M. M., TEIXEIRA, H. C. G., 2010, *Controles Típicos de Equipamentos e Processos Industriais*. Blucher. ISBN: 978-85-212-0552-4.

ERGUN, S., 1952, "Fluid flow through packed columns". .

FOO, K. Y., HAMEED, B. H., 2010, "Insights into the modeling of adsorption isotherm systems", *Chemical Engineering Journal*, v. 156, n. 1, pp. 2–10. doi: <https://doi.org/10.1016/j.cej.2009.09.013>. Availability: <http://www.sciencedirect.com/science/article/pii/S1385894709006147>.

FULLER, E. N., SCHETTLER, P. D., GIDDINGS, J. C., 1966, "NEW METHOD FOR PREDICTION OF BINARY GAS-PHASE DIFFUSION COEFFICIENTS", *Industrial & Engineering Chemistry*, v. 58, n. 5 (maio), pp. 18–27. doi: <10.1021/ie50677a007>. Availability: <https://doi.org/10.1021/ie50677a007>.

FULLER, E. N., ENSLEY, K., GIDDINGS, J. C., 1969, "Diffusion of halogenated hydrocarbons in helium. The effect of structure on collision cross sections", *The Journal of Physical Chemistry*, v. 73, n. 11 (nov.), pp. 3679–3685. doi: <10.1021/j100845a020>. Availability: <https://doi.org/10.1021/j100845a020>.

GABRUŚ, E., NASTAJ, J., TABERO, P., et al., 2015, "Experimental studies on 3A and 4A zeolite molecular sieves regeneration in TSA process: Aliphatic alcohols dewatering–water desorption", *Chemical Engineering Journal*, v. 259 (jan.), pp. 232–242. doi: <10.1016/j.cej.2014.07.108>. Availability: <https://doi.org/10.1016/j.cej.2014.07.108>.

GIRAUDET, S., PRE

, P., CLOIREC, P. L., 2009, "Modeling the Heat and Mass Transfers in Temperature-Swing Adsorption of Volatile Organic Compounds onto Activated Carbons", *Environmental Science & Technology*, v. 43, n. 4 (fev.), pp. 1173–1179. doi: <10.1021/es801494a>. Availability: <https://doi.org/10.1021/es801494a>.

HUANG, C.-C., FAIR, J. R., 1988, "Study of the adsorption and desorption of multiple adsorbates in a fixed bed", *AIChE Journal*, v. 34, n. 11 (nov.), pp. 1861–1877. doi: <10.1002/aic.690341112>. Availability: <https://doi.org/10.1002/aic.690341112>.

HUANG, C.-C., FAIR, J. R., 1989, "Parametric analysis of thermal swing cycles for multicomponent adsorption", *AIChE Journal*, v. 35, n. 10 (out.), pp. 1667–1677. doi: <10.1002/aic.690351011>. Availability: <https://doi.org/10.1002/aic.690351011>.

JOSS, L., GAZZANI, M., MAZZOTTI, M., 2017, "Rational design of temperature swing adsorption cycles for post-combustion CO 2 capture", *Chemical Engineering Science*, v. 158 (fev.), pp. 381–394. doi: <10.1016/j.ces.2016.10.013>. Availability: <https://doi.org/10.1016/j.ces.2016.10.013>.

KAPOOR, A., RITTER, J. A., YANG, R. T., 1990, "An extended Langmuir model for adsorption of gas mixtures on heterogeneous surfaces", *Langmuir*, v. 6, n. 3 (mar.), pp. 660–664. doi: <10.1021/la00093a022>. Availability: <https://doi.org/10.1021/la00093a022>.

KAST, W., 1988, *Adsorption Aus Der Gasphase Ingenieurwissenschaftliche Grundlagen U Technische Verfahren*. Wiley-VCH. ISBN: 3527267190. Availability: <https://www.xarg.org/ref/a/3527267190/>.

KATZ, D. L., KURATA, F., 1940, "RETROGRADE CONDENSATION", *Industrial & Engineering Chemistry*, v. 32, n. 6 (jun.), pp. 817–827. doi: <10.1021/ie50366a018>. Availability: <https://pubs.acs.org/doi/abs/10.1021/ie50366a018>.

KIM, M.-B., MOON, J.-H., LEE, C.-H., et al., 2004, "Effect of heat transfer on the transient dynamics of temperature swing adsorption process", *Korean Journal of Chemical Engineering*, v. 21, n. 3 (May), pp. 703–711. doi: <10.1007/BF02705509>. Availability: <https://doi.org/10.1007/BF02705509>.

KO, D., KIM, M., MOON, I., et al., 2001, "Novel Thermal Swing Adsorption Process with a Cooling Jacket for Benzene-Toluene-p-Xylene Purification", *Industrial & Engineering Chemistry Research*, v. 40, n. 22 (out.), pp. 4973–4982. doi: <10.1021/ie000515z>. Availability: <https://doi.org/10.1021/ie000515z>.

KUENEN, J. P., 1892, *Communications from the Laboratory of Physics at the University of Leiden, No. 4*.

LI, P., 2007, *Adsorption and separations for methane, carbon dioxide, nitrogen and oxygen gases*. Thesis, University of Ottawa (Canada). Availability: <http://ruor.uottawa.ca/handle/10393/29444>.

MARX, D., JOSS, L., HEFTI, M., et al., 2016, "Temperature Swing Adsorption for Postcombustion CO2Capture: Single- and Multicolumn Experiments and Simulations", *Industrial & Engineering Chemistry Research*, v. 55, n. 5 (jan.), pp. 1401–1412. doi: <10.1021/acs.iecr.5b03727>. Availability: <https://doi.org/10.1021/acs.iecr.5b03727>.

MOATE, J. R., LEVAN, M. D., 2010, "Temperature swing adsorption compression: Effects of nonuniform heating on bed efficiency", *Applied Thermal Engineering*, v. 30, n. 6-7 (maio), pp. 658–663. doi: <10.1016/j.applthermaleng.2009.11.013>. Availability: <https://doi.org/10.1016/j.applthermaleng.2009.11.013>.

MOKHATAB, S., 2019, *Handbook of natural gas transmission and processing : principles and practices*. Oxford, Gulf Professional Publishing. ISBN: 978-0-12-815817-3.

MOREIRA, R. F. P. M., SOARES, J. L., CASARIN, G. L., et al., 2006, "Adsorption of CO $_2$ on Hydrotalcite-like Compounds in a Fixed Bed", *Separation Science and Technology*, v. 41, n. 2 (fev.), pp. 341–357. doi: <10.1080/01496390500496827>. Availability: <https://www.tandfonline.com/doi/full/10.1080/01496390500496827>.

MYERS, A. L., PRAUSNITZ, J. M., 1965, "Thermodynamics of mixed-gas adsorption", *AIChE Journal*, v. 11, n. 1 (jan.), pp. 121–127. doi: <10.1002/aic.690110125>. Availability: <https://doi.org/10.1002/aic.690110125>.

NASTAJ, J., AMBROŻEK, B., 2009, "Modeling of Drying of Gases Using Solid Desiccants", *Drying Technology*, v. 27, n. 12 (nov.), pp. 1344–1352. doi: <10.1080/07373930903383679>. Availability: <https://doi.org/10.1080/07373930903383679>.

NETUSIL, M., DITL, P., 2011, "Comparison of three methods for natural gas dehydration", *Journal of Natural Gas Chemistry*, v. 20, n. 5, pp. 471–476. doi: <10.1016/S1003-9953(10)60218-6>. Availability: <http://dx.doi.org/10.1016/S1003-9953(10)60218-6>.

NTIAMOAH, A., LING, J., XIAO, P., et al., 2016, "CO2 Capture by Temperature Swing Adsorption: Use of Hot CO2-Rich Gas for Regeneration", *Industrial & Engineering Chemistry Research*, v. 55, n. 3 (jan.), pp. 703–713. doi: <10.1021/acs.iecr.5b01384>. Availability: <https://doi.org/10.1021/acs.iecr.5b01384>.

OBERLAENDER, D. T., 2015, *SIMULAÇÃO E OTIMIZAÇÃO DE UMA UNIDADE DE DESIDRATAÇÃO DE GÁSNATURAL OFFSHORE: UMA ANÁLISE COM APLICAÇÃO OPERACIONAL*. Master thesis, EQ/UFRJ, Rio de Janeiro, RJ, Brazil.

OPEC, 2019. "OPEC Annual Statistical Bulletin 2019". Availability: <https://asb.opec.org/index.php/pdf-download>.

PAUL, E. L., 2003, *Handbook of Industrial Mixing: Science and Practice*. Wiley-Interscience. ISBN: 9780471269199. Availability: <https://www.xarg.org/ref/a/0471269190/>.

PENG, D.-Y., ROBINSON, D. B., 1976, "A New Two-Constant Equation of State", *Industrial & Engineering Chemistry Fundamentals*, v. 15, n. 1 (fev.), pp. 59–64. doi: <10.1021/i160057a011>. Availability: <https://doi.org/10.1021/i160057a011>.

PIRNGRUBER, G. D., GUILLOU, F., GOMEZ, A., et al., 2013, "A theoretical analysis of the energy consumption of post-combustion CO2 capture processes by temperature swing adsorption using solid sorbents", *International Journal of Greenhouse Gas Control*, v. 14 (maio), pp. 74–83. doi: <10.1016/j.ijggc.2013.01.010>. Availability: <https://doi.org/10.1016/j.ijggc.2013.01.010>.

RIBEIRO, R. P., SAUER, T. P., LOPES, F. V., et al., 2008, "Adsorption of CO2, CH4, and N2in Activated Carbon Honeycomb Monolith", *Journal of Chemical & Engineering Data*, v. 53, n. 10 (out.), pp. 2311–2317. doi: <10.1021/je800161m>. Availability: <https://doi.org/10.1021/je800161m>.

RITTER, R. B., LENOIR, J. M., SCHWEPPE, J. L., 1958, "Find specific gravities by nomograph", *Petroleum Refiner*, v. 37(11), pp. 225–232.

ROUQUEROL, J., AVNIR, D., FAIRBRIDGE, C. W., et al., 1994, "Recommendations for the characterization of porous solids (Technical Report)", *Pure and Applied Chemistry*, v. 66, n. 8 (jan.), pp. 1739–1758. doi: <10.1351/pac199466081739>. Availability: <https://doi.org/10.1351/pac199466081739>.

RUTHVEN, D. M., 1984, *Principles of Adsorption and Adsorption Processes*. Wiley-Interscience. ISBN: 9780471866060. Availability: <https://www.xarg.org/ref/a/0471866067/>.

SALVADOR, F., MARTIN-SANCHEZ, N., SANCHEZ-HERNANDEZ, R., et al., 2015, "Regeneration of carbonaceous adsorbents. Part I: Thermal Regeneration", *Microporous and Mesoporous Materials*, v. 202 (jan.), pp. 259–276. doi: <10.1016/j.micromeso.2014.02.045>. Availability: <https://doi.org/10.1016/j.micromeso.2014.02.045>.

SANTOS, M. G. R. S., 2016, *Molecular Sieve Dehydration of Natural Gas with High CO2 Content: Simulation and Aspects of Behavior*. Master thesis, EQ/UFRJ, Rio de Janeiro, RJ, Brazil.

SCHORK, J. M., FAIR, J. R., 1988, "Parametric analysis of thermal regeneration of adsorption beds", *Industrial & Engineering Chemistry Research*, v. 27, n. 3 (mar.), pp. 457–469. doi: <10.1021/ie00075a016>. Availability: <https://doi.org/10.1021/ie00075a016>.

SHAFEEYAN, MOHAMMAD SALEH WAN DAU AND, W. M. A. S. A., 2014, "A Review of Mathematical Modeling of Fixed-bed Columns for Car-

bon Dioxide Adsorption", *Chemical Engineering Research and Design*, v. 92, pp. 961–988. doi: <10.1016/j.cherd.2013.08.018>.

SHEIKHOLESLAMI, M., GANJI, D. D., 2017, "Nanofluid Forced Convection Heat Transfer". In: *Applications of Nanofluid for Heat Transfer Enhancement*, Elsevier, pp. 127–193. Availability: <https://doi.org/10.1016/b978-0-08-102172-9.00003-4>.

SUWANAYUEN, S., DANNER, R. P., 1980, "Vacancy solution theory of adsorption from gas mixtures", *AIChE Journal*, v. 26, n. 1 (jan.), pp. 76–83. doi: <10.1002/aic.690260113>. Availability: <https://doi.org/10.1002/aic.690260113>.

SZOSTAK, R., 1992, *Handbook Of Molecular Sieves: Structures*. Springer. ISBN: 0442318995. Availability: <https://www.xarg.org/ref/a/0442318995/>.

TANG, X., RIPEPI, N., STADIE, N. P., et al., 2016, "A dual-site Langmuir equation for accurate estimation of high pressure deep shale gas resources", *Fuel*, v. 185 (dez.), pp. 10–17. doi: <10.1016/j.fuel.2016.07.088>. Availability: <https://doi.org/10.1016/j.fuel.2016.07.088>.

TERRIGEOL, A., 2012, "Molecular Sieves Contaminants: Effects, Consequences and Mitigation", *GPA Europe, Annual Conference*.

TLILI, N., GRÉVILLOT, G., VALLIÈRES, C., 2009, "Carbon dioxide capture and recovery by means of TSA and/or VSA", *International Journal of Greenhouse Gas Control*, v. 3, n. 5 (set.), pp. 519–527. doi: <10.1016/j.ijggc.2009.04.005>. Availability: <https://doi.org/10.1016/j.ijggc.2009.04.005>.

TSAI, M. C., WANG, S. S., YANG, R. T., 1983, "Pore-diffusion model for cyclic separation: Temperature swing separation of hydrogen and methane at elevated pressures", *AIChE Journal*, v. 29, n. 6 (nov.), pp. 966–975. doi: <10.1002/aic.690290615>. Availability: <https://doi.org/10.1002/aic.690290615>.

TSAI, M. C., WANG, S. S., YANG, R. T., et al., 1985, "Temperature-swing separation of hydrogen-methane mixture", *Industrial & Engineering Chemistry Process Design and Development*, v. 24, n. 1 (jan.), pp. 57–62. doi: <10.1021/i200028a010>. Availability: <https://doi.org/10.1021/i200028a010>.

VALENZUELA, D. P., MYERS, A. L., TALU, O., et al., 1988, "Adsorption of gas mixtures: Effect of energetic heterogeneity", *AIChE Journal*, v. 34, n. 3 (mar.), pp. 397–402. doi: <10.1002/aic.690340306>. Availability: <https://doi.org/10.1002/aic.690340306>.

WAKAO, N., FUNAZKRI, T., 1978, "Effect of fluid dispersion coefficients on particle-to-fluid mass transfer coefficients in packed beds", *Chemical Engineering Science*, v. 33, n. 10, pp. 1375–1384. doi: <10.1016/0009-2509(78)85120-3>. Availability: <https://doi.org/10.1016/0009-2509(78)85120-3>.

WOOD, K. R., LIU, Y. A., YU, Y., 2018, *Design, Simulation and Optimization of Adsorptive and Chromatographic Separations*. Wiley-VCH Verlag GmbH & Co. KGaA. Availability: <https://doi.org/10.1002/9783527815029>.

WYNNYK, K. G., 2019, *High-pressure Adsorption Equilibria Aimed at Optimizing Sour Gas Conditioning*. Ph.D. Thesis, University of Calgary, 4.

ZOU, X., 2019, *Microporous Materials for Separation Membranes*. Wiley-VCH. ISBN: 3527343970. Availability: <https://www.xarg.org/ref/a/3527343970/>.